Hungarian University of Agriculture and Life Sciences

Development of innovative rapid methods for the qualification and authentication of fruits and fruit products

Flóra Vitális

Budapest

2024

PhD School/ Program

Name Doctoral School of Food Science

Field: Food Science

Head: **Livia Simon-Sarkadi, DSc**

Department of Nutrition

Institute of Food Science and Technology

Hungarian University of Agriculture and Life Sciences

Supervisor:

Zoltan Kovacs, PhD

Department of Food Measurements and Process Control

Institute of Food Science and Technology

Hungarian University of Agriculture and Life Sciences

The applicant met the requirement of the PhD regulations of the Hungarian University of Agriculture and Life Science and the thesis is accepted for the defense process.

....

Head of Doctoral School Supervisor

Table of Contents

LIST OF ABBREVIATIONS

Abbreviation	Meaning
1st der	first derivative spectral pre-treatment
2nd der	second derivative spectral pre-treatment
ANNs	artificial neural networks
BB	“Bigarreau Burlat” sweet cherry variety
CBE	cranberry extract
con	index of fruits prepared without conidium suspension (control samples)
CV	cross-validation
deTr	detrending spectral pre-treatment
DMC	dry matter content
EL	“Elena” plum variety
EMA	economically motivated adulteration
g	index of statistical model(s) based on spectra recorded on the immature side of fruit
GSE	grapeseed extract
HCA	hierarchical cluster analysis
HPLC	high performance liquid chromatography
HSI	hyperspectral imaging
IFST	Institute of Food Science and Technology (MATE)
inf	index of fruits infected with conidial suspension (infected samples)
IPP	Institute of Plant Protection (MATE)
KJ	“Kántorjánosi” sour cherry variety
k-NN	k-nearest neighbours
LD	linear discriminant variable
LDA	linear discriminant analysis
LOSO	leave one sample out
MATE	Hungarian University of Agriculture and Life Sciences
MÉ	Codex Alimentarius Hungaricus, Magyar Élelmiszerkönyv
MI	maturation index
msc	multiplicative scatter correction spectral pre-treatment
NIRS	near infrared spectroscopy
Nr	number of spectra used in modelling
NrLV	number of latent variables used in regression modelling
NrPC	number of principal components used in LDA modelling
PCA	principal component analysis
PCA-LDA	PCA-based LDA
PGE	pomegranate extract
PLS-DA	partial least squares discriminant analysis
PLSR	partial least squares regression
r	index of statistical(s) model based on spectra recorded on the mature side of fruit

RAE	retinol activity equivalents
R_C^2	coefficient of determination of calibration
R_{CV}^2	coefficient of determination of validation
$RMSE_C$	root mean square error of calibration
$RMSE_{CV}$	root mean square error of validation
ROI	region of interest
sgol	Savitzky-Golay smoothing spectral pre-treatment
SIMCA	soft independent modelling of class analogies
SSC	soluble solid content
ST	“Stanley” plum variety
SVM	support vector machine
TSS	total soluble solid content
TA	total acidity
TAC	total anthocyanin content
TD	“Topend” plum variety
TP	“Topend plus” plum variety
UF	“Újfehértói” sour cherry variety
VC	“Valery Chkalov” sweet cherry variety
VOCs	volatile organic compounds

LIST OF UNITS

Unit	Meaning
% m/m	mass percent (dry matter content)
% V/V	volume percent
% brix	soluble solid concentration
con. / µL	conidium concentration in suspension
g/ 100 mL	extract concentration in fruit juices
mg/ g	malic acid content in fruit puree
mg/ L	anthocyanin content in fruit juice

1. INTRODUCTION

Food consumption trends have evolved significantly over the recent years, particularly in the context of health consciousness, environmental awareness, and the impacts of the COVID-19 pandemic. These trends can be particularly tracked in the consumption of fruits and fruit products, which have seen fluctuations in demand influenced by various socio-economic influences, consumer preferences and public health messages.

One of the most notable trends in food consumption is the increasing demand for healthy and organic food options that is driven by a growing consumer consciousness regarding the perceived benefits. Research indicates that consumers are increasingly prioritizing organic fruits and vegetables, which are often associated with higher nutritional value and lower pesticide residues (Wang, Pham, and Dang 2020). This trend also appears in developing regions, where consumers are becoming more discerning about the quality of food, they consume. The COVID-19 pandemic has further accelerated this trend, as individuals have become more focused on maintaining their health through dietary choices (Boca 2021; Guiné et al. 2022; Śmiglak-Krajewska and Wojciechowska-Solis 2021).

The impact of marketing on consumer behaviour is significant. The promotion of health benefits associated with fruit consumption has been a key strategy. Public health campaigns emphasize the importance of fruits in a balanced diet, which has contributed to increased awareness and demand (Goryńska-Goldmann 2019). Additionally, the rise of social media and digital marketing has allowed for targeted advertising, further shaping consumer preferences towards healthier food options, including fruits (Whitham et al. 2021). In terms of fruit products, there has been a notable increase in the consumption of processed fruit products, such as juices and dried fruits. These products are often marketed as convenient, appealing and healthy options. It is essential to consider the nutritional quality of these products, as some may contain added sweeteners, preservatives that can detract from their health benefits (Laguna et al. 2020; S. Li et al. 2021). As a result, consumers are becoming more vigilant about reading labels and understanding the ingredients in processed products, reflecting a broader trend towards informed consumption (Gopal 2023).

The production and consumption of fruits, which are subject to various consumer trends, are influenced by numerous factors. Ensuring the quality expected by buyers and consumers poses a significant challenge. In discussing this, even without striving for exhaustive detail, we cannot ignore the social, health-related, and environmental crises affecting our world. These include, but are not limited to, the impacts of war, pandemics, and extreme climatic conditions. For fruits to reach store shelves in the form, degree of processing, and quality we seek, they have to go through a very complex journey, through the food chain as we know it. The first challenges arise right in the orchards, consider the mild winters, frosty springs, drought-stricken summers, and the multitude of pests. Then comes the critical question of when to begin harvesting. How long, where, and under what conditions should fruits be ripened and/or stored, so that the industry can process them in so many of ways. Here, do not forget to mention the transparent processing and distribution processes.

In fruit production and quality control practice, the commonly applied assessments are often based on empirical, and often destructive methods. By empirical, we refer to when producers determine the start of harvest based on traits such as how easily the fruit detaches from the stalk, how easily the fruit flesh cracks, or how sweet is the fruit after degustation (Kállay et al. 2007), which are inherently subjective. A more objective approach involves the instrumental measurement of fruit weight, colour, firmness, and sugar content. These are destructive techniques, each designed to assess a single characteristic at a time. However, on their own, they are insufficient for capturing the full spectrum of quality differences or alterations. Ensuring the authenticity and traceability of food products is almost unimaginable without the use of digital solutions throughout the production and logistic processes. Today, innovative rapid methods allow us to conduct non-destructive and even contactless analyses directly on-site. During such analyses, hundreds or even thousands of data at a time can be collected, forming the "fingerprint" of a given sample. Based on these fingerprints, paired with reference characteristics and chemometric modelling, the non-destructive qualification of previously unknown samples become possible.

We increasingly rely on tuneable digital solutions that can be trained to address a wide range of questions, that is fundamentally driven by chemometric modelling, often translated into different digital agricultural strategies, like Digital Agricultural Strategy (DAS) and Digital Food Strategy (DÉS). In line with this trend, the objectives of this doctoral research were realised in cooperation with Agricolae Ltd., a company based in the Szatmár region (Hungary), renowned for its fruit production. The focus of the thesis is on the widespread application of spectroscopy-based techniques in fruit production and quality assessment (Cattaneo and Stellari 2019), specifically at certain critical points within the fruit supply chain. Within the framework of the collaboration, fruit species and varieties have been included that hold significant economic importance both within and beyond national borders. Additionally, determining their physiological state (e.g., ripeness, microbiological contamination) or detecting specific manipulations of products made from them that poses particular challenges.

Near infrared (NIR) spectroscopy is one of the advanced correlative analytical methods that are widely used in routine laboratory or industrial monitoring systems, utilising the wavelength range of 780 to 2500 nm (Manley 2014). The proliferation of miniaturisation techniques and their application in image processing technologies, like hyperspectral imaging, has made it possible to study complex biological systems in an intact way. During our investigations, we addressed the question of the efficiency of NIR spectroscopy and hyperspectral imaging coupled with chemometric modelling for the determination of fruit ripeness and thus the determination of harvest time, the efficiency of detecting inadequate fruit storage and brown rot as well as food fortification of whole stone fruits or fruit juices.

2. OBJECTIVES

The aim of the thesis was the application and development of *state-of-the-art* correlative analytical methods for non-destructive characterization of fruits and fruit products (namely fruit juices). In this doctoral research three main objectives were established, which, with the corresponding tasks, are as follows.

I. **Determining the applicability of NIR spectroscopy to determine the ripeness of various stone fruits.** Achieving this aim was supported by the following tasks:
   - Spectral tracing of maturation and ripening processes with hand-held spectrometer,
   - Model development for the classification of fruits according to their ripeness levels,
   - Model development for the prediction of certain quality traits of fruits.

II. **Determining the applicability of NIR spectroscopy and hyperspectral image processing for the detection of brown rot caused by *Monilinia* on different stone fruits.** Achieving this aim was supported by the following tasks:
   - Monitoring changes during refrigerated or room temperature storage of intact and damaged fruits contaminated with different concentrations of *Monilinia* conidium suspension,
   - Conducting investigations with hand-held NIR spectrometer and hyperspectral imaging,
   - Model development for pinpointing the effect of different storage conditions,
   - Model development for the detection of fruits contaminated with *Monilinia* in various ways and to various degrees,
   - Development of sorting models for the early detection of fruits suspected for brown rot.

III. **Determining the applicability of NIR spectroscopy for the detection of enrichment/manipulation of fruit juices with plant extracts.** Achieving this aim was supported by the following tasks:
   - Spectral analyses of fruit juices enriched with plant extracts in various combination and concentration using hand-held and benchtop NIR spectrometers,
   - Model development for the classification according to the type of extract, and dosed concentration,
   - Model development for the prediction of added extract content.

3. LITERATURE OVERVIEW

In this section, we have summarised the available literature on the topics under investigation, in alignment with the objectives of the thesis.

3.1. The importance of stone fruit consumption from different perspectives

3.1.1. Fruit production statistics in Hungary and in the world

The Hungarian fruit production plays a significant role in the country's agricultural landscape, that is characterised by wide range of fruit varieties. Comparing the production of major fruit species in Hungary, pomme fruits (i.e., apple, pear, quince, etc.) and stone fruits (i.e., apricot, peach, plum, cherries, etc.) are of utmost importance, with apple production being particularly noteworthy (KSH 2017, 2024). In Hungary, there is a strong tradition of breeding and preserving the authenticity of the mentioned fruit species. Fruit cultivation trends can be observed not only by region but even by county, the outstanding significance of the Szatmár region, located in the easternmost part of Hungary, is particularly striking (Figure 1).

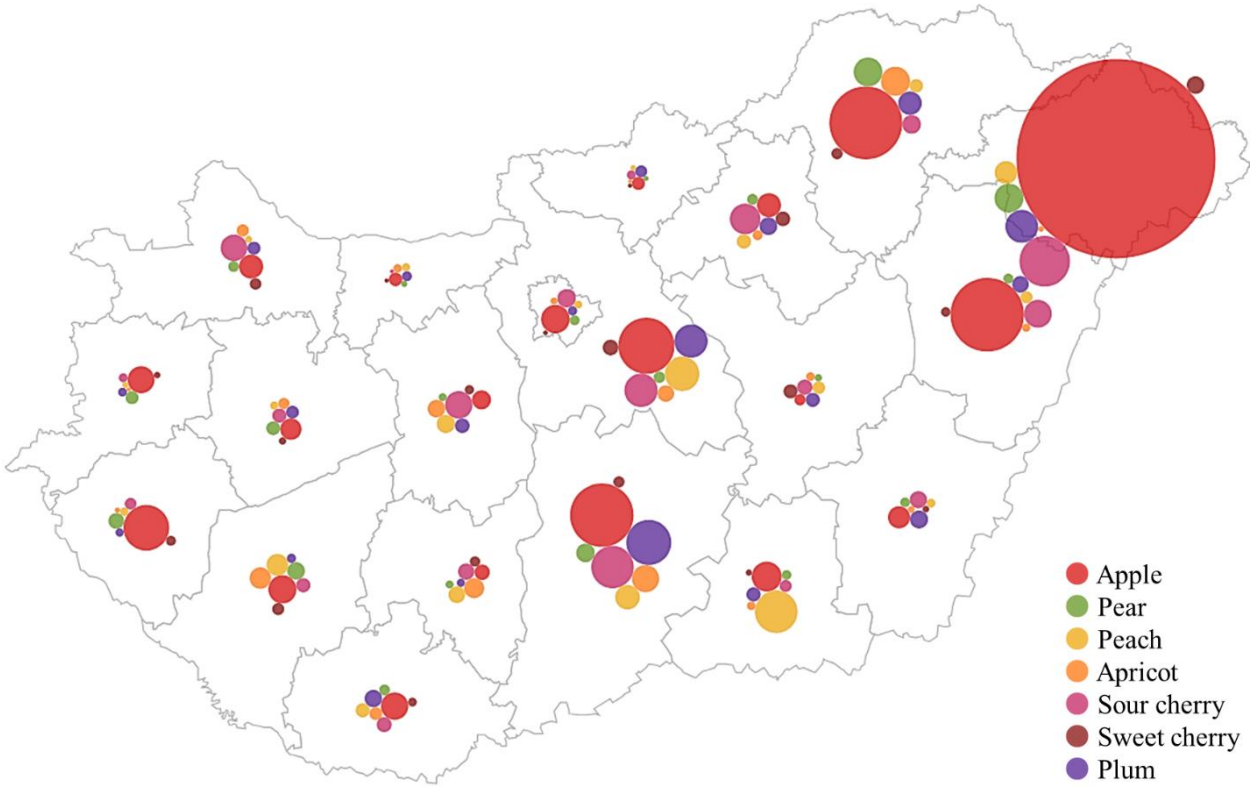

Figure 1. Distribution of economically important fruit production in Hungary by counties in 2016 (KSH 2017, 2024).

Szatmár region is recognized as a favourable area for fruit production due to a combination of its geographical, climatic, and soil. This region, benefits from a temperate continental climate, which is conducive to the growth of a variety of fruit species in the region (Kondész 2005; Papp, Nyéki, and Soltész 2004). The climate features, warm summers and cold winters, provide a distinct

seasonal variation that is essential for the proper development of many fruit crops, including apples, cherries, and plums. Besides the production of this region, it is also famous for its special quality and Hungarikum products (Lovas Kiss 2014).

After apple, sour cherry and plum are considered the most important fruits in Hungary. As in the doctoral research, various cherry and plum varieties were primarily involved, the focus will be more on these varieties in the following sections. The quantity of these fruits harvested each year fluctuates, averaging around 70 176 and 40 656 tonnes, respectively over the last 10 years. Comparing the average production of sour cherries and plums, the demand for sour cherries is nearly double that of plums (Figure 2).

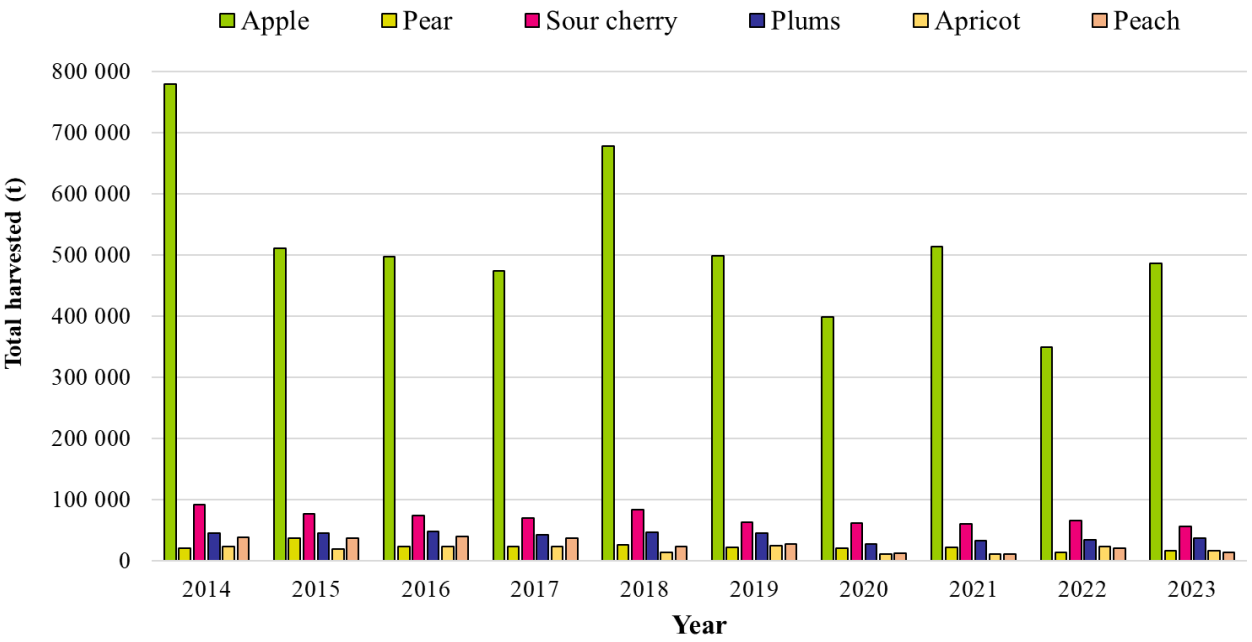

Figure 2. Harvested quantities of economically important fruits in Hungary between 2014 and 2023 (KSH 2024).

Interestingly, on a global scale, production indicators show a different trend. According to annual reports published by FAO, considering the period from 2014 to 2022, worldwide sweet cherry production has shown a slow but steady increase, with annual production exceeding 2 million tonnes. Sour cherry production has grown from 1.3 to nearly 1.6 million tonnes, while the annual production for plums and sloes has consistently exceeded 12 million tonnes since 2018 (FAO 2023a). Figure 3 illustrates the key production regions for sweet cherries, sour cherries and plums worldwide, based on data recorded and averaged between 2014 and 2022. In 2022, Turkey, Chile, Uzbekistan, and the United States were listed among the largest sweet cherry-producing countries. For sour cherries, the main producers included Russia, Poland, Ukraine, Turkey and Serbia. For plums and sloes, China's annual production was more than ten times that of Romania and Serbia, respectively (FAO 2023b).

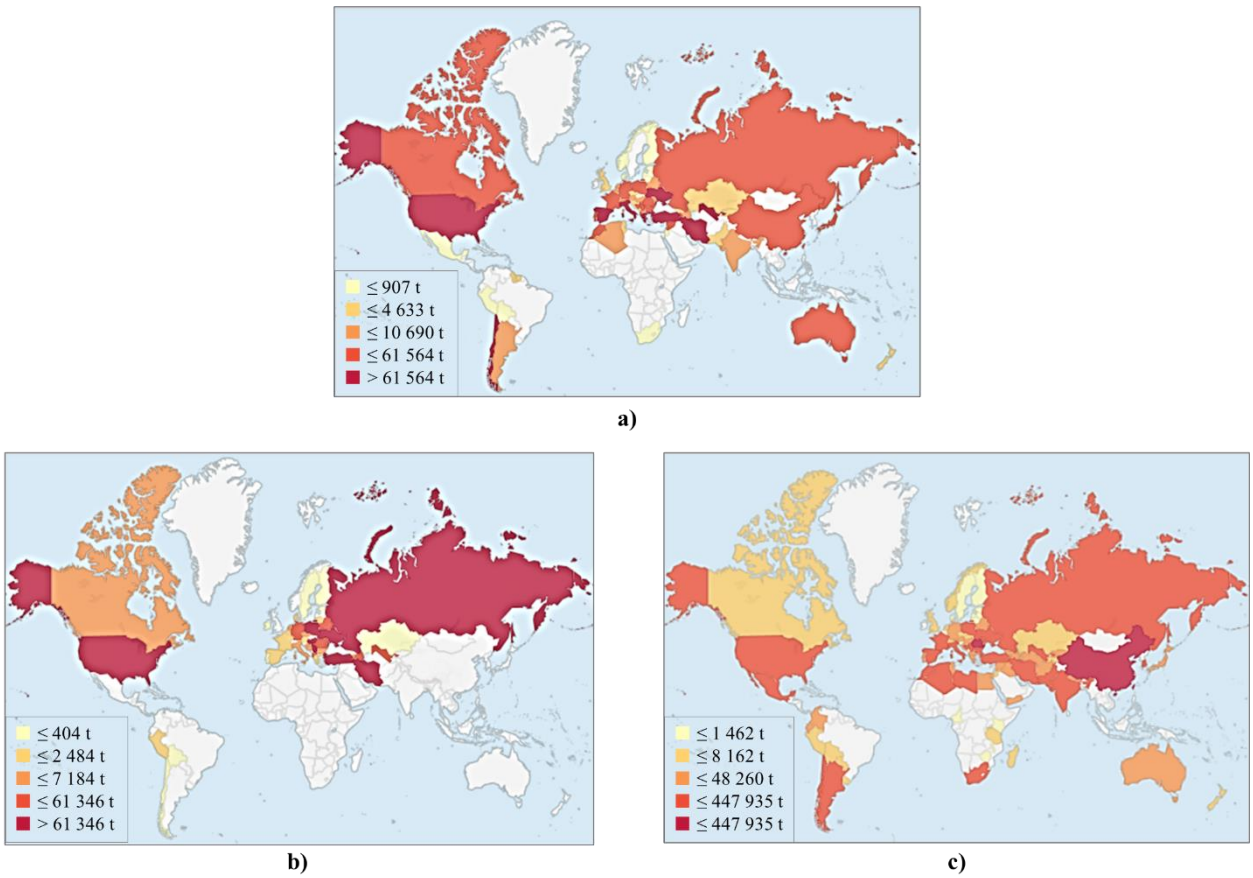

Figure 3. Average production quantities of sweet cherries (a), sour cherries (b), plums and sloes (c) by country between 2014 and 2022 (FAO 2023b).

3.1.2. The origin and improvement of stone fruits

The genus *Prunus* includes a lot of economically important members such as peach, apricot, cherry, plum and almond (Das, Ahmed, and Singh 2011). The origins and genetic improvement of sweet and sour cherries, specifically *Prunus avium* (sweet cherry) and *Prunus cerasus* (sour cherry), are rooted in a complex interplay of evolutionary biology, hybridization, and agricultural practices.

Sweet cherries have their origins primarily traced back to wild *Prunus avium*, which is native to regions between the Black and Caspian Seas (Sharpe et al. 2022a, 2022b). The domestication process of sweet cherries has involved selective breeding practices aimed at enhancing desirable traits. Genetic studies have shown that wild populations of *P. avium* serve as a significant genetic reservoir for breeding programs, providing traits that can be introduced into cultivated varieties (Guarino et al. 2009; Panda et al. 2003).

The cultivated sour cherry is believed to have arisen from hybridization involving sweet cherries and ground cherries, specifically *Prunus fruticosa* (Brettin et al. 2000; Hauck et al. 2006). This hybridization has led to a rich genetic diversity within the sour cherry population, which is essential for its adaptation and cultivation across various climates. The origin mapping of sour cherries reveals that multiple wild *Prunus* species may have contributed to the genetic makeup of cultivated sour cherries. For instance, studies indicate that the maternal parent of sour cherries

could involve different populations of *P. fruticosa* or other *Prunus* species, suggesting a complex ancestry that merits further investigation (Bird et al. 2022).

The origin and genetic improvement of plums, particularly focusing on *Prunus domestica* (European plum) and *Prunus salicina* (Japanese plum), reflect a rich history of domestication, hybridization, and modern breeding practices. The domestication of plums is believed to have occurred independently in several regions, including Southern Europe, Asia Minor and China, where distinct species such as *P. domestica* and *P. salicina* emerged as important fruit crops (Callahan 2008; Hussain et al. 2021). Studies have proven that plums are among the most polymorphic species within the *Prunus* genus that can be largely attributed to recurrent hybridization history. This explicitly characterises reflected in Japanese plums, which are interspecific hybrids involving *P. salicina*, *P. simonii* (apricot plum) and *P. cerasifera* (cherry plum) (Huang et al. 2021; Sottile et al. 2022).

In recent years, advancements in genomic technologies have significantly enhanced the understanding of genetics. Whole-genome resequencing has provided insights into the genetic diversity of the studied fruit species, revealing numerous alleles associated with important agronomic and quality traits (Xiao et al. 2021). Mapping of the genetic diversity present in wild populations is crucial for ongoing breeding programs, particularly in the face of climate change, emerging pests and diseases. In addition to these, it also enables the identification of specific genes linked to desirable fruit characteristics, such as fruit size and flavour (Valderrama-Soto et al. 2021).

The conservation of genetic resources is a critical aspect of cherry and plum improvement. Many traditional and local cultivars are being preserved in germplasm and in breeding collections. According to some sources, 135 sweet and 74 sour cherry cultivars have been reported since the mid-1990s. Europe's role in the cherry breeding programmes is outstanding, Germany, Czechia, Russia, Hungary, Estonia, France, Romania and Italy being among the most important countries (Kappel et al. 2012). In case of plums, the estimated number of cultivars are over 6 000 belonging to 19-40 species, depending on the taxonomist (Butac 2020; Topp et al. 2012).

3.1.3. The composition of stone fruits

Sweet cherries, sour cherries and plums are stone fruits in which the flesh is the most important part that surrounds a single shell (stone) of endocarp with the kernel inside. These fruits are characterized with rich nutritional composition and delightsome flavour. All these stone fruits offer a variety of macronutrients, micronutrients, and phytochemicals that contribute to their health benefits as well. Understanding the nutritional profile of these fruits is essential for appreciating their role in a balanced diet and their potential health-promoting properties.

Table 1 shows a comparative summary about the composition of the fruits in focus according to various sources. These fruits are characterised by a relatively low-calorie content, that being the lowest for plums. A common characteristic is that water, exceeding 80%, is the major constituent of the fruits. Sweet cherries are primarily composed of carbohydrates, which constitute approximately 13-16% of their total weight, predominantly in the form of natural sugars such as fructose and glucose. Sour cherries contain slightly lower carbohydrate levels, typically around

10-14% (Kelley, Adkins, and Laugero 2018). Plums have a carbohydrate content that ranges from 11-15%, with a similar sugar profile to cherries, including fructose and sorbitol, which contributes to their sweetness. Starch is present in very low amounts in the fruits, since its concentration decreases during maturation (Sinha 2012).

All three fruits are low in protein, with sweet cherries containing about 0.6-1%, sour cherries slightly less, and plums around 0.5-1% (Igwe and Charlton 2016; Kole and Abbott 2012). However, the protein present includes essential amino acids, which are vital for various bodily functions (Kelley et al. 2018). The fat content in these fruits is negligible, generally less than 0.5%, making them suitable for low-fat diets.

Table 1 also summarises the micronutrients present in cherries and plums. The main minerals of these fruits include potassium, magnesium, calcium and phosphorus, with potassium being particularly abundant, contributing to cardiovascular health by helping to regulate blood pressure (Khan et al. 2022). Additionally, minerals like iron, manganese, copper, zinc and selenium are also present in trace amounts (Serradilla et al. 2016). These fruits contain almost no sodium, which supports current dietary recommendations related to salt intake.

These fruits are rich in vitamins as well, particularly in vitamin C, which is crucial for immune function and skin health. Sweet cherries typically contain about 7-10 mg of vitamin C per 100 grams, while sour cherries can have slightly higher concentrations, ranging from 10-15 mg (Kelley et al. 2018). This vitamin plays a significant role in collagen synthesis and enhances the absorption of iron from plant-based foods. In addition to vitamin C, these stone fruits contain a variety of B vitamins, including B1 (thiamine), B2 (riboflavin), B3 (niacin), B5 (pantothenic acid), and B6 (pyridoxine) (Serradilla et al. 2016), which are essential for energy metabolism, and the proper functioning of the nervous system. These fruits, in general, contain little or no amount of vitamin E and D which can be related to low fat content.

While discussing the composition of cherries and plums, one cannot neglect to mention their valuable antioxidant properties, as these fruits are highly regarded for their abundance of phenolic compounds and polyphenols. These secondary metabolites, produced in plant tissues through photosynthesis, play a crucial role in determining the quality of plant-derived foods. They significantly affect the fruits' colour, taste and flavour, also offering notable health benefits. Published literature suggested that sour cherries have higher concentrations of total phenolic compounds, while the sweet cherries contained more anthocyanins (Habib et al. 2017). Among the major phenolic compounds, these fruits contain anthocyanins (cyanidin-3-rutinoside, cyanidin-3-O-glucoside, peonidin-3-O-rutinoside), hydroxycinnamates (3-caffeoylquinic acid, 3-p-coumaroylquinic acid), flavanols (catechin, epicatechin) and flavonols (quercetin 3-O-glucoside, quercetin-3-O-rutinoside) (Lara et al. 2020; Neveu et al. 2010; Serradilla et al. 2016).

Table 1. Comparison of the approximate nutritional composition of raw sweet cherry, sour cherry and plum according to different nutritional databases.

Component	Unit	Sweet cherry			Sour cherry		Plum		
		USDA (2019b)	Frida Food Data (2024a)	Bíró and Lindner (1995)	USDA (2019a)	Bíró and Lindner (1995)	USDA (2019c)	Frida Food Data (2024b)	Bíró and Lindner (1995)
Energy	kcal	63	61	63	50	52	46	46	59.7
Energy	kJ	263	258	265	209	218	192	195	250
Water	g	82.2	83.8	83.6	86.1	85.9	87.2	87.1	84.7
Protein	g	1.1	1.0	0.8	1.0	0.8	0.7	0.3	0.7
Total lipid (fat)	g	0.2	0.0	0.0	0.3	0.0	0.3	0.0	0.0
Carbohydrate, by difference	g	16.0	14.8	14.0	12.2	11.0	11.4	12.3	13.1
Dietary fibre	g	2.10	1.20		1.60		1.40	2.00	
Sucrose	g	0.15	0.00		0.80		1.57	1.05	
Glucose	g	6.59	6.17		4.18		5.07	3.65	
Fructose	g	5.37	5.35		3.51		3.07	3.11	
Maltose	g	0.12	0.00		0.00		0.08	0.00	
Minerals		USDA (2019b)	Frida Food Data (2024a)	EFSA (2021)	USDA (2019a)	EFSA (2021)	USDA (2019c)	Frida Food Data (2024b)	EFSA (2021)
Sodium	mg	0	0		3		0	0.125	
Potassium	mg	222.00	200.00	212.29	173.00	173.83	157.00	173.00	198.43
Calcium	mg	13.00	8.78	18.14	16.00	12.51	6.00	7.45	11.71
Magnesium	mg	11.00	8.12	9.97	9.00	8.00	7.00	7.08	8.67
Iron	mg	0.360	0.200	0.360	0.320	0.410	0.170	0.111	0.290
Copper	mg	0.060	0.072	0.070	0.104	0.080	0.057	0.051	0.070
Zinc	mg	0.070	0.055	0.080	0.100	0.100	0.100	0.100	0.090
Manganese	mg	0.070	0.062		0.112		0.052	0.058	
Selenium	µg	0	0.333	0.240	0	0.550	0	0.175	0.100
Phosphorus	mg	21.00	20.30	20.97	15.00	18.23	16.00	14.40	18.71
Vitamins		USDA (2019b)	Frida Food Data (2024a)	EFSA (2021)	USDA (2019a)	EFSA (2021)	USDA (2019c)	Frida Food Data (2024b)	EFSA (2021)
Vimamin A	RAE	3.00	4.28		64.00		17.00	29.50	
Retinol	µg	0	0		0		0	0	
Beta-carotene	µg	38.0	25.7		770		190	177	
Vitamin D	µg		0					0	
Vitamin E (α-TE*)	mg	0.070	0.152	0.150	0.070	0.120	0.260	0.392	0.770
Thiamin (Vitamin B1)	mg	0.027	0.016	0.040	0.030	0.030	0.028	0	0.050
Riboflavin (Vitamin B2)	mg	0.033	0.021	0.040	0.040	0.040	0.026	0.015	0.060
Niacin (Vitamin B3)	mg	0.154	0.025	0.580**	0.400	0.460**	0.417	0.168	0.730**
Pantothenic acid (Vitamin B5)	mg	0.199	0.123		0.143		0.135	0.168	
Pyridoxine (Vitamin B6)	mg	0.049	0.037	0.050	0.044	0.050	0.029	0.029	0.050
Folate (Vitamin B9)	µg	4.00	6.48		8.00		5.00	0	
Ascorbic acid (Vitamin C)	mg	7.00	6.72		10.00		9.50	3.06	
Choline, total	mg	6.10	6.10		6.10		1.90	1.90	

* alpha-tocopherol equivalent

** niacin equivalent

3.1.4. The health benefits of stone fruit consumption

Both cherries and plums are low in calories and high in essential nutrients. They are rich in carbohydrates, primarily in the form of natural sugars, and provide dietary fibre that have a regulatory function by selecting the microflora present in the intestines (Cui et al. 2019). Sweet cherries typically contain about 13-16% carbohydrates, while sour cherries and plums have similar carbohydrate content, with plums also being a good source of sorbitol, a sugar alcohol that can aid in digestion (Alsolmei et al. 2019). The fibre content in these fruits contributes to satiety, helping to control appetite and manage weight (Stacewicz-Sapuntzakis 2013).

The beneficial effects of stone fruit consumption can be enhanced by consuming it in dried form, this is of particular interest for plums, also known as prunes (Stacewicz-Sapuntzakis 2013). These fruits are known for their moderate laxative effects, which can help alleviate constipation and promote bowel movements, and support a healthy microbiome (Shamloufard, Kern, and Hooshmand 2017). Earlier studies attributed these effects of prunes on the digestion to the presence of phenolics (chlorogenic acid) and sorbitol, together with its high fibre content (Igwe and Charlton 2016; Stacewicz-Sapuntzakis 2013). The role of fibre in human health is mainly protective against disease, for example, of the gastrointestinal tract, circulation-related, and metabolic diseases (Padayachee et al. 2017).

Stone fruits are an important source of an array of secondary metabolites that may reduce the risk of various diseases. Numerous epidemiological studies support the concept that regular consumption of foods and beverages rich in antioxidant flavonoids is associated with a decreased health risk. Such components have been shown to combat oxidative stress and reduce inflammation (Bakuradze et al. 2019; Fotirić Akšić et al. 2023). The antioxidant capacity of these fruits is linked to a lower risk of chronic diseases such as cardiovascular disease, diabetes, and certain cancers (El-Beltagi et al. 2019; Igwe and Charlton 2016). The anthocyanins in cherries have been associated with improved endothelial function and reduced blood pressure (Igwe et al. 2017). Studies indicate that the regular consumption of cherries and plums can lead to significant improvements in lipid profiles, particularly in individuals with hypercholesterolemia (Walkowiak-Tomczak, Regula, and Smidowicz 2018).

Plums, particularly prunes, have been linked to improved cholesterol levels and reduced inflammation, contributing to overall heart health (Hong et al. 2021). The combination of fibre, antioxidants, and other phytochemicals in these fruits plays a crucial role in maintaining cardiovascular functions (Blando and Oomah 2019; Faienza et al. 2020; Kelley et al. 2018). Prunes also garnered attention for their bone health benefits. Researches have demonstrated that prune consumption can prevent and even reverse bone loss in postmenopausal women, who are particularly at risk for osteoporosis (Arjmandi et al. 2017). The polyphenolic compounds in prunes enhance bone formation and mineralization while inhibiting bone resorption (Graef et al. 2018). This dual action makes dried plums a valuable addition to the diet for maintaining bone density and overall skeletal health.

3.2. Processes during the development of stone fruits

The maturation and ripening processes of sweet cherries, sour cherries and plums are complex physiological phenomena that involve a series of biochemical changes leading to the development of fruit quality attributes such as colour, flavour, texture and nutritional value. Each species exhibits unique characteristics during these stages, influenced by varietal, environmental, and physiological factors (Serradilla et al. 2016, 2017). This summary explores the main maturation and ripening processes, enzymatic and postharvest changes in the named fruits. Understanding and tracking these processes are crucial for optimising harvesting and postharvest practices, as well as for enhancing fruit quality, shelf life and support possible further processing.

3.2.1. Stone fruit maturation

Maturation refers to the developmental phase of cherries and plums when the fruit transitions from a hard, immature state to a soft, ripe condition (Li 2012). This phase is characterized by significant physiological changes, a biphasic growth pattern including rapid cell division, followed by a slower phase of cell expansion (Prinsi et al. 2016), which contribute to the overall size and shape of the fruit. The maturation of these stone fruits involves the accumulation of soluble solids, primarily sugars, organic acids, and phenolic compounds is a critical aspect of maturation, influencing the flavour profile and overall quality of the fruit. The latter is a key indicator of maturation, with the fruit becoming sweeter as it ripens (Mahmood et al. 2012; Serradilla et al. 2010).

The maturation of sweet cherries is marked by a rapid increase in fruit size and the accumulation of sugars, primarily glucose and fructose, which contribute to the fruit's sweetness. During this phase, the total soluble solids (TSS) content rises, while titratable acidity (TA) remains relatively stable (Di Matteo et al. 2017; Mulabagal et al. 2009). The maturation process typically spans approximately 50 days from pollination to full ripening (Li et al. 2015), with the fruit transitioning from a hard, green state to a softer, more palatable form (Serradilla et al. 2010). Another salient feature of cherry fruit maturation is the transition from an initial green colour to shades of red, violet or black, driven by the formation of anthocyanins and the breakdown of chlorophyl (Habib et al. 2017). The accumulation of anthocyanins, particularly cyanidin-3-O-rutinoside, imparts the characteristic red colour to ripe cherries (Mulabagal et al. 2009).

Sour cherries undergo a similar maturation process, but the timing and specific biochemical pathways may differ due to the distinct characteristics of the fruit. Sour cherries are characterized by a higher acidity level and organic acid content, primarily malic acid, which provide their tart flavour (Serrano et al. 2005). The balance between sugars and acids is crucial for determining the overall taste profile of sour cherries, and this maturation index (MI) is often used to assess fruit quality (Wojdyło et al. 2014). The maturation period for sour cherries is generally shorter than that of sweet cherries, making them more sensitive to harvest timing.

The maturation of plums is similar to cherries, demonstrate an increase in TSS and a decrease in acidity during maturation. The maturation process is influenced by environmental factors such as temperature and sunlight, which can affect the rate of growth and the accumulation of sugars and

acids (Kodagoda et al. 2021; Kuhn et al. 2020). The maturation of plums is also marked by changes in colour, with the fruit transitioning from green to yellow, red or purple, depending on the cultivar (Fazzari et al. 2008).

3.2.2. Stone fruit ripening

Ripening is the subsequent phase that follows maturation and is characterized by a series of biochemical, physiological and sensorial changes that enhance the fruit's palatability and nutritional value (Li 2012; Serradilla et al. 2017). During the ripening process, sweet cherries, sour cherries and plums exhibit a significant increase in pigment production, mainly anthocyanin, which is responsible for their characteristic colour. The biosynthesis of anthocyanins is regulated by various transcription factors, and their accumulation is closely linked to the ripening stage (Wang et al. 2023; Wei et al. 2015).

Sweet cherries are classified as non-climacteric fruits, meaning their ripening is not driven by ethylene production (Chen et al. 2022; Tijero et al. 2016). Instead, ripening is primarily regulated by abscisic acid (ABA), which promotes softening and colour development (Kuhn et al. 2020). During ripening, the fruit undergoes significant softening due to the breakdown of cell wall components, primarily pectin, mediated by enzymes such as polygalacturonase. The accumulation of anthocyanins continues during ripening, enhancing the fruit's colour and antioxidant properties (Serrano et al. 2009).

Sour cherries also exhibit a non-climacteric ripening process, with ethylene playing a minimal role. The ripening of sour cherries is characterized by a decrease in acidity and an increase in sugar content, leading to a more balanced flavour profile (Wojdyło et al. 2014). The accumulation of anthocyanins during ripening is crucial for developing the characteristic red colour of ripe sour cherries, and the flavour is influenced by the balance of sugars and organic acids (Viljevac et al. 2012). The softening of the fruit is facilitated by enzymatic activity, similar to that observed in sweet cherries.

Plums are classified as climacteric fruits, meaning their ripening is associated with a peak in ethylene production (Fang et al. 2016). Ethylene regulates various physiological processes during ripening (María-Jesús Rodrigo et al. 2012), including softening, colour change, and the production of volatile compounds that contribute to aroma and flavour (Álvarez-Herrera, Deaquiz, and Rozo-Romero 2021; Li et al. 2019). The softening of plums is mediated by enzymes such as pectinase and cellulase, which break down cell wall components. The accumulation of anthocyanins during ripening contributes to the fruit's colour, and the production of esters and alcohols enhances the aroma. The ripening process in plums is also influenced by environmental factors, with temperature and humidity playing critical roles in determining fruit quality (Vargas et al. 2017).

3.2.3. Enzymatic changes in stone fruits

Enzymatic activity is a key element of the maturation and ripening processes in all three fruit species. Enzymatic reactions are influenced by genetic factors and environmental conditions, emphasizing the importance of cultivar selection and growing practices in determining fruit quality.

In sweet cherries, the softening process during ripening is associated with increased activity of enzymes such as polygalacturonase, β-galactosidase, and pectin methylesterase, that break down cell wall components and lead to fruit softening (Mahfoudhi and Hamdi 2015). These enzymatic changes are essential for achieving the desired texture and mouthfeel of ripe cherries. The activity of enzymes involved in cell wall degradation increases during ripening, leading to softening and changes in fruit texture.

In sour cherries, similar enzymatic changes occur, with the breakdown of pectins and other cell wall components facilitating softening (Viljevac et al. 2012). The production of volatile organic compounds (VOCs) contributing to the characteristic aroma of ripe cherries, is also regulated by enzymatic reactions (Serradilla et al. 2010). The production of esters, alcohols, and aldehydes increases during ripening, enhancing the sensory attributes of the fruit (Serradilla et al. 2016; Villavicencio et al. 2021).

In plums, the enzymatic activity associated with ripening is more pronounced due to their climacteric nature. Ethylene production triggers the expression of genes encoding enzymes involved in softening and flavour development (Fang et al. 2016). The activity of antioxidant enzymes in plums, including superoxide dismutase, catalase, and ascorbate peroxidase, play an important role in protecting the fruit from oxidative stress during ripening (Martínez-Esplá et al. 2017). The activity of these enzymes can be influenced by preharvest treatments, like salicylates or melatonin, which have been shown to enhance the antioxidant capacity and storability of plums (Cortés-Montaña et al. 2023).

3.2.4. Postharvest changes in stone fruits

Postharvest handling of sweet cherries, sour cherries, and plums is critical for maintaining fruit quality and extending shelf life. In the days following harvest, fruits continue to ripen, although at a slower rate compared to on-tree ripening (Serrano et al. 2009), and phenolic content tends to increase and generally remains stable throughout the storage (Habib et al. 2017). Factors such as storage temperature, humidity and ethylene exposure significantly impact the postharvest ripening dynamics (Serradilla et al. 2017). For instance, treatments with plant hormones like salicylic acid can delay ripening and preserve fruit quality during storage (Mahfoudhi and Hamdi 2015; Valero et al. 2011).

Sour cherries are primarily processed into juices, jams, and other products, and their postharvest handling focuses on preserving quality during processing (Horváth-Kerkai and Stéger-Máté 2012). The high respiration rate of sour cherries necessitates careful management of storage conditions to prevent spoilage (Milić et al. 2021). Researches have shown that the ripening processes can be influenced by preharvest treatments. The application of gibberellins or melatonin can enhance fruit quality attributes and antioxidant systems. These treatments can lead to improved colour development, increased sugar content, and enhanced flavour profiles, ultimately benefiting consumers (Carrión-Antolí et al. 2022; Michailidis et al. 2021).

Plums stored at higher temperatures may experience accelerated ripening and increased susceptibility to spoilage (Wu et al. 2011). For this species, it has been proven that the use of

preharvest treatments, such as gibberellins and abscisic acid, also enhance fruit quality attributes and extend shelf life (Time et al. 2021).

As a fruit moves beyond peak of ripeness, it undergoes a process of degradation and decay. This stage, known as senescence, is not merely a simple breakdown but represents the final phase of the fruit's life cycle. During senescence, a series of typically irreversible physiological and biochemical processes take place, leading to the deterioration of cells and ultimately the death of the fruit (Li 2012).

3.3. Decay during pre- and postharvest of stone fruits

The preharvest and postharvest decay processes in sweet cherries, sour cherries and plums are critical factors influencing the quality and marketability of these fruits. Understanding decay processes is essential for applying effective intervention, management practices to reduce losses and maintain fruit quality throughout the supply chain. Cherries and plums are highly perishable that ripen quickly after harvest, thus resulting in short postharvest life that is determined by fruit ripeness at harvest, and handling during transport and storage (Habib et al. 2017).

There are differences among varieties but in general, non-climacteric cherries have a shelf life of 7-14 days in cold storage, and plums have a shelf life of around 2-6 weeks, even when stored at 0 °C (Miranda-Castro 2016). Therefore, efforts must be undertaken to minimize the losses in the postharvest stage and maximize the storage life of the fruit. An essential demand of the consumers is for products that are safe, meaning free of pathogens and chemical residues.

The losses caused by postharvest diseases in fruits are inevitable as they can cause production loss of even up to 50% (Elik et al. 2019). Several pathogens such as fungi and bacteria attack orchards before and after harvest. These are mostly weak air-borne pathogens in the sense that they can only invade damaged individuals, and are typical for harvested and stored fruits. Environmental stress such as low temperature, heat, and oxygen shortage can cause physiological damage of the tissues that increases the sensitivity of stored fruit by forming locations vulnerable to the invasion of pathogens (Barkai-Golan 2001). Nowadays, brown rot caused by various *Monilinia spp*. is a major problem threatening the production of stone fruit crops such as cherries and plums worldwide (Aiello et al. 2019; Singh and Sharma 2018).

3.3.1. Description of brown rot

Brown rot, primarily caused by the fungal pathogens *Monilinia fructicola*, *Monilinia laxa*, and *Monilinia fructigena*, is a significant disease affecting sweet cherries, sour cherries and plums. This disease poses a major threat to fruit production, leading to substantial economic losses during both preharvest and postharvest stages and can result in losses of up to 80% under favorable environmental conditions for the fungus.

Latent infection can occur when *Monilinia* spp. causes the infection of young fruit in the orchard, but develop symptoms only after fruit ripening (Barkai-Golan 2001). Even when the fungal spores reach the specific host, they are capable to cause the disease only under appropriate conditions for germination. The disease cycle begins with the germination of conidia, which can penetrate fruit

through natural openings or wounds. Once established, the fungus produces abundant spores, facilitating further spread (Garcia-Benitez et al. 2016). Figure 4. illustrates the schematic life cycle of brown rot caused by *Monilinia spp.* using peaches as an example (Oliveira Lino et al. 2016).

The pathogen can infect blossoms, fruit, and twigs, with significant damage occurring during storage and transport (Aiello et al. 2019). The optimum temperature for growth of most fungi attacking fruits in storage is about 20-25 °C, though some species prefer lower or, more often higher temperatures. The effect of temperature is interrelated with that of the relative humidity (Yahaya and Mardiyya 2019). High relative humidity needed for the protection of fruits from dehydration and weight loss may promote the growth of pathogens during fruit storage (Barkai-Golan 2001).

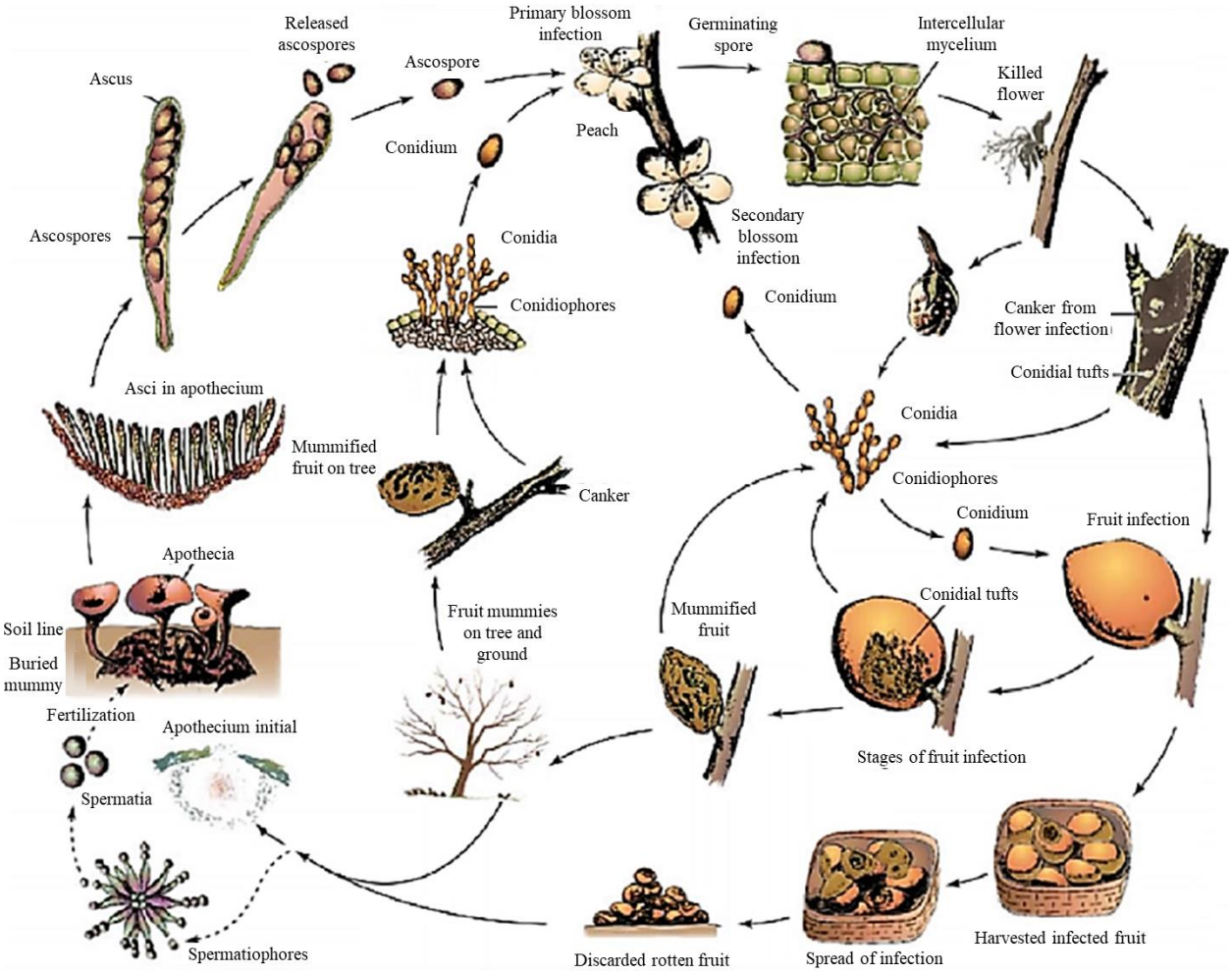

Figure 4. Life cycle of *Monilinia* spp. (source: Plant Pathology. Copyright 2005. Elsevier Ltd.) (Oliveira Lino et al. 2016).

Monilinia species are notorious for causing brown rot, which manifests as soft, brown lesions on fruit, leading to decay both pre- and post-harvest (Astacio et al. 2023; Oliveira Lino et al. 2016). The infection contributes to the penetration and development of other pathogens till the fruit is completely consumed. However, these processes can be delayed and inhibited by the phenolic compound of the fruits (Oliveira Lino et al. 2016).

To minimize postharvest losses, it is crucial to sort any suspected or infected fruits from the batch to preserve the product quality expected by consumers. This approach helps prevent further fungal contamination and limits the processing of spoiled produce, ultimately contributing to increased agricultural profits. In connection with this, Petróczy (2009) has extensively studied the latest and environmentally friendly possibilities for the control of various *Monilinia* species.

3.3.2. *Monilinia* species that pose the greatest threat to stone fruits

Monilinia fructigena

M. fructigena is a major concern for pomme fruit, particularly apple and pear production, but also affect stone fruits (Gell et al. 2008). It was already widespread in Europe in the 1800s, and its morphology and biology were known in details. It has also been reported in other regions, including parts of Asia and North America (Hrustić, Mihajlović, and Tanović 2020). It is a quarantine pathogen in Canada, United States, Australia and New Zealand (De Miccolis Angelini et al. 2022). This pathogen can also infect blossoms and twigs, leading to blossom blight and twig cankers, which can significantly impact overall fruit yield (Van Leeuwen, Holb, and Jeger 2002). *M. fructigena* is unable to secrete cell wall degrading enzymes, thus can spread through contact after contamination via mechanical injury.

Monilinia laxa

M. laxa is one of the most dangerous fruit tree pathogens. It primarily damages flowers and shoots, causing wilting and drying, while also inducing cankers on woody parts as a result of the infection. It also causes substantial damage to stone fruits through fruit rot (Batra 1991). The pathogen is found throughout Europe, with the exception of the northernmost regions. *M. laxa* is known to be able to secrete cell wall-degrading enzymes to infect primarily stone fruits. The fungus causes significant crop loss, and the infected fruit can pose a serious threat as it may serve as a source of further contamination. Research shows that *M. laxa* can germinate at temperatures up to 30°C, with optimal growth occurring between 20-25°C (Bernat et al. 2017).

Monilinia fructicola

M. fructicola is the most prevalent species associated with brown rot in stone fruits, including sweet cherries, sour cherries and plums. It can infect fruit at any developmental stage, but susceptibility increases dramatically as the fruit matures (Martínez-García et al. 2023; Villarino et al. 2012). *M. fructicola* is primarily found in North America, South America, New Zealand and Australia, with its presence increasingly noted in Europe due to the importation of infected fruits (Fan et al. 2010; Ivić et al. 2014; Pereira et al. 2019). The pathogen has been identified in various countries. For Hungary, the pathogen was introduced through infected Italian and Spanish peaches and was later identified in domestic plantations in 2006 (Petróczy and Palkovics 2005, 2006). Research indicates that this pathogen can germinate at temperatures up to 35 °C, making it resilient to various climatic conditions (Bernat et al. 2017). Additionally, it demonstrates varying sensitivity to extreme growth conditions, with some isolates exhibiting greater resistance compared to others (Hrustić et al. 2020).

3.4. Challenges in the production of fruit-based products

Stone fruits, like cherries and plums, are seasonal fruits. To preserve their valuable nutritional value over the long term, preservation methods are essential. Due to the highly diverse techno-functional properties of stone fruits, a wide variety of products can be made, including pulps, juices, concentrates, canned goods, sauces, dried, or even frozen fruits (Stéger-Máté 2012). The following section details the technological process of juice production, quality standards and their possible manipulation particularly relevant to this research work.

3.4.1. Production of fruit beverages

The primary raw materials for fruit beverages in international trade include citruses, pomme fruits, stone fruits, grapes, various berries, etc. As fruit juice consumption increases, the production of raw materials and the actual consumption of juice have become increasingly separated, both geographically and temporally. This has led to a shift toward using fruit pulps and concentrates, which are easier to store and transport (Horváth-Kerkai and Stéger-Máté 2012).

Fruits intended for industrial processing must meet several requirements, such as being resistant to fruit diseases and mechanical harvesting, ripen uniformly to produce large yields. From a technological point of view, traits like soluble solid content (SSC), acidity, and pigment concentration are crucial. After harvesting, the fruits delivered to the plant undergo quantitative receipt, visual inspection, and objective quality assessment. These results provide essential information for planning the processing steps (e.g., the intensity of preparatory operations and the level of concentration required). The production of filtered juices and other fruit beverages, which is the focus of this research is summarised in Figure 5.

Preparatory operations

The fruits arriving at the processing facility are tipped into a flotation flume, from where they are transported to the initial stages of the preparation process. Washing, as the primary cleaning operation, aims to improve the physical, chemical, and microbiological cleanliness of the raw material. With proper efficiency, it can reduce the microbial count by 3-5 orders of magnitude (Barta and Körmendy 2008). Meanwhile, the cleaned raw material undergoes sorting, during which foreign plant materials, non-plant parts, and fruits with quality defects (i.e., inappropriate colour, damage, infection) are removed. Optical sorters (colour graders) are the most commonly used for this step. Certain fruits, such as sweet cherries, sour cherries and berries, arrive with stems for processing, and the chlorophyll content of the stem necessitates the de-stemming step particularly important for preserving the colour and flavour of the product (Barta and Körmendy 2007).

Juice extraction

There are several preparatory operations before the actual juice extraction. Cracking, crushing and smashing fruits are generally applied operations to increase the surface area and initiate the release of cell fluids. The intensity of this process depends on the specific juice extraction method used afterward. This step can potentially damage valuable compounds or trigger enzymatic reactions that result in the formation of undesirable substances.

To mitigate the lysing effects, the crushed fruits are immediately subjected to further treatments such as heat, enzymatic processes, freezing, vibration, or ultrasound electroplasmolytic and ionic irradiation. The aim of the mentioned treatment is to increase juice yield, reduce undesirable physical, biochemical changes, and also to enhance the formation of better colour, aroma, flavour properties.

In the further processing of cracked fruits, heat treatment, enzymatic treatment or a combination of these are perhaps the most commonly used preparatory operations. Enzymatic treatment is used to break down the components that give the fruit its structure, in particular its pectins and cellulose. The pectin-degrading enzymes (e.g., pectin esterase, pectin lyase, polygalacturonase) rapidly reduces the viscosity of the fruit mash; however, the fruit raw materials contain varying types and amounts of pectins depending on the species and variety. It essential to select enzyme preparations with these in mind, as the depolymerization allows for more efficient extraction of juice from the fruit pulp.

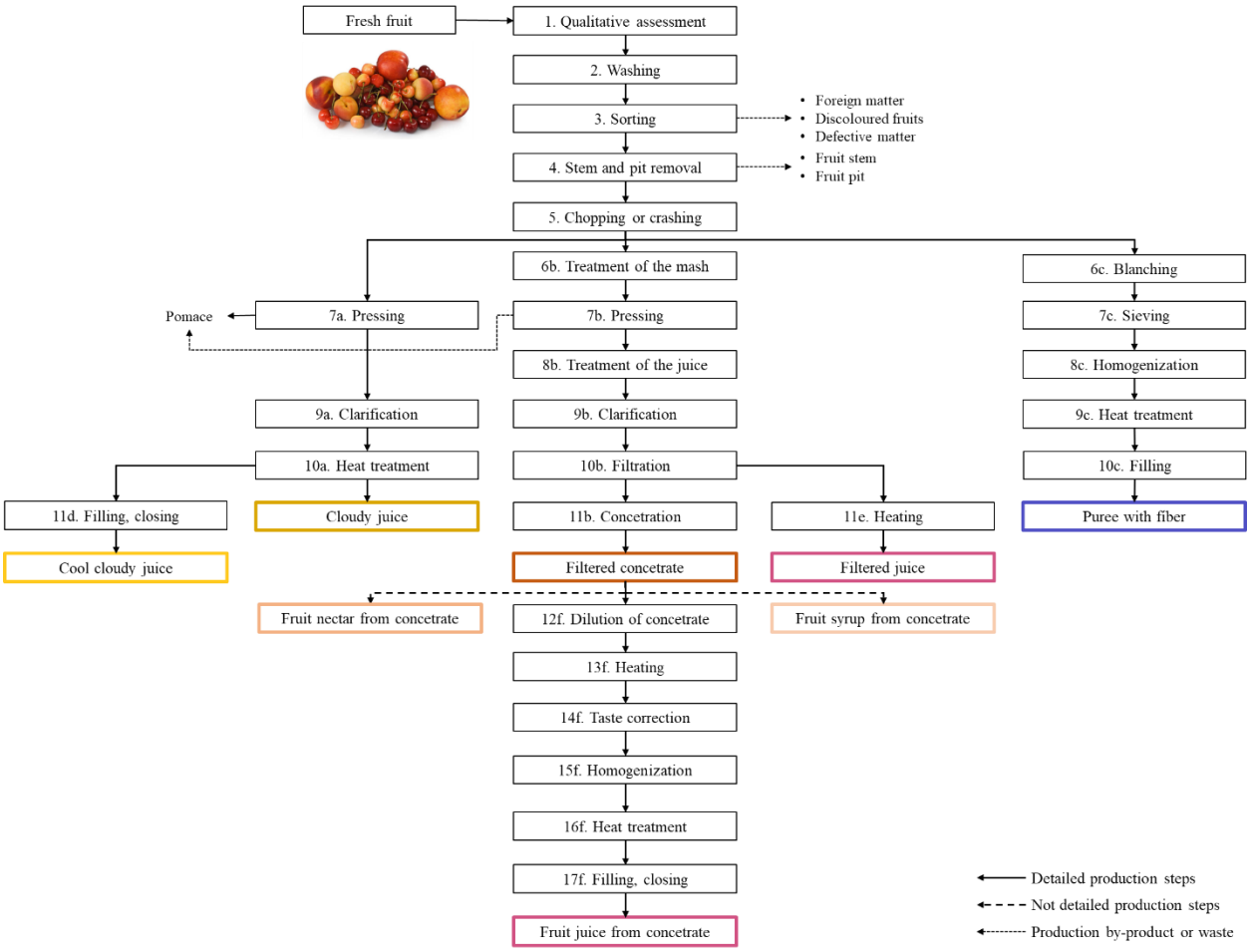

Figure 5. Flow chart of fruit beverages production (adapted from Barta and Körmendy (2007, 2008); Horváth-Kerkai and Stéger-Máté (2012)).

After the mash treatment, juice extraction typically follows, usually carried out by pressing. The objective of this process is to separate the solid parts (i.e., fruit tissues) from the liquid to obtain the juice. The most important parameter during pressing is the liquid yield, which refers to the

percentage of juice extracted compared to the initial raw material. Juice yield largely depends on the type of pressing equipment used, as well as the quality and preparation of the raw material. The leftover by-product at the end of the process is known as pomace or marc.

Juice clarification

Extracted fruit juice typically appear cloudy due to the presence of insoluble plant particles like fibres, cellulose, hemicellulose, protopectin, starch and lipids, as well as colloidal macromolecules such as pectins, soluble starch fractions, proteins, certain polyphenols, and their oxidized or condensed forms. Depending on the desired final product, these components need to be partially or fully removed to prevent turbidity and sedimentation, thereby enhancing the juice's sensory qualities. Juice clarification can be achieved using physicochemical, mechanical techniques, or a combination of both approaches.

The first step in juice clarification involves eliminating protective colloids, as they can obstruct sedimentation and impact concentration stability, potentially leading to turbidity during storage. Enzymatic treatment is also vital for degrading pectin, ensuring the production of high-quality concentrates. For optimal results, it is crucial to completely break down pectin, as well as starch, hemicellulose and araban. The development of multifunctional enzymatic agents customized to suit specific fruit species, varieties and ripening stages, enhancing the overall quality of the juice products is of manufacturers' interest.

Physicochemical clarification is used after the decomposition of colloidal components and are essential for removing turbidity-causing substances from fruit juices. This method entails adding clarification agents that promote the precipitation of insoluble particles and macromolecules, which can then be separated using mechanical processes. This usually involves the addition of substances with charge and/or surface activity to the juice to be further clarified, in varying concentrations. Such substances include bentonite, silica sol, activated carbon or even gelatine.

Physicochemical clarification is typically followed by mechanical purification to eliminate suspended fibres and precipitation, usually performed in centrifuges or filters. The filtration process can be carried out by conventional filtration methods or by membrane filtration (e.g., ultrafiltration). Ultrafiltration offers the significant benefit of using membranes with carefully selected pore sizes that can selectively retain larger molecules (proteins, starch, pectin fragments), whilst smaller molecules, including dissolved sugars, acids and aromatic compounds, are allowed to pass through along with the solvent. This selective process enhances the quality and concentration of fruit juice by effectively separating undesirable components while preserving essential flavours and nutrients.

Further processing of the juice

Clarified, filtered or cloudy juices are now ready for preservation for later use. If the processing of the raw fruit does not immediately lead to beverage production, the juices are concentrated into semi-finished products. These products are later completed, sometimes at different production plants. The objective of juice concentration is to enhance the dry matter content while reducing water content, which helps to prolong shelf life and improves transportation and storage efficiency.

This process should be carried out with minimal loss of nutritionally important components and minimal impact on sensory attributes. Common methods for concentrating juice include evaporation, freeze concentration and membrane procedures like reverse osmosis. The extent of concentration is described by the ratio of the outlet concentration to the inlet concentration, known as the concentration ratio.

From all those mentioned above, we would underline evaporation as it is perhaps the most widely used concentration method. Due to the heat sensitivity of valuable juice components, it is important to utilize short-duration, low-temperature condensation techniques. To achieve a lower boiling point, this process is conducted under vacuum conditions with multiple effect evaporator systems, The process itself significantly impacts the product's compositional, thermal and rheological properties. Typically, evaporator systems are integrated with aroma recovery units, that are connected to the initial stages of evaporation to condense the most volatile aroma compounds. The condensed aromas are often reintroduced into the concentrate to enhance its aroma and flavour.

The resultant concentrates, with a soluble solid content of around 62-65%, are semi-finished product, normally stored in bag-in-drum or bag-in-box packaging until further use (Horváth-Kerkai and Stéger-Máté 2012; Pátkai 2012). The fruit concentrates can be used to make various fruit drinks such as juices, nectars and syrups. They are also highly sought-after ingredients in the bakery, confectionery and dairy industries, serving as natural sources of colour and sweetness (Pátkai 2012). The production of fruit juices relevant to the present research starts with the dilution of concentrate to normal juice concentration (10-20% brix) whilst heating the juice. In aseptic technology, this is followed by flavour correction and homogenisation. The process is completed by heat treatment, followed by filling and sealing.

3.4.2. Regulations and directives on fruit juices and similar products

Regulations of the European Community

In order to protect consumer interests, various regulations establish criteria related to the handling, processing and distribution of fruits and fruit products. As a member of the European Economic Community, Hungary is obliged to obliged to adapt its provisions. Regulation (EC) No 178/2002 of the European Parliament and of the Council describes the concept and principles of food law, risk analysis, and food safety requirements. According to the regulation, “the traceability of food, and any other substance intended to be, or expected to be, incorporated into a food or feed shall be established at all stages of production, processing, and distribution” (EC 2002). Commission Implementing Regulation (EU) No 543/2011 summarises the detailed rules applicable to the fruit and processed fruit sectors (EU 2011a).

The European Commission's Directive 2001/112/EC provides guidance on fruit juices and certain similar products intended for human consumption. The directive aims to specify requirements regarding the composition, reserved names, manufacturing characteristics, and labelling of fruit juices. It applies to fruit juice, fruit juice made from concentrate, concentrated fruit juice, dehydrated fruit juice powder and fruit nectar products (EC 2001). If the product is made from a single type of fruit, the name of that fruit must be used in place of the word “fruit”. For products

made from two or more types of fruit, except for the specific exception mentioned, the product name should be supplemented with a list of the fruits used, in descending order of the amount of fruit juice or puree used. However, for products made from three or more types of fruit, the names of the fruits can be replaced by the term “several fruits” or a similar expression, or by indicating the number of fruits used (EU 2015).

The directive specifies that in terms of permitted ingredients, fruit juice products must have the aroma, pulp, and cells reintroduced if they were removed during processing. In the case of fruit juice made from concentrate, materials extracted from the same type of fruit or even from other fruits of the same type may be reintroduced. The enzymes, flavourings and additives that can be used in the production of the product, as well as their concentration, are defined in regulations No 1332/2008 (EC 2008a), No 1334/2008 (EC 2008c), and No1333/2008 (EC 2008b) of the European Parliament and Council, respectively. According to the tables of permitted additives by food category in Commission Regulation (EU) No 1129/2011, the presence of food colour is not permitted in fresh and processed fruit products by virtue of the carry over principle (EU 2011b). The use of so-called “novel foods” in various food products is regulated by Regulation (EU) No 2015/2283 of the European Parliament and of the Council (FAO and WHO n.d.), and their specifications are provided in Commission Implementing Regulation (EU) No 2018/1023 (EU 2018).

Strict regulations regarding labelling are found in the directive, which are complemented by Regulation (EU) No 1169/2011 of the European Parliament and of the Council. The regulation details provisions on labelling, particularly concerning the accurate display of ingredients and the indication of allergens (EU 2011c).

Codex Alimentarius

The Codex Alimentarius Commission was established in 1963 as part of the food standardization program initiated by two United Nations specialized agencies: the Food and Agriculture Organization (FAO) and the World Health Organization (WHO). The purpose of the work carried out by the Codex Alimentarius organization is to develop internationally adopted food standards, guidelines and related documents (FAO and WHO n.d.).

According to Codex Alimentarius standard 247-2005, fruit juice is defined as a non-fermented, but fermentable liquid obtained from the edible part of healthy, properly ripened, and fresh fruit. The juice can also be extracted from fruit that has been kept in a healthy condition using appropriate post-harvest treatments, in line with the relevant regulations of the Codex Alimentarius Commission. The juice may appear cloudy or clear and can include recovered aromas and volatile flavour components extracted through appropriate physical methods, and these must come from the same type of fruit (FAO and WHO 2005).

The standard allows the addition of fruit pulp and cells obtained by suitable physical methods from the same fruit. The characteristic colour, aroma and taste of the juice or nectar must resemble that of the fruit from which it is made, and any residual water from processing must be minimal. Juice can only be obtained from a single fruit type, while mixed fruit juice is created by blending juices

or juices with purees from different fruit types. The standard distinguishes two methods of juice extraction, direct mechanical extraction, and reconstitution from concentrate using potable water. Technological aids such as clarifying agents, filtration aids, flocculating agents and enzyme preparations may be used, provided they stay within specified maximum limits. Fruit juices and nectars may undergo testing for authenticity, composition, and quality (FAO and WHO 2005).

The requirements specifically applicable in Hungary are defined by the Committee of Codex Alimentarius Hungaricus (MÉ) in alignment with above mentioned EU regulations. Specific provisions on fruit juices and certain similar products (i.e., fruit purées and nectars) intended for human consumption are laid down in Commission Regulation No 1-3-2001/112 (Magyar Élelmiszerkönyv Bizottság 2009). The MÉ directive No 2-601 provides guidance on the production of fruit products preserved by heat-treated, such as syrups, jams and fruit preserves, along with specific quality criteria. The latter refers to the fruit content, soluble solids (% brix), acidity (% m/m), and in certain cases, sand content (% m/m) (Magyar Élelmiszerkönyv Bizottság 2013). The guidelines regarding certain processed fruit products marked with distinctive quality label is specified in MÉ directive No 2-101. The directive establishes minimum requirements for fruit content, allowable sweeteners and additives for special quality jams and fruit syrups. It outlines specific standards that must be met to ensure the product's quality and authenticity (Magyar Élelmiszerkönyv Bizottság 2010).

3.4.3. The phenomena of food fraud

For fruits to reach our tables in the desired processed form and quality, they must undergo a complex journey. The well-known interlaced food supply chain is burdened with numerous hardly predictable problems and risks. This path includes stages such as harvesting, transportation, processing, packaging and distribution, each of which may introduce challenges that can impact the quality and safety of the final product. Nothing demonstrates the vulnerability of the food supply chain more clearly than its response to societal crises that test the resilience of the food chain, revealing the limitations in logistics, production, and distribution networks.

The issues or challenges that may occur in the food chain are well illustrated by the protection risk matrix. As highlighted in Table 2, a distinction can be made between intentional and unintentional acts, and according to whether the motive is economic gain or even environmental threat (Spink 2014; Spink and Moyer 2011). In the previous sub-chapters, certain aspects of food quality and safety, in particular of fruit, have been discussed in detail. Unfortunately, however, with the introduction of fruits into the food chain, the potential for food fraud should be also discussed.

Food fraud is a deliberate act with the almost sole purpose of economic gain that also includes economically motivated adulteration (EMA). As defined by the US Food and Drug Administration (FDA) EMA is the “fraudulent, intentional substitution or addition of a substance in a product for the purpose of increasing the apparent value of the product or reducing the cost of its production” (FDA 2009). As colourful as the food chain is, the quality and extent of fraud can vary. At any stage in the chain, there are many opportunities for fraud, including deception, substitution and counterfeiting (BRC, FDF, and SSA 2016).

Table 2. The food protection risk matrix (Spink and Moyer 2011).

Food quality	**Food fraud ***
Food safety	**Food defense**
Unintentional	Intentional

Action

Motivation
Economic gain

Harm
Public health, economic, or terror

* Includes the subcategory of economically motivated adulteration and food counterfeiting

Ever since mankind started producing food, food fraud has gone together with the production. Food adulteration hazards can be riskier than "traditional" food safety hazards because the contaminants are unknown and unconventional. Counterfeiters are not interested and/or do not have sufficient knowledge, expertise or resources to determine the extent to which product manipulation poses to consumers. Accordingly, a difference can be made between direct risk (e.g., toxic or allergenic contaminants), indirect risk in the case of long-term exposure (e.g., chronic diseases) and technical risk due to for example misleading product documentation. in addition, the concentration of beneficial compounds in food also reduces.

Spink and colleagues have carried out several investigations relating to scientific and media reports on food adulteration cases. Their observations show that the most frequent incidents since 1980 have been reported for olive oil, milk, honey, saffron, fruit juice (e.g., orange, apple) and coffee in the scholarly records; fish and seafood, honey, olive oil, spices (including chilli, black pepper, paprika, saffron, turmeric, etc.), milk, etc., in other records (Everstine, Spink, and Kennedy 2013; Moore, Spink, and Lipp 2012). In general, the following intentional fraudulent activities may occur in food production (Csapó, Albert, and Csapóné Kiss 2016):

- repackaging,
- misleading use of a protected designation of origin (PDO), protected geographical indication (PGI) or the adulteration of such product,
- traditionally produced "organic" product,
- selling imported products as domestic or local,
- incorrect and/or misleading indication of origin,
- use of unauthorised ingredients and/or manufacturing practices,
- use of raw materials of apparently poor quality or deteriorating quality,
- reuse of expired products in the manufacturing,
- marketing of product not meeting legal quality standards.

In addition to those mentioned above, specifically in relation to fresh fruits, there may be accelerated ripening (e.g., with Ca-carbide, oxytocin), pesticide (e.g., Cu-sulphate, chlorpyrifos, etc.) and metal contamination (e.g., Pb-arsenate). In the case of fruit products, dilution with water, pulp wash, or the addition of lower quality juices may occur. Besides, flavour enhancement (e.g., with sweeteners, acidity regulators), consistency improvement (e.g., with starch hydrolysates) and colour correction with natural or artificial colourants may be used to produce products with more

saleable organoleptic properties for consumers (Csapó et al. 2016; Dasenaki and Thomaidis 2019; Johnson 2014).

There are many reports in the literature of studies that aimed to determine and present the actual composition of foods as accurately as possible. This is particularly interesting in the quality assurance of products whose producer declares the presence of specific component(s) with beneficial effects at a certain concentration. There are several reasons why an ingredient containing beneficial compounds may be administered. Fruit processing, especially heat treatment, has a detectable effect on sensory and internal quality attributes (Toydemir et al. 2013). To compensate for this, manufacturers have the possibility to "feed back" the lost components, which are typically vitamins and flavourings (FAO and WHO 2005).

In addition to this, we would like to highlight another direction, fortification, when a product poor in certain components is supplemented and/or enriched with ingredients that are rich in the lacking component. The quality and quantity of such materials that can be admitted are normally defined in legislations. The natural fortification of fruit juices relevant for the present research can be achieved by the addition e.g., probiotic bacterial cultures (Naseem et al. 2023), super fruit juices, concentrates (Hasan et al. 2014), or even plant extracts (Furulyás et al. 2024; Ivanišová et al. 2015). The quantity of these must be indicated on the product packaging (EU 2011c).

3.5. Techniques used in the qualification of fresh fruits and their products

There are many different approaches in determining the quality of fruit for fresh consumption and processing, because of their compositional and structural diversity. In addition, the analytical methods can be quite specific to the fruit as well. In fruit production, processing, and product quality assessment, one can encounter empirical, targeted and non-targeted controlling methods.

3.5.1. Generally used indicators in fruit quality assurance

Classically, especially in orchards, the time of harvesting is typically determined and planned following empirical investigation. This may be done, for example, by comparing ripening fruit to different colour scales or by the force required to remove fruit from the stalk (Chełpiński, Ochmian, and Forczmański 2019; Kállay et al. 2007). Empirical methods can compromise the reproducibility of studies, leading to subjective decision-making. This may be mitigated by the use of small or large laboratory-based approaches and assays. For both fresh and processed fruit products, sweetness (SSC), acidity (TA, pH), colour and texture are among the most important measures of value (Li 2012). If these properties are mapped for fruit products not only in general terms, but also using compound-specific profiling, a much more accurate analytical image of the condition of the subject can be obtained.

The characteristic sugar, acid and polyphenol profiles of the fruit can be used to infer the progress of ripeness. This is also true of certain amino acids and esters (e.g., ethyl butanol, β, γ-butylene glycol), increased amounts of which indicate over-ripening and the initiation of spoilage processes. The amino acid and volatile profiles are an excellent way to detect dilution of fruit products, either with water, protein hydrolysates or by mixing in other fruit. Fruit products can be characterised not only by their characteristic components but also by their specific proportions. Thus, differences

in, for example, the ratio of L- and D-organic acids, total nitrogen-amino-nitrogen, free, L- and D-amino acids or isotopes can be revealing (Csapó et al. 2016; Johnson 2014).

The most commonly used methods allow targeted determination and quantification due to their reliability and sensitivity. Various DNA-based techniques, such as polymerase chain reaction (PCR), real-time PCR, etc., have proved to be effective for varietal and origin identification, similarly, stable isotope analysis with isotope ratio mass spectrometry (IRMS) or site-specific natural isotope fractionation-nuclear magnetic resonance (SNIF-NMR), and elemental analysis with inductively coupled plasma-mass spectrometry (ICP-MS). Separation techniques such as capillary electrophoresis, gas or liquid chromatography combined with MS can be applied to determine with high accuracy the organic acid, sugar, amino acid, and anthocyanin profiles along with their concentrations in the fruit products (Dasenaki and Thomaidis 2019; Kamiloglu 2019).

These analyses are characterised by the fact that they typically require sample preparation involving the destruction of the sample, that be time and financially expensive to obtain the also finite number of analytical results. In addition, the application of these analytical methods requires almost complete knowledge of the component(s) to be determined in the test samples. For this reason, unexpected quality differences may not be detected. The introduction and use of non-destructive, non-targeted correlative approaches as opposed to targeted determination is justified.

3.5.2. Recent trends in fruit quality assessment

Presentation of non-targeted NIR spectroscopy and hyperspectral imaging

The development of methods determining the conformity of foodstuffs, i.e., their quality and safety, is a key task for the scientific community, quality assurance and industry. Over the last 10-15 years or so, the development of non-targeted, also called “fingerprinting” methodologies based on the evaluation of broad analytical profiles, in place of the targeted ones, has become very much in the focus (Creydt and Fischer 2020). Analyses based on data captured using such approach allow patterns in the data to be rapidly mapped, supporting effective decision-making and intervention where needed in the food chain (Walsh, McGlone, and Han 2020). A very wide range of methods can be classified as non-targeted, the most important of which include various “-omics” disciplines (e.g., genomics, metabolomics, proteomics-based, etc.), chromatographic, spectrometric, spectroscopic and multisensorial techniques techniques (Aouadi et al. 2020; Esslinger, Riedl, and Fauhl-Hassek 2014). Together, results from targeted and non-targeted analyses can contribute to the formation of huge databases, whose multivariate statistical analysis provides the basis for trainable artificial intelligent solutions. Numerous scholarly articles and reviews available regarding how the mentioned analytical techniques performed in the quality assessment of fruit products, therefore, in the following, the methods that form an inseparable part of the doctoral research work presented are detailed.

Near infrared (NIR) spectroscopy belongs to vibrational spectroscopic techniques, and associated with Frederick William Herschel, who discovered the invisible absorption spectrum in the 1800s (Manley, Downey, and Baeten 2008). The agricultural implementation of the NIR technique was initiated in the 1950s by Karl Norris, an American engineer and researcher, through the

determination of grain moisture and protein content (Norris 1964, 1992; Williams and Norris 1987). The first promoter of the methodology in Hungary and its world-renowned pioneer was Professor Károly Kaffka (Salgó 2014). Besides agriculture, many other industries have discovered the benefits of its application, like the pharmaceutical, petrol, textile, and cosmetic industry (Manley 2014).

NIR spectroscopy fundamentally relies on illuminating the sample under study with light of wavelengths ranging from 780 to 2500 nm, which produces a response signal, alias spectrum, dependent on the material quality of the sample. When a sample, especially food, is illuminated with NIR light, the inter-atomic bonds of the molecular functional groups containing carbon, nitrogen, oxygen, and hydrogen are excited to such an extent that they result in broad and overlapping absorbance bands in the spectrum (Qu et al. 2015). By measuring absorbance, one can infer the approximate composition of the sample in the determined wavelength range without knowing the specific components. NIR instruments exist in various constructions, measurement arrangements, sizes. Some features of the commercially available NIR spectroscopic instruments are summarised in Table 3 (Manley et al. 2008):

Table 3. Features of commercially available NIR spectrometers

Instrument size:	**Illumination:**	**Sample presentation:**	**Type of detector:**
- benchtop, - portable, - hand-held.	- discrete, - full spectrum.	- diffuse reflectance, - transmittance, diffuse transmittance, - transflectance, - interactance.	- single channel, - multichannel.

The advantage of the NIR technique is that one can obtain comprehensive information about the examined sample in an intact manner without causing any damage. As a result of the extensive miniaturization of NIR instruments, investigations that had not been heard or thought before are now possible. Let's consider here online integrable devices or field studies even under extreme conditions (Beć, Grabska, and Huck 2022). The disadvantage of this approach is that it can only obtain mean spectral information from a relatively small investigated area at a time. However, combined with the vision system, not only non-destructive but also contactless measurements can be achieved. For the presented research, one of the important representatives is hyperspectral image processing.

According to Park and Lu (2015), the fundamental techniques for hyperspectral image processing are rooted in the optics, the digital signal processing dealing with one-dimensional time- and frequency-domain signals and the digital image processing dealing with multidimensional space- and space-time-domain signals such as images and videos. Hyperspectral imaging (HSI) is more than “conventional” spectroscopy in the sense that images contain spectral data by pixel, allowing for the simultaneous acquisition of localizable spatial and spectral information in a contactless

way. A HSI system typically records several hundreds of discrete wavelength data points at each image pixel.

The generated data is three-dimensional and combines information from x-y spatial and λ spectral coordinates (Manley 2014). Fundamentally, there are four approaches to recording the so-called hypercubes, and Figure 6 summarises how the different scanning systems build them up. Spectral scanning (also known as "staring" HSI) captures the data in a single wavelength at a time. The two primary spatial scanning methods are whiskbroom and pushbroom scanning. In the former case, system records the spectrum at a single point, while the latter records the spectral information in a complete line. Perhaps one of the most compact solution for hyperspectral imaging is snapshot (or single shot) HSI, that records spatial and spectral features in a single exposure (Wu and Sun 2013).

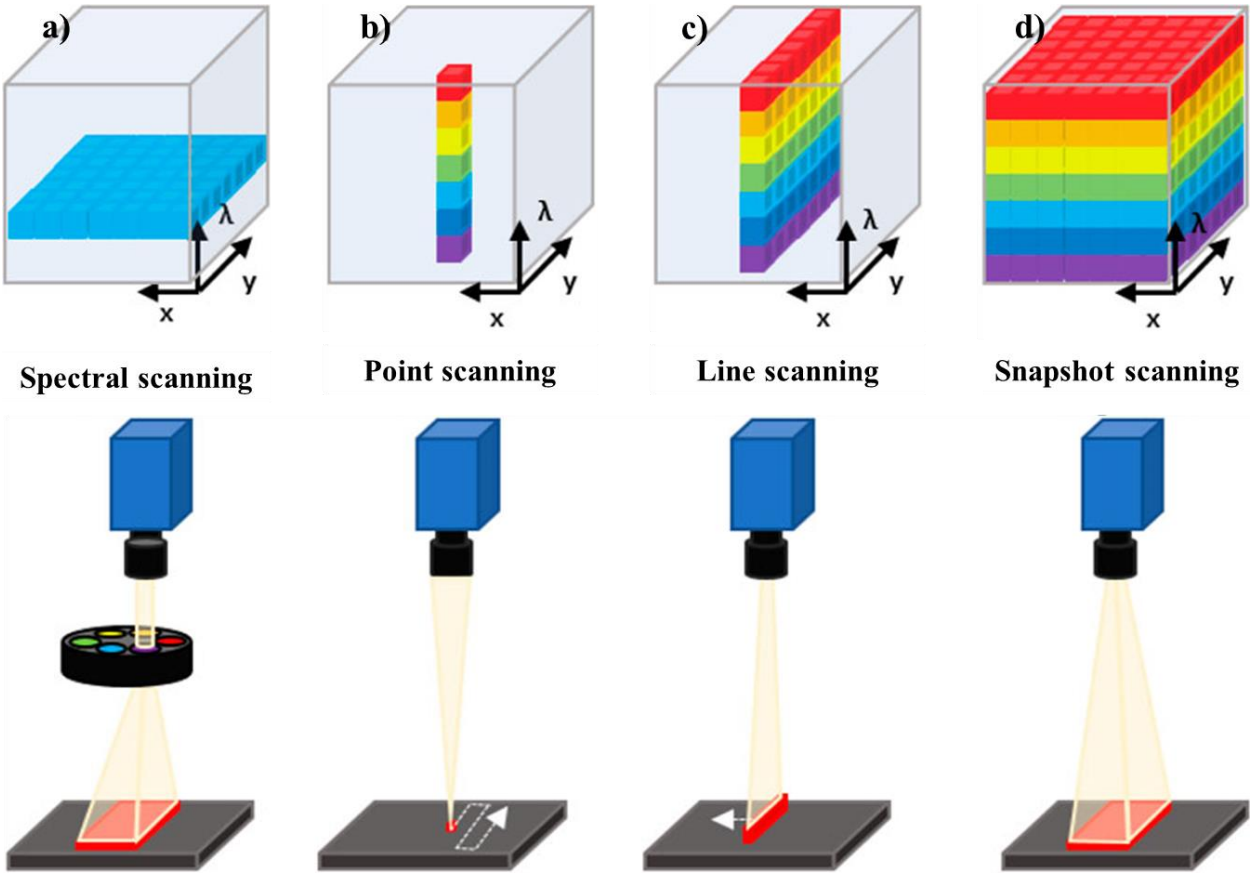

Figure 6. Schematic diagrams of hyperspectral data cube acquisition: Spectral scanning (a); Point scanning or wiskbroom imaging (b); Line scanning or pushbroom imaging (c); Snapshot imaging (d). Adapted from: (Wu et al. 2022).

Due to the recording specificities of the mentioned scanning approaches, each method presents different challenges. In case of spectral, point and line scanning, the records have to be combined afterwards. These methods are generally time-consuming and sensitive to positioning; therefore, their stable installation is essential. Nevertheless, the continuous scanning in one direction during line scanning, makes it particularly suitable in conveyor belt systems commonly used in the food industry. In terms of time efficiency, the performance of snapshot imaging is outstanding, making it an attractive choice for field studies when the hypercube needs to captured real-time, even at

video frame rates, crucial for fast decision making (Jung et al. 2019; Jung, Michels, and Rainer 2018). However, the technology is new enough that it presents limited spectral and spectral resolution (Femenias et al. 2022; Wu and Sun 2013).

Similar to those listed for NIR spectrometers, HSI systems are also available in different measurement designs. According to the position of the detector, the three main measurement arrangements are as reflectance, transmittance and interactance (Table 3). One of the beginning steps in hyperspectral image processing is to delimitate spatial locations to be analysed. This process typically starts with image segmentation with a thresholding operation on a spectral image band. The accurate determination of regions of interest (ROIs) in HSI is similar to correct sampling (Park and Lu 2015). Subsequently, HSI enables the visualisation of NIR light absorbing component distribution in heterogenous samples.

The spectra obtained through spectroscopy and hyperspectral imaging must first be subjected to various pre-processing steps in order to eliminate unwanted effects. Based on the preliminary inspection of the data, outliers can be removed, and the applicable spectrum pre-treatment methods can be defined. As extensively summarised and reviewed by (Geladi, Grahn, and Manley 2010; Zaukuu et al. 2022), supervised and unsupervised quality-based classifications and quantitative predictions can take place subsequently. Examples of the most commonly used spectral pre-processing and chemometric tools are listed in the following.

Pre-processing of the spectral data:

- smoothing,
- multiplicative scatter correction (msc),
- extended multiplicative scatter correction (emsc),
- normalisation,
- detrending (deTr),
- standard normal variate (snv),
- derivatives.

Qualitative analysis of the spectral data:

- principal component analysis (PCA),
- hierarchical cluster analysis (HCA),
- discriminant analysis (linear, quadratic, factorial),
- partial least squares discriminant analysis (PLS-DA),
- soft independent modelling of class analogies (SIMCA),
- support vector machine (SVM),
- artificial neural networks (ANNs),
- k-nearest neighbours (k-NN).

Quantitative analysis of the spectral data:

- multiple linear regression (MLR),
- principal component regression,
- partial least squares regression (PLSR).

Recent application of NIR spectroscopy and hyperspectral imaging in fruit quality assessment

NIR spectrum-based chemometric modelling is widely used in fruit quality assessment for various purposes (Cattaneo and Stellari 2019; Shah et al. 2020). Relating to stone fruits in focused of the present work, Li et al. (2018) examined the relationship between ripeness, SSC, and pH based on HSI images of 550 cherries in the 874-1734 nm region. The authors could classify the fruits according to ripeness with over 96% accuracy and estimated the two quality traits with coefficients of determination (R^2) above 0.8 using genetic algorithm-combined MLR. Escribano et al. (2017) associated DMC and SSC with the NIR spectra of cherries. The R^2 ranged between 0.67 to 0.73 for DMC, and 0.73 to 0.89 for SSC, respectively by variety. When evaluating fruit firmness beside SSC with HSI, Pullanagari and Li (2021) could predict the former attribute with an R^2 of 0.60 and RMSE of 0.38 N. Fodor et al. (2023) also conducted studies on the ripeness of plums and the predictability of certain internal characteristics. The classification models distinguished between mature and immature fruits with 100% accuracy in all cases. The DMC, SSC and TA regression models predicted with an RMSE of less than 0.7% m/m. In a series of experiments conducted on marian plums, Posom et al. (2020) concluded that the used wavelength range has a significant impact on the accuracy of the SSC, pH and TA models compared to the integration time.

When it comes to fruits intended for fresh consumption, it is important that their storage ensures the preservation of their quality. In fruits, qualitative changes can also be well monitored using NIR spectral patterns. Szabo et al. (2023) investigated the applicability of NIR spectroscopy to detect the effect of various storage conditions (packed as control or modified atmosphere; stored at 3 or 5 °C) on sour cherries of different varieties and perceived ripeness. SIMCA modelling discriminated samples with apparent error rates between 0 and 0.5 during prediction regardless of fruit maturity. Li et al. (2017) applied the NIR technique to predict firmness, flesh colour properties (L*, a*, b*), SSC, TA and pH in “Friar” plums. Based on their results, the flesh colour proved to be an important feature in post-ripening during low-temperature storage. Guo et al. (2022) employed various classification models (e.g., LDA, SVM, PLS, general LM) to determine storage time also for plums stored in cold environment.

In case of stored fruits, unfortunately, unwanted decay processes due to damage or microbial contamination must be taken into account in many cases. Screening out crops that are going bad is also important for food safety. NIR spectroscopy and hyperspectral image processing have been shown to be suitable for the detection of unwanted processes and components, the scheme of which is illustrated in Figure 7 using kernels as an example. Shao et al. (2019) combined Vis-NIR reflection spectroscopy and least square-support vector machine (LS-SVM) to sort intact, slightly, and severely damaged cherries with 93% classification accuracy. Zhao et al. (2016) could distinguish plums with browning flesh with 100% accuracy when combined NIR spectroscopy with back propagation-ANN. Castillo-Girones et al. (2024) evaluated the feasibility of spectral imaging and convolutional neural network for subsurface bruise detection in plums and achnieved almost 100% accuracy when classifying the bruised fruits with the highest impact energy of 0.50 J.

Using modelling based on hyperspectral data, Li et al. (2021) could classify bruising peaches with up to 100% accuracy at 12, 24, 36 and 48 hours after mechanical impact.

There is relatively limited source material available on the control of fungal infection in stone fruit. Therefore, Sun, Xiao, et al. (2018) developed a 360° rotating hyperspectral imaging system to detect *Rhizopus stolonifera* infection of different degrees on peaches. The detection accuracies of sound, slight-decayed, moderate-decayed and severe-decayed samples were 95, 66.29, 100 and 100%, respectively, when three single-band images were evaluated (709, 807, 874 nm). Sun, Wei, et al. (2018) also conducted experiments on peaches infected with *Botrytis cinerea*, *R. stolonifera* and *Colletotrichum acutatum*. The authors reported 82.5, 92.5 and 100% classification accuracies for slightly-decayed, moderately-decayed and severely-decayed samples, respectively, when combined hyperspectral image processing and deep belief network (DBN). NIR spectral detection of brown rot was first addressed by Liu et al. (2020), also for peaches. With HSI and PCA, the authors could completely distinguish samples according to the degree of infection (acceptable, moldy, highly moldy), and achieved R^2 of 0.84 and RMSE of 0.78 when predicting fungal colony counts. Vitalis et al. (2021a, 2021b) examined the effects of ambient and refrigerated storage on NIR spectral properties of plums infected with *M. fructigena* mycelium in different ways. Based on their results, the authors could indisputably detect samples that did not yet show visible signs of infection.

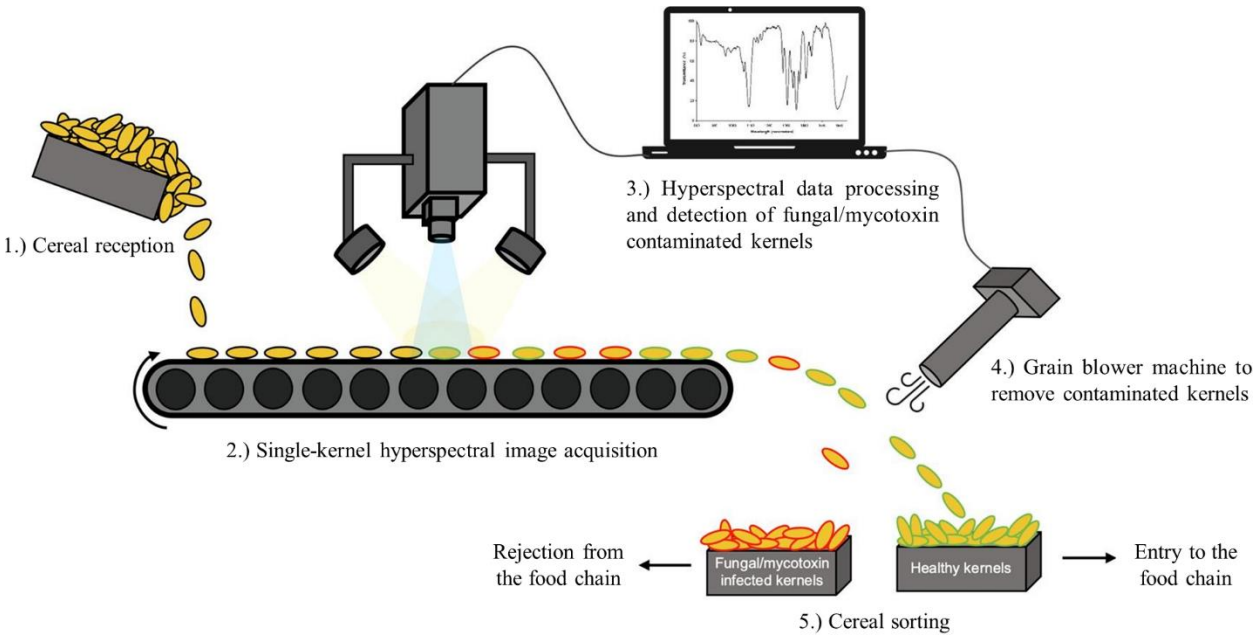

Figure 7. Hyperspectral imaging for the classification of individual cereal kernels according to fungal and mycotoxins contamination (graphical abstract by Femenias et al. (2022)).

For fruit products, NIR spectroscopy has a very important role in determining and controlling authenticity and quality, which also has a large literature. Relating to fresh fruit product control, Siedliska et al. (2017) applied various HSI-based algorithms to detect sour cherry pits and/or fragments in transmittance measurement arrangement.

The majority of frauds affecting fruit juices can be associated with apple, orange, and pomegranate juices, the latter being considered superfood due to its very valuable nutritional composition. Aykas and Rodriguez-Saona (2024) assessed fruit juices purchased from US stores in their research. The authors involved 28 single and 40 blended juices in their study, and simultaneously estimated their SSC, sucrose, glucose, fructose, total sugars, TA, citric and ascorbic acid content with high correlation ($R_{cv}^2 > 0.93$). Aykac, Cavdaroglu, and Ozen (2023) have conducted research regarding the dilution of pomegranate juices when binary and ternary blends were prepared with 5-10% doses of sour cherry and black carrot juices. After pre-processing the spectra, PLS-DA and OPLS-DA always resulted in 100% calibration and 97% validation accuracies. Cassani et al. (2018) developed Fourier transform (FT) mid infrared-based PLS models for the simultaneous prediction of simple sugars and exogenously added fructooligosaccharides in strawberry juices preserved with non-thermal treatment (geraniol or vanillin+ultrasound) up to 14 days. The authors obtained predictive models with R^2 higher than 0.97. Vitalis et al. (2023) have preliminary results regarding the probiotic enrichment of fruit juice blends, demonstrating that the simple and mixed bacterial cultures could be well distinguished, as well as the fermentation time and acidity could be predicted with high accuracy.

The literature reviewed on changes during cherry and plum ripening, storage, and on the qualification of processed fruit products reports a wide range of analytical approaches that can be applied to determine the physiological state (e.g., ripeness, decay), quality (e.g., physical, chemical, biological traits) and authenticity of fruits and fruit products. Chemometric modelling results based on NIR- and hyperspectral analyses, which are the focus of this thesis, report a particularly high accuracy in predicting fruit ripeness through their certain physical and chemical quality characteristics (e.g., firmness, SSC, TA, etc.). Similarly, studies on storage monitoring and juice composition in general. Nevertheless, it was found that there is little literature discussing the impact of maturity stage and the location of spectrum acquisition on the accuracy of the modelling. There is almost no available literature on the spectral monitoring of sour cherry and plum postharvest worsen by *Monilinia* contamination. There are also relatively few literature sources available regarding the control of fruit juice enrichment with plant derivatives. Overall, these substantiated the formulated research objectives.

4. MATERIALS AND METHODS

This chapter details the materials and methods employed throughout the series of experiments involved in the thesis.

4.1. Materials

4.1.1. Fruit samples analysed during the ripeness assessment studies

The non-destructive determination of ripeness, and thus the optimal harvest time of various stone fruits was carried out by analysing fruit samples from Szabolcs-Szatmár-Bereg county. During the summer months of 2021, seasonal sweet cherries, sour cherries and plums were examined. According to the ripening period of the fruits, the harvesting took place in June, July and August. Harvesting was done in two distinct phases, one week apart per fruit species. After each harvest, the fruits were promptly transported to the to the Institute of Food Science and Technology (IFST), Hungarian University of Agriculture and Life Sciences (MATE).

The incoming batches exhibited significant variability; their ripeness ranged from unsuitable for consumption to fully ripe. After sample arrival, the stem removal and sorting of the fruit was started as soon as possible to avoid any undesirable perishing processes. The preliminary classification of the fruits according to their presumed ripeness was based on the overall visible colour shade differences, varying from the very green to deep red or purple. The sample sets into which a relatively large number of fruits were initially sorted were further divided into subsets.

Table 4 summarises the total number of pre-classified sample sets per fruit variety obtained with the assistance of the experts of the Department of Food Chemistry and Analysis (Institute of Food Science and Technology, MATE). To facilitate the interpretation of research outcomes, the pre-classified sample sets were then grouped into larger ripeness clusters. This was necessary subsequently, because there were pre-classified sample groups with overlapping ripeness levels but harvested at different dates. The possible uses of the defined ripeness levels based on experts' opinion are shown Table 5.

Table 4. The quantity of fruits pre-classified prior ripeness assessment by variety**.**

Fruit	Variety	Abbreviation	Pre-classified groups	Sample size of NIRS
Sweet cherries	Bigarreau Burlat	BB	26	130
	Valery Chkalov	VC	21	105
Sour cherries	Kántorjánosi	KJ	20	100
	Újfehértói	UF	21	105
Plums	Elena	EL	20	100
	Stanley	ST	20	100

Table 19 summarises how many actual pre-classified sample sets cover the ripeness levels established between the L1 (immature) and L6 (very ripe) categories. When determining the boundaries between the maturity levels, the experts aimed for an equal distribution.for each fruit specie. The shading used in the table shows the colour by which clusters were marked during the

data analysis. From the pre-selected sample sets, 5 fruits were started to be analysed using non-destructive analytical methods (see Table 4), and the rest were analysed using destructive analytical methods.

Table 5. The ripeness levels and usability of the fruits analysed.

Ripeness level	Ripeness stage	Utilisation
L1	fully unripe	no use
L2	slight colouration	no use
L3	intensive maturation	production of preserves
L4	ripe	production pf fresh/ frozen/ juice/ concentrate/ jam
L5	fully ripe	production pf fresh/ frozen/ juice/ concentrate/ jam
L6	very ripe/ overripe	variable use

4.1.2. Fruit samples analysed during the *Monilinia* detection studies

Fruit sampling

For the non-destructive study of the processes involved in brown rot of stone fruits, different sour cherry and plum varieties were included in the research. The harvest and examination of the fruit varieties were conducted at different times. The experiments on "Érdi bőtermő" (EB) and "Újfehértói" (UF) sour cherries, as well as "Topend" (TD) plums, were conducted in 2021. The experiments on "Topend plus" (TP) plums were carried out in 2022. The pre-selected experimental fruits were uniform in ripeness, colour, and free from any visible damage for each variety.

Process of *Monilinia* isolation

Isolation of *Monilinia* species causing brown rot was performed from the surface of various fruits (e.g., sour cherry, plum). After several attempts, it was possible to successfully isolate and propagate *M. fructigena* on culture media. The fruits intended for conidium production were disinfected with ethanol solution (70% V/V), wounded using a sterile lancet needle, and agar discs overgrown with mycelium from a pure pathogen culture were placed into the wounds. To produce conidia, sour cherries were inoculated for the sour cherry experiment in 2021, plums for the plum experiment in 2021, and apples for the plum experiment in 2022. This step was necessary because *Monilinia* species do not produce conidia on culture media. The inoculated fruits were stored in a Fitotron growth chamber on 21°C with a 12-hour light cycle. After approximately seven days, conidia formed on the surface of the inoculated fruits were collected using sterile wooden sticks moistened with sterile water, then transferred into 2 mL Eppendorf tubes containing sterile water (Figure 8).

The conidial suspensions were adjusted to a concentration of approximately 10^5 conidium/ mL using a Bürker counting chamber. This was followed by tenfold, hundredfold, and thousandfold serial dilutions with sterile water. These suspensions were subsequently used to inoculate the sour cherry and plum samples involved in the latter studies. The approximate concentrations of the conidial suspensions used in each experiment are shown in (Table 7). The isolation of the fungi

and the preparation of conidial suspensions were conducted under the supervision of experts from the Institute of Plant Protection (MATE), in accordance with Horváthné Petróczy (2009).

a) b) c)

Figure 8. Preparation steps for *M. fructigena* conidial suspension: propagation of fungal isolates (a); conidium formation on the surface of fruits (b); collection of fungal conidia (c).

Infection of the fruit samples

Before starting the sample actual preparation, the stems of the sour cherries and plums were removed and their surface was gently cleaned with precision wipes soaked in ethanol solution (70% V/V). This step was necessary because in these series of experiments, we focused solely on the detectability of *Monilinia* and aimed to minimize any potential spoilage processes caused by unwanted other microbes.

After cleaning, a 5 mm incision was made with the tip of a disinfected knife on the surface of a portion of the fruits into which 20 μL of undiluted (~10^2 conidium/ μL) or diluted *M. fructigena* conidial suspension was pipetted (Table 7). These fruits constituted the "$Injury_{inf}$" samples. For another portion of the fruits, 20 μL of the suspensions was applied without making any incisions, constituting the "$Intact_{inf}$" samples. The remaining fruits were not inoculated, serving as the "$Intact_{con}$" and "$Injury_{con}$" samples, the latter was prepared only for *Topend plus* plums.

The prepared fruits were subjected to seven days of refrigerated (around 5 °C) or room temperature (above 20 °C) storage under controlled conditions. In the case of room temperature storage, the storage environment was adjusted to the room temperature typical at the time of fruit preparation. The average temperature and relative humidity values recorded during storage are included in Table 6.

Table 6. Temperature and relative humidity recorded during the storage of stone fruits (average ± 2 σ).

Fruit	variety	Refrigerated storage		Room temperature storage	
		Temperature	Humidity	Temperature	Humidity
Sour cherries	Érdi bőtermő	4.34 ± 1.99 °C	62.64 ± 12.94%	25.94 ± 1.66 °C	81.04 ± 10.09%
	Újfehértói	5.64 ± 1.89 °C	59.32 ± 9.33%	25.83 ± 0.15 °C	84.85 ± 4.64%
Plums	Topend	5.97 ± 2.89 °C	52.36 ± 22.43%	22.26 ± 0.86°C	75.92 ± 16.58%
	Topend plus	5.41 ± 1.54 °C	73.46 ± 18.46%	22.64 ± 1.01 °C	83.87 ± 13.38%

The decaying processes were investigated using two distinct non-destructive analytical techniques, NIR spectroscopy and hyperspectral imaging, for which two identically prepared sample sets were established. For each sample group, five replicates were prepared, resulting in the following sample sizes:

- **Sour cherry varieties:**
  Érdi bőtermő (EB)
  $((Intact_{con} + 4\ Injury_{inf} + 4\ Intact_{inf}) \times 2$ storage conditions$) \times 5$ replicates =
  90 sour cherry samples
  Újfehértói (UF)
  $((Intact_{con} + 4\ Injury_{inf} + 4\ Intact_{inf}) \times 2$ storage conditions$) \times 5$ replicates =
  90 sour cherry samples
- **Plum varieties:**
  Topend (TD)
  $((Intact_{con} + 3\ Injury_{inf} + 3\ Intact_{inf}) \times 2$ storage conditions$) \times 5$ replicates =
  70 plum samples
  Topend plus (TP)
  $((Intact_{con} + Injury_{con} + 3\ Injury_{inf} + 3\ Intact_{inf}) \times 2$ storage conditions$) \times 5$ replicates =
  80 plum samples

Table 7. Sample groups for investigating the detectability of *M. fructigena* on stone fruits

Fruit	**Variety**	**Suspension concentration** (conidium/ µL)	**Injured**		**Intact**	
			~ 5 °C	**~ 20 °C**	**~ 5 °C**	**~ 20 °C**
Sour cherry	**Érdi bőtermő** EB	0	—	—	5	5
		~ 0,15	5	5	5	5
		~ 1,5	5	5	5	5
		~ 15	5	5	5	5
		~ 150	5	5	5	5
	Újfehértói UF	0	—	—	5	5
		~ 0,17	5	5	5	5
		~ 1,7	5	5	5	5
		~ 17	5	5	5	5
		~ 170	5	5	5	5
Plum	**Topend** TD	0	—	—	5	5
		~ 1,05	5	5	5	5
		~ 10,5	5	5	5	5
		~ 105	5	5	5	5
	Topend plus TP	0	5	5	5	5
		~ 2,31	5	5	5	5
		~ 23,1	5	5	5	5
		~ 231	5	5	5	5

— – no sample preparation

4.1.3. Samples analysed during the fruit juice enrichment studies

Preparation of fruit juice mixtures

For these experiments, juices prepared from sour cherry and plum concentrates were analysed to minimise the risk of unwanted and unknown product manipulation in our samples. Based on the initial concentration of fruit juice concentrates (approx. 65% brix), pure stock juices were prepared of about 20% brix in SSC by dilution with distilled water. Cranberry (CBE), grape seed (GSE) or pomegranate extracts (PGE) were added to the juices at six concentration levels so that their total concentration ranged between 0.5 and 2.5 g/100 mL. These formed the simple blends, which were then mixed in equal proportions by concentration level to produce binary and ternary juice blends. In these cases, the aim was also to ensure that the total extract content of the resulting juice blends remained between 0.5 and 2.5 g/100 mL (Table 20). For easier understanding, the blending procedure has been partly illustrated in Figure 9.

During the preparation of the fruit juice blends, three parallel juice samples were prepared per sample group. For the pure sour cherry and plum juices five replicate samples were prepared. These samples represented the 0 g/100 mL concentration level. The sample sizes for each fruit juice were as follows (Eq. 1, 2):

(5 pure juices) + (3 extracts × 6 conc. level × 3 replicates) + (3 binary mixtures × 6 conc. level × 3 replicates) + (1 tertiary mixtures × 6 conc. level × 3 replicates) = **131 blends of sour cherry juice** (1)

(5 pure juices) + (3 extracts × 6 conc. level × 3 replicates) + (3 binary mixtures × 6 conc. level × 3 replicates) + (1 tertiary mixtures × 6 conc. level × 3 replicates) = **131 blends of plum juice** (2)

Heat treatment of the fruit juice blends

The prepared fruit juice samples were pipetted into 15 mL autoclavable centrifuge tubes, closed and subjected to heat treatment. For this, a drying chamber was preheated to 85 °C (MMM Medcenter Einrichtungen GmbH, Planegg, Germany). A "blank" 15 mL centrifuge tube, containing stock juice equilibrated to the same temperature as the experimental samples (e.g., room temperature), was prepared; this liquid was not used in subsequent analyses. A hole was drilled in the centre of a centrifuge tube cap, large enough to accommodate a Pt100 thermometer (Fluke Corporation, Everett, Washington, USA). The cap was then attached to the thermometer, ensuring that the tip of the thermometer was centred within the tube. The sample tubes, along with the blank sample tube, were placed into a holder and positioned within the drying chamber, with the thermometer display remaining outside for temperature monitoring. Once the thermometer indicated 85 °C - reflecting the temperature at the cold point of the blank tube - the samples were held for 60 seconds at constant temperature. Subsequently, the samples were removed from the chamber, allowed to cool to room temperature, and were refrigerated until non-destructive analytical methods.

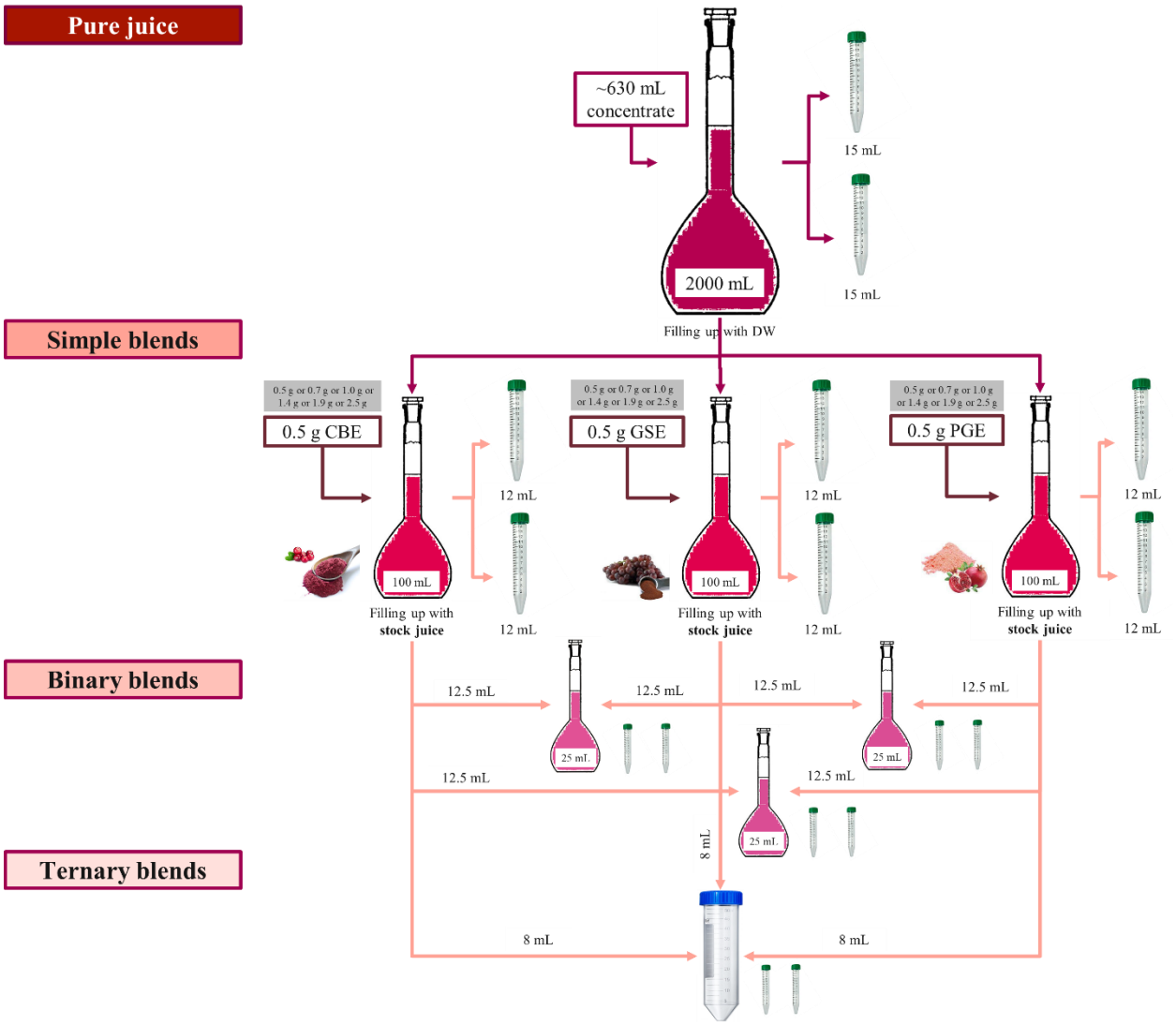

Figure 9. Excerpt from the blending scheme of fruit juices containing different concentrations of various plant extracts.

4.2. Applied methods

This subsection summarises the reference methods used in the ripeness assessment studies as well as the non-destructive correlative analytical methods and chemometric modelling used in the determination of fruit ripeness, detection of *Monilinia* and fruit juice enrichment.

4.2.1. Reference methods applied in the fruit ripeness assessment studies

The reference methods used in the examination of stone fruit of different ripeness were performed separately for each pre-classified sample sets (see Table 19). An example of a selected sample set is shown in Figure 10 to illustrate how the measuring processes followed each other, and the sample amounts required. The colour measurement was done by fruit, analytical measurement was done by pre-classified sample group at the Department of Food Chemistry and Analysis (MATE IFST).

Determination of colour characteristics of stone fruits

The colour characteristics of stone fruits of varying ripeness were determined using a ColorLite sph850 spectrophotometer (ColorLite GmbH, Germany). Following calibration, the instrument was used to measure the colour attributes, such as lightness (L*), green-red (a*), and blue-yellow (b*), on both the immature and mature sides of the fruits. All five parallel samples of the pre-classified sample groups were measured respectively in a randomised measurement order. Three consecutive measurements were taken for each colour attribute. The averages of these measurements were used in the subsequent data analysis.

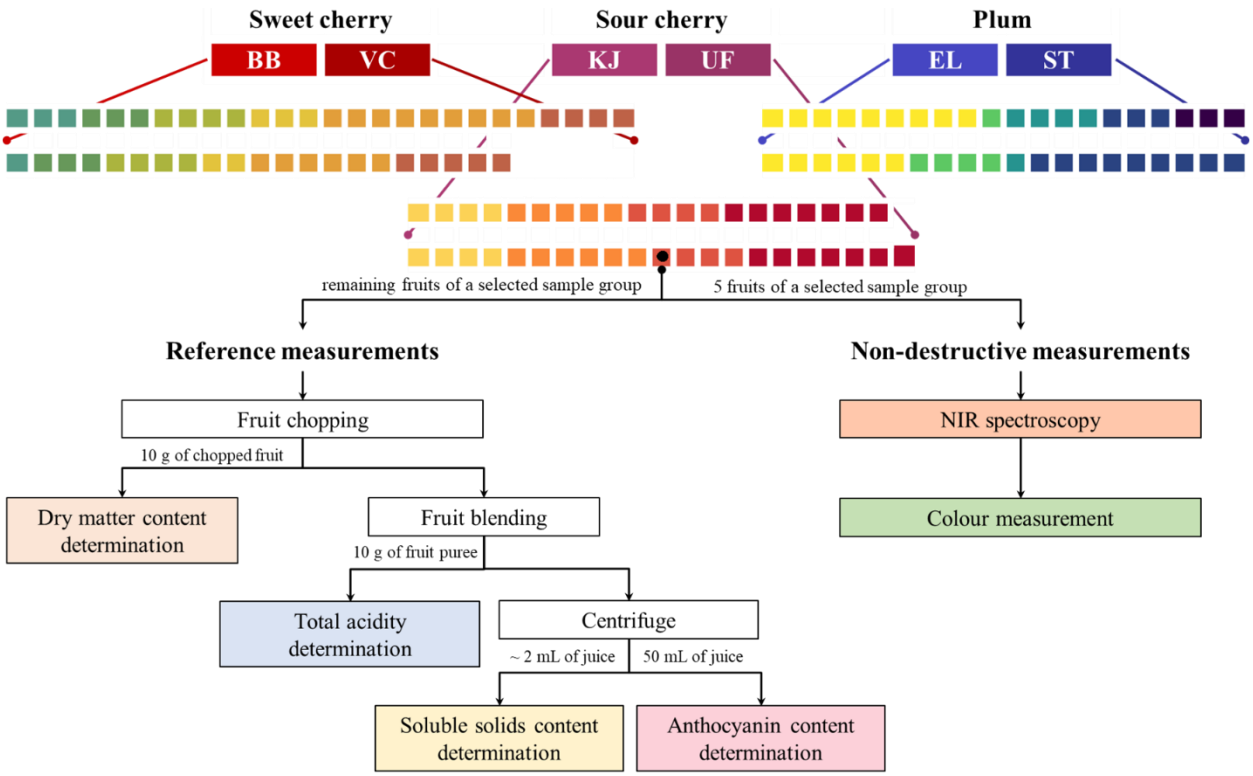

Figure 10. Destructive and non-destructive analytical analyses performed separately for pre-classified sample groups per fruit variety, presented on a case example.

Determination of dry matter content of stone fruits

To determine the dry matter content (DMC) of stone fruits of varying ripeness, the flesh of the fruits was chopped by pre-classified sample sets. Approximately 10 g of chopped fruits were measured in and gently dried at 70 °C in an air-conditioned airing cupboard (Memmert, Schwabach, Germany) to constant weight. Due to the high sugar content of the samples, gentle drying was necessary to avoid damaging them. The dry matter content was calculated as the ratio of the dry weight to the initial weight (Schuck, Dolivet, and Jeantet 2012). Three measurements were conducted for each sample group, respectively, and the averages of these were used for subsequent data analysis.

Determination of total acidity of stone fruits

To determine the total acidity (TA) of stone fruits of varying ripeness, the previously chopped fruits were pureed with a kitchen stick blender (Philips, Amsterdam, Netherlands). Approximately

10 g of fruit puree was measured in and the acid concent was determined by potentiometric titration with 0.1 mol/ dm³ sodium hydroxide solution (pH 8.2) in the presence of phenolphthalein indicator. During the measurement, a Hanna HI2209 benchtop pH meter was utilised (Hanna Instruments, Smithfield, USA). The total acidity was calculated and expressed as mg/ g (fresh weight) malic acid (Tyl and Sadler 2017). Three measurements were conducted for each pre-classified sample group, respectively, and the averages of these were used in the subsequent data analysis.

Determination of total soluble solid content of stone fruits

To determine the total soluble solid content (SSC) of stone fruits of varying ripeness, the previously blended fruits were measured in a tube of 50 mL, centrifuged at 6000 rpm for 20 min (Micro 22R Hettich, Germany), and a few drops of the supernatant juice were measured with a digital refractometer (Pocket PAL-1, ATAGO, Tokyo, Japan). Following calibration with distilled water, the device provided results of fruit juice soluble solid content expressed in % brix (Chockchaisawasdee et al. 2016). Three measurements were conducted for each pre-classified sample group, respectively, and the averages of these was used in the subsequent data analysis.

Determination total anthocyanin content of stone fruits

To determine total anthocyanin content (TAC) of stone fruits of different ripeness, the previously prepared supernatant juice was measured in and analysed using the pH differential method (Lao and Giusti 2016; Lee et al. 2005, 2016), as described in the studies by Fodor et al. (2022, 2023). These measurements required the use of a pH meter (Hanna Instruments, Smithfield, USA) and UV-Vis spectrophotometer (Thermo Electronic UV-Vis 2.02, Thermo Fisher Scientific, Waltham, MA, USA). The results were expressed in cyanidin-3-glucoside equivalent in mg/ L. Three measurements were performed for each pre-classified sample group, and the averages of these measurements was used in the subsequent data analysis.

4.2.2. Near infrared spectroscopy for the fruit quality assessment studies

Application of hand-held NIR spectrometer for the determination of stone fruit ripeness

To non-destructively model the harvest maturity of various stone fruits, near-infrared (NIR) spectroscopy was applied. The investigations were conducted with a hand-held reflection-based NIR spectrometer (NIR-S-G1, InnoSpectra Co., Hsinchu, Taiwan). The device enables contact measurement with internal illumination in a total of 256 spectral bands in the 900-1700 nm wavelength range using the Hadamard method. For the fruits, spectra were recorded on both the immature and mature sides of the five parallel samples of the pre-classified sample sets. At each measurement position, three consecutive spectrum recording was performed. The fruits were scanned in a randomised measurement order.

In the presentation of the results obtained from the chemometric modelling, the sun-yellow (–) colour indicates the models that were based on the whole dataset for each variety, respectively. In green (–) and index “g” is used after the abbreviation of the variety to indicate the model results based on the spectra recorded on the immature side of the fruit. Modelling results based on spectra

recorded on the mature side of the fruit are indicated in burgundy (–) in the case of cherries or in navy blue (–) in the case of plums, and index "r" is used after the abbreviation of the variety.

Application of hand-held NIR spectrometer for the detection of *Monilinia* on stone fruits

The hand-held NIR instrument and setup used for the non-destructive analysis of sour cherries and plums infected with *M. fructigena* and stored under different conditions were consistent with the configuration described above. On sour cherries, spectra were recorded along the horizontal axis of the fruits; on plums, they were captured along the vertical axis, with three measurement points per fruit, as indicated in Figure 11a. The second measurement point was always the point of inoculation on the fruit. At each measurement position, three consecutive spectrum recording was performed. After each measurement position, the contact surface of the device was disinfected with alcohol-soaked precision wipes to prevent cross-contamination. Spectral data collection was performed daily throughout the seven-day long storage. The fruits were scanned in a randomised measurement order.

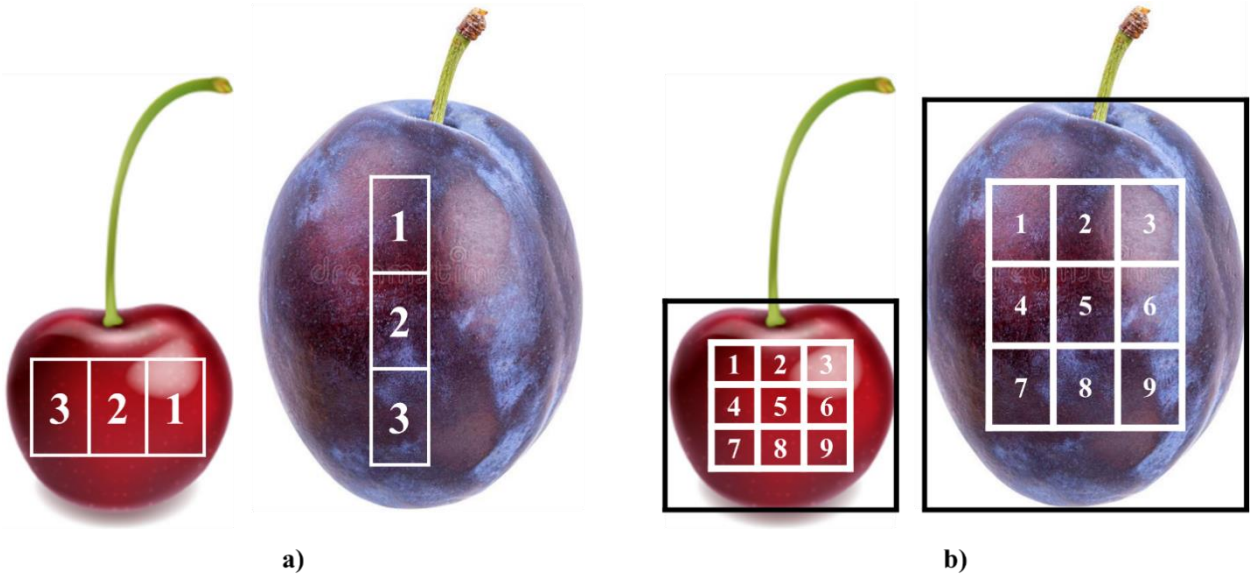

Figure 11. Spectral measurement locations for detecting *M. fructigena* on stone fruits: measurement points for hand-held NIR spectrometer (a); spectral acquisition points during hyperspectral image processing (b).

Application of hand-held NIR spectrometer for the control of enriched fruit juices

For the examination of plant extract-enriched fruit juice blends, a hand-held MicroNIR spectrometer (Viavi, Scottsdale, USA) was employed in transflectance measurement arrangement. The device enables contact measurement with internal illumination in a total of 125 spectral bands in the 900-1700 nm wavelength range. The spectra of the juices were recorded in a cylindrical glass cuvette with a reflective surface that provided a layer thickness of 0.5 mm. To compensate the initially large number of fruit juice blends, the pure fruit juices were scanned multiple times. Specifically, the five replicate samples of sour cherry and plum juice were each scanned three times in total. Three consecutive spectra were recorded during each sample loading. Between each sample measurement, the cuvette was thoroughly cleaned with distilled water and ethanol (70% V/V), then dried and rinsed with the upcoming juice sample to prevent cross-contamination.

The juices were scanned in a randomized measurement order. These measurements were conducted at the Institute of Analytical Chemistry and Radiochemistry (University of Innsbruck, Austria).

Application of benchtop NIR spectrometer for the control of enriched fruit juices

The spectral properties of the fruit juices were also examined in a transmission measurement arrangement. A modular Fourier transform spectrometer was utilized for this purpose (NIRFlex N-500, Büchi Labortechnik AG, Flawil, Switzerland), acquiring data in a total of 1178 spectral bands within the wavelength range of 1000-1890 nm. Similarly, as detailed above, the samples were analysed in a randomized order with three consecutive scanning using a glass cuvette with a path length of 1 mm. The cuvette was cleaned as described above with additional drying with compressed purified air to remove as much of the excess cleaning moisture from the cuvette as possible. The cuvette was also rinsed with the upcoming juice sample. These measurements were conducted at the Institute of Analytical Chemistry and Radiochemistry (University of Innsbruck, Austria).

4.2.3. Hyperspectral imaging for the detection of *Monilinia* contamination on stone fruits

For the non-destructive and contactless analysis of sour cherries and plums infected with *M. fructigena* and stored under various conditions, a desktop Headwall Photonics XEVA-1648 XC134 hyperspectral imaging (HSI) system was utilised (Specim spectrograph, Xenics InGaAs 14-bit sensor, 256 × 320 px spectral and spatial resolution). This system allowed the NIR spectral and spatial characterization of fruits at the same time. The instrument operated in a push-broom configuration, capturing a total of 155 spectral bands in the 900-1700 nm wavelength range, with a spectral resolution of 5 nm and a spatial resolution of 0.475 mm per pixel. The measuring system was operated using the department-developed Argus software (Firtha 2011). Randomised HSI was performed daily on the plum samples and on six days in total for the sour cherry samples during their seven-day long storage.

To compensate spectral inconsistencies, on every measurement day, the system's spectral and spatial calibration preceded the measurements. Under full illumination of lamps (~79 mm linear tungsten halogen bulbs, 150 W) positioned on two sides in 45° angle with the moving platform, a white teflon (PTFE) standard (NCS 0300) was used for the light reference scanning. The measurement of the dark surface was done by scanning after completely covering optics preventing any external light from entering the system. The data matrix measured at this time was considered homogeneous and stable over time based on previous experiences. After correctly setting the measurement arrangement, illumination, optical aperture, and AD parameters, saving dark and light reference images could eliminate inhomogeneity and increase the signal level (Firtha, 2008), also enabling the calculation of relative reflectance from the raw data.

The segmentation of fruit-related pixels from the data recorded in a hypercube with the HSI system was performed using a department-developed HyperGrab hyperspectral image processing software (GillaySoft, Budapest, Hungary). The software allowed to extract the average absorbance values from nine surface areas per measurement at a time as illustrated in Figure 11b. Examples

of the defined region of interests (ROI) during the segmentation are provided in Figure 60 and Figure 61.

4.3. Evaluation of the research results

The organization, evaluation, and illustration of the data were performed using Miscrosoft Excel 365 (Microsoft Corporation, Redmond, Washington, USA), Origin Pro 2018 (OriginLab Corp. Northampton, MA, USA), R-project (version 3.6.3) and the "aquap2" package (Pollner and Kovacs 2016). This section summarises the methods used to evaluate the study results.

4.3.1. Evaluation of results obtained with reference measurements

Reference measurements are only available on the samples analysed during the ripeness determination studies. The colour (L*, a*, b*) and compositional characteristics (i.e., DMC, SSC, TA, TAC) obtained from the pre-classified sample sets were averaged according to ripeness clusters shown in Table 5 and Table 19. These average values are discussed in chapter RESULTS AND DISCUSSION.

4.3.2. Evaluation of results obtained using correlative analytical methods

Pre-processing of the spectral data

The spectra obtained through NIR spectroscopy and hyperspectral image processing were first truncated to the wavelength ranges intended for evaluation, followed by the removal of outliers and subsequent multivariate statistical analyses. In experiments where the efficiency of different instruments was compared (e.g., benchtop and hand-held NIR devices), the evaluations were performed within the same wavelength ranges. The number of spectra used as a basis for chemometric modelling in the three different studies and the considered wavelength ranges are summarised in Table 8. In neither case were the spectra averaged.

Table 8. Spectrum counts and wavelength ranges used during chemometric modelling.

Study	Variety	Hand-held device(s)	Benchtop device(s) *	Wavelength range
Ripeness assessment				
Sweet cherries	BB	780 spectra	–	950 – 1650 nm
	VC	627 spectra	–	950 – 1650 nm
Sour cherries	KJ	597 spectra	–	950 – 1650 nm
	UF	621 spectra	–	950 – 1650 nm
Plums	EL	600 spectra	–	950 – 1650 nm
	ST	597 spectra	–	950 – 1650 nm
***Monilinia* detecion**				
Sour cherries	EB	4421 spectra	3579 spectra	1000 – 1650 nm
	UF	5022 spectra	3224 spectra	1000 – 1650 nm
Plums	TD	3872 spectra	3084 spectra	1000 – 1650 nm
	TP	4294 spectra	3462 spectra	1000 – 1650 nm
Fruit juice control				
Sour cherry juices	–	423 spectra	421 spectra	1000 – 1650 nm
Plum juices	–	423 spectra	422 spectra	1000 – 1650 nm

* By benchtop device is meant here the hyperspectral imaging system in *Monilinia* detection studies or the FT-NIR spectrometer in fruit juice analysis.

For noise reduction in the spectra, Savitzky-Golay smoothing (second-order polynomial) was applied (Savitzky and Golay 1951), along with other spectral pre-processing methods (e.g., scatter correction, detrending, derivatives) to optimise statistical modelling. The combinations of spectral pre-processing methods and their application purposes are summarised in Table 21 and Table 22. Table 9. summarises all the variables according to which it was possible to filter the data or build classification models.

Principal component analysis of the spectral data

Principal component analysis (PCA) was applied to compress the highly correlated NIR spectral data into variables (principal components, PCs) that no longer correlate with each other. Additionally, this method allowed for the identification of outliers by detecting data points that fell outside the 95% confidence interval. This function of the PCA was only used for the evaluation of experimental results aimed at monitoring storage and detectability of *Monilinia*-caused decay on stone fruits.

PCA modelling was also used as a preliminary pattern exploration on smoothed (Savitzky-Golay smoothing with 2nd order polynomial, 21 data points; "sgol-2-21-0") and multiplicative scatter-corrected (msc) data. Furthermore, the results revealed how individual wavelengths correlate with the PCs, which were illustrated on loading plots. PCA models were built on the whole dataset by fruit variety, respectively, to recognise patterns in fruit ripeness, in *Monilinia*-infected fruit handling and storage, or in total added extract content in enriched fruit juices.

Soft independent modelling of class analogies

Soft independent modelling of class analogies (SIMCA) was only used to evaluate the experimental results of *Monilinia* detection studies. The method was applied alongside the PCA results, except that modelling was performed on data recorded at the beginning (day 1), middle (day 4) and end of storage (day 7), also after smoothing and msc pre-treatments. This supervised classification method helped to better understand the similarities and differences between the sample groups which for these evaluations were the different treatments (mode of inoculation and storage condition together).

SIMCA models the multivariate space formed by a given sample group and calculates whether a given observation belongs to a specific group based on the interclass distances and the importance of variables (i.e., wavelengths). This approach also gives the discriminating power of the variables, significantly contributing to group differentiation and thereby facilitating the identification of absorbance bands associated with spectral differences (Wold and Sjostrom 1977).

Linear discriminant analysis of the spectral data

Linear discriminant analysis (LDA) was performed as a supervised classification method to discriminate and classify samples according to various classification variables (see Table 9). In our specific application, principal component scores served as the input values for the LDA models. The optimal number of principal components (NrPCs) used in the modelling process was determined by an R-based algorithm that collected and compared the LDA model calibration and validation accuracies up to a predefined 20 NrPCs, using three-fold cross-validation. The NrPCs

that yielded the smallest difference between model calibration and validation accuracy, as well as the highest validation accuracy, was selected for the actual modelling. The PCA-LDA models were built on data filtered to certain data sets, pre-processed then further optimised for NrPCs. The models were tested using leave-one-sample replicate-out (LOSO) validation.

The classification results (%) obtained during the construction and testing of the models are summarised in so-called confusion tables. The optimal spectral pre-treatment(s) and NrPCs for the PCA-LDA modelling of a given dataset are displayed at the bottom of the summary tables, specifically following * symbols. In addition, this method also assisted in identifying absorbance bands which contributed greatly to the differentiation between sample groups.

In the ripeness studies, models classifying by ripeness levels were first built by fruit variety, and then separately on the data obtained on the more mature and immature sides of the fruits. This was performed to explore the influence of the location of spectrum acquisition on classification accuracy. Model construction was done by omitting data of one parallel sample from the five available per pre-classified sample sets at a time. During testing, the data of the previously omitted samples were projected into the constructed PCA-LDA model. Model building and testing were completed cyclically until all data for each sample were included at least once in the modelling.

Table 9. Summary of variables used to filter or model the data

Study	Classification variables	Levels of classification
Ripeness assessment:	Fruit variety:	BB – VC; KJ – UF; EL – ST
	Ripeness level:	L1 ▸▸▸ L6
	Measurement side:	immature – mature
Monilinia detection:	Fruit variety:	EB – UF; TD – TP
	Suspension concentration:	~ 0.1, 1, 10, 100 conidia/ μL
	Storage condition:	5 °C; 24 °C
	Mode of conidial inoculation:	$Intact_{con}$ – $Inact_{inf}$ – $Injury_{con}$ – $Injury_{inf}$
	Treatment groups:	5 °C $Intact_{con}$; 5 °C $Intact_{inf}$; 5 °C $Injury_{con}$; 5 °C $Injury_{inf}$; ~ 20 °C $Intact_{con}$; ~ 20 °C $Intact_{inf}$; ~ 20 °C $Injury_{con}$; ~ 20 °C $Injury_{inf}$
	Appearance time of visible infection signs	- 6 days ▸▸▸ + 6 days
Fruit juice control:	Fruit juice:	sour cherry; plum
	Type of extract:	Juice; Juice + CBE; Juice + GSE; Juice + PGE; Juice + CBE + GSE; Juice + GSE + PGE; Juice + PGE + CBE; Juice + CBE + GSE + PGE
	Type of juice blend:	pure juice; simple; binary; ternary
	Added extract concentration:	0.0, 0.5, 0.7, 1.0, 1.4, 1.9, 2.5 g/ 100 mL

In the experiments related to *Monilinia* detectability, classification models were built by treatment group based on spectral pre-processing- and NrPC-optimised data recorded the day after sample

inoculation to determine the detectability of the initial conidial contamination on the fruit surface. For this modelling, the classification was done for conidium contamination levels of about 0.1, 1, 10, 100 conidia/ µL. In addition, the spectral trend of samples that were found to undergo *Monilinia*-induced spoilage during storage was also modelled. This only concerned fruits that were infected through injury and stored at room temperature ("~ 20 °C $Injury_{inf}$"). After specifically determining on which storage day the fruits exhibited visible signs of *Monilinia* infection (marked as "0 day"), data covering ± 2-day interval relative to data for "day 0" were included in this modelling. In both modelling cases, the model building was done by omitting data of one sample from the five parallelly prepared per sample group at a time. During testing, the data of the previously omitted samples were projected into the constructed PCA-LDA model. Model building and testing were completed cyclically until all data for each sample were included at least once in the modelling.

PCA-LDA was also applied for the qualitative classification of fruit juice blends enriched with plant extracts in various concentration. Models were built to detect the type of extracts administered in simple, binary, or ternary combinations, as well as to group them based on the total added extract concentration. In these cases, the model building and testing involved the cyclic omission of one of the three samples prepared in parallel and their projection into the constructed model.

Partial least squares regression on the spectral data

Partial least squares regression (PLSR) was applied to predict quantitative compositional attributes based on the spectral data. PLSR models were developed individually for each fruit variety using filtered, spectral pre-processing- and latent variable- (NrLV) optimised data. Model validation was conducted through leave-one-sample replicate-out (LOSO) validation, ensuring robust assessment of predictive performance. The accuracy and reliability of the models were quantified by the coefficient of determination (R^2) and the root mean square error (RMSE). The model fitting accuracies obtained during the model building (C) and testing (CV) by predicted attribute are arranged in summarising tables. The optimal spectral pre-treatment(s) and NrLVs for the PLSR modelling of a given dataset are included in the corresponding columns of the summary tables. In addition, the regression vectors were also obtained as partial results, which provide information on the degree to which each variable is correlated with the actually predicted parameter.

In the ripeness studies, PLSR models were employed to non-destructively predict certain quality traits (colour, DMC, SSC, TA, TAC) of fruits of different ripeness. The models were first built by fruit variety, and then on the data obtained on the more mature and immature sides of the fruits, respectively, to explore its influence on the prediction accuracy. Model construction was done by omitting data of one parallel sample from the five available per pre-classified sample sets at a time. During testing, the data of the previously omitted samples was projected into the constructed PLSR model. Model training and testing were completed cyclically until all data for each sample were included at least once in the modelling.

PLSR modelling was also applied to predict the added extract concentration in fruit juices enriched to varying degrees. The models were first built using juice samples by fruit species, and then filtered according to simple, binary, and ternary blends when estimating CBE, GSE, PGE, and total extract content. As described in detail above, model building and testing involved the cyclic omission of data corresponding one of the three samples prepared in parallel and their projection into the constructed model.

Identification of frequently occurring absorption bands in chemometric modelling

For each of the different chemometric modelling approaches, the extent to which each wavelength supports the performance of the current modelling approach was determined. The wavelengths relevant to each modelling approach were identified based on the peaks in the PCA loadings, SIMCA and LDA discriminating powers and PLSR regression vectors. By fruit species and analytical method, the frequency with which each variable (i.e., wavelength) occurs in the modelling was summarised together, using spectral windows of approximately 10 nm. The resulting absorbance bands with their corresponding incidence values were plotted on line diagrams.

5. RESULTS AND DISCUSSION

This chapter summarises the main results and findings obtained during the assessment of stone fruit ripeness, detectability of *Monilinia* contamination, and prediction of fruit juice enrichment with plant extracts. The summary presents the best classification and prediction results.

5.1. Determination of the stone fruit ripeness with NIR spectroscopy

This subsection presents a summary for each fruit type regarding the effectiveness of a hand-held NIR spectrometer in predicting the ripeness and certain quality attributes of stone fruits.

5.1.1. Determination of sweet cherry ripeness

For the sweet cherries harvested at various stages of ripeness, a total of 26 and 21 pre-classified sample sets were analysed, respectively. The colours of the sweet cherries ranged from a completely immature green to close to overripe deep red. The pre-classified fruit samples were graded into six ripeness clusters. Table 10 presents the averages of the measured physical and compositional properties for each ripeness level across the pre-classified samples.

Table 10. Quality characteristics of sweet cherry varieties of different ripeness (average values).

	L*	**a***	**b***	**Dry matter**	**Total acidity**	**Soluble solids**	**Anthocyanin content**
				% m/m	mg/ g	% brix	mg/ L
BB_L1	48.72	9.71	16.83	17.19	6.41	9.20	0.00
BB_L2	37.13	24.30	12.99	16.26	5.73	9.91	0.00
BB_L3	28.98	24.62	10.73	19.77	5.81	11.26	0.61
BB_L4	24.76	22.22	10.09	22.62	5.53	12.18	2.31
BB_L5	18.26	13.22	4.98	26.84	7.44	16.09	45.38
BB_L6	16.06	6.92	2.85	32.45	7.41	17.49	79.31
VC_L1	51.60	8.43	13.70	18.67	7.74	9.23	0.00
VC_L2	44.28	19.70	11.61	18.93	7.34	10.49	2.15
VC_L3	31.61	27.65	11.88	19.43	6,56	11.73	2.47
VC_L4	25.57	24.39	10.12	20.62	6.27	12.98	8.19
VC_L5	18.50	11.07	4.67	28.58	6.95	15.43	72.45
VC_L6	16.13	6.40	2.70	27.05	7.79	18.64	131.01

As Table 10 shows, the L* values indicating fruit lightness, tended to decrease as ripening progressed, signifying a darkening of the fruits' skin colour. Similarly, the a* values representing the green-red hue, also showed a decreasing trend across most ripeness levels. The relatively low a* values observed for the two varieties at lower ripeness levels (L1, L2) are due to that the colour coordinates included in the table represent the average of the values recorded on the immature and mature sides of the fruits. At these ripeness levels, solar radiation on skin colour development resulted in more pronounced differences on the immature and more mature measurement sides of the fruits. The b* values indicating the blue-yellow hue, decreased with advancing ripeness as

well. Trends in colour coordinate values have been reported in other researches as well. Chełpiński, Ochmian and Forczmański (2019) found that "Burlat" cherries achieve their optimum harvesting ripeness when L* is within 30.0 to 20.0, a* is within 30.0 to 0.0, and b* is within 10.0 to 0.0.

Among the compositional traits, the dry matter, soluble solids, and total anthocyanin content consistently increased as ripening progressed. In the case of the VC cherries, the anthocyanin content was nearly double compared to the BB variety. As for the acidity, a decline was observed from the L1 to L3 or L4 ripeness stages, followed by an increase at higher ripeness levels. The DMC of the ripe fruits was slightly higher than usually reported in the literature, while the SSC and TA were almost the same (Serradilla et al. 2016). According to some sources, the TAC may vary between 2 and 300 mg/ 100 g depending on variety and season, overlapping with our results (Valero and Serrano 2010).

Figure 62 presents the raw spectra recorded on the mature and immature sides of the sweet cherries. Due to the inhomogeneity of the samples and spectral scatter, clear separation based on ripeness levels is not immediately apparent. However, following the application of smoothing (sgol-2-21-0) and the 2nd derivative (sgol-2-17-2) pre-processing, the significance of the wavelength range around 1100, 1300 and 1400 nm becomes evident, indicating its importance for distinguishing between ripeness levels.

After smoothing and msc correction on the spectra recorded on both the mature and immature sides of the sweet cherries, PCA was performed (Figure 12). This analysis aimed to assess the reliability of the ripeness levels we identified, using an unsupervised method to determine how well these levels corresponded to the actual variations in the dataset. For the BB and VC cherries, the first four principal components (PCs) explained about 99% of the variance in the data.

Based on the PCA score plots (Figure 12a), for the BB variety, the greatest separation of ripeness levels is observed along the second and third PCs. In contrast, for the VC variety, the separation appears most clearly in the combination of the first and third PCs. In the PCA modelling based on ripeness, specific wavelengths (i.e., loadings) that contributed the most were identified for each principal component. Based on the two PCA loadings highlighted per variety, the relevant wavelengths that best describe separation according to ripeness are the following:

- **Bigarreau Burlat (BB) sweet cherries**
  PC 1 loading: 1062.9, 1173.5, 1356.3, 1435.8, 1545.1 nm;
  PC 3 loading: 1078.9, 1265.2, 1393.0, 1454.2, 1530.6 nm;

- **Valery Chkalov (VC) sweet cherries**
  PC 2 loading: 1072.8, 1212.7, 1363.0, 1442.3 nm;
  PC 3 loading: 1265.2, 1393.0, 1454.2, 1535.8 nm.

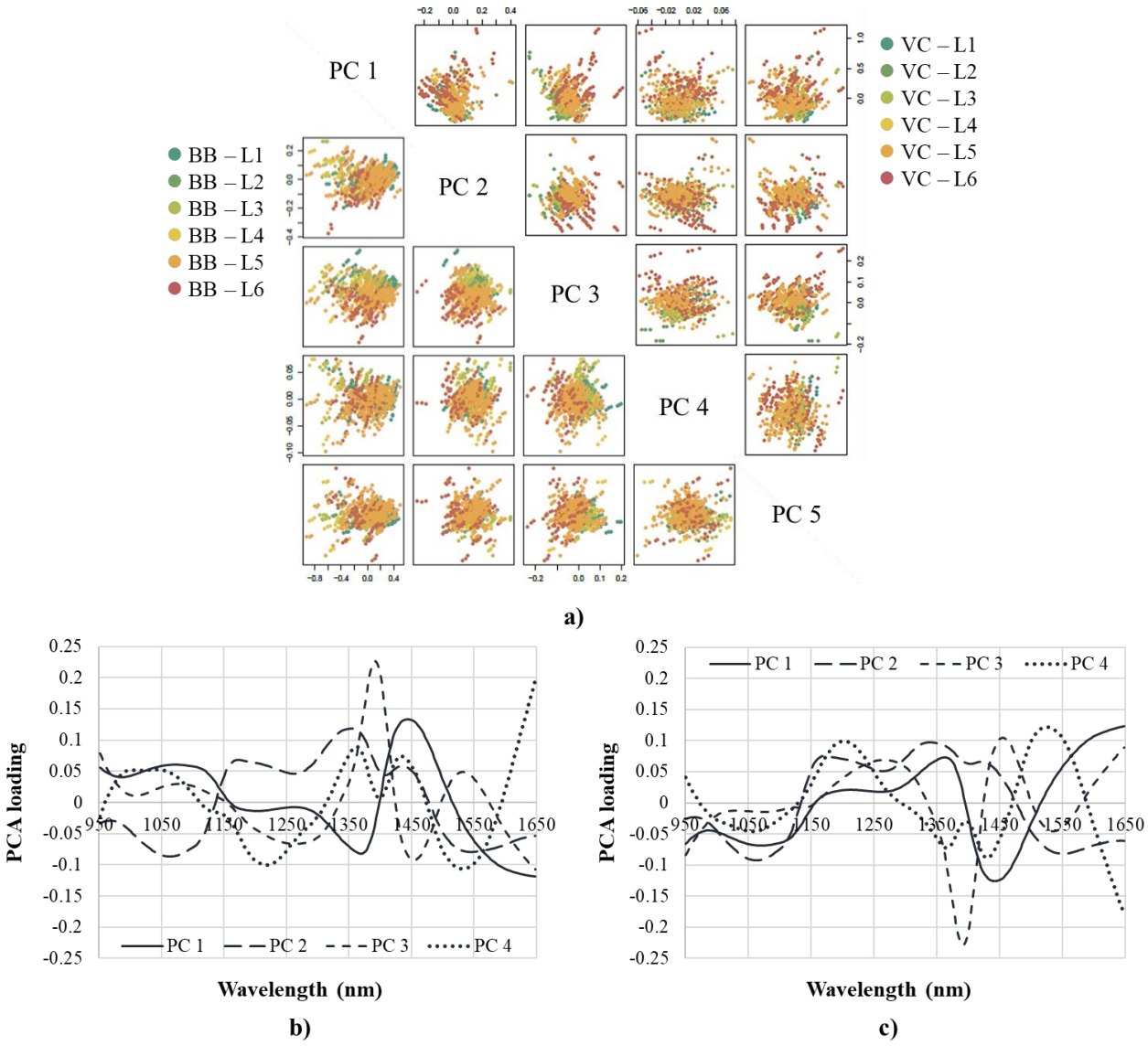

Figure 12. Preliminary PCA on the NIR spectra of sweet cherries when colouring was based on fruit ripeness (sgol-2-21-0; msc): PCA score plots of sweet cherries of different ripeness (a); PCA loading plot of BB cherries (b); PCA loading plot of VC cherries (c).

For sweet cherries harvested at different ripeness levels, classification models by variety were developed based on whole dataset collected on both mature and immature, as well as on the data respectively by measuring sides. This approach aimed to enable a more accurate classification. The results obtained after the optimised spectral pre-processing are illustrated in Figure 13. In both sweet cherry varieties, the different ripeness levels were distinctly separated along a semi-circular path. For the VC variety, the data points representing green ripe fruits clustered more sharply. The first two discriminant variables (LD) depicted in the figures accounted for 85.68% of the variance in the BB variety and 93.61% in the VC variety, respectively.

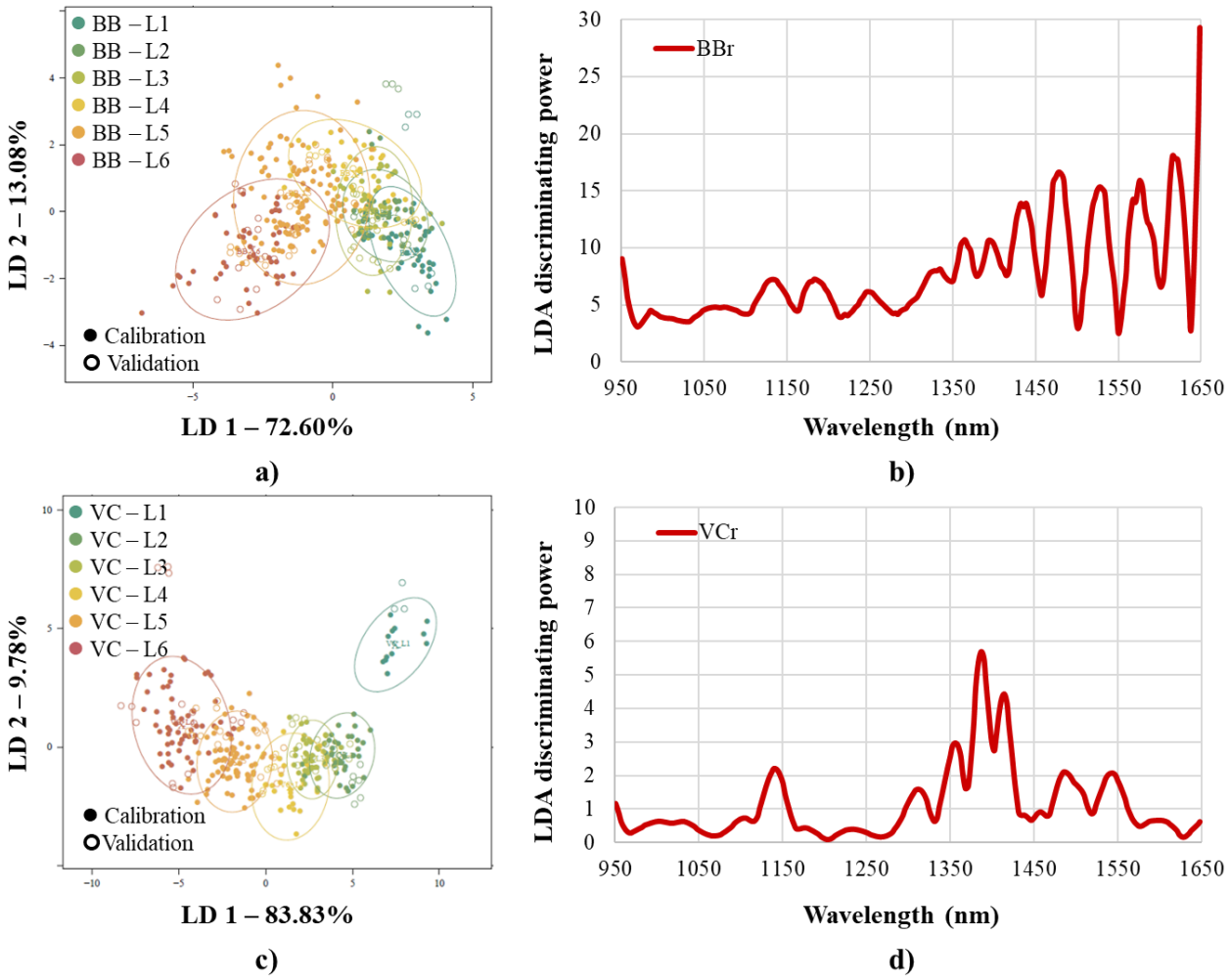

Figure 13. PCA-LDA on NIR spectra of sweet cherries when classification was based on fruit ripeness: PCA-LDA score plot on BBr (a); LDA discriminating power plot on BBr (b); PCA-LDA score plot on VCr (c); LDA discriminating power plot on VCr cherries (d).

The classification results of the PCA-LDA models by variety are summarised in Table 23 and Table 24, detailing the model building and validation accuracies. When comparing the classification results of sweet cherries, models based on data from the more mature side generally performed better. The average correct classification rates during model validation were between 42.5 - 55.5% for the BB variety, and between 48.8 - 78.0% for the VC variety. Misclassification typically occurred at adjacent ripeness levels. In addition to this, wavelengths that played a significant role in discrimination among ripeness levels were identified based on their discriminating power. These modelling results based on the spectra recorded from the mature side of the sweet cherries are presented in Figure 13b and Figure 13d, and the corresponding wavelengths are the following:

- **BBr**: 1062.9, 1133.8, 1183.0, 1249.0, 1335.0, 1365.3, 1396.3, 1432.5, 1477.8, 1527.4, 1576.1, 1615.6 nm;

- **VCr**: 1139.9, 1312.3, 1356.3, 1387.5, 1415.0, 1486.3, 1545.1 nm.

Similar to our series of experiments, Fodor (2022) investigated the grading of sweet and sour cherries together by maturity. Using the maturity index (MI) of the fruits, calculated as the ratio of SSC and TA values, QDA discriminated cherries with 98.4% accuracy.

The PLSR models for predicting various quality characteristics of sweet cherries were constructed separately based on spectra collected from both mature and immature, as well as from both sides of the cherries, respectively. This was done following optimised spectral pre-processing. The accuracies obtained during model calibration and validation are summarised in Table 25 and Table 26. The accuracy of predicting various physical and compositional characteristics was highly dependent on the cherry variety and the location of the spectral measurements. For sweet cherries, the best predictions were achieved for those characteristics that either increased or decreased monotonically as ripening progressed. For both sweet cherry varieties, the most accurate models were obtained during the prediction of average L*, dry matter, soluble solid, and anthocyanin content.

Figure 14 shows the best model fits found for the BB variety. The DMC prediction accuracy was with a maximal R^2 of 0.88 - 0.83 and RMSE of 2.07 - 2.50% m/m. The prediction of SSC was achieved with an R^2 of 0.89 - 0.86 and RMSE of 1.09 - 1.23% brix. The prediction of TAC was achieved with an R^2 of 0.86 - 0.83 and RMSE of 12.14 - 13.51 mg/ L during calibration and validation, respectively. The regression vectors showcasing the wavelengths that played a crucial role in the fittings of the selected models are the following:

- **DMC (BBg)**: 985.3, 1028.1, 1107.1, 1147.1, 1177.1, 1193.7, 1236.1, 1274.5, 1312.3, 1344.0, 1365.3, 1396.3, 1415.0, 1432.5, 1454.2, 1519.1, 1535.8, 1564.8, 1585.3, 1601.5, 1626.7 nm;
- **SSC (BBr)**: 1003.0, 1116.9, 1166.3, 1236.1, 1274.5, 1322.5, 1353.0, 1387.5, 1420.5, 1459.5, 1489.5, 1530.6, 1582.2, 1590.4, 1598.5 nm;
- **TAC (BBr)**: 1010.5, 1062.9, 1076.5, 1126.6, 1173.5, 1225.6, 1274.5, 1331.6, 1365.3, 1393.0, 1408.5, 1430.3, 1466.0, 1489.5, 1519.1, 1548.3, 1593.4, 1621.7 nm.

Figure 15 shows the best model fits found for the VC variety. The SSC prediction accuracy was a maximal R^2 of 0.95 - 0.93 and RMSE of 0.69 - 0.79% brix. The prediction of TAC was achieved with an R^2 of 0.91 - 0.87 and RMSE of 16.20 - 19.86 mg/ L. The prediction of average L* was achieved with an R^2 of 0.83 - 0.78 and RMSE of 4.76 - 5.44 during calibration and validation, respectively. The regression vectors showcasing the wavelengths that played a crucial role in the fittings of the selected models are the following:

- **SSC (VCg)**: 982.8, 1045.5, 1103.5, 1150.7, 1212.7, 1267.5, 1337.2, 1372.0, 1405.2, 1442.3, 1477.8, 1548.3, 1612.6 nm;
- **TAC (VCg)**: 1016.8, 1062.9, 1116.9, 1169.9, 1229.1, 1281.4, 1331.6, 1368.6, 1393.0, 1427.1, 1450.9, 1486.3, 1519.1, 1559.6, 1587.3 nm;
- **L* average. (VCr)**: 1020.6 1147.1 1193.7, 1236.1, 1271.0, 1347.4, 1399.7, 1430.3, 1457.4, 1504.3, 1519.1, 1574.0, 1618.7, 1626.7, 1635.7 nm

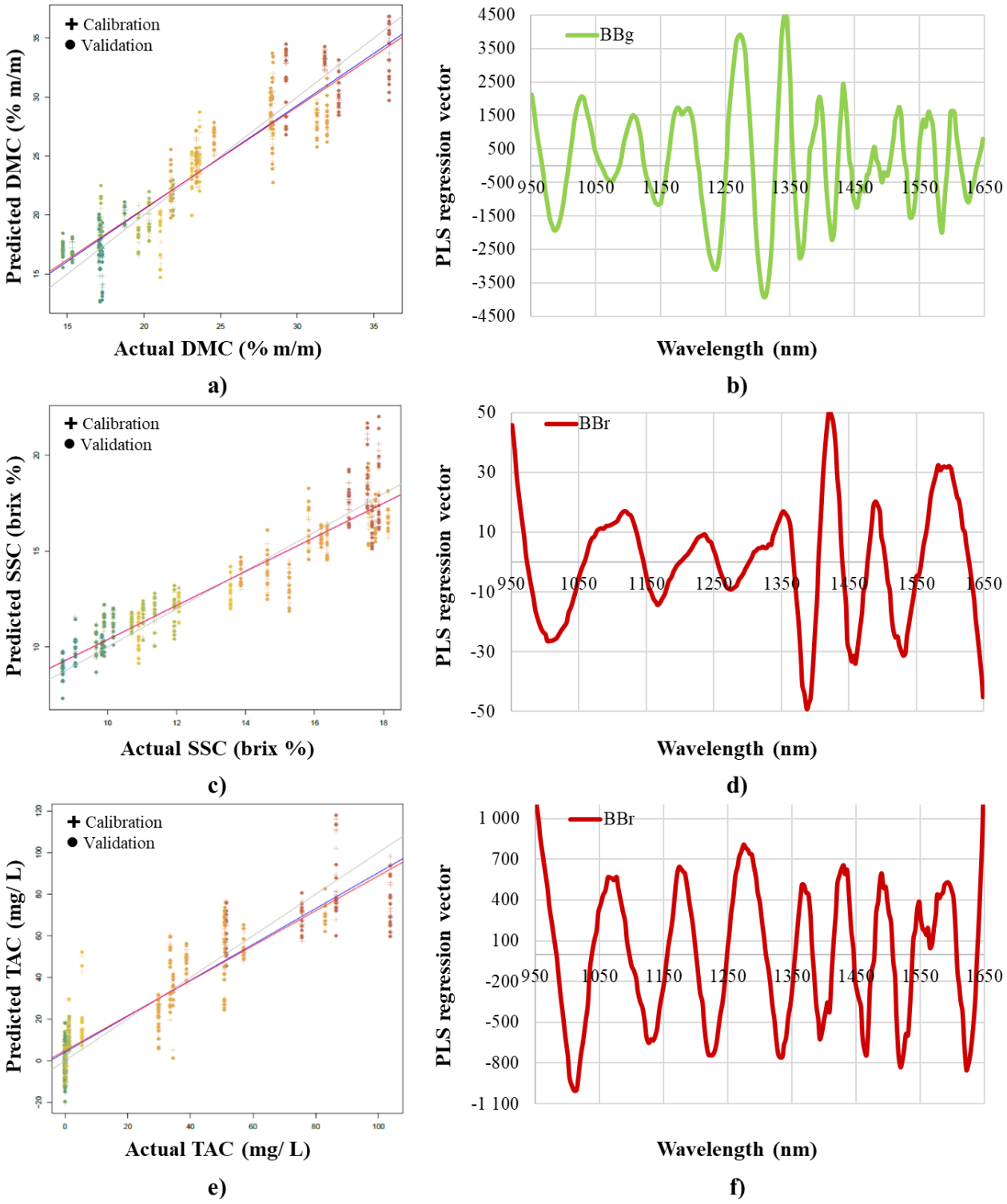

Figure 14. PLSR prediction results of certain quality traits of BB sweet cherries of different ripeness: Y-fit of DMC prediction on BBg(a); regression vectors of DMC prediction on BBg (b); Y-fit of SSC prediction on BBr (c); regression vectors of SSC prediction on BBr (d); Y-fit of average TAC prediction on BBr (e); regression vectors of average TAC prediction on BBr (f).

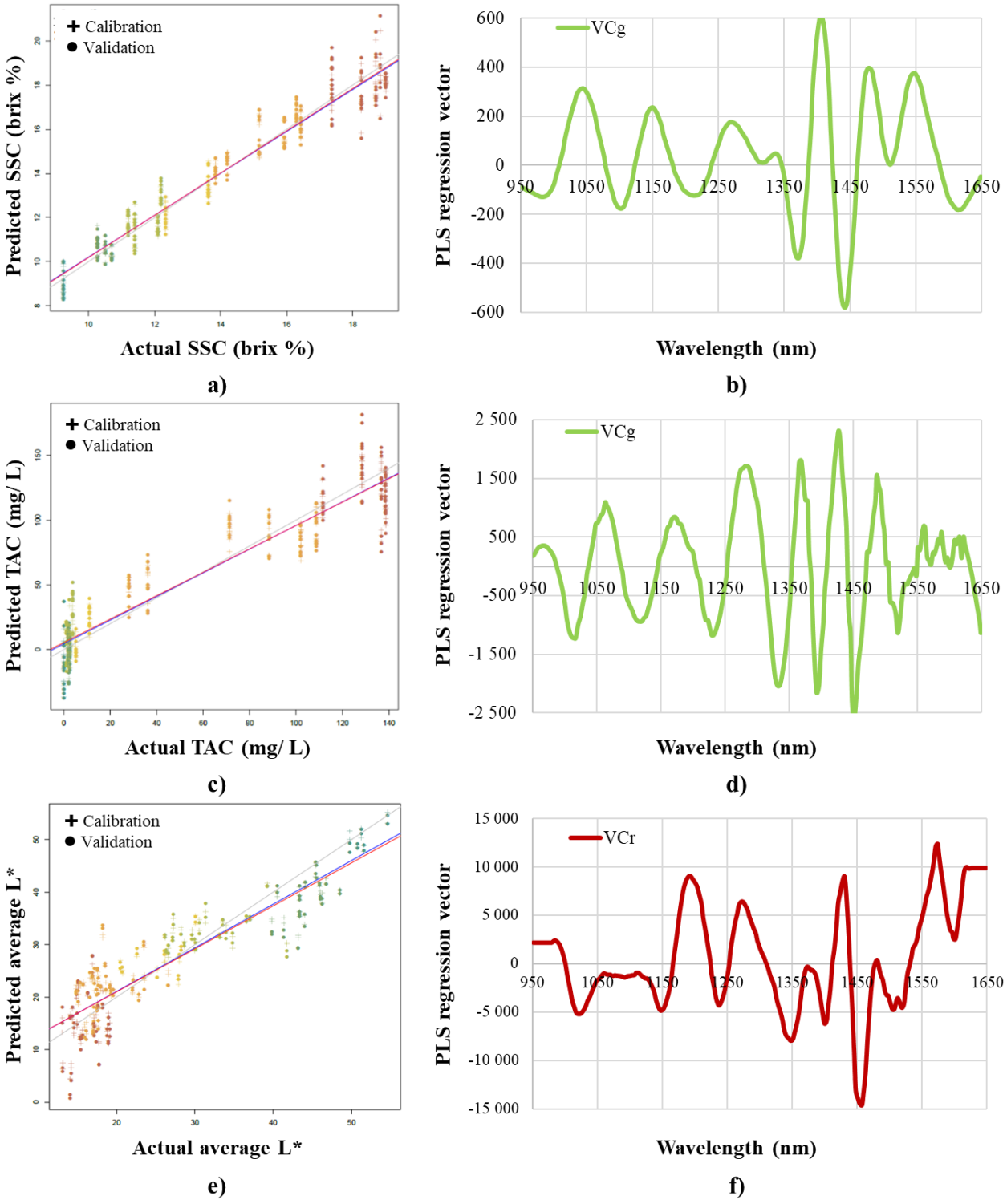

Figure 15. PLSR prediction results of certain quality traits of VC sweet cherries of different ripeness: Y-fit of SSC prediction on VCg (a); regression vectors of SSC prediction on VCg (b); Y-fit of TAC prediction on VCg (c); regression vectors of TAC prediction on VCg (d); Y-fit of average L* prediction on VCr (e); regression vectors of average L* prediction on VCr (f).

Prominent wavelengths obtained as a result of the PCA, PCA-LDA and PLSR models built on NIR spectral data of sweet cherries of different ripeness were summarised. Taking into account the most contributing wavelengths of the two studied varieties together, Figure 16 presents the absorption bands of successful chemometric modelling with their approximate frequency values.

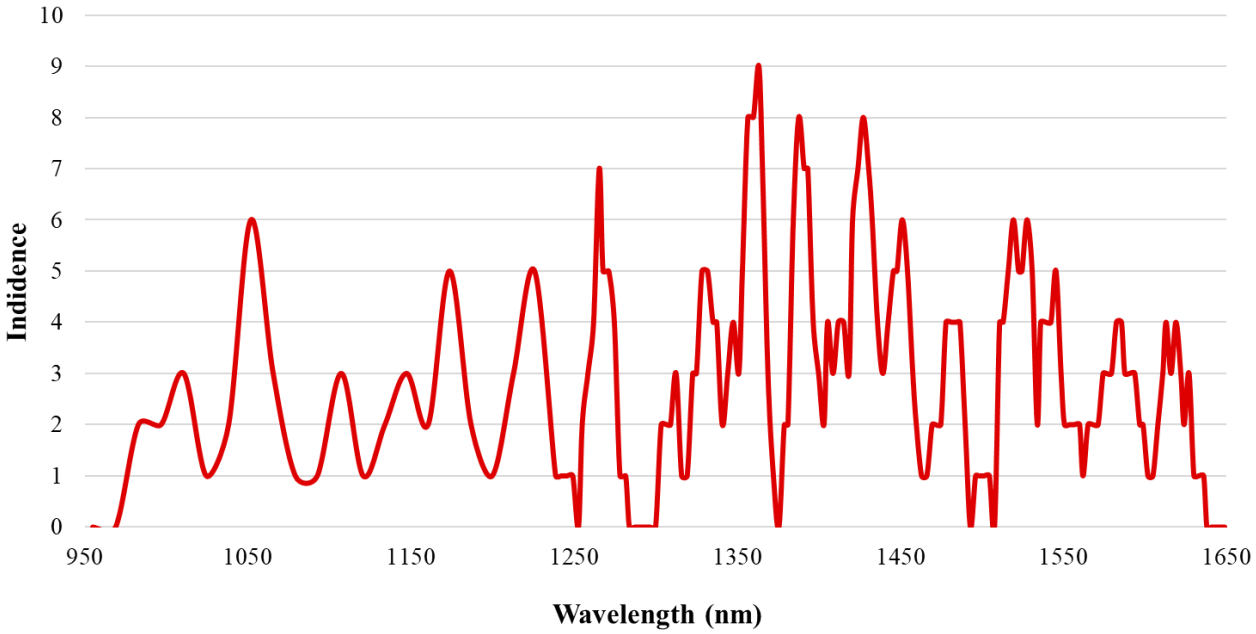

Figure 16. Absorbance bands frequently observed in chemometric modelling results of sweet cherry ripening with hand-held NIR spectrometer.

The ripening of cherries and the non-destructive determination of certain physical and organoleptic properties of cherries have been the subject of a number of studies reported in the literature. Escribano et al. (2017) combined the NIR spectral data (729-975 nm) with DMC and SSC of "Chelan" and "Bing" cherries. The authors reported prediction of DMC with R^2 between 0.67 - 0.73 and SSC between 0.73 - 0.89, respectively by variety. Toivonen, Batista, and Lannard (2017) developed DMC predicting models based on the spectral data of "Lapins" cherries obtained in the 858-1008 nm wavelength range with a portable Vis/NIR spectrometer. The predictive efficiency of the developed model was validated on three other cherry cultivars (Staccato, Sentennial, Sovereign) when Rp^2 were 0.96, 0.94, and 0.99, and RMSEp values were 0.51, 0.74, and 0.56% m/m, respectively. Li et al. (2018) used the hyperspectral data (874-1734 nm) of 550 "Hongdeng" cherries to determine the relationship between ripeness, SSC and pH. The authors could classify the fruits according to ripeness with over 96% accuracy with LDA and estimated SSC and pH with R^2 above 0.82 and RMSEp of 1.21% brix and 0.06, respectively, when genetic algorithm (GA) variable selection method was applied prior MLR. Wang et al. (2018) developed a cloud-based qualification system called "SeeFruits" that also involves a hand-held NIR spectrometer (DLP NIRscan Nano) to predict fruit cherry ripeness and SSC. The authors compared the performance of the developed system with hyperspectral imaging and found satisfying results during support vector classification (0.89) and PLSR prediction (Rp^2 = 0.83; RMSEP = 1.52% brix).

5.1.2. Determination of sour cherry ripeness

For the sour cherries harvested at various stages of ripeness, a total of 20 and 21 pre-classified sample sets were analysed, respectively. The colours of the cherries ranged from a light pink to a ripe deep red. The pre-classified fruit samples were graded into four ripeness clusters. Table 11 presents the averages of the measured physical and compositional properties for each ripeness level across the pre-classified samples.

Table 11. Quality characteristics of sour cherry varieties of different ripeness (average values).

	L*	a*	b*	Dry matter	Total acidity	Soluble solids	Anthocyanin content
				% m/m	mg/ g	% brix	mg/ L
KJ_L2	32.58	21.55	15.04	23.36	27.81	13.47	24.34
KJ_L3	23.80	21.34	10.26	24.59	22.98	12.82	57.24
KJ_L4	20.19	13.49	5.78	25.71	22.64	14.93	118.52
KJ_L5	18.32	5.73	3.00	29.69	21.40	16.40	141.05
UF_L2	33.62	21.01	16.49	25.34	22.02	10.98	12.28
UF_L3	22.67	20.39	9.26	22.89	24.07	12.78	67.75
UF_L4	19.60	12.64	5.59	23.21	23.31	14.92	140.79
UF_L5	19.01	6.42	2.66	24.59	22.97	16.59	149.55

As Table 11 shows, the L* values indicating lightness tended to decrease as ripening progressed, signifying a darkening of the fruits skin colour. Similarly, a* (green-red hue) and b* (blue-yellow hue) values also decreased with advancing ripeness. Among the compositional traits, the soluble solids and anthocyanin content consistently increased as ripening progressed. In the various ripening stages, the KJ variety exhibited a consistent trend of increasing dry matter and decreasing acidity, whereas the UF variety showed ambiguity at the L2 ripeness stage. These trends are very similar to those detailed for sweet cherries, with the difference that for sour cherries, acidity decreases overall as ripening progresses. When investigating Hungarian sour cherry cultivars, Desiderio et al. (2023) found consistent tendencies, especially regarding fruit skin colouration.

Figure 17 presents the raw spectra recorded on the mature and immature sides of sour cherries. Despite spectral scatter, clear separation based on ripeness levels is visible. It can be seen that the absorption of the fruit increases as the ripening progresses. With the application of smoothing and the 2nd derivative pre-processing, the significance of the wavelength range around 1100, 1300 and 1400 nm is also observable, indicating its importance for distinguishing between ripeness levels.

After smoothing and msc treatments on the spectra recorded from both the mature and immature sides of the sour cherries, PCA was performed (Figure 63). This analysis aimed to assess the reliability of the ripeness levels defined, using an unsupervised method to determine how well these levels corresponded to the actual variations in the dataset. In both varieties, it was characteristic that the different ripening stages became distinguishable along the first three principal components. For the two varieties, the first five principal components (PCs) explained about 99% of the variance in the data.

Based on the PCA score plots (Figure 63a), for the KJ variety, the greatest separation of ripeness levels is observed along the first and third PCs. In contrast, for the UF variety, the separation appears most clearly in the combination of the first and second PCs. In the PCA modelling based on ripeness, specific wavelengths that contributed the most were identified for each principal component. Based on the two PCA loadings highlighted per variety, the relevant wavelengths that best describe separation according to ripeness are the following:

- **Kántorjánosi (KJ) sour cherries**
  PC 1 loading: 1065.4, 1210.3, 1347.4, 1435.8 nm;
  PC 3 loading: 1028.1, 1163.9, 1265.2, 1387.5, 1466.0 nm;

- **Újfehértói (UF) sour cherries**
  PC 1 loading: 1062.9, 1203.2, 1359.7, 1442.3 nm;
  PC 2 loading: 1055.5, 1199.7, 1319.1, 1439.0, 1561.7 nm.

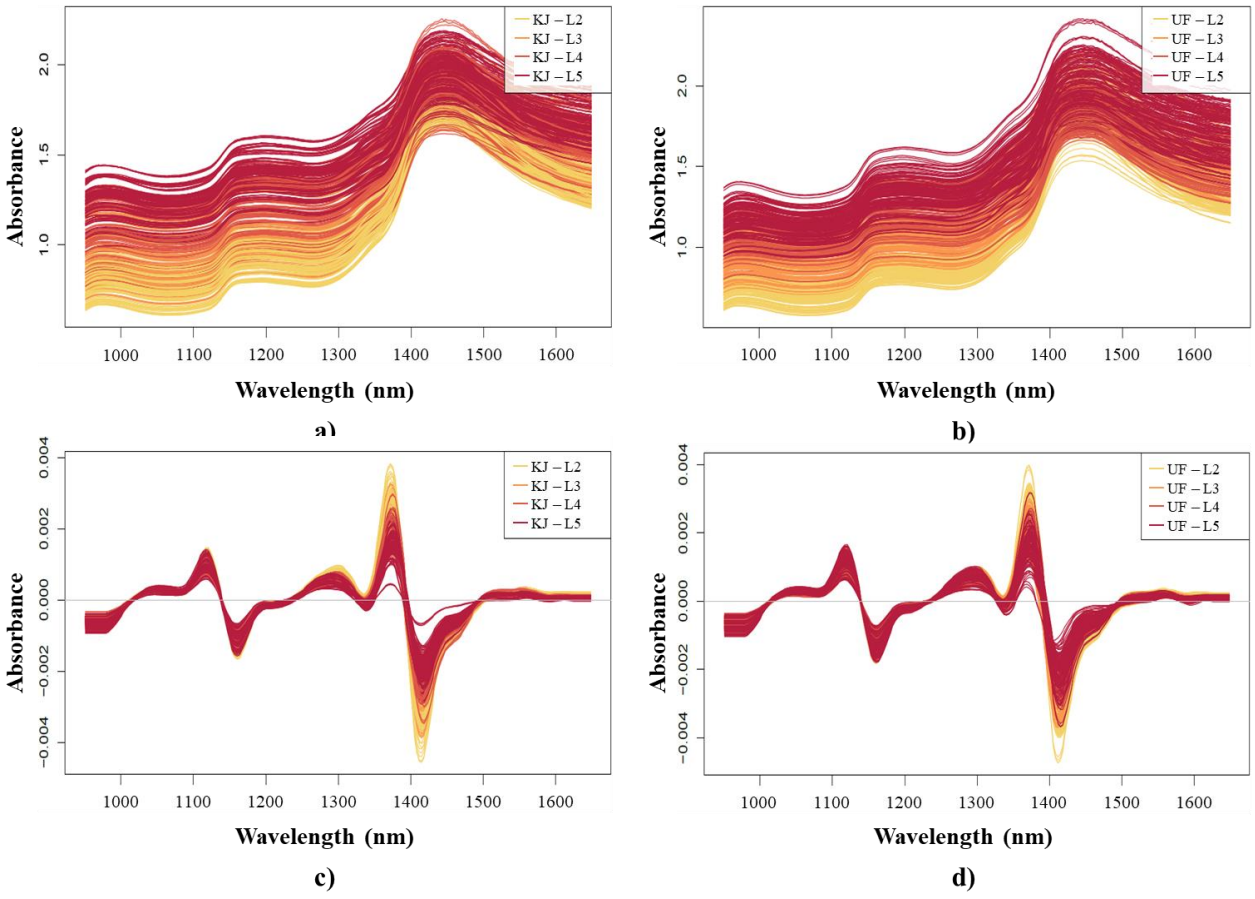

Figure 17. NIR spectra of sour cherries of different ripeness: raw spectra of KJ cherries (a); raw spectra of UF cherries (b); 2nd derivative spectra of KJ cherries (c); 2nd derivative spectra of UF cherries (d).

For sour cherries harvested at different ripeness levels, classification models were also developed separately based on spectra collected from both mature and immature, as well as from both sides of the cherries, respectively. The results obtained after the optimised spectral pre-processing are illustrated in Figure 18. In both sour cherry varieties, the different ripeness levels were very well separated along LD 1. Interestingly, for both varieties, a slight separation along LD2 was observed

for the L4 ripeness level. The first two LDs depicted in the figures accounted for the 97.13 and 90.13% of the variance in the KJ and UF variety, respectively.

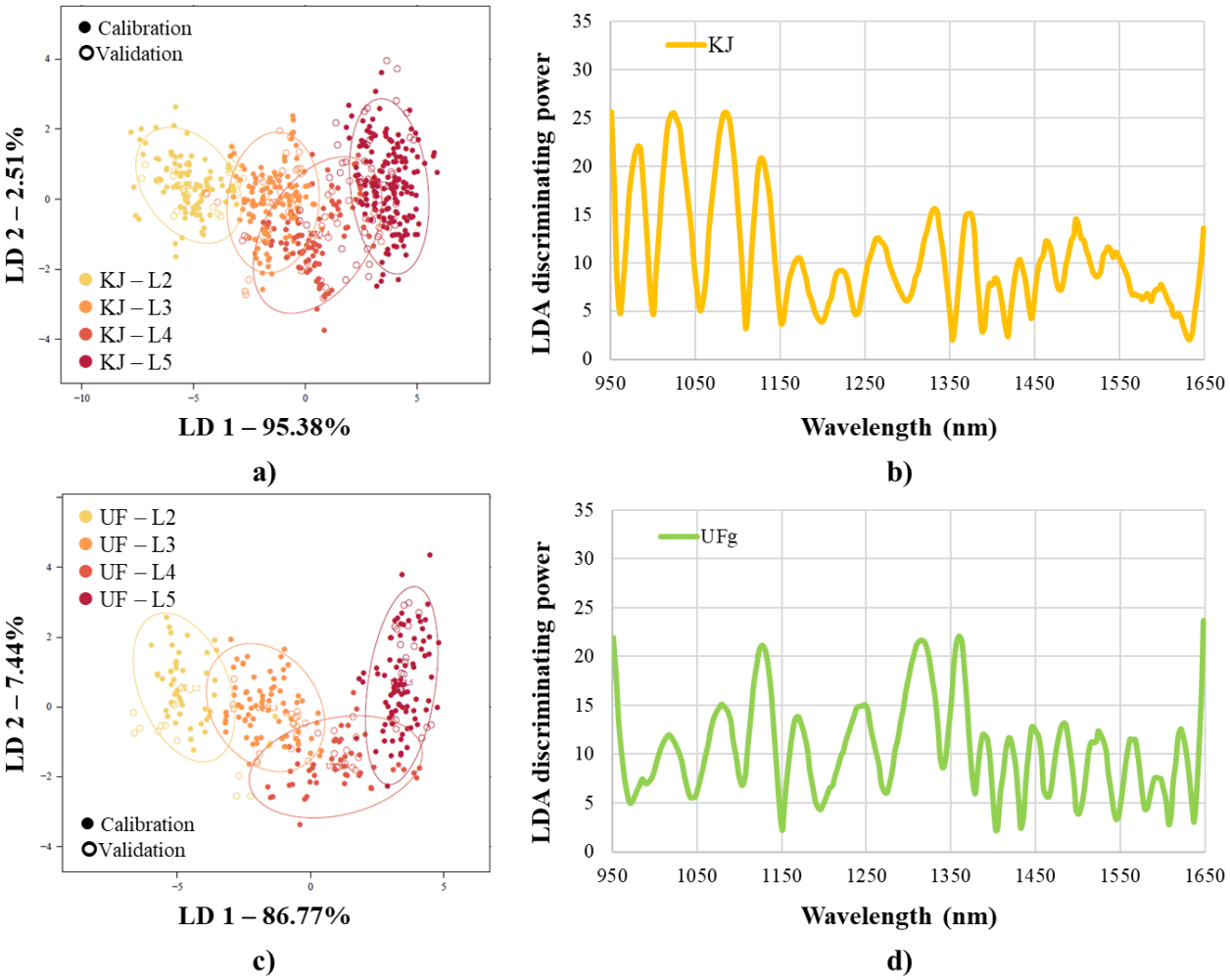

Figure 18. PCA-LDA on NIR spectra of sour cherries when classification was based on fruit ripeness: PCA-LDA score plot on KJ (a); LDA discriminating power plot on KJ (b); PCA-LDA score plot on UFg (c); LDA discriminating power plot on UFg (d).

The classification results of the PCA-LDA models by variety are summarised in Table 27 and Table 28, detailing the model calibration and validation accuracies. The classification accuracies for sour cherries varied according to measurement location by variety. The average correct classifications during model validation were between 76.8 - 82.4% for the KJ variety, and between 78.30 - 80.9% for the UF variety. Misclassification typically occurred at adjacent ripeness levels. In addition to this, wavelengths that played a significant role in discrimination among sample groups were identified based on their discriminating power. These modelling results based on the data of KJ and UFg are presented in Figure 18b and Figure 18d, and the corresponding wavelengths are the following:

- **KJ**: 982.8, 1024.3, 1086.3, 1126.6, 1169.9, 1223.2, 1265.2, 1331.6, 1372.0, 1403.0, 1432.5, 1462.8, 1498.0, 1535.8, 1582.2, 1598.5 nm;

- **UFg**: 985.3, 1016.8, 1078.9, 1126.6, 1169.9, 1249.0, 1315.7, 1359.7, 1387.5, 1418.3, 1447.7, 1484.2, 1524.3, 1561.7, 1593.4, 1621.7 nm.

The PLSR models for predicting various quality characteristics of sour cherries were also constructed separately based on spectra collected from both mature and immature, as well as from both sides of the cherries, respectively. The accuracies obtained during model calibration and validation are summarised in Table 29 and Table 30. The accuracy of predicting various physical and compositional characteristics was dependent on the sour cherry variety and the location of the spectral measurements. For sour cherries, the best predictions were found for characteristics that either clearly increased or decreased with ripening. For both sour cherry varieties, the most accurate models were obtained for predicting average L*, b*, dry matter or soluble solid, and anthocyanin content.

Figure 19 shows the best model fits found for the KJ variety. The DMC prediction accuracy was a maximal R^2 of 0.79 - 0.72 and RMSE of 1.47 - 1.67% m/m. The prediction of TAC was achieved with an R^2 of 0.91 - 0.87 and RMSE of 15.14 - 18.03 mg/ L. The prediction of average b* was achieved with an R^2 of 0.93 - 0.91 and RMSE of 1.26 - 1.51 during calibration and validation, respectively. The regression vectors showcasing the wavelengths that played a crucial role in the fittings of the selected models are the following:

- **DMC (KJr)**: 1006.8, 1020.6, 1041.8, 1139.9, 1210.3, 1308.9, 1353.0, 1384.2, 1430.3, 1498.0, 1564.8 nm;
- **TAC (KJg)**: 1016.8, 1069.1, 1139.9, 1177.1, 1249.0, 1296.3, 1353.0, 1393.0, 1420.5, 1454.2, 1481.0, 1495.8, 1542.0, 1593.4 nm;
- **b* average (KJg)**: 985.3, 1014.3, 1072.8, 1139.9, 1190.2, 1281.4, 1347.4, 1384.2, 1418.3, 1454.2, 1495.8, 1535.8, 1585.3 nm.

Figure 20 shows the best model fits found for the UF variety. The prediction of SSC was achieved with a maximal R^2 of 0.87 - 0.83 and RMSE of 0.98 - 1.10% brix. The prediction of TAC was achieved with an R^2 of 0.89 - 0.87 and RMSE of 18.67 - 20.98 mg/ L. The prediction of average b* was achieved with an R^2 of 0.91 - 0.89 and RMSE of 1.54 - 1.78 during calibration and validation. The regression vectors showcasing the wavelengths that played a crucial role in the fittings of the selected models are the following:

- **SSC (UFr)**: 982.8, 1031.8, 1082.6, 1130.2, 1169.9, 1210.3, 1308.9, 1331.6, 1353.0, 1380.9, 1408.5, 1432.5, 1486.3, 1519.1, 1559.6, 1582.2, 1607.6 nm;
- **TAC (UFg)**: 985.3, 1076.5, 1139.9, 1199.7, 1287.1, 1347.4, 1408.5, 1439.0, 1450.9, 1498.0, 1582.2, 1635.7 nm;
- **b* average (UFg)**: 1014.3, 1069.1, 1130.2, 1196.1, 1274.5, 1340.6, 1380.9, 1418.3, 1459.5, 1489.5, 1533.7, 1607.6, 1615.6 nm.

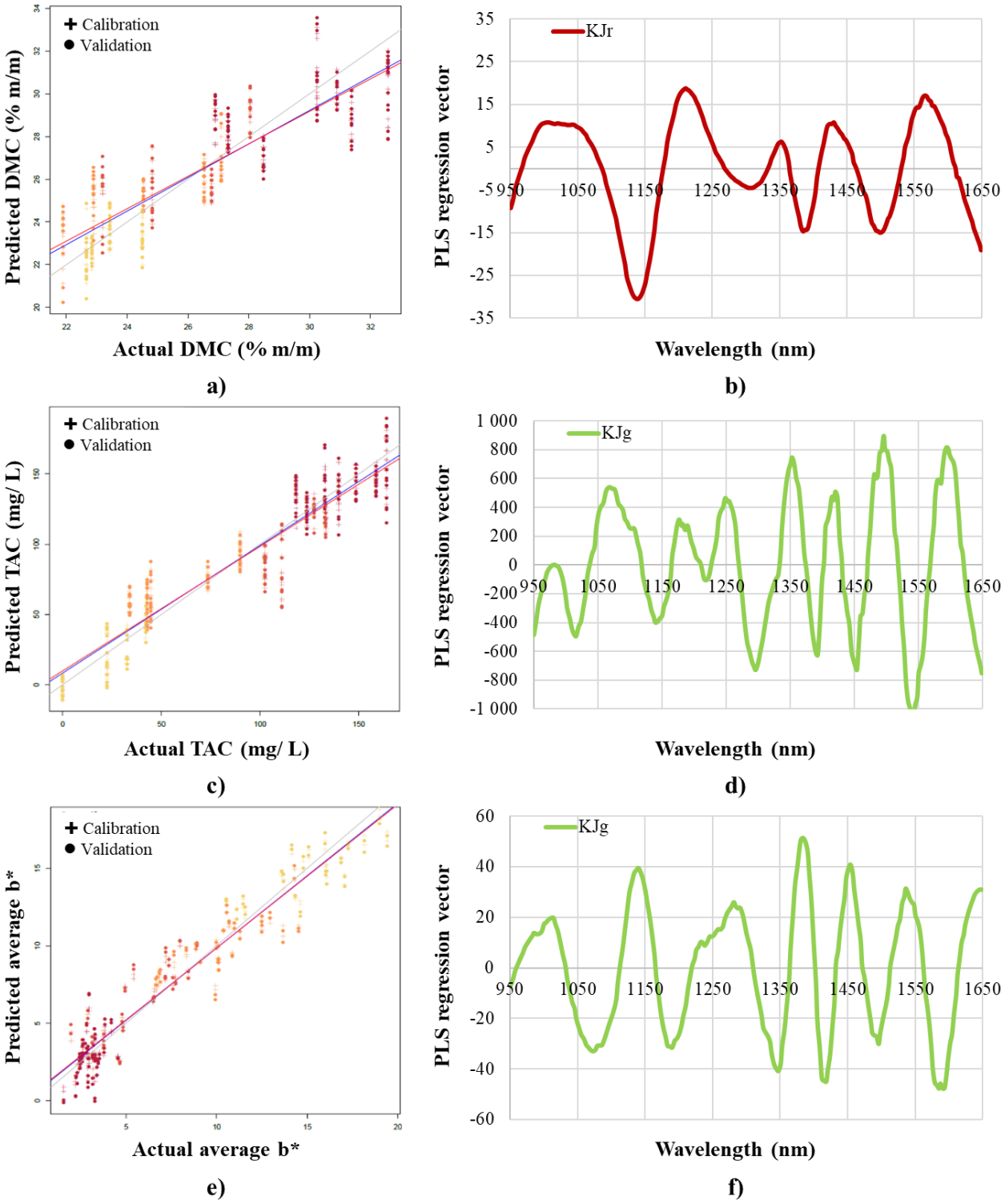

Figure 19. PLSR prediction results of certain quality traits of KJ sour cherries of different ripeness: Y-fit of DMC prediction on KJr (a); regression vectors of DMC prediction on KJr (b); Y-fit of TAC prediction on KJg (c); regression vectors of TAC prediction on KJg (d); Y-fit of average b* prediction on KJg (e); regression vectors of average b* prediction on KJg (f).

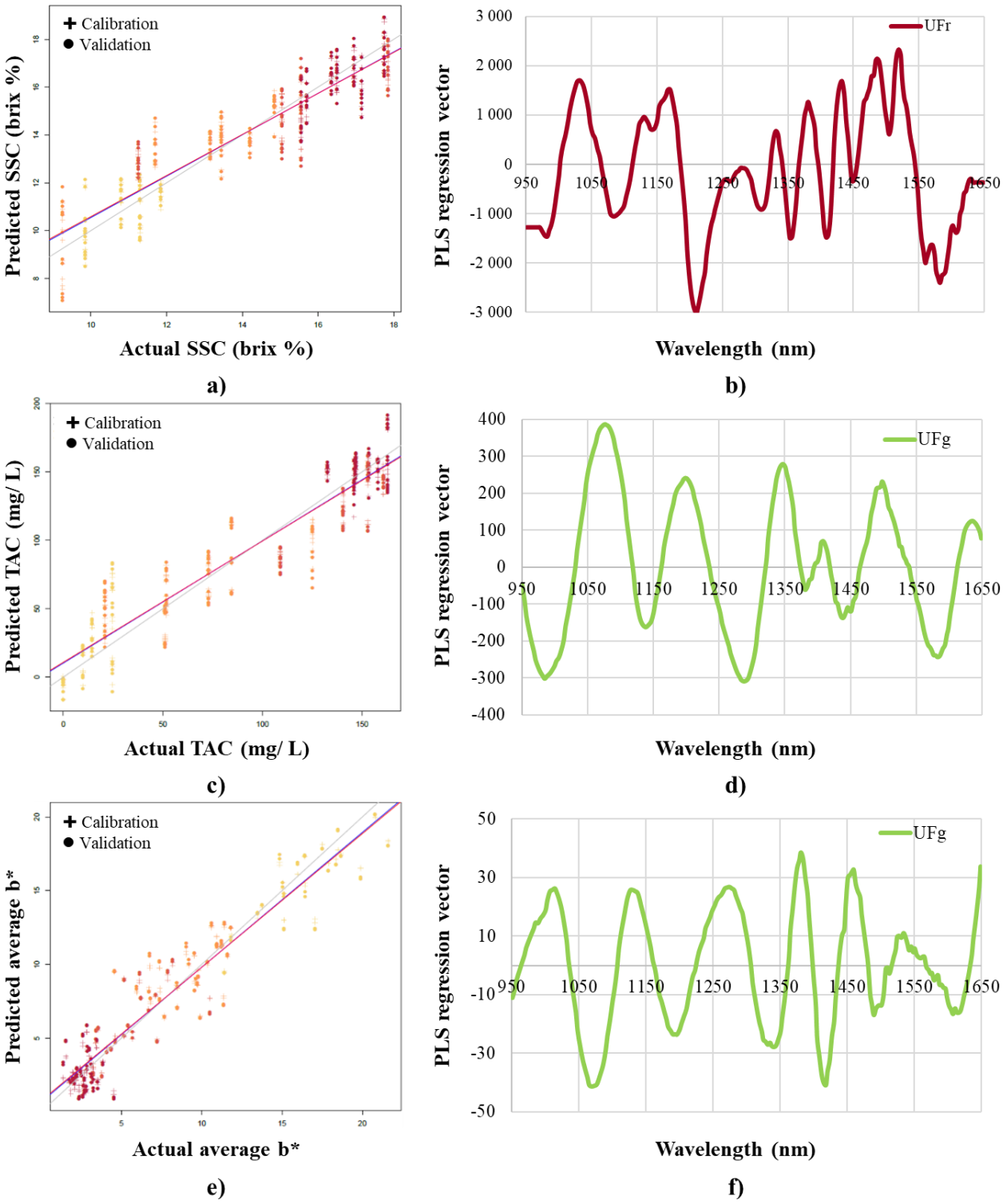

Figure 20. PLSR prediction results of certain quality traits of UF sour cherries of different ripeness: Y-fit of SSC prediction on UFr (a); regression vectors of SSC prediction on UFr (b); Y-fit of TAC prediction on UFg (c); regression vectors of TAC prediction on UFg (d); Y-fit of average b* prediction on UFg (e); regression vectors of average b* prediction on UFg (f).

Prominent wavelengths obtained as a result of the PCA, PCA-LDA and PLSR models built on NIR spectral data of sour cherries of different ripeness were summarised. Taking into account the most contributing wavelengths of the two studied varieties together, Figure 21 presents the absorption bands of successful chemometric modelling with their approximate frequency values.

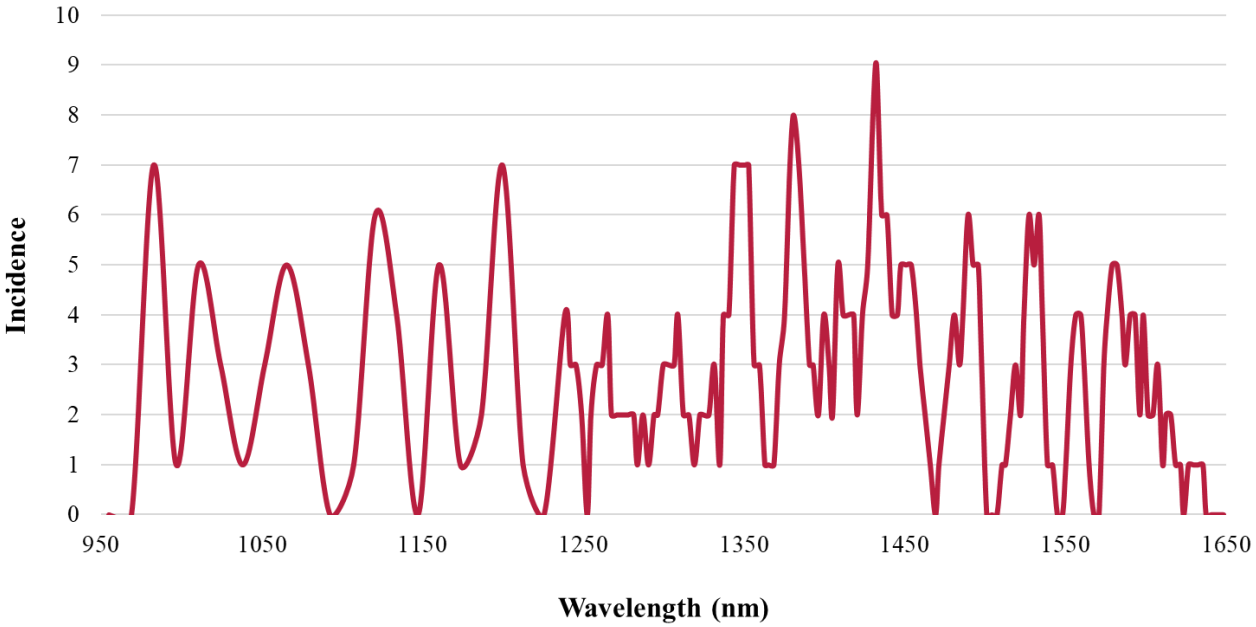

Figure 21. Absorbance bands frequently observed in chemometric modelling results of sour cherry ripening with hand-held NIR spectrometer.

In contrast to cherries, there is a relatively limited literature available on non-destructive NIR spectroscopic assessment of intact sour cherries. Analysing sweet cherries ("Bigarreau Burlat", "Valery Chkalov") and sour cherries ("Kántorjánosi", "Újfehértói") together, Fodor (2022) could predict DMC with Rcv^2 of 0.95 and RMSEcv of 1.25% m/m, SSC with Rcv^2 of 0.91 and RMSEcv of 0.97% brix, TA with Rcv^2 of 0.97 and RMSEcv of 0.14% m/m, and TAC with Rcv^2 of 0.89 and RMSEcv of 17.5 mg/ 100 g during seven-fold cross-validation.

5.1.3. Determination of plum ripeness

For the plums harvested at different stages of ripeness, a total of 20 and 20 pre-classified sample sets were analysed. The colour of the plums ranged from unripe green to a dark purple. The pre-classified fruit samples were put into five and four ripeness clusters, respectively by variety. The sample populations were characterized by a significant presence of unripe fruits and displayed considerable heterogeneity. Table 12 presents the averages of the measured physical and compositional properties for each ripeness level across the pre-classified samples.

Table 12. Quality characteristics of plum varieties of different ripeness (average values).

	L*	a*	b*	Dry matter	Total acidity	Soluble solids	Anthocyanin content
				% m/m	mg/ g	% brix	mg/ L
EL_L1	40.47	-6.82	22.25	18.70	16.66	9.19	0.00
EL_L2	38.27	-1.49	16.96	21.44	15.72	9.43	0.00
EL_L3	27.94	2.92	10.50	20.31	10.56	12.35	0.61
EL_L4	23.21	6.15	6.62	19.09	9.65	12.73	0.95
EL_L5	19.43	4.42	2.12	20.16	8.39	13.39	4.23
ST_L1	38.94	-3.16	19.15	16.95	14.36	8.19	0.00
ST_L2	36.49	0.07	15.40	18.87	13.89	8.43	0.00
ST_L3	25.01	6.09	5.59	18.37	10.14	11.47	0.00
ST_L4	24.28	5.92	4.77	18.64	10.11	11.03	3.94

Table 12 shows that the L* values tended to decrease as ripening progressed, signifying a darkening of the fruits' skin colour. Similarly, the b* values (blue-yellow hue), decreased with advancing ripeness as well, while the a* generally exhibited higher values in the more mature sample groups. The combination of these two coordinates suggests the accumulation of purplish components in the fruit skin. Among the compositional traits, the soluble solids, anthocyanin, and acidity of the plums developed as expected, with the latter decreasing as ripening progressed. However, no clear trend could be established based on the data of dry matter content, and this variability can be attributed to the inhomogeneity of the samples. The relatively low TAC values may be due to the fact that at the time of plum harvesting, the skin of the fruit contained higher concentrations of anthocyanins and the flesh of the fruit less, and therefore the anthocyanin concentration of the supernatant juice obtained from blending and centrifuging these samples may have been negligible. Usenik et al. (2008, 2009) reported similar findings for L* and b* values, as well as for SSC, malic acid and TAC of plums of different cultivars and ripeness.

Figure 64 presents the raw spectra recorded on the mature and immature sides of plums. Despite spectral scatter, separation based on ripeness levels is visible. It can be seen that the absorption of the fruits increases as the ripening process progresses. With smoothing and 2nd derivative pre-treatment, the significance of the wavelengths around 1100, 1300 and 1400 nm is also evident in these samples.

After smoothing and msc treatments on the spectra recorded from both the mature and immature sides of the plums, PCA was performed (Figure 22). This analysis aimed to assess the reliability of the ripeness levels we identified, using an unsupervised method. In both varieties, it was characteristic that the different ripening stages were distinguishable along the first three principal components. For the EL plums, the first five, for the ST plums, the first seven PCs accounted about for the 99% of the variance in the data.

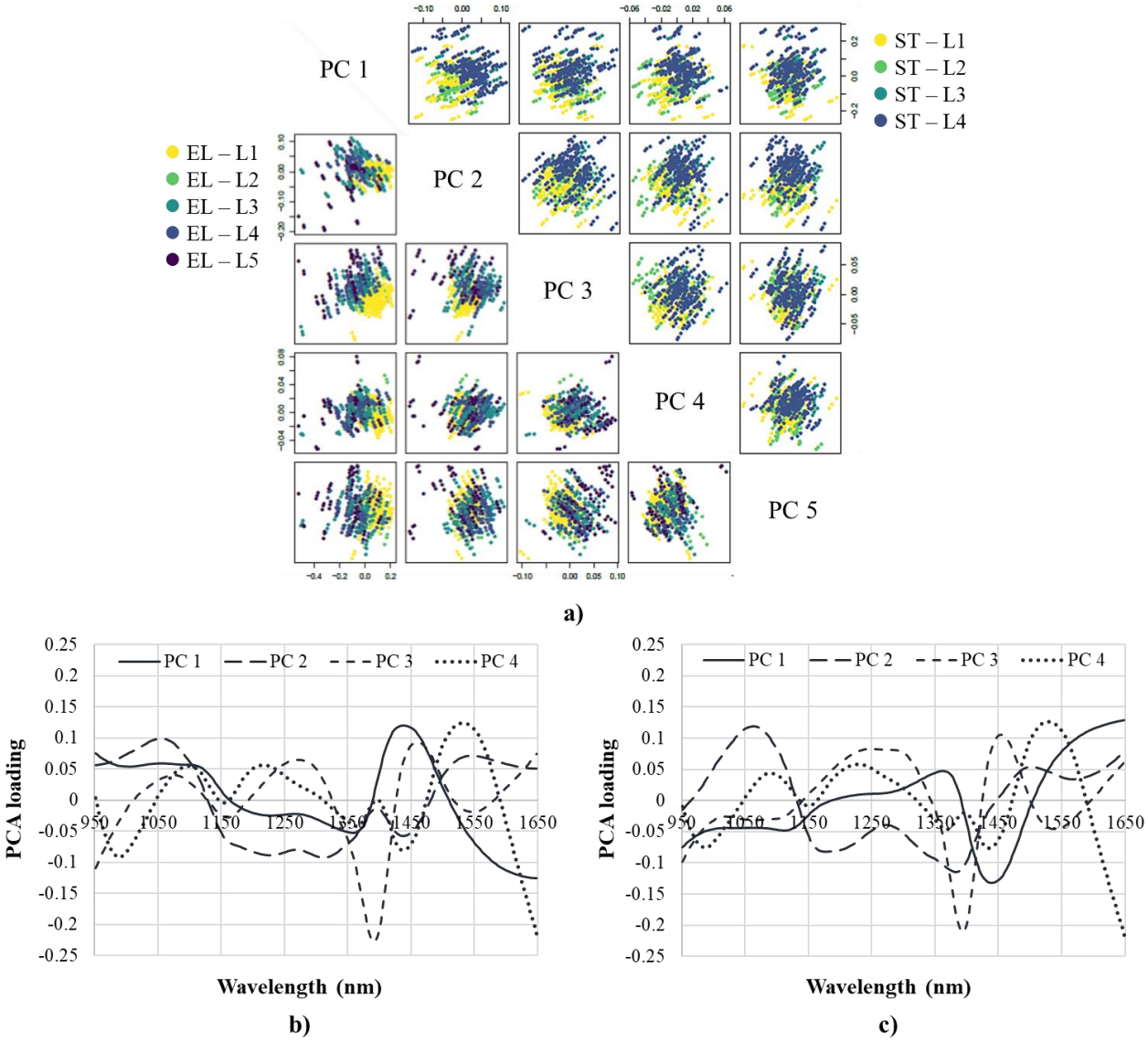

Figure 22. Preliminary PCA on the NIR spectra of plums when colouring was based on fruit ripeness (sgol-2-21-0, msc): PCA score plots of plums of different ripeness (a); PCA loading plot of EL plums (b); PCA loading plot of ST plums (c).

Based on the PCA score plots (Figure 22a), for the EL variety, the greatest separation of ripeness levels is observed along the first and third PCs. For the UF variety, the separation appears most clearly in the combination of the first and second PCs. In the PCA modelling based on ripeness, specific wavelengths that contributed the most were identified. The highlighted two PCA loadings per variety, the relevant wavelengths that best describe separation according to ripeness are the following:

- **Elena (EL) plums**
  PC 1 loading: 1055.5, 1229.1, 1359.7, 1439.0 nm;
  PC 3 loading: 1076.5, 1160.3, 1271.0, 1390.8, 1459.5, 1548.3 nm;

- **Stanely (ST) plums**
  PC 1 loading: 1034.3, 1113.2, 1363.0, 1439.0 nm;
  PC 2 loading: 1062.9, 1177.1, 1384.2, 1501.1 nm.

For plums harvested at different ripeness levels, classification models were also developed separately based on spectra collected from both mature and immature, as well as from both sides of the plums, respectively. The results obtained after the optimised spectral pre-processing are illustrated in Figure 23. For both varieties, the very unripe fruits and those showing slight coloration distinctly separated along LD 1, while within these clusters, the points representing riper fruits grouped along LD 2. The first two LDs shown in the figures accounted for the 92.34 and 99.38% of the variance in the EL and ST variety, respectively.

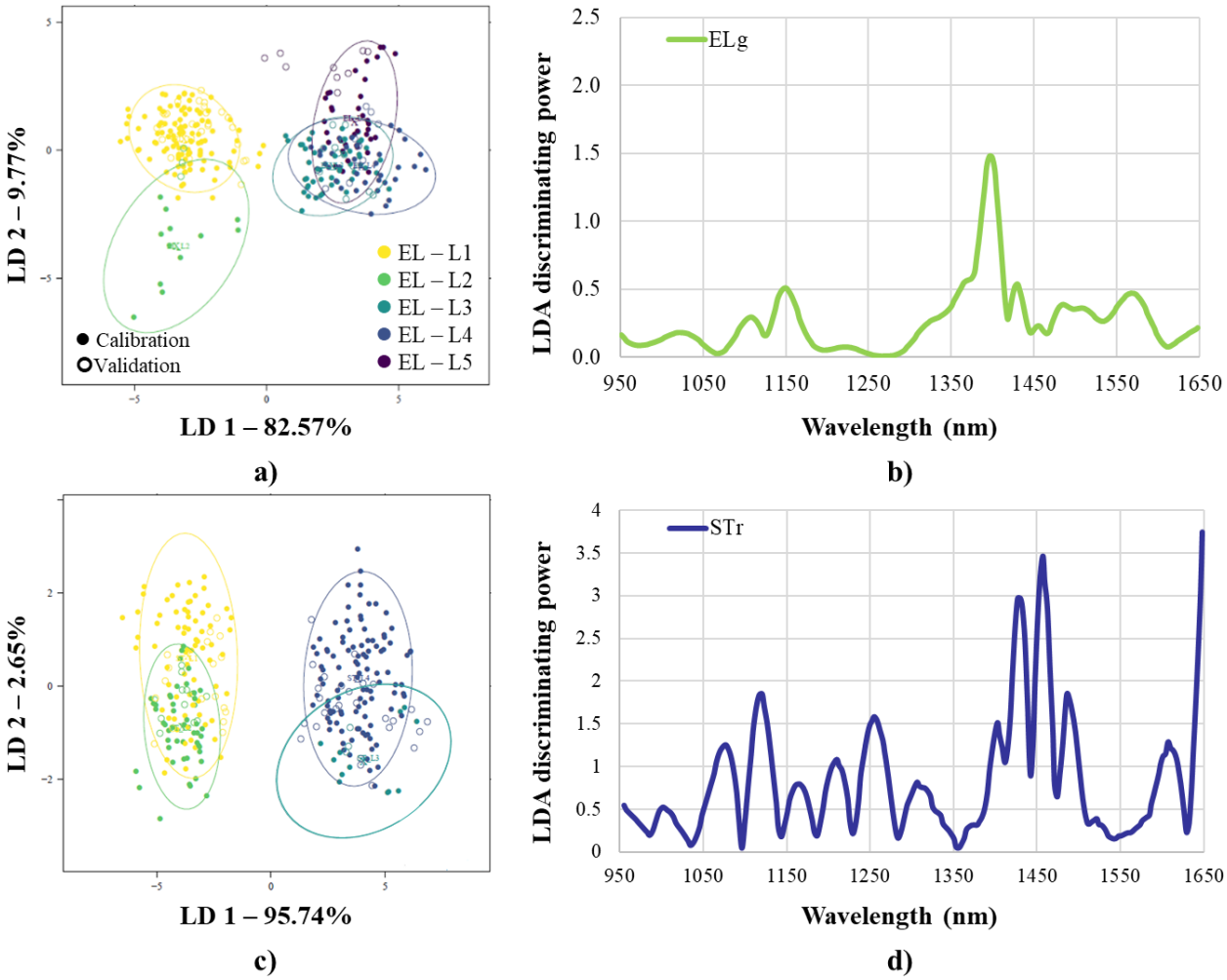

Figure 23. PCA-LDA on NIR spectra of plums when classification was based on fruit ripeness: PCA-LDA score plot on ELg (a); LDA discriminating power plot on ELg (b); PCA-LDA score plot on STr (c); LDA discriminating power plot on STr (d).

The classification results of the PCA-LDA models by plum variety are summarised in Table 31 and Table 32, detailing the model calibration and validation accuracies. The classification accuracies for plums varied as well according to measurement location and variety. The average correct classifications during model validation were between 60.1 - 70.7% for the EL variety, and between 58.7 - 68.0% for the ST variety. Misclassification typically occurred at adjacent ripeness levels. There was no misclassification between the two previously observed large ripeness clusters. In addition to this, wavelengths that played a significant role in discrimination among sample groups were identified based on their discriminating power. These modelling results based on the data of ELg and STr are presented in Figure 23b and Figure 23d, and the corresponding wavelengths are the following:

- **ELg**: 1107.1, 1150.7, 1396.3, 1430.3, 1486.3, 1507.5, 1567.9 nm;
- **STr**: 1000.5, 1076.5, 1120.5, 1163.9, 1210.3, 1254.8, 1306.6, 1403.0, 1430.3, 1457.4, 1486.3, 1522.2, 1607.6 nm.

Similarly, to our studies, Fodor et al. (2023) also investigated the applicability of the NIR technique for EL and ST plums to classify fruits classified as immature and ripe based on their SSC, TA and maturity index. The classification models they used (e.g., LDA, MDA, QDA) distinguished between the two sample groups with an accuracy of 100% in all cases. A sharp separation of plums by ripeness was also observed in our results, even though we applied a different approach for the preliminary assessment of fruit ripeness.

The PLSR models for predicting various quality characteristics of plums were also constructed separately based on spectra collected from both mature and immature, as well as from both sides of the cherries, respectively. The accuracies obtained during model calibration and validation is summarised in Table 33 and Table 34. The accuracy of predicting various physical and compositional characteristics was dependent on the plum variety and the location of the spectral measurements. For plums as well, the best predictions were found for characteristics that either clearly increased or decreased with ripening. For both plum varieties, the most accurate models were obtained for predicting colour properties, soluble solids an acidity.

Figure 24 shows the best model fits found for the EL variety. The prediction of SSC was achieved with a maximal R^2 of 0.97 - 0.95 and RMSE of 0.32 - 0.41% brix The prediction of TA was achieved with an R^2 of 0.97 - 0.95 and RMSE of 0.58 - 0.74 mg/ g. The prediction of average b* was achieved with an R^2 of 0.92 - 0.88 and RMSE of 2.40 - 2.84 during calibration and validation, respectively. The regression vectors showcasing the wavelengths that played a crucial role in the fittings of the selected models are the following:

- **SSC (ELg)**: 1006.8, 1020.6, 1041.8, 1139.9, 1210.3, 1308.9, 1353.0, 1384.2, 1430.3, 1498.0, 1564.8 nm;
- **TA (ELg)**: 1016.8, 1069.1, 1139.9, 1177.1, 1249.0, 1296.3, 1353.0, 1393.0, 1420.5, 1454.2, 1481.0, 1495.8, 1542.0, 1593.4 nm;

- **b* average (ELr)**: 985.3, 1014.3, 1072.8, 1139.9, 1190.2, 1281.4, 1347.4, 1384.2, 1418.3, 1454.2, 1495.8, 1535.8, 1585.3 nm.

Figure 25 shows the best model fits found for the ST variety. The prediction of SSC was achieved with a maximal R^2 of 0.93 - 0.86 and RMSE of 0.40 - 0.55% brix The prediction of TA was achieved with an R^2 of 0.94 - 0.90 and RMSE of 0.52 - 0.66 mg/ g. The prediction of average L* was achieved with an R^2 of 0.86 - 0.82 and RMSE of 2.75 - 3.12 during calibration and validation, respectively. The regression vectors showcasing the wavelengths that played a crucial role in the fittings of the selected models are the following:

- **SSC (STg)**: 982.8, 1031.8, 1082.6, 1130.2, 1169.9, 1210.3, 1308.9, 1331.6, 1353.0, 1380.9, 1408.5, 1432.5, 1486.3, 1519.1, 1559.6, 1582.2, 1607.6 nm;
- **TA (STr)**: 985.3, 1076.5, 1139.9, 1199.7, 1287.1, 1347.4, 1408.5, 1439.0, 1450.9, 1498.0, 1582.2, 1635.7 nm;
- **L* average (ST)**: 1014.3, 1069.1, 1130.2, 1196.1, 1274.5, 1340.6, 1380.9, 1418.3, 1459.5, 1489.5, 1533.7, 1607.6, 1615.6 nm.

Fodor et al. (2023) have also determined the accuracy with which DMC, SSC and TA could be predicted in "Elena" and "Stanley" plums after applying different combined spectral pre-treatments. The authors could predict DMC with an Rcv^2 of 0.86 and RMSEcv of 0.66% m/m, SSC with an Rcv^2 of 0.95 and RMSEcv of 0.72% brix, and TA with an Rcv^2 of 0.95 and RMSEcv of 0.07 mg/g. Louw and Theron (2010) also used an FT-NIR reflectance spectroscopy (800–2700 nm) to assess the predictability of weight, firmness, SSC, TA and MI in "Pioneer", "Laetitia", "Angeleno" and multi-cultivar plums harvested throughout 7 weeks of ripening period over two seasons (2007, 2008). Regarding the intrinsic quality traits, the authors reported varying validation accuracies for SSC (R^2 = 0.82–0.96; RMSEp = 0.45–0.61% brix), TA (R^2 = 0.61 - 0.83; RMSEp = 0.11 - 0.19% m/m), and MI (R^2 = 0.72 - 0.89; RMSEp = 0.61 - 1.59). It was also found that despite the multi-cultivar models outperformed the single-cultivar models on R^2 values, they had higher prediction errors. The models are nevertheless robust in terms of seasonality and sample collection period. Costa and de Lima (2013) investigated the effectiveness of the NIR spectroscopy when predicting SSC and pH in European and Japanese plums. After combined spectral pre-treatments, including smoothing and msc as well as various variable selection methods, the authors found the best model fit for SSC when variable selection was not used (Rp^2 = 0.95; RMSEp = 0.45% brix), while for pH when GA was applied prior PLSR (Rp^2 = 0.90; RMSEp = 0.07).

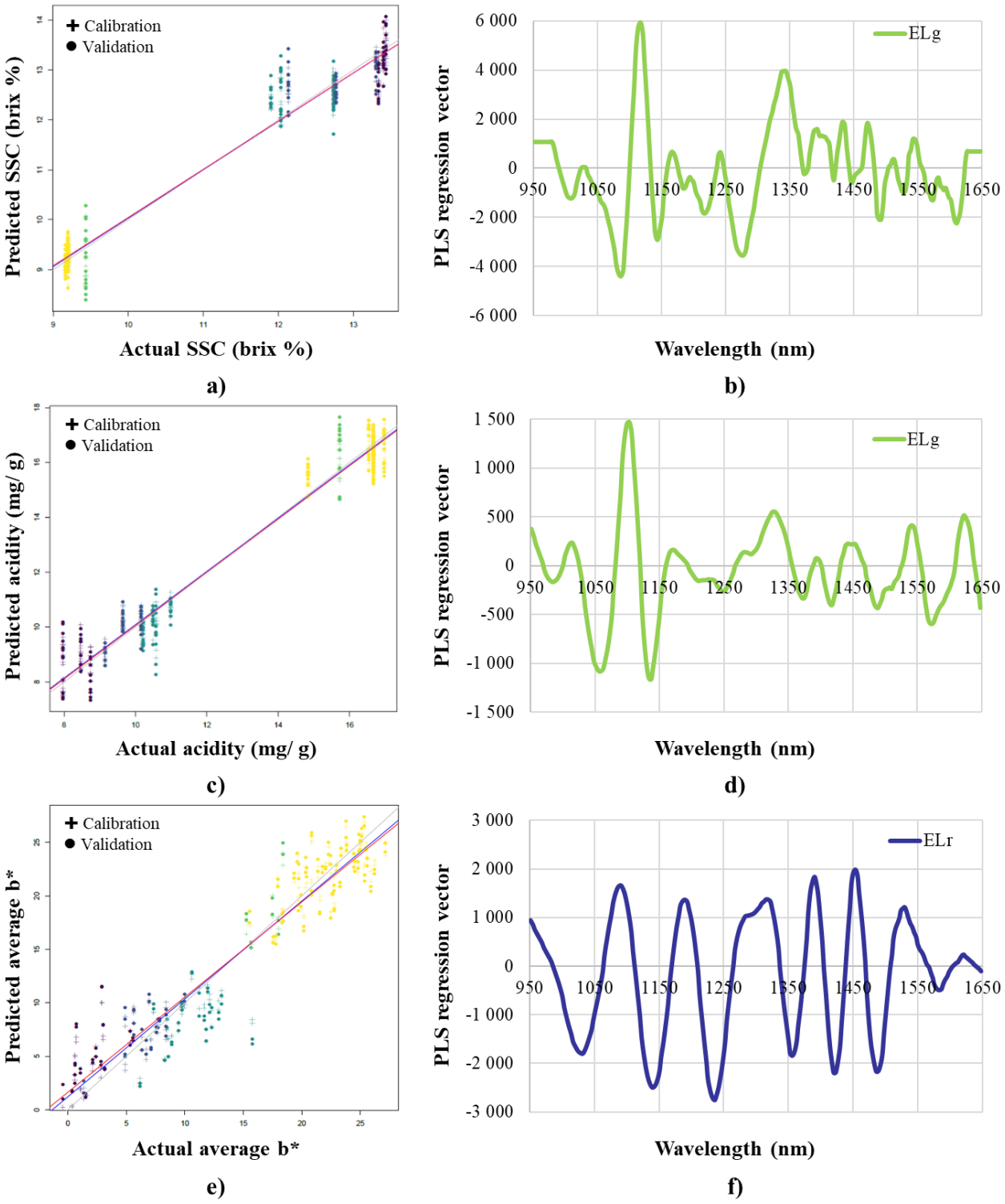

Figure 24. PLSR prediction results for certain quality traits of EL plums of different ripeness: Y-fit of SSC prediction (a); regression vectors of SSC prediction (b); Y-fit of acidity prediction (c); regression vectors of acidity prediction (d); Y-fit of average L* prediction (e); regression vectors of average L* prediction (f).

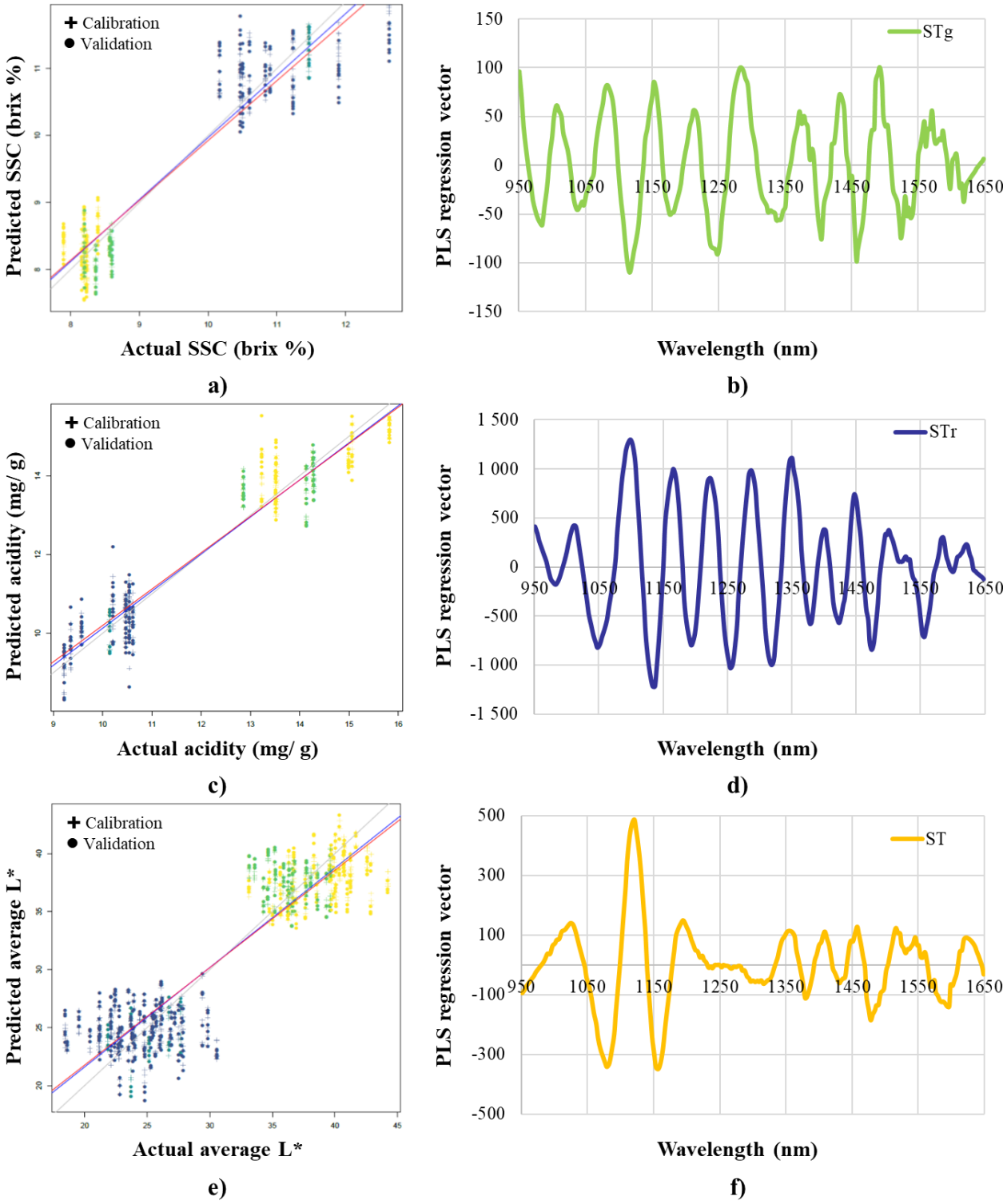

Figure 25. PLSR prediction results for certain quality traits of ST plums of different ripeness: Y-fit of SSC prediction (a); regression vectors of SSC prediction (b); Y-fit of acidity prediction (c); regression vectors of acidity prediction (d); Y-fit of average L* prediction (e); regression vectors of average L* prediction (f).

Prominent wavelengths obtained as a result of the PCA, PCA-LDA and PLSR models built on NIR spectral data of plums of different ripeness were summarised. Taking into account the most contributing wavelengths of the two studied varieties together, Figure 26 presents the absorption bands of successful chemometric modelling with their approximate frequency values.

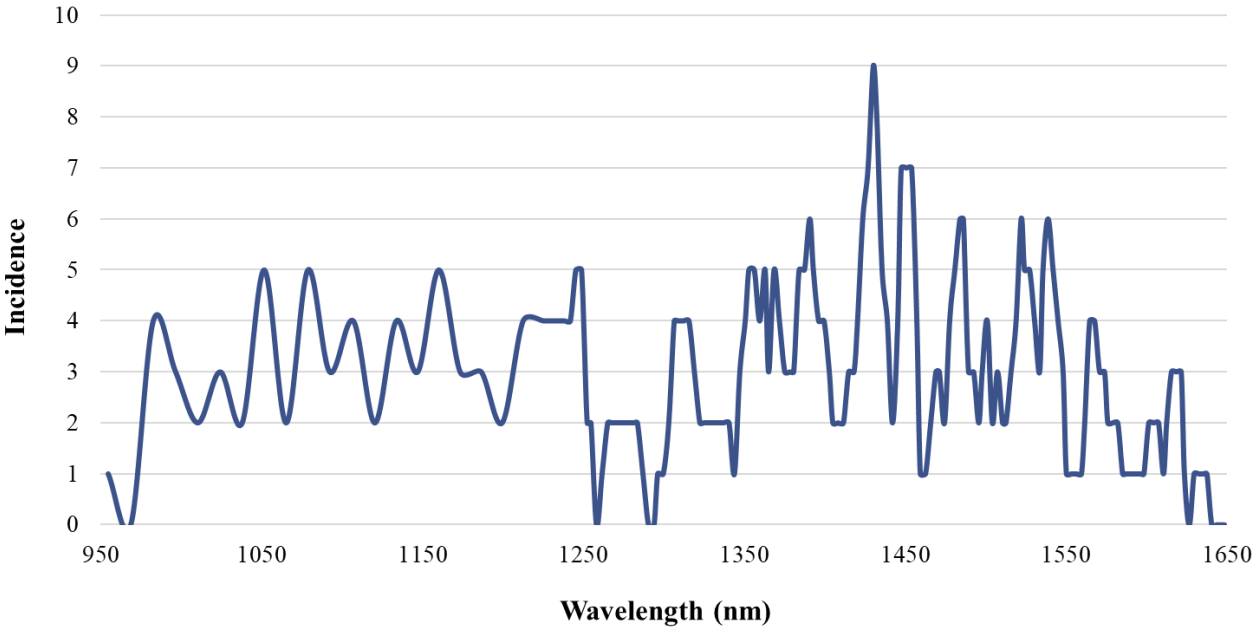

Figure 26. Absorbance bands frequently observed in chemometric modelling results of plum ripening with hand-held NIR spectrometer.

5.2. Detection of *Monilinia* contamination on stone fruits based on spectral characteristics

This subsection summarises the effectiveness of using a hand-held NIR device and hyperspectral image processing to distinguish between differently infected and stored sour cherries and plums. The findings also demonstrated the potential for early detection of spoilage caused by *Monilinia*. The results in this topic are discussed in two separate chapters because, although the fruit samples were prepared in the same way for both instruments, the analyses were conducted on different sets of samples.

5.2.1. Detection results with a hand-held NIR spectrometer

Investigation results on sour cherries

Figure 65 illustrates the spectra obtained with a hand-held NIR spectrometer for cherries that were prepared and stored under different conditions. For the EB variety, the spectra showed significant overlap, indicating minimal differentiation based on storage conditions. In contrast, for the UF variety, a trend was observed: the higher the storage temperature and the more injured the sample, the lower the absorbances as storage progressed.

The smoothing and msc correction performed on the NIR spectral data, followed by PCA analysis, confirmed the significant impact of storage conditions on the light absorption properties of the samples (Figure 27). For the two varieties, the first six components explained the 99% of the total variance in the data. Based on the PCA score plots (Figure 27a), for the EB variety, the greatest separation of treatment groups is observed along the first and third PCs. For the UF variety, the separation appears most clearly in the combination of the second and third PCs. The PCA loadings for the highlighted two PCs per variety (Figure 27b, c), the relevant wavelengths that best describe separation according to fruit handling are the following:

- **Érdő bőtermő (EB) sour cherries**
  PC 1 loading: 1069.1, 1190.2, 1372.0, 1450.9 nm;
  PC 3 loading: 1062.9, 1245.5, 1393.0, 1466.0, 1548.3 nm;

- **Újfehértói (UF) sour cherries**
  PC 2 loading: 1065.4, 1163.9, 1390.8 nm;
  PC 3 loading: 1051.7, 1238.5, 1290.6, 1396.3, 1459.5 nm.

The data, which had already been pre-processed with smoothing and msc correction for PCA, was subjected to SIMCA to determine the statistical significance of differences between infection methods and storage conditions for the two cherry varieties. Models were created for data filtered to the initial, middle, and final days of storage to analyse changes over time. Figure 28 and Figure 66 illustrate the distances between sample groups at specific storage days, showing the evolution of separations across time. For the EB variety, SIMCA models generally indicated increasing differences between groups as storage progressed (Figure 28a, c, e). Interestingly, the opposite trend was observed for the UF variety, where distinctions between sample groups tended to diminish over time (Figure 66a, c, e). On the one hand, this could imply that the storage conditions may have a different impact on the spectral characteristics of each variety, potentially due to

differences in their response to the infection methods or their inherent fruit properties. On the other hand, it is also possible that, over time, spectral data of a certain variety may be so scattered that they result in relatively large overlaps of calculated data points in multidimensional space.

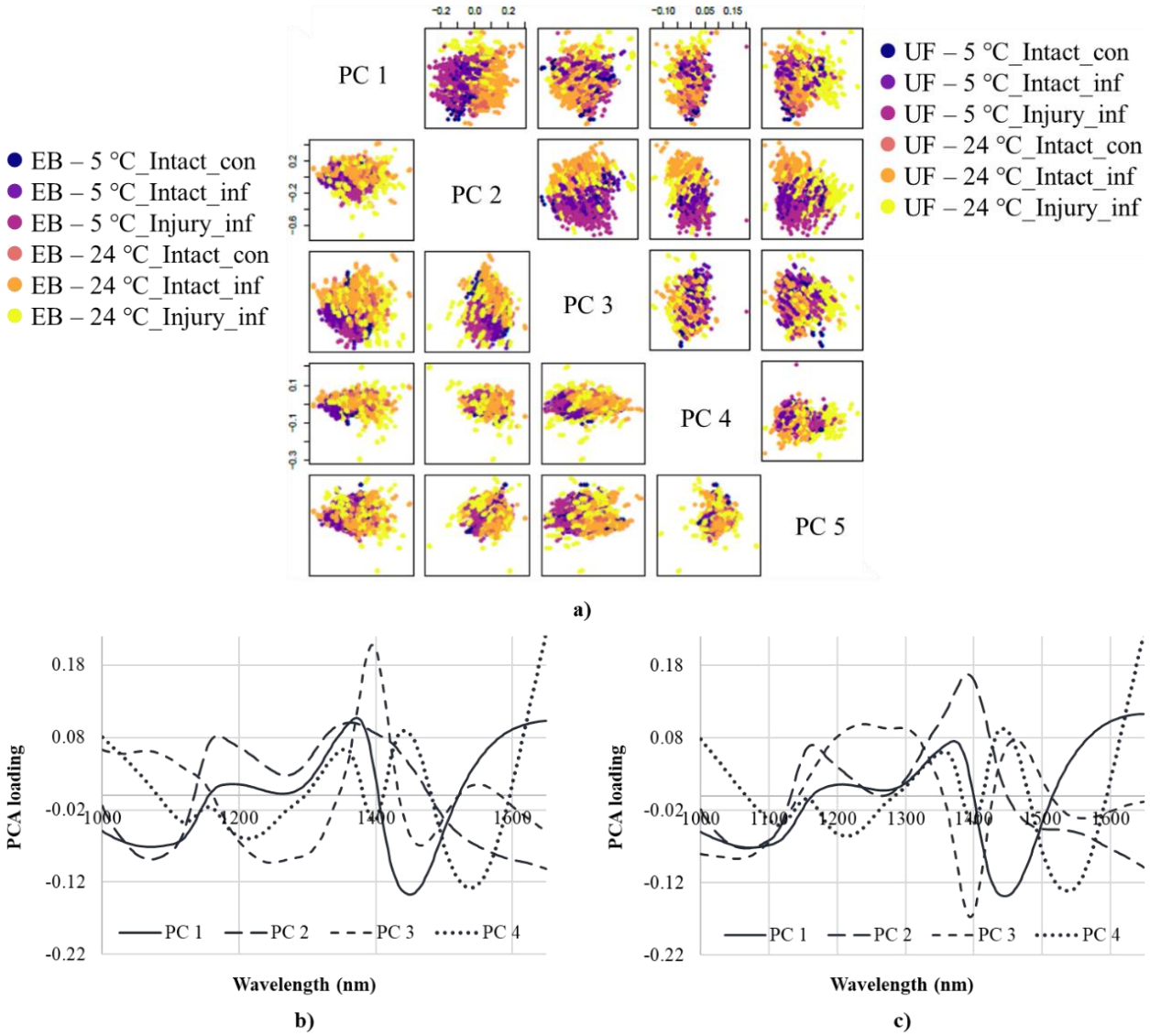

Figure 27. Preliminary PCA on the NIR spectra of sour cherries when colouring was based on fruit treatment (sgol-2-21-0, msc): PCA score plots of cherries treated in different ways (a); PCA loading plot of EB cherries (b); PCA loading plot of UF cherries (c).

The impact of storage temperature is evident, whereas the method of sample preparation is less so. Overall, no significant interclass distances were observed for any of the sample sets. This indicates that while storage temperature plays a crucial role in the storage of the cherries, the mode of preparation methods employed did not lead to detectable differences in the data analysed. During the SIMCA, prominent wavelengths contributing to the discriminations were also identified based on the discriminating power plots and are the following, by variety (Figure 28b, d, f, and Figure 66b, d, f):

- **EB sour cherries:**

  Day 1: 1082.6, 1147.1, 1238.5, 1340.6, 1380.9, 1427.1, 1474.6, 1548.3, 1635.7 nm;

  Day 4: 1090.0, 1156.7, 1258.3, 1294.0, 1390.8, 1420.5, 1477.8, 1579.1, 1587.3, 1637.7 nm;

  Day 7: 1034.3, 1139.9, 1232.6, 1423.8, 1486.3, 1559.6, 1632.7 nm;

- **UF sour cherries:**

  Day 1: 1078.9, 1143.5, 1249.0, 1340.6, 1423.8, 1469.2, 1538.9, 1626.7 nm;

  Day 4: 1045.5, 1143.5, 1252.5, 1378.6, 1420.5, 1471.3, 1559.6, 1629.7 nm;

  Day 7: 1034.3, 1103.5, 1236.1, 1303.2, 1384.2, 1427.1, 1459.5, 1522.2, 1590.4.

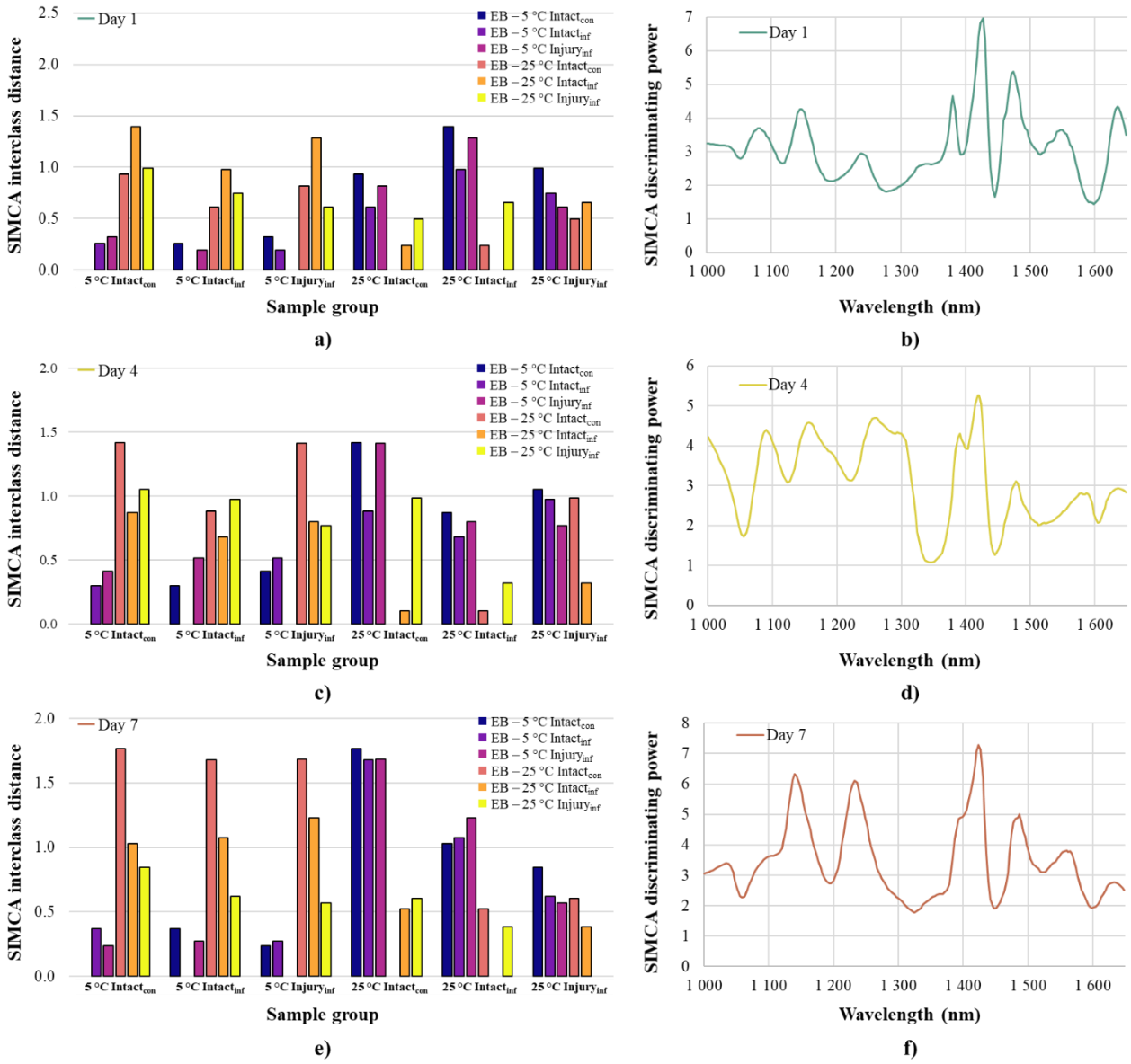

Figure 28. SIMCA on NIR spectra of EB cherries when discrimination was based on fruit treatment on certain storage days (sgol-2-21-0, msc): SIMCA interclass distances on the 1st day of storage (a); SIMCA discrimination power plot on the 1st day of storage (b); SIMCA interclass distances on the 4th day of storage (c); SIMCA discrimination power plot on the 4th day of storage (d); SIMCA interclass distances on the 7th day of storage (e); SIMCA discrimination power plot on the 7th day of storage (f).

As a supervised classification, spectral pre-treatment and NrPC-optimised LDA modelling was used to determine the accuracy with which the initial *Monilinia* conidium concentration can be determined based on the NIR spectra of sour cherries. For this classification, spectra recorded the day after inoculation were utilized. These spectra were further filtered based on sample preparation and storage conditions. This step was necessary because storage of the fruit under controlled environmental conditions started immediately after inoculation and we endeavoured to reduce the impact of environmental factors during the modelling.

In the case of sour cherries, the classification was for a total of four different levels of conidial contamination. Table 35 and Table 36 summarise the classification performance regarding the initial conidial contamination of EB and UF cherries, respectively, and show quite a large variability in the classification accuracies. For the samples stored under refrigerated conditions, the average correct classification rates were between 63.1 - 85.1% during calibration and between 30.5 - 42.0% during validation. For the samples stored at room temperature, the average correct classification rates during calibration were between 58.2 - 75.4%, while during validation, they ranged from 23.5 to 31.5%. Overall, the classification of samples stored in the refrigerator was slightly more accurate. The classification results are supported by the PCA-LDA score plots shown in Figure 29, Figure 30 and Figure 67. In the form of LDA discriminanting power plots, the wavelengths that contributed in some way to the classification were also obtained.

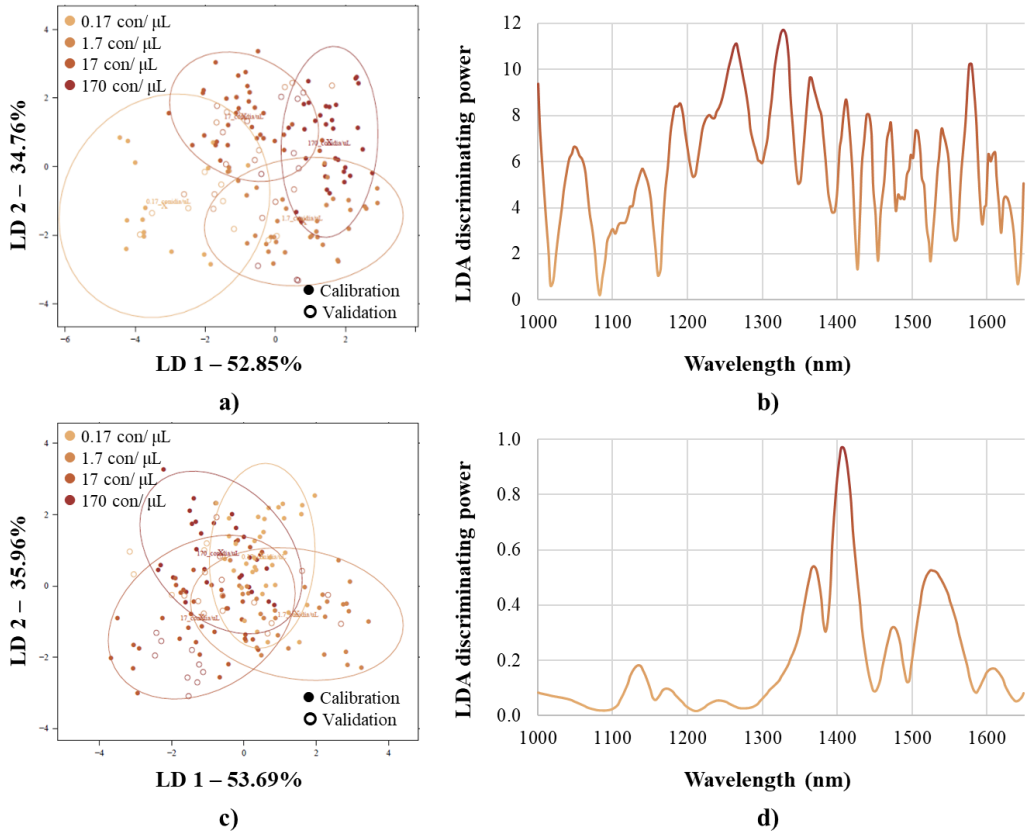

Figure 29. PCA-LDA on NIR spectra of UF cherries when classification was based on initial conidial contamination: PCA-LDA score plot of "5 °C Injury" samples (a); LDA discriminating power plot of "5 °C Injury" samples (b); PCA-LDA score plot of "5 °C Intact" samples (c); LDA discriminating power plot of "5 °C Intact" samples (d).

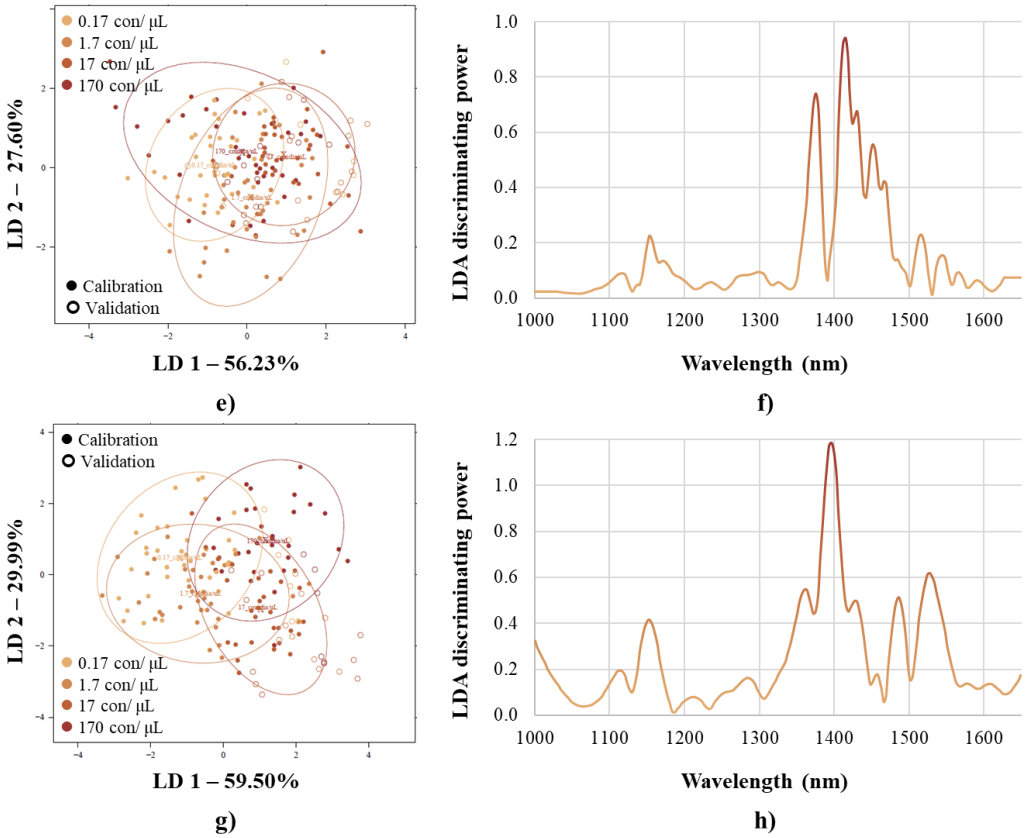

Figure 30. PCA-LDA on NIR spectra of UF cherries when classification was based on initial conidial contamination: PCA-LDA score plot of "25 °C Injury" samples (e); LDA discriminating power plot of "25 °C Injury" samples (f); PCA-LDA score plot of "25 °C Intact" samples (g); LDA discriminating power plot of "25 °C Intact" samples (h).

Due to the reproductive characteristics of the *M. fructigena* species involved in the experiments, only the samples infected through injury and stored at room temperature exhibited fungal activity. Table 13 shows, the specific fruits (i.e., parallelly prepared samples) that demonstrated the signs of *Monilinia*-caused decaying by sample group. This variation may be attributed to the structural and compositional inhomogeneity of the cherries. It was observed for each variety, that a higher initial concentration of conidia in the samples resulted in a greater likelihood and earlier manifestation of brown rot.

Table 13. Date of appearance of visible signs of infection in sour cherries analysed by the hand-held NIR device, inoculated with conidial suspension in various concentrations through injury and stored at 25 °C.

Variety	Initial conidium concentration	Sample 1	Sample 2	Sample 3	Sample 4	Sample 5
EB	~ 0.15 con./ µL	–	–	–	–	–
	~ 1.5 con./ µL	day 7	–	–	–	–
	~ 15 con./ µL	day 4	day 6	–	day 6	–
	~ 150 con./ µL	day 4	day 4	–	day 4	day 4
UF	~ 0.17 con./ µL	–	–	–	–	–
	~ 1.7 con./ µL	–	–	–	–	day 3
	~ 17 con./ µL	day 3	day 2	day 4	day 2	day 2
	~ 170 con./ µL	day 2	day 3	day 3	day 3	day 2

– There were no clear signs of *Monilinia* activity in these samples

It was considered important to examine the spectral trend of samples showing signs of brown rot on different days of storage. For this, optimised PCA-LDA modelling was employed using only the spectra of those samples that exhibited signs of decay during the 7-day long storage. Prior modelling, we sample specifically filtered the data corresponding to the day of appearance of the rot (marked as "day 0") ± 2-day interval and used this information to develop the classification models. A day-wise separation is illustrated in Figure 31 showing a semi-circular separation trend for the EB variety. Figure 31b and Figure 31d illustrate the discriminating power, the wavelengths that significantly contributed to highlight the mentioned trend.

- **EB sour cherries**
  1048.0, 1130.2, 1229.1, 1290.6, 1322.5, 1359.7, 1390.8, 1415.0, 1466.0, 1498.0, 1553.4, 1590.4, 1618.7 nm;
- **UF sour cherries**
  1072.8, 1147.1, 1199.7, 1258.3, 1350.7, 1384.2, 1418.3, 1450.9, 1495.8, 1556.5, 1601.5 nm.

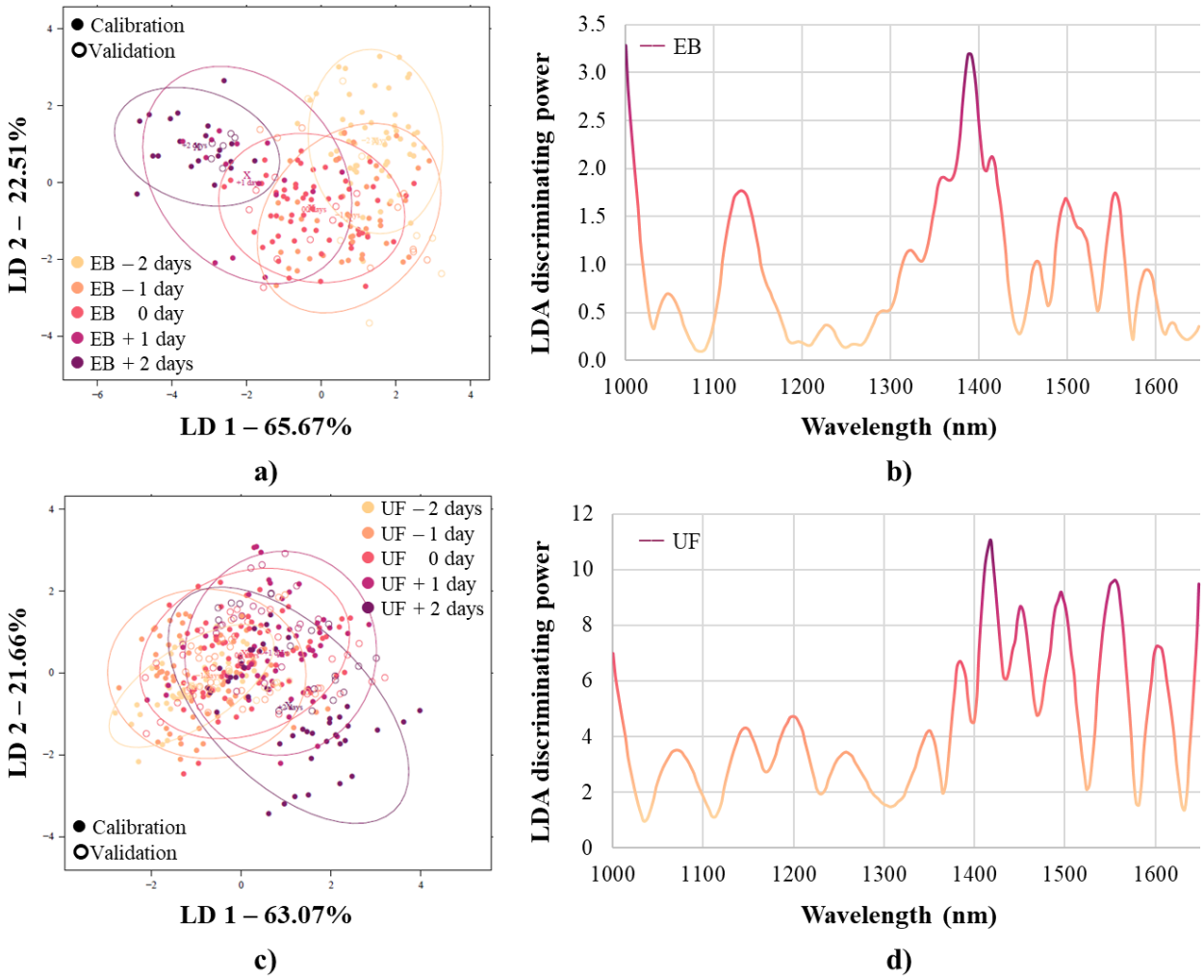

Figure 31. PCA-LDA on NIR spectra of sour cherries showing monilial activity when classification was based on the day of appearance of visible infection signs ± 2 days: PCA-LDA score plot of EB cherries (a); LDA discriminating power plot of EB cherries (b); PCA-LDA score plot of UF cherries (c); LDA discriminating power plot of UF cherries (d).

Table 37 summarises the average correct classification rates during model building and validation for the EB variety (77.2, 48.2%), and the UF variety (49.1, 31.7%), respectively. The results indicate that more accurate outcomes were characteristic of the EB variety. A higher degree of misclassification predominantly occurred between the data of adjacent days.

Prominent wavelengths obtained as a result of the PCA, SIMCA and PCA-LDA models built on the NIR spectral data of sour cherries infected with *Monilinia* conidia and stored under various conditions were summarised. Taking into account the most contributing wavelengths of the two studied varieties together, Figure 32 presents the absorption bands of successful chemometric modelling with their approximate frequency values.

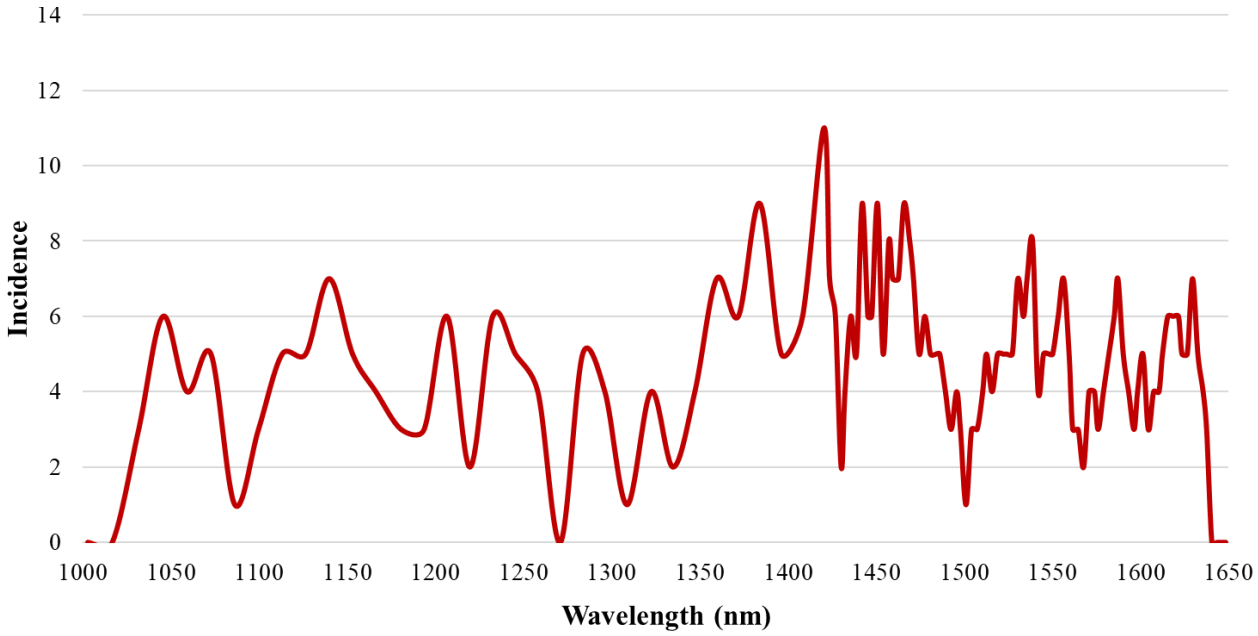

Figure 32. Absorbance bands frequently observed in chemometric modelling results of *Monilinia* detection on sour cherries with a hand-held NIR spectrometer.

Research on the inappropriate management of cherries was conducted by Shao et al. (2019) who combined Vis-NIR reflection spectroscopy and least square-support vector machine (LS-SVM). The authors reported classification accuracy of 93% when discriminating intact, slightly, and severely damaged cherries. Szabo et al. (2023) investigated the applicability of NIR spectroscopy to detect the effect of various storage conditions (packed as control or modified atmosphere; stored at 3 or 5 °C) on sour cherries. With SIMCA, the authors distinguised samples with apparent error rates between 0 and 0.5 during prediction regardless of fruit maturity.

Investigation results on plums

Figure 68 illustrates the spectra obtained with a hand-held NIR spectrometer for plums that were prepared and stored under different conditions. The spectra of TD and TP plums demonstrated significant overlap and scatter, indicating minimal differentiation based on storage conditions. The smoothing and msc correction performed on the NIR spectral data, followed by PCA analysis, confirmed the impact of storage conditions on the absorption properties of the samples (Figure 33). For the TD variety, the first five components, for the TP variety, the first four components explained the 99% of the total variance in the data.

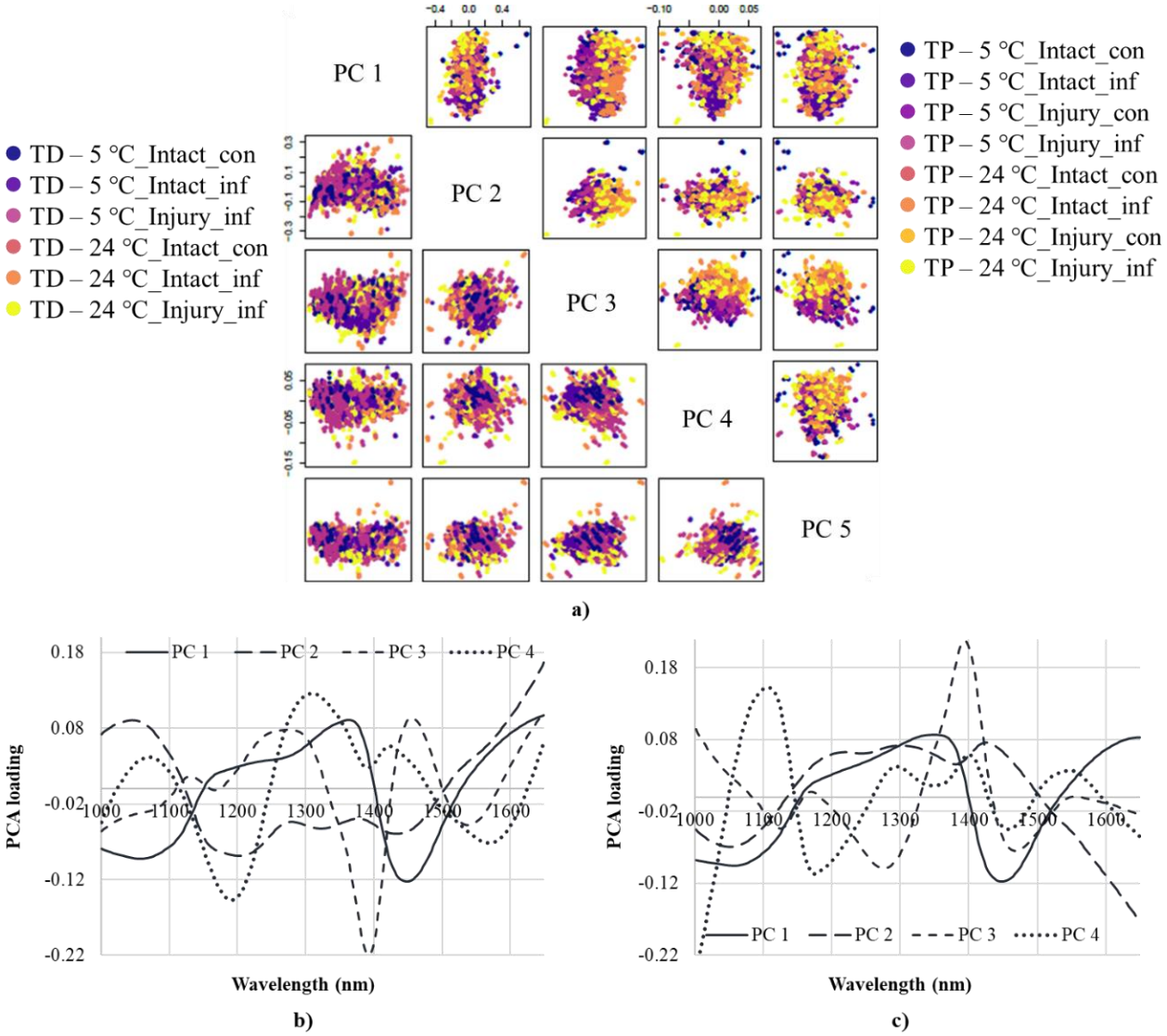

Figure 33. Preliminary PCA on the NIR spectra of plums when colouring was based on fruit treatment (sgol-2-21-0, msc): PCA score plots of plums treated in different ways (a); PCA loading plot of TD plums (b); PCA loading plot of TP plums (c).

In the case of the TD variety, the PCA score plots indicate quite sparse results. In contrast, a more pronounced trend emerges for the TP variety, particularly along the third PC. This difference suggests that the TP variety exhibits more distinct patterns in the obtained spectral data, potentially making it easier to classify based on its spectral characteristics (Figure 33a). The PCA loadings

for the highlighted two PCs per variety (Figure 33b, c), the relevant wavelengths that best describe separation according to fruit handling are the following:

- **Topend (TD) plums**
  PC 1 loading: 1055.5, 1363.0, 1447.7 nm;
  PC 3 loading: 1130.2, 1274.5, 1393.0, 1454.2, 1535.8 nm;

- **Topoend plus (TP) plums**
  PC 2 loading: 1052.9, 1221.1, 1301.1, 1424.9 nm;
  PC 3 loading: 1125.4, 1275.8, 1395.3, 1470.2 nm.

The data, which had been pre-processed with smoothing and msc correction for PCA, was subjected to SIMCA to determine the statistical significance of differences between infection methods and storage conditions for the two plum varieties. Models were created for data filtered to the initial, middle, and final days of storage to analyse changes over time. Figure 34 and Figure 69 illustrate the distances between sample groups at specific storage days, showing the evolution of separations across time.

For the TD variety, SIMCA models based on recorded NIR spectra showed slight increasing differences between groups from day 1 to day 4, then moderation by day 7. (Figure 69a, c, e). Interestingly, in the case of the TP variety, the highest interclass distances were observed on the day 1. These interclass distances markedly decreased by the day 4, followed by a slight increase on day 7 (Figure 34a, c, e). These patterns suggest an initial clear separation in characteristics, which then diminished, possibly due to similar progression in the fruit's condition over time. The slight resurgence on day 7 might indicate changes in spoilage factors that led to renewed differentiation among the groups. The reduction in the distances between sample groups can mean that the spectra were significantly dispersed, meaning that the calculated data points overlap and thus less distant from each other in multidimensional space.

Unlike the spectra recorded for the sour cherries infected in different ways, the different storage conditions had a less pronounced effect on the plum sample set. This suggests that the plums physical characteristics were not as sensitive to temperature variation during storage. Overall, no significant interclass distances were observed for any of the evaluated datasets. During the SIMCA modelling, prominent wavelengths were also identified. These plots highlight the specific wavelengths contributing to the discrimination were also identified based on the discriminating power plots. The absorption bands showing the peaks are nearly coincident (Figure 34b, d, f, and Figure 69b, d, f):

- **TD plums**
  Day 1: 1062.9, 1173.5, 1274.5, 1384.2, 1427.1, 1481.0, 1535.8, 1635.7 nm;
  Day 4: 1045.5, 1126.6, 1212.7, 1277.9, 1368.6, 1405.2, 1469.2, 1585.3 nm;
  Day 7: 1045.5, 1122.9, 1166.3, 1238.5, 1277.9, 1363.0, 1405.2, 1447.7, 1474.6, 1522.2, 1610.6 nm

- **TP plums**

  Day 1: 1049.2, 1144.8, 1234.0, 1270.0, 1327.2, 1379.8, 1452.0, 1514.6, 1585.8, 1631.0 nm

  Day 4: 1021.7, 1108.4, 1125.4, 1250.3, 1388.7, 1473.4, 1496.8, 1511.5, 1585.8, 1596.9 nm;

  Day 7: 1021.7, 1042.9, 1074.0, 1121.8, 1288.5, 1395.3, 1461.6, 1488.3, 1566.4, 1577.7, 1600.0, 1628.0 nm

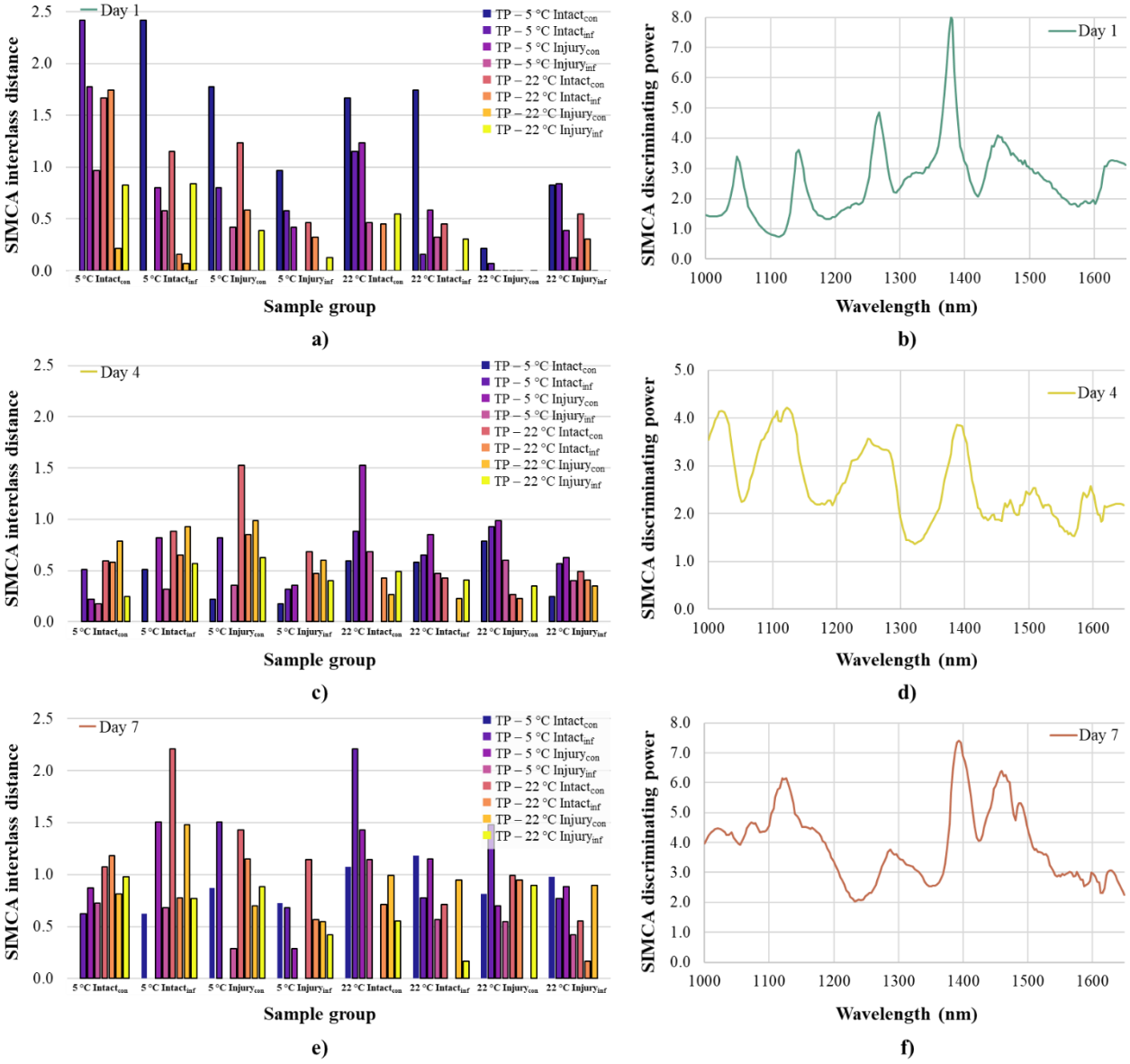

Figure 34. SIMCA on NIR spectra of TP plums when discrimination was based on fruit treatment on certain storage days (sgol-2-21-0, msc): SIMCA interclass distances on the 1st day of storage (a); SIMCA discrimination power plot on the 1st day of storage (b); SIMCA interclass distances on the 4th day of storage (c); SIMCA discrimination power plot on the 4th day of storage (d); SIMCA interclass distances on the 7th day of storage (e); SIMCA discrimination power plot on the 7th day of storage (f).

As a supervised classification, optimised PCA-LDA modelling was used to determine the accuracy with which the initial *Monilinia* conidium concentration could be determined from the NIR spectra of plums. For this purpose, spectra recorded the day after inoculation were utilized. These spectra

were further filtered according to sample preparation and storage conditions to reduce the impact of environmental factors during the modelling process as the fruit under controlled environmental conditions started immediately after inoculation.

In the case of plums, the classification was for a total of three different levels of conidial contamination. Table 38 and Table 39 summarise the classification performance regarding the initial conidial contamination of TD and TP plums, respectively. For the samples stored under refrigerated conditions, the average correct classification rates were between 74.2 - 92.9% during calibration and between 34.0 - 50.4% during validation. For the samples stored at room temperature, the average correct classification rates during calibration were between 77.8 - 89.4%, while during validation, they ranged from 39.2 to 51.6%. Overall, the classification of samples stored at room temperature was slightly more accurate.

The classification results are supported by the PCA-LDA score plots shown in Figure 35, Figure 36 and Figure 70. In the form of LDA discriminating power plots, the wavelengths that contributed in some way to the classification were also obtained and included in the figures.

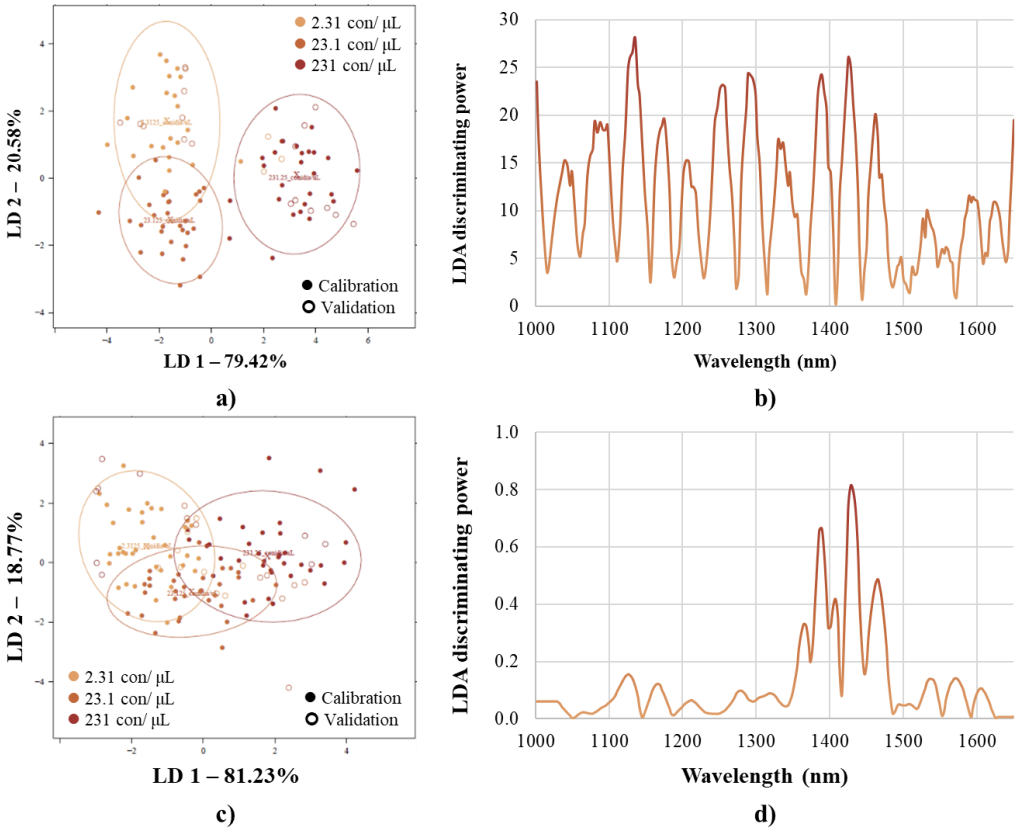

Figure 35. PCA-LDA on NIR spectra of TP plums when classification was based on initial conidial contamination: PCA-LDA score plot of "5 °C Injury" samples (a); LDA discriminating power plot of "5 °C Injury" samples (b); PCA-LDA score plot of "5 °C Intact" samples (c); LDA discriminating power plot of "5 °C Intact" samples (d).

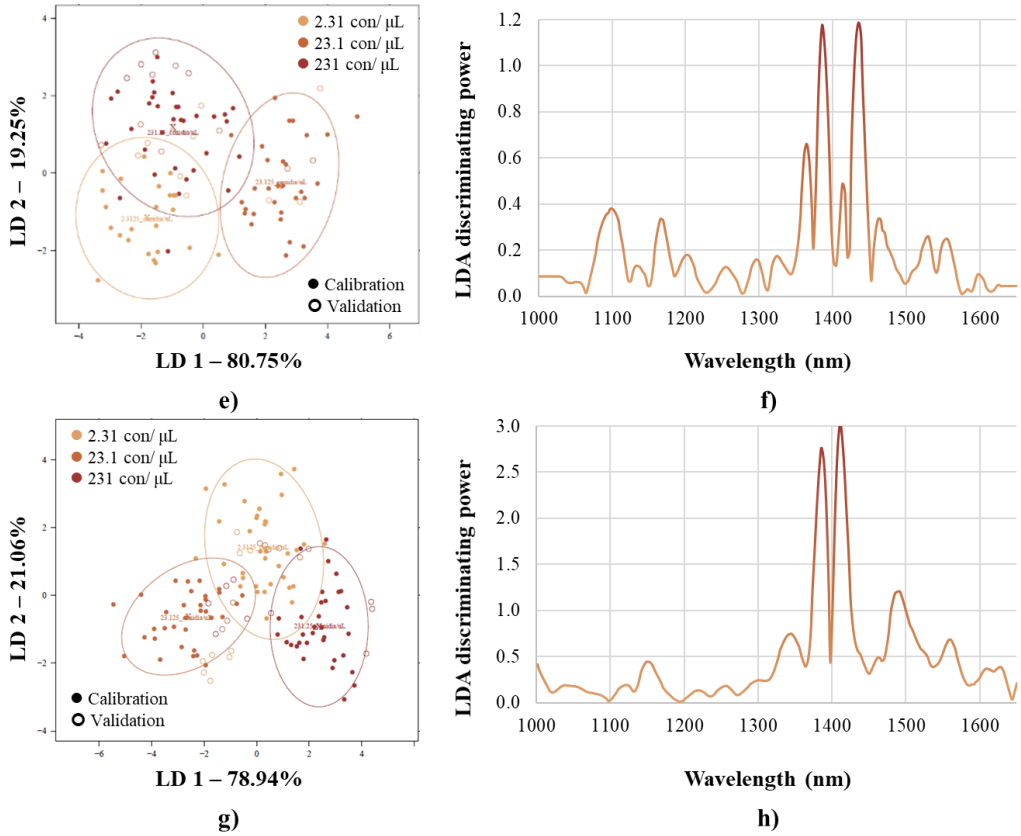

Figure 36. PCA-LDA on NIR spectra of TP plums when classification was based on initial conidial contamination: PCA-LDA score plot of "22 °C Injury" samples (e); LDA discriminating power plot of "22 °C Injury" samples (f); PCA-LDA score plot of "22 °C Intact" samples (g); LDA discriminating power plot of "22 °C Intact" samples (h).

It was also observed for plums that *Monilinia* activity was visible in samples that were inoculated via injury and stored at room temperature. The fungal proliferation was inhomogeneous, even in samples that were prepared the same way. This variability is fruit specifically summarised in Table 14. This variation can also be attributed to the structural and compositional inhomogeneity of the plums. Unlike the sour cherries, several plum samples showed signs of rotting even with relatively low initial conidium contamination. This difference can be partly attributed to the lower acidity of plums compared to sour cherries, and thus have more favourable conditions for fungal growth. The acidity in fruits often acts as a natural inhibitor to fungal proliferation.

Table 14. Date of appearance of visible signs of infection in plums analysed by a hand-held NIR device, inoculated with conidial suspension in different concentrations through injury and stored at 22 °C.

Variety	Initial conidium concentration	Sample 1	Sample 2	Sample 3	Sample 4	Sample 5
TD	~ 1.05 con./ µL	–	day 5	day 3	day 5	day 5
	~ 10.5 con./ µL	–	day 3	day 4	day 3	day 7
	~ 105 con./ µL	day 3	day 3	–	day 4	day 3
TP	~ 2.31 con./ µL	*day 8*	day 7	–	–	day 5
	~ 23.1 con./ µL	day 4	day 3	day 6	day 4	day 7
	~ 231 con./ µL	–	day 3	day 3	day 6	day 3

– There were no clear signs of *Monilinia* activity in these samples

For plums, we also considered it important to examine the spectral trend of samples showing signs of brown rot on different days of storage. For this, optimised PCA-LDA modelling was employed using only the spectra of those samples that exhibited signs of decay during the 7-day long storage. Prior modelling, we sample specifically filtered the data corresponding to the day of appearance of the rot (marked as "day 0") ± 2-day interval and used this information to develop the classification models. The day-wise separation is illustrated in Figure 37 revealing a semi-circular separation trend for the TD variety. Figure 37b and Figure 37d show the discriminating power, the wavelengths that significantly contributed to classify the mentioned trend.

- **TD plums**

  1072.8, 1107.1, 1133.8, 1160.3, 1242.0, 1312.3, 1353.0, 1399.7, 1423.8, 1469.2, 1492.7, 1515.9, 1545.1, 1576.1, 1604.6, 1629.7 nm;

- **TP plums**

  1066.5, 1114.5, 1155.6, 1250.3, 1279.3, 1311.3, 1371.0, 1392.0, 1424.9, 1458.4, 1545.9, 1600.0, 1635.9 nm.

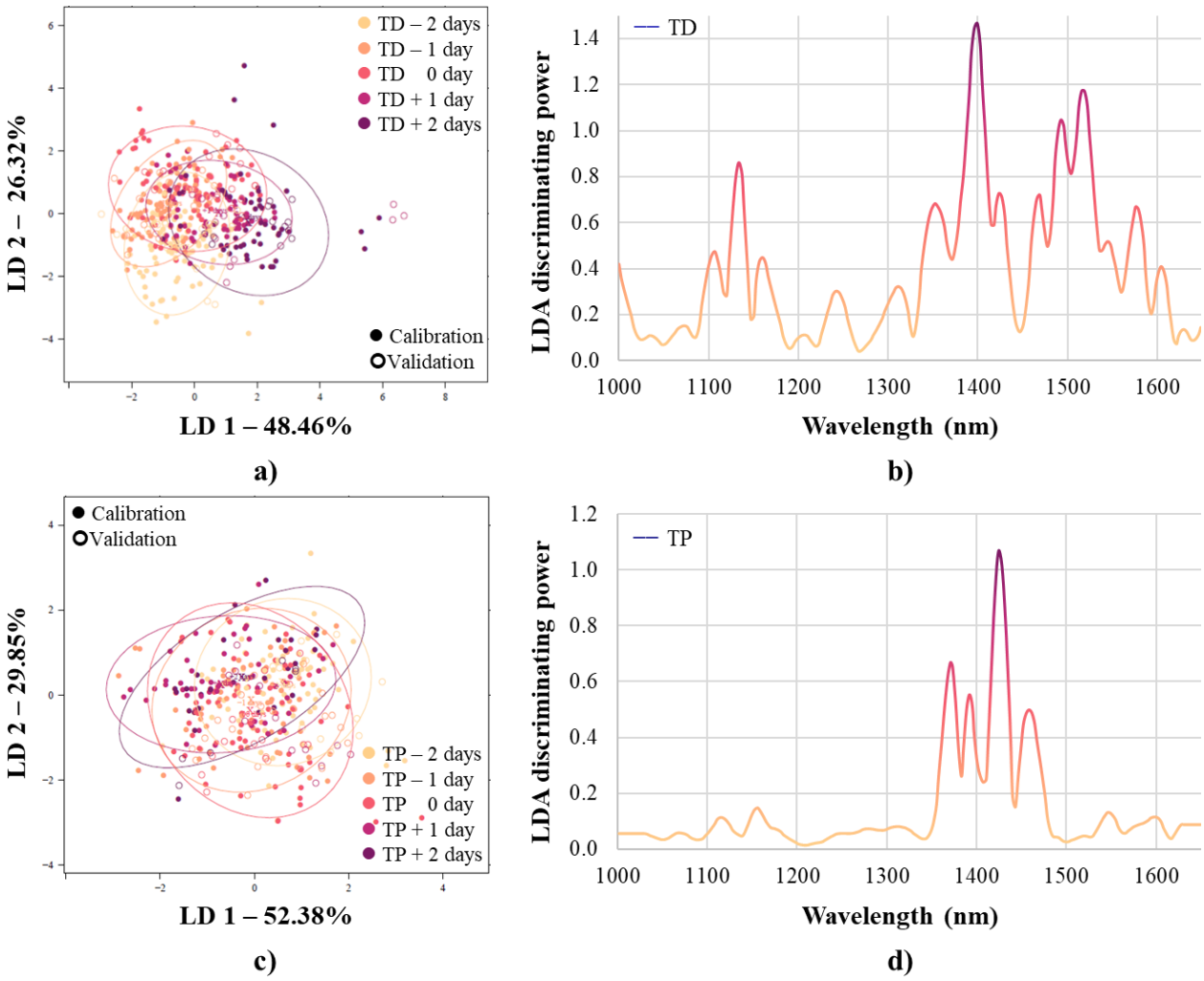

Figure 37. PCA-LDA on NIR spectra of plums showing monilial activity when classification was based on the day of appearance of visible infection signs ± 2 days: PCA-LDA plot of TD plums (a); LDA discriminating power plot of TD plums (b); PCA-LDA plot of TP plums (c); LDA discriminating power plot of TP plums (d).

Table 40 summarises the average correct classification rates during model building and validation for the TD (61.0, 49.6%) and TP variety (38.9, 25.3%), respectively. The overlap of the calculated data points, especially for the TP variety, is also reflected in the classification results. A high degree of misclassification mostly occurred between adjacent days for the TD variety.

Prominent wavelengths obtained as a result of the PCA, SIMCA and PCA-LDA models built on the NIR spectral data of plums infected with *Monilinia* conidia and stored under various environmental conditions were summarised. Taking into account the most contributing wavelengths of the two studied varieties together, Figure 38 presents the absorption bands of successful chemometric modelling with their approximate frequency values.

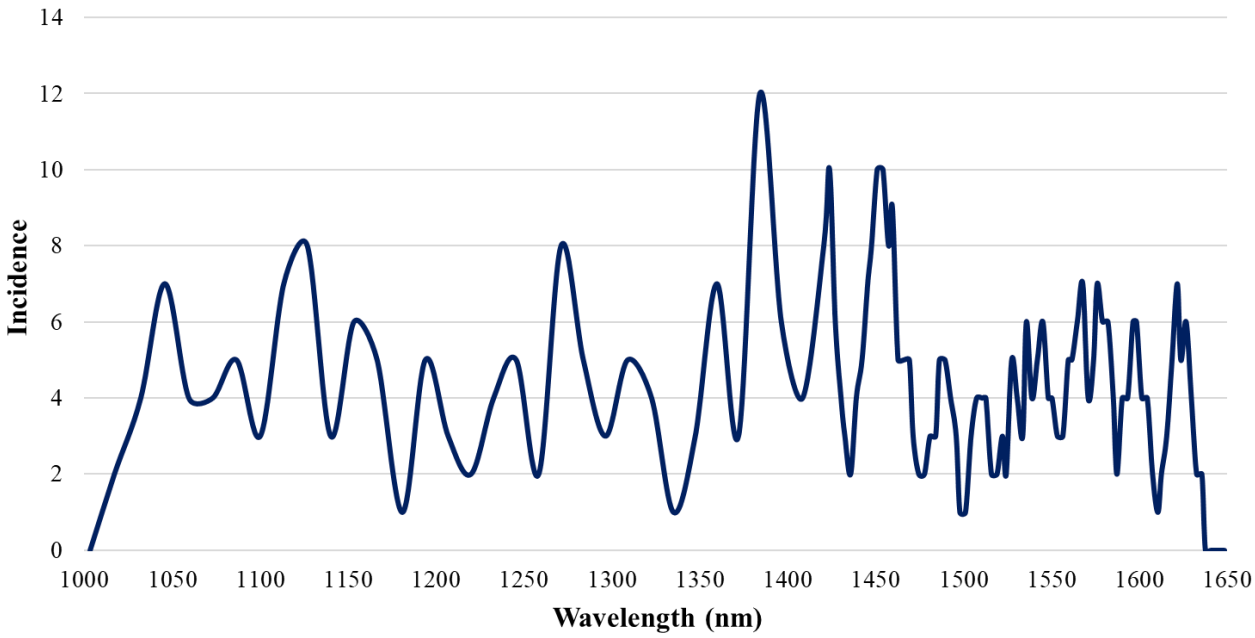

Figure 38. Absorbance bands frequently observed in chemometric modelling results of *Monilinia* detection on plums with hand-held NIR spectrometer.

Li et al. (2017) conducted research specifically related to the storage of plums with NIR technique to predict certain quality traits (e.g., firmness, flesh colour, SSC, TA, pH) in "Friar" plums. Their results showed that the flesh colour is be an important feature in post-ripening during low-temperature storage. Guo et al. (2022) employed various classification models (e.g., LDA, SVM, PLS, general LM) to determine storage time also for plums stored in cold environment, and achieved accuracy above 0.9 with LDA. Zhao et al. (2016) combined NIR spectroscopy with back propagation-ANN and could discriminate plums with browning flesh with 100% accuracy. Vitalis et al. (2021a, 2021b) also examined the effects of ambient and refrigerated storage on NIR spectral properties of plums infected with *M. fructigena* mycelium in different ways. The authors could indisputably detect samples that did not yet show visible signs of infection with PCA-LDA.

5.2.2. Detection results with a hyperspectral imaging

Investigation results on sour cherries

Figure 71 illustrates the spectra acquired with a benchtop hyperspectral imaging system from sour cherries prepared and stored under different conditions. In both varieties, overlapping, at the same time consistent trend emerges in the average spectra obtained on specific surfaces of the fruits. The raw and second derivative spectra potently demonstrate how deviations from optimal storage conditions manifest in the spectral properties.

The smoothing and msc correction performed on the HSI spectral data, followed by PCA analysis, confirmed the significant impact of storage conditions on the absorption properties of the samples (Figure 39). For the EB variety, the first three, for the UF variety, the first four PCs explained the 99% of the total variance in the data.

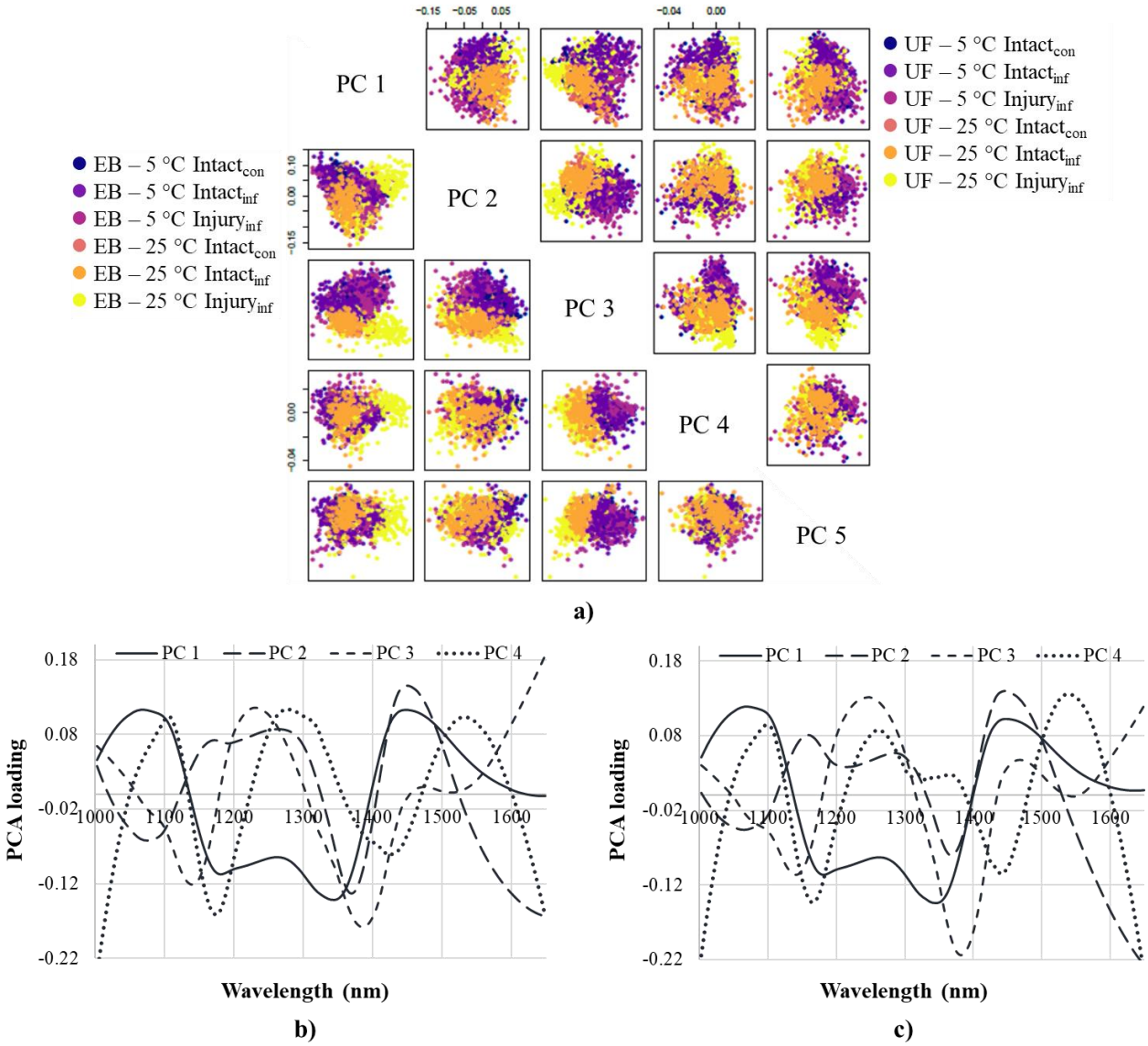

Figure 39. Preliminary PCA on the HSI spectra of sour cherries when colouring was based on fruit treatment (sgol-2-21-0, msc): PCA score plots of cherries treated in different ways (a); PCA loading plot of EB cherries (b); PCA loading plot of UF cherries (c).

Based on the PCA score plots (Figure 39a), for the EB variety, the greatest separation of treatment groups is observed along the first and third PCs, while for the UF variety, it was more evident along the second and third PCs. The PCA loadings for the highlighted two PCs per variety (Figure 39b, c), the relevant wavelengths that best describe separation according to fruit handling are the following:

- **Érdő bőtermő (EB) sour cherries**
  PC 1 loading: 1069.8, 1180.9, 1345.0, 1446.4 nm;
  PC 3 loading: 1137.4, 1229.2, 1383.7 nm;

- **Újfehértói (UF) sour cherries**
  PC 2 loading: 1065.0, 1156.7, 1287.1, 1369.2, 1446.4 nm;
  PC 3 loading: 1142.3, 1248.5, 1383.7, 1465.7 nm.

The data pre-treated for PCA was also subjected to SIMCA to determine the statistical significance of differences between infection methods and storage conditions for the two cherry varieties. Models were created for data filtered to the initial, intermediate, and final days of storage to analyse changes over time. Figure 40 and Figure 72 illustrate how the interclass distances evolved on specific storage days.

The SIMCA models based on HSI spectra of the EB variety showed nearly uniform differences around the middle of storage, however, the impact of the different storage conditions became more pronounced close to the end of storage (Figure 40a, c, e). The UF variety exhibited the same trend, though the interclass distances were smaller, indicating less pronounced differences between the groups (Figure 72a, c, e).

These results support those obtained during PCA, and that the samples analysed with HSI showed similar trends during controlled storage, however, no significant interclass distances were observed for any of the sample sets. It was confirmed that storage temperature plays a crucial role in the storage of the cherries, the mode of preparation methods employed did not lead to detectable differences During the SIMCA modelling, prominent wavelengths were also identified. These plots highlight the specific wavelengths that significantly contribute to the discrimination of the sample groups. The SIMCA discriminanting power plots illustrate this in Figure 40b, d, f for the EB variety, and Figure 72b, d, f for the UF variety, respectively.

- **EB sour cherries**
  Day 1: 1040.9, 1132.6, 1243.6, 1369.2, 1403.0, 1456.1, 1543.0, 1610.6 nm;
  Day 4: 1050.5, 1094.0, 1161.6, 1248.5, 1330.6, 1393.3, 1441.6, 1557.5, 1615.4 nm;
  Day 7: 1031.2, 1094.0, 1147.1, 1238.8, 1369.2, 1441.6, 1586.4 nm;

- **UF sour cherries**
  Day 1: 1045.7, 1132.6, 1238.8, 1253.3, 1354.7, 1388.5, 1446.4, 1523.7, 1615.4 nm;
  Day 3: 1036.0, 1132.6, 1224.3, 1238.8, 1330.6, 1378.8, 1431.9, 1465.7, 1586.4, 1620.2 nm;
  Day 7: 1031.2, 1127.8, 1234.0, 1374.0, 1446.4, 1518.8, 1591.3 nm.

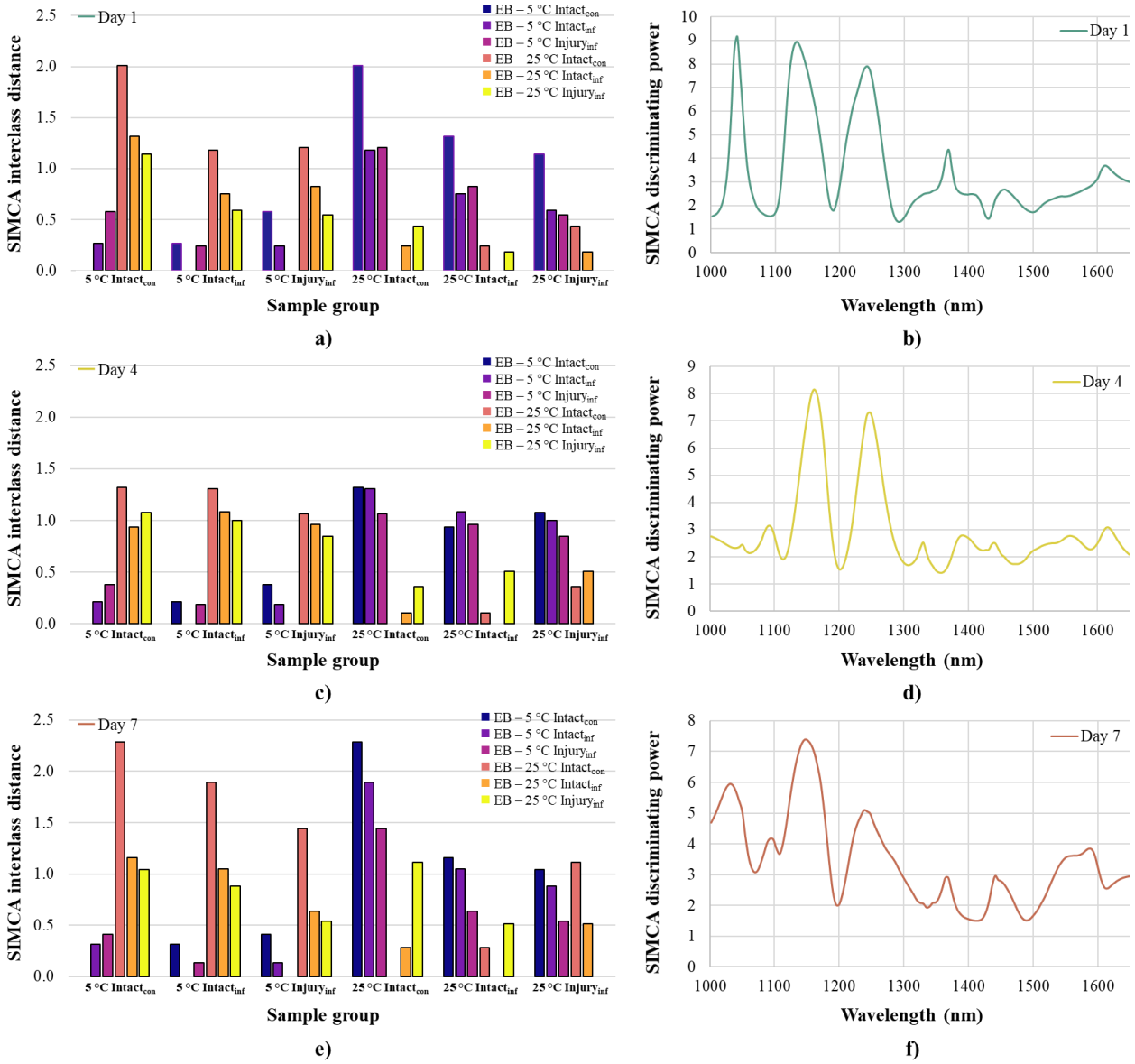

Figure 40. SIMCA on the HSI spectra of EB cherries when discrimination was based on fruit treatment on certain storage days (sgol-2-21-0, msc): SIMCA interclass distances on the 1st day of storage (a); SIMCA discrimination power plot on the 1st day of storage (b); SIMCA interclass distances on the 4th day of storage (c); SIMCA discrimination power plot on the 4th day of storage (d); SIMCA interclass distances on the 7th day of storage (e); SIMCA discrimination power plot on the 7th day of storage (f).

Optimised PCA-LDA modelling was used as supervised classification to determine the accuracy with which the initial *Monilinia* conidium concentration can be determined from the HSI spectra of sour cherries. For this classification, spectra recorded the day after inoculation were utilized. The spectra were further filtered according to mode of infection and storage conditions to reduce the impact of environmental factors during the modelling.

In the case of sour cherries, the classification was for a total of four different levels of conidial contamination. Table 41 and Table 42 summarise the classification performance regarding the initial conidial contamination of EB and UF cherries, respectively. For the samples stored under refrigerated conditions, the average correct classification rates were between 85.5 - 98.0% during calibration and between 33.1 - 53.3% during validation. For the samples stored at room

temperature, the average correct classification rates during calibration were between 61.6 - 89.1%, during validation, they ranged from 32.5 - 46.3%. The classification accuracy of the HSI was better than that of the data recorded with the hand-held NIR instrument.

The classification results are supported by the PCA-LDA score plots shown in Figure 41, Figure 42 and Figure 73. In the discriminant space bounded by LD 1 and LD 2, the data points (i.e., scores) representing the concentration levels of each suspension were less overlapped in contrast to the data recorded with the hand-held NIR device. In the form of LDA discriminanting power plots, the wavelengths that contributed in some way to the classification were also obtained.

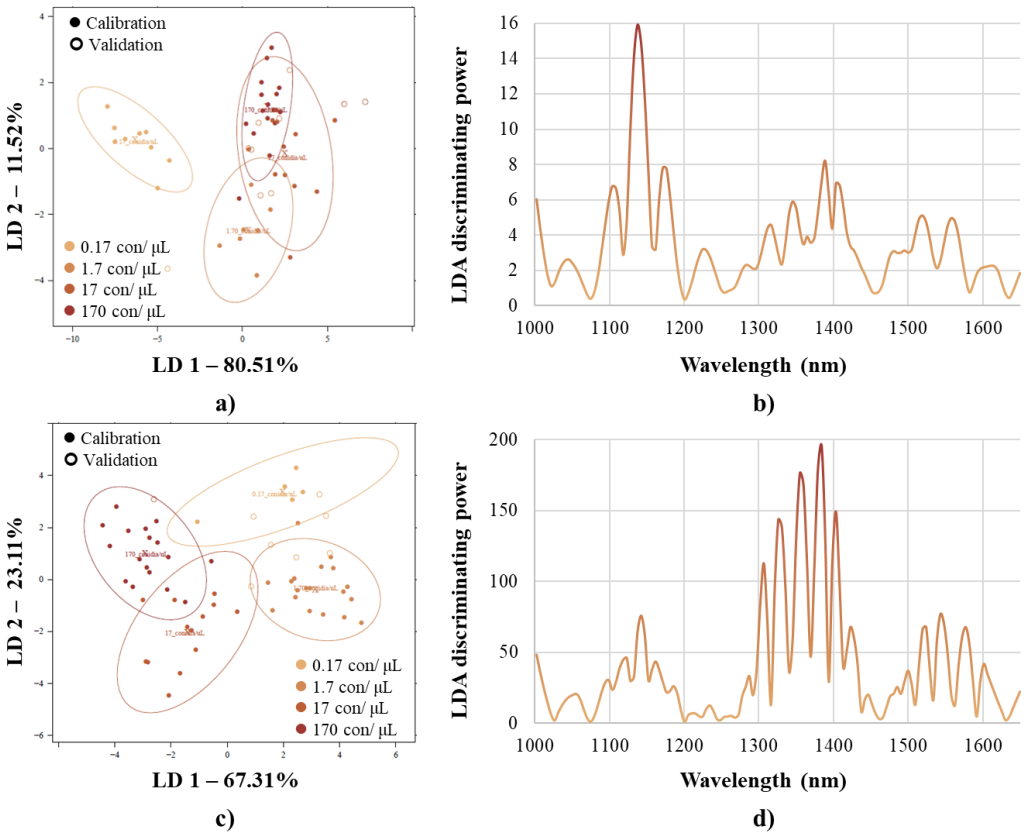

Figure 41. PCA-LDA on the HSI spectra of UF cherries when classification was based on initial conidial contamination: PCA-LDA score plot of "5 °C Injury" samples (a); LDA discriminating power plot of "5 °C Injury" samples (b); PCA-LDA score plot of "5 °C Intact" samples (c); LDA discriminating power plot of "5 °C Intact" samples (d).

In case of sour cherries analysed with HSI, it was also typical that *Monilinia* activity was visible in the samples that were inoculated via injury and stored at room temperature. It was also true for the cherry samples prepared for HSI measurements that fungal proliferation was also inhomogeneous, even for samples prepared in the same way, as shown in Table 15. Similar to the sour cherries examined with the hand-held NIR spectrometer, the EB samples exhibited more moderated *Monilinia* activity even for relatively high initial conidium concentration. This could be attributed to the less favourable physicochemical properties of this variety, which may not have supported the spread of the fungus. Such properties may include a more bounded tissue structure, higher acidity, or the presence of compounds with antioxidant properties in the fruits.

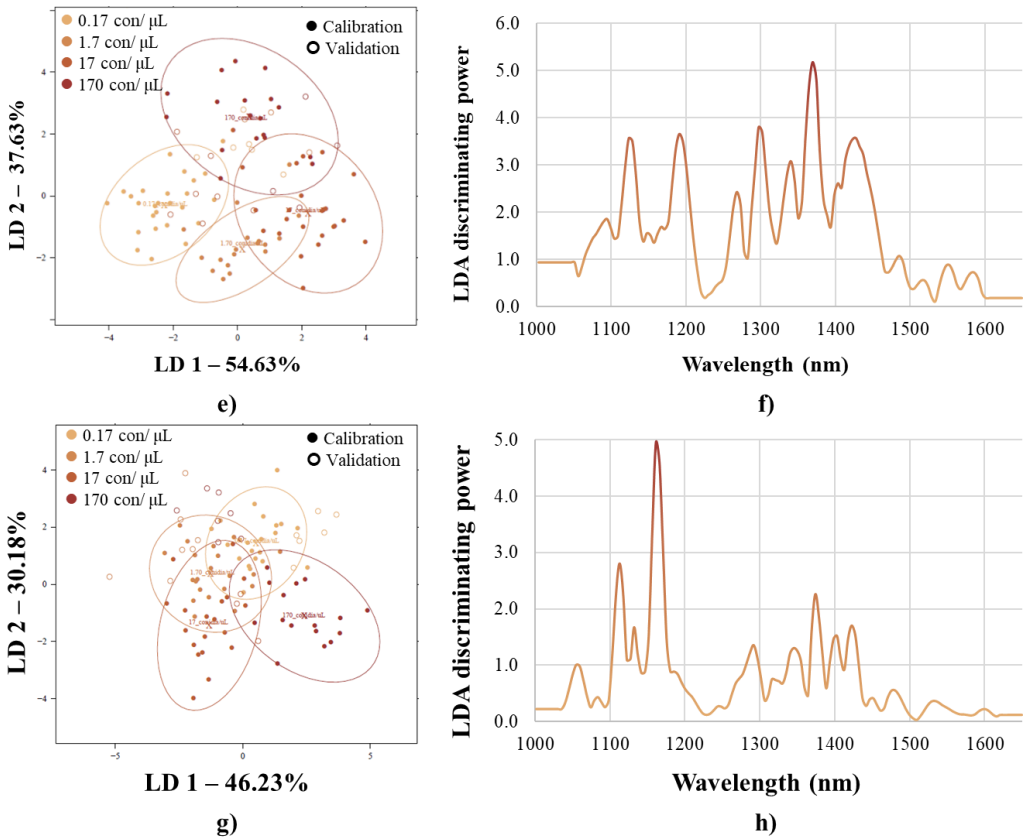

Figure 42. PCA-LDA on the HSI spectra of UF cherries when classification was based on initial conidial contamination: PCA-LDA score plot of "25 °C Injury" samples (e); LDA discriminating power plot of "25 °C Injury" samples (f); PCA-LDA score plot of "25 °C Intact" samples (g); LDA discriminating power plot of "25 °C Intact" samples (h).

It was considered essential to investigate the effectiveness of HSI in tracking the spectral variation of fruits in decay, quasi-independently of the day of storage when visible signs of infection appeared on the fruits. Optimised PCA-LDA was employed on specific data corresponding to samples that exhibited signs of decay during the 7-day long storage and the day of appearance of the rot (marked as "day 0") ± 2-day interval.

Table 15. Date of appearance of visible signs of *Monilinia* infection in sour cherries analysed by HSI, inoculated with conidial suspension of different concentrations through injury and stored at 25 °C.

Variety	Initial conidium concentration	Sample 1	Sample 2	Sample 3	Sample 4	Sample 5
EB	~ 0.15 con./ µL	–	–	–	–	–
	~ 1.5 con./ µL	–	–	–	–	–
	~ 15 con./ µL	day 4	–	day 4	–	–
	~ 150 con./ µL	day 2	day 4	day 3	day 3	day 6
UF	~ 0.17 con./ µL	–	–	–	–	–
	~ 1.7 con./ µL	–	–	–	–	–
	~ 17 con./ µL	day 5	day 5	day 5	day 5	day 5
	~ 170 con./ µL	day 5	day 2	day 2	day 3	day 5

– There were no clear signs of *Monilinia* activity in these samples

Table 43 summarises the classification accuracies during model building and validation for the EB variety (72.6, 25.9%) and for the UF variety (86.5, 57.4%), respectively. More accurate outcomes were characteristic of the UF variety, while there was significant misclassification to adjacent days for the EB samples. In the PCA-LDA score plots shown in Figure 43, a reversed V-shaped separation trend appears across the different days. The "0 day" data points, representing the samples that began showing signs of decay, are prominently noticeable in this separation. The dominant wavelengths of these specific analyses are shown in Figure 43b and Figure 43d, and listed below:

- **EB sour cherries**

  1065.0, 1108.5, 1147.1, 1166.4, 1267.8, 1301.6, 1349.9, 1374.0, 1412.6, 1441.6, 1470.6, 1543.0 1576.8 nm;

- **UF sour cherries**

  1060.2, 1113.3, 1132.6, 1147.1, 1166.4, 1263.0, 1296.8, 1330.6, 1359.5, 1378.8, 1407.8, 1431.9, 1480.2, 1538.2, 1596.1nm.

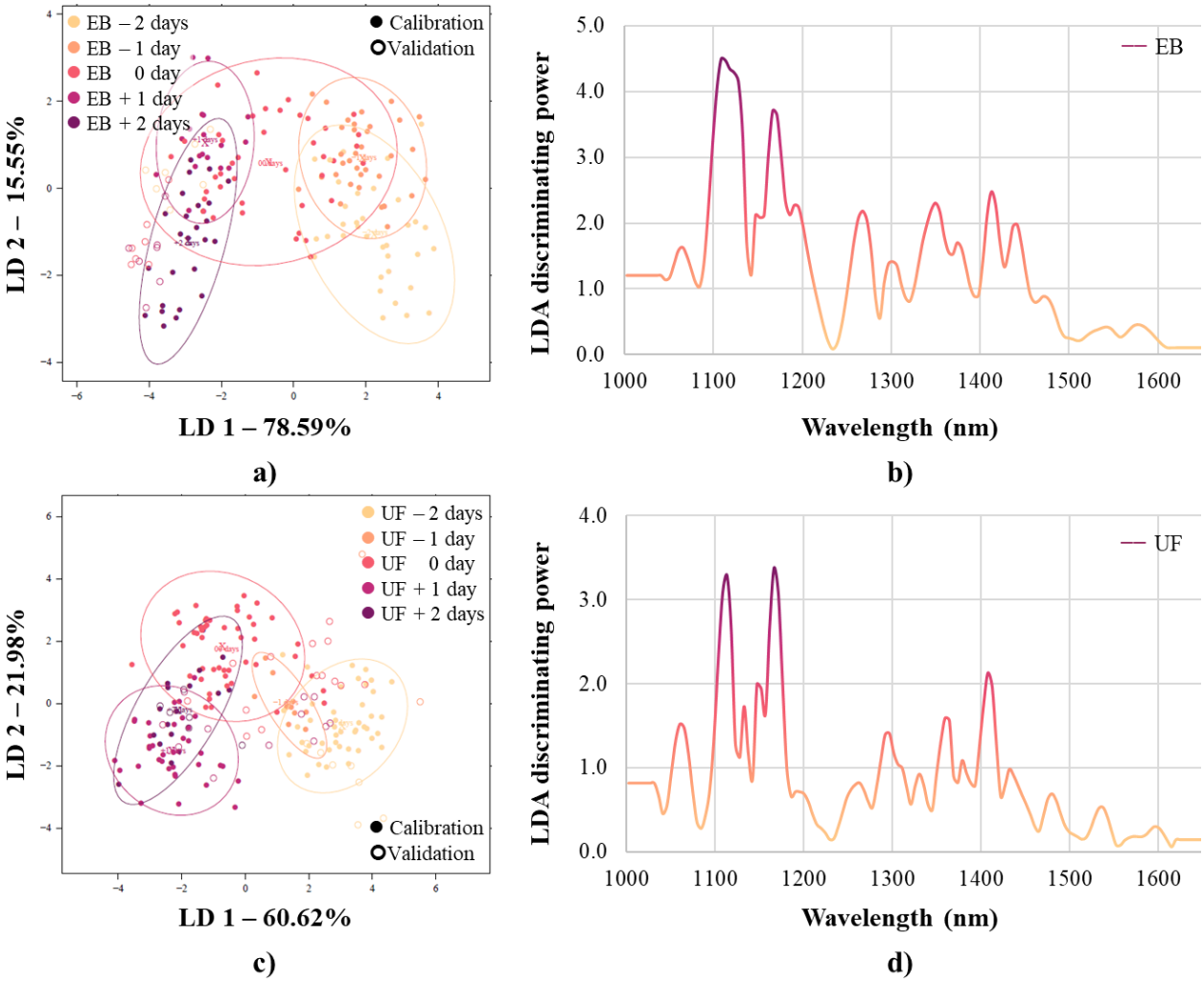

Figure 43. PCA-LDA on the HSI spectra of sour cherries showing monilial activity when classification was based on the day of appearance of visible infection signs ± 2 days: PCA-LDA score plot of EB cherries (a); LDA discriminating power plot of EB cherries (b); PCA-LDA score plot of UF cherries (c); LDA discriminating power plot of UF cherries (d).

Prominent wavelengths obtained as a result of the PCA, SIMCA and PCA-LDA models built on the hyperspectral data of sour cherries infected with *Monilinia* conidia and stored under various environmental conditions were summarised. Taking into account the most contributing wavelengths of the two studied varieties together, Figure 44 presents the absorption bands of successful chemometric modelling with their approximate frequency values.

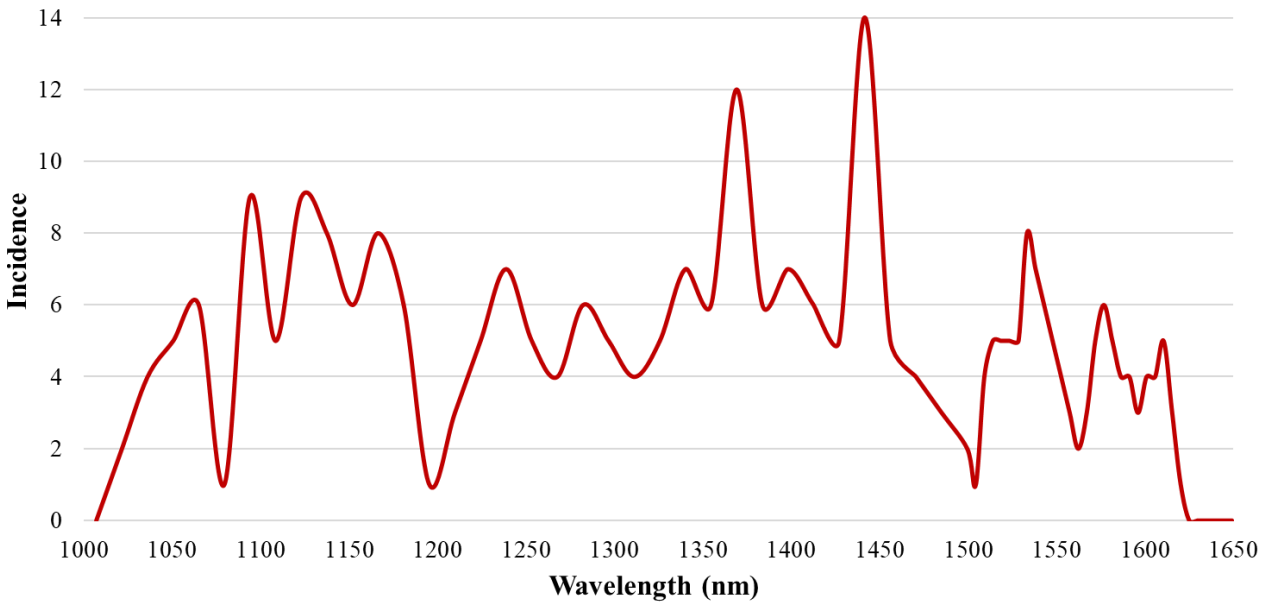

Figure 44. Absorbance bands frequently observed in chemometric modelling results of *Monilinia* detection on sour cherries with hyperspectral imaging.

There are relatively few examples in the literature of hyperspectral analysis of deterioration of intact cherries, however, also stone fruit peach is significant. Sun, Wei, et al. (2018) conducted experiments on peaches infected with *Botrytis cinerea*, *R. stolonifera* and *Colletotrichum acutatum*. The authors reported 82.5, 92.5 and 100% classification accuracies for slightly-decayed, moderately-decayed and severely-decayed samples, respectively, when combined hyperspectral image processing and deep belief network (DBN). To our knowledge, the first spectral *Monilinia* detection was performed by Liu et al. (2020), who could completely distinguish peaches with HIS-based PCA according to the degree of infection (acceptable, moldy, highly moldy), and achieved R^2 of 0.84 and RMSE of 0.78 when predicting fungal colony counts.

Investigation results on plums

Figure 45 illustrates the spectra acquired with a benchtop hyperspectral imaging system from plums prepared and stored under different conditions. In both varieties, overlapping, at the same time consistent trend emerges in the average spectra obtained on specific spatial areas of the fruits. The raw and second derivative spectra demonstrate indubitably how deviations from optimal storage conditions manifest in the spectral properties.

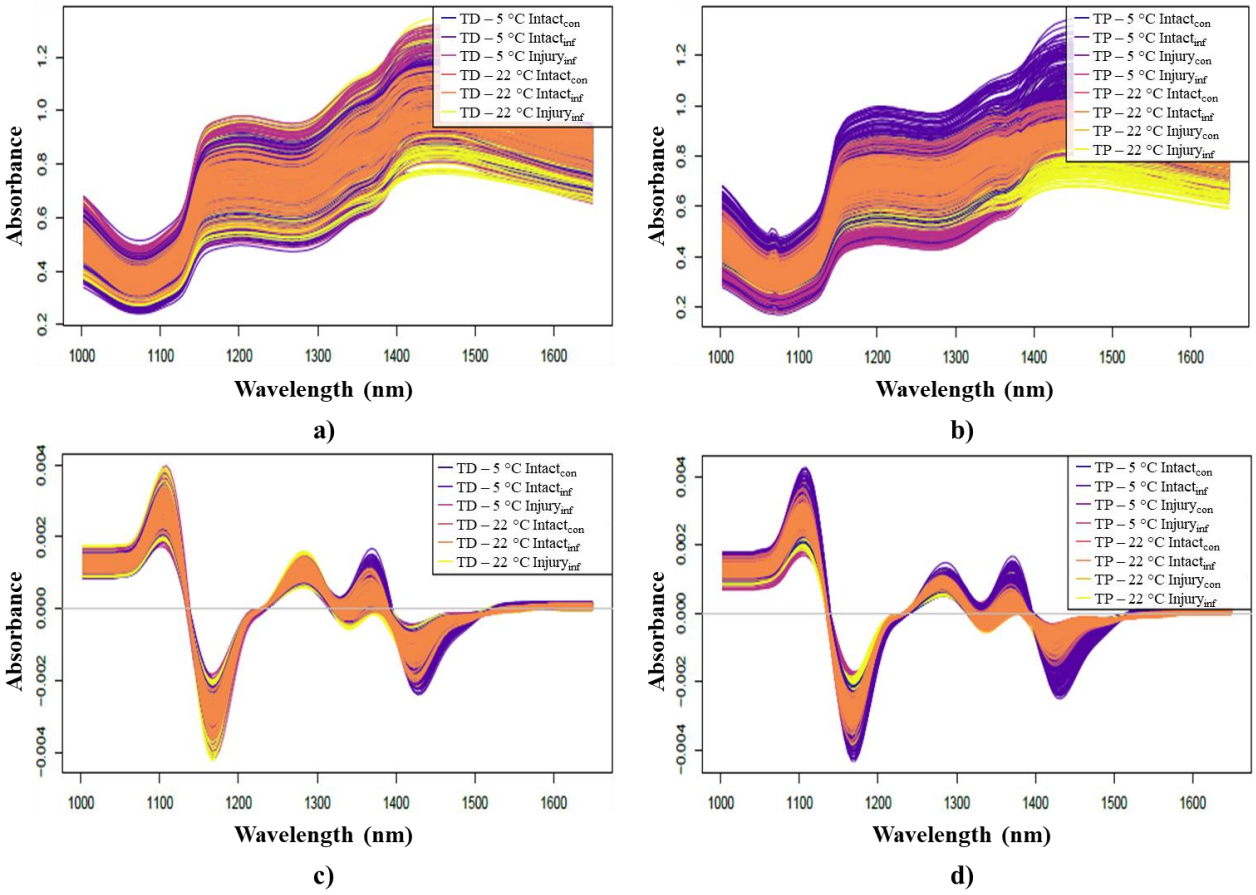

Figure 45. HSI spectra of plums treated in different ways: raw spectra of TD plums (a); raw spectra of TP plums (b); 2nd derivative spectra of TD plums (c); 2nd derivative spectra of TP plums (d).

Smoothing and msc correction performed on the HSI spectral data of plums, followed by PCA confirmed the impact of storage conditions on the absorption characteristics of the samples. For the two plum varieties, the first three PCs explained the 99% of the total variance in the data. Based on the PCA score plots (Figure 74a), it can be observed how sharply the spectral differences along the third PC are outlined, especially for the TP variety. Respectively for the TD and TP variety, the main PCA loadings that best describe separation according to fruit handling are the following (Figure 74b, c):

- **Topend (TD) plums**

  PC 2 loading: 1069.8, 1151.9, 1263.0, 1364.3, 1446.4 nm;

  PC 3 loading: 1122.9, 1238.8, 1374.0, 1465.7 nm;

- **Topend plus (TP) plums**

  PC 2 loading: 1079.5, 1142.3, 1267.8, 1369.2, 1456.1 nm;

  PC 3 loading: 1132.6, 1243.6, 1383.7 nm.

The pre-treated data for PCA was subjected to SIMCA to determine the statistical significance of differences between infection methods and storage conditions for the two plum varieties. Models were created for data filtered to the initial, intermediate, and final days of storage to evaluate changes over time. Figure 46 and Figure 75 illustrate how the interclass distances evolved on specific storage days.

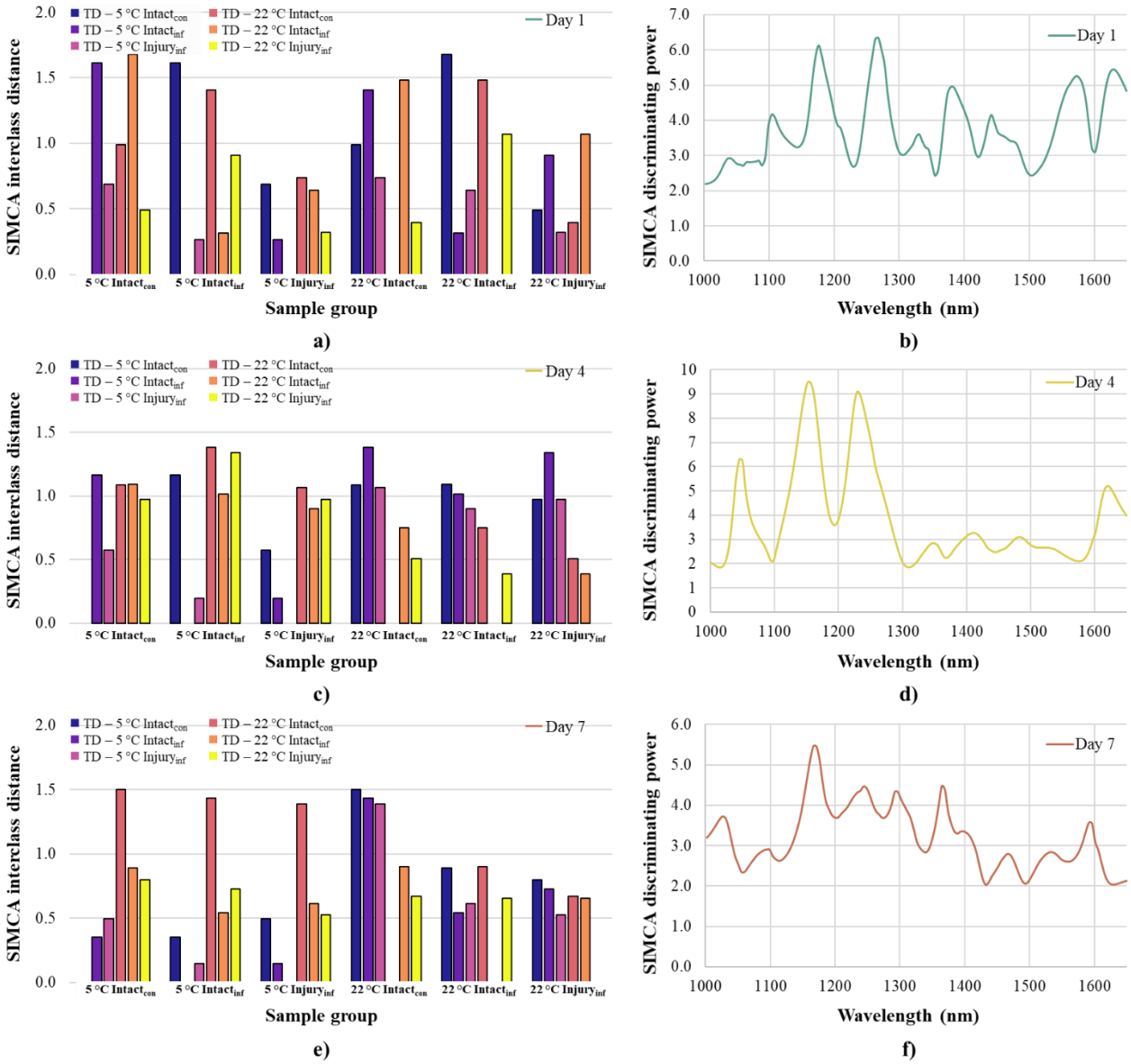

Figure 46. SIMCA on the HSI spectra of TD plums when discrimination was based on fruit treatment on certain storage days (sgol-2-21-0, msc): SIMCA interclass distances on the 1st day of storage (a); SIMCA discrimination power plot on the 1st day of storage (b); SIMCA interclass distances on the 4th day of storage (c); SIMCA discrimination power plot on the 4th day of storage (d); SIMCA interclass distances on the 7th day of storage (e); SIMCA discrimination power plot on the 7th day of storage (f).

According to the SIMCA based on HSI spectra of the TD variety, bigger interclass distances were characteristic on the first day of storage, which almost levelled out by the middle of the storage period, and then showed overall smaller, but staggered distances by the end of storage (Figure 46a, c, e). In case of the TP variety, the different storage conditions were more evident in the interclass distances. By the middle of the storage period, the distances demonstrated salient differences (Figure 75a, c, e). Samples of the TD variety appeared to be less affected by storage under different conditions compared to TP samples, and this also supports the findings of PCA.

Overall, no significant interclass distances were observed for any of the sample sets indicating that while storage temperature can play a crucial role in the storage of the plums, the mode of preparation did not lead to significant differences During the SIMCA modelling, prominent wavelengths were also identified. The SIMCA discriminating power plots highlight the specific wavelengths that significantly contribute to the discrimination of the sample groups, respectively (Figure 46b, d, f and Figure 75b, d, f):

- **TD plums**
  Day 1: 1040.9, 1103.6, 1176.1, 1267.8, 1330.6, 1378.8, 1441.6, 1572.0, 1629.9 nm;
  Day 4: 1045.7, 1151.9, 1229.2, 1349.9, 1412.6, 1480.2, 1523.7, 1620.2 nm;
  Day 7: 1026.4, 1094.0, 1166.4, 1243.6, 1291.9, 1364.3, 1398.1, 1465.7, 1533.3, 1591.3 nm;

- **TP plums**
  Day 2: 1050.5, 1084.3, 1166.4, 1214.7, 1253.3, 1417.5, 1494.7, 1576.8, 1639.6 nm;
  Day 4: 1026.4, 1089.1, 1166.4, 1214.7, 1253.3, 1316.1, 1340.2, 1427.1, 1489.9, 1562.3 nm;
  Day 7: 1036.0, 1103.6, 1151.9, 1229.2, 1374.0, 1412.6, 1480.2, 1586.4 nm.

Optimised PCA-LDA modelling was used to determine the accuracy with which the initial *Monilinia* conidium concentration can be determined from the HSI spectra of plums. For this classification, spectra recorded the day after inoculation were utilized. The spectra were further filtered according to mode of infection and storage conditions to reduce the impact of environmental factors during the modelling.

In the case of plums, the classification was for a total of three different levels of conidial contamination. Table 44 and Table 45 summarise the classification performance regarding the initial conidial contamination of TD and TP plums, respectively. For the samples stored under refrigerated conditions, the average correct classification rates were between 83.8 - 96.9% during calibration and between 50.0 - 69.5% during validation. For the samples stored at room temperature, the average correct classification rates during calibration were between 81.6 - 100%, while during validation, they ranged from 42.8 to 75.2%. It was also true for plums that the classification accuracy of the HSI was better than that of the data recorded with the hand-held NIR instrument. These results are supported by the PCA-LDA score plots presented in Figure 47 and Figure 76. In the discriminant space bounded by LD 1 and LD 2, the data points (i.e., scores) representing the concentration levels of each suspension separated well, in some cases almost completely. In the form of LDA discriminating power plots, the most contributing wavelengths were also determined.

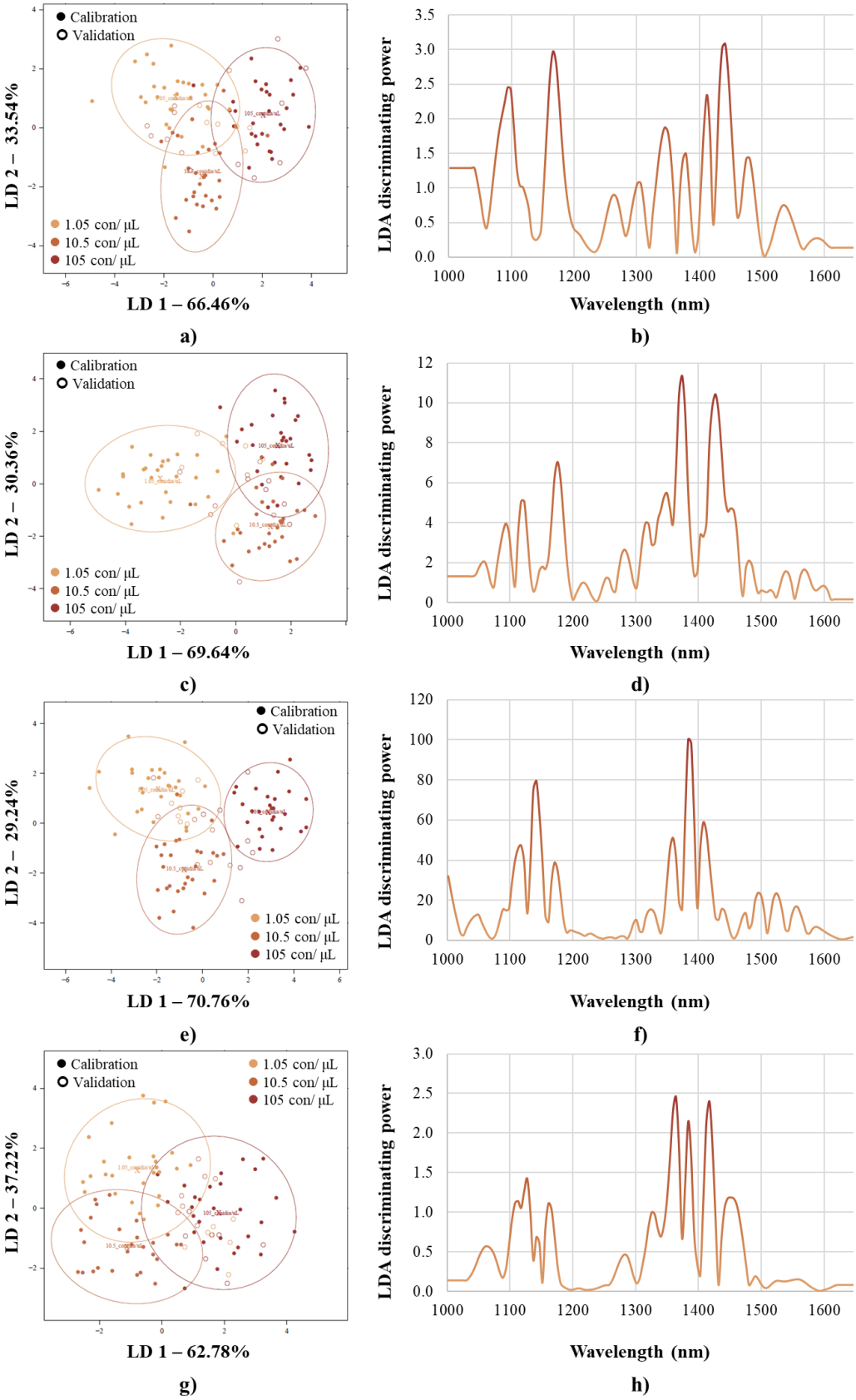

Figure 47. PCA-LDA on the HSI spectra of TD plums when classification was based on initial conidial contamination: PCA-LDA score plot of "5 °C Injury" samples (a); LDA discriminating power plot of "5 °C Injury" samples (b); PCA-LDA score plot of "5 °C Intact" samples (c); LDA discriminating power plot of "5 °C Intact" samples (d); PCA-LDA score plot of "22 °C Injury" samples (e); LDA discriminating power plot of "22 °C Injury" samples (f); PCA-LDA score plot of "22 °C Intact" samples (g); LDA discriminating power plot of "22 °C Intact" samples (h).

In case of plums analysed with HSI, it was also typical that *Monilinia* activity was visible in the samples that were inoculated via injury and stored at room temperature. It was also true for the plum samples prepared for HSI measurements that fungal proliferation was inhomogeneous, even for samples prepared in the same way, as shown in Table 16. Similar to the samples analysed with the hand-held instrument, plum samples showed signs of the infection even at relatively low initial conidium concentrations. This is due to the more favourable characteristics for *Monilinia* reproduction in the fruits.

Table 16. Date of appearance of visible signs of *Monilinia* infection in plums analysed by HSI, inoculated with conidial suspensions of different concentrations through injury and stored at 22 °C.

Variety	Initial conidium concentration	Sample 1	Sample 2	Sample 3	Sample 4	Sample 5
TD	~ 1.05 con./ µL	–	day 4	day 3	day 5	day 5
	~ 10.5 con./ µL	day 5	day 3	day 3	day 3	–
	~ 105 con./ µL	–	day 4	day 5	day 2	–
TP	~ 2.31 con./ µL	day 4	–	day 5	day 6	day 7
	~ 23.1 con./ µL	day 4	day 4	day 6	day 3	day 3
	~ 231 con./ µL	day 4	day 4	day 2	day 3	day 4

– There were no clear signs of *Monilinia* activity in these samples

It was considered essential to investigate the effectiveness of HSI in tracking the spectral variation of plums in decay, quasi-independently of the day of storage when visible signs of infection appeared on the fruits. Optimised PCA-LDA was employed on specific data corresponding to samples that exhibited signs of decay during the 7-day long storage and the day of appearance of the rot (marked as "day 0") ± 2-day interval. Table 46 summarises the classification accuracies during model building and validation for the TD (65.3, 46.5%) and TP variety (57.3, 33.5%), respectively. The results indicate more accurate outcomes for the TD variety, while for the TP, there was significant misclassification not only to adjacent days. In the PCA-LDA score plots of the two varieties (Figure 48a, c), almost identical V-shaped separation trend appears in the discriminant space displayed. The dominant wavelengths for this specific modelling are the following (Figure 48b, d):

- **TD plums**
  1060.2, 1113.3, 1132.6, 1147.1, 1171.2, 1234.0, 1296.8, 1320.9, 1349.9, 1383.7, 1403.0, 1431.9, 1470.6, 1494.7, 1523.7, 1557.5, 1596.1 nm;

- **TP plums**
  1065.0, 1113.3, 1147.1, 1267.8, 1282.3, 1316.1, 1378.8, 1417.5, 1436.8, 1475.4, 1514.0, 1547.8, 1586.4 nm.

Prominent wavelengths obtained as a result of the PCA, SIMCA and PCA-LDA models built on the hyperspectral data of plums infected with *Monilinia* and stored under various environmental conditions were summarised. Taking into account the most contributing wavelengths of the two studied varieties, Figure 50 presents the absorption bands of successful chemometric modelling with their approximate frequency values.

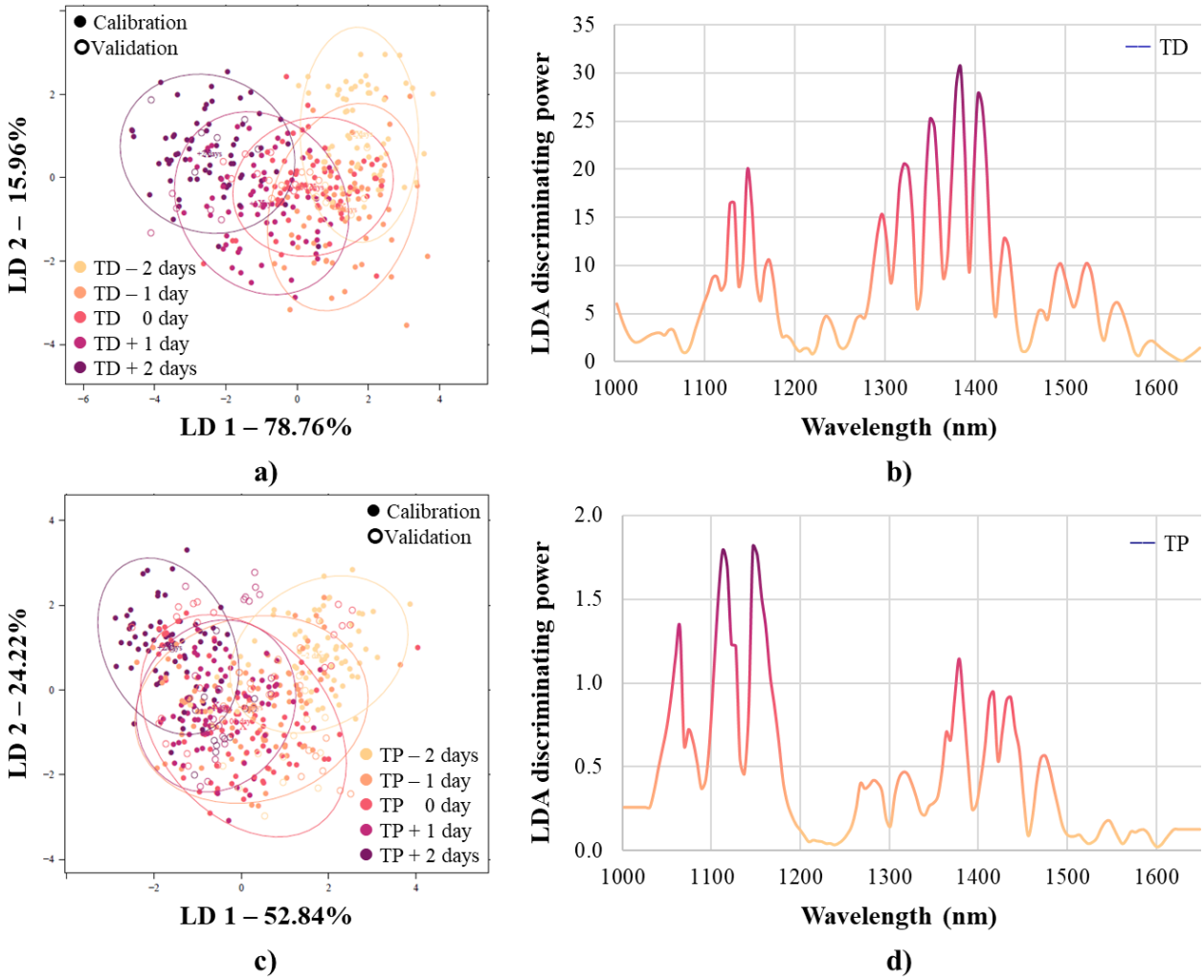

Figure 48. PCA-LDA on the HSI spectra of plums showing monilial activity when classification was based on the day of appearance of visible infection signs ± 2 days: PCA-LDA score plot of TD plums (a); LDA discriminating power plot of TD plums (b); PCA-LDA score plot of TP plums (c); LDA discriminating power plot of TP plums (d).

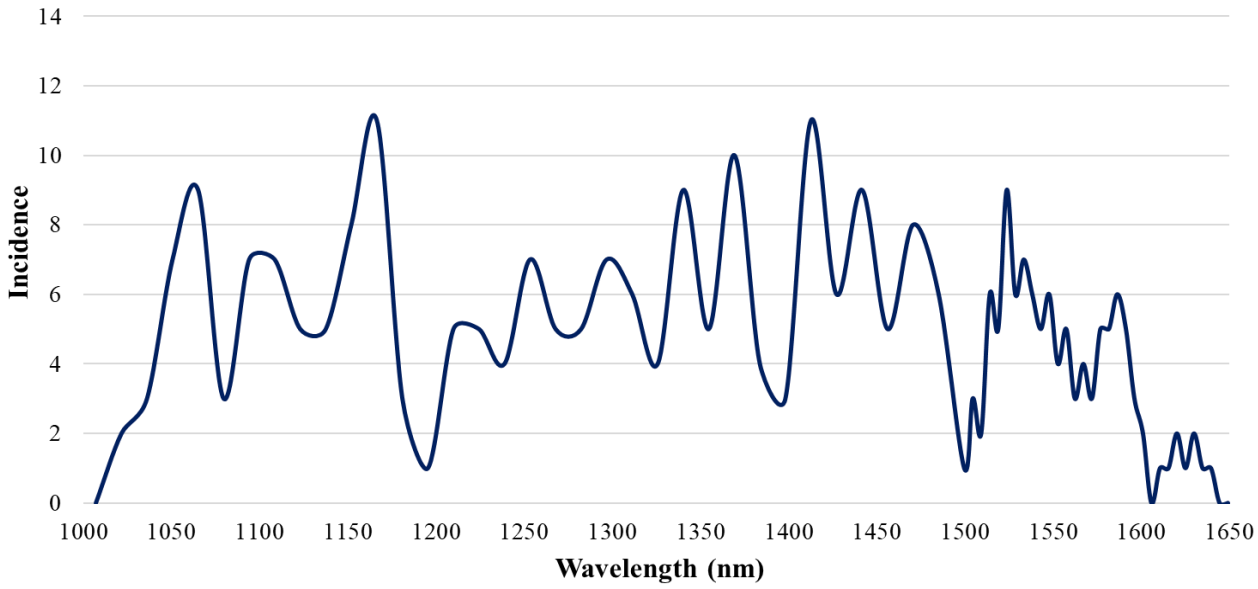

Figure 49. Absorbance bands frequently observed in chemometric modelling results of *Monilinia* detection on plums with hyperspectral imaging.

5.3. Determination of fruit juice enrichment with NIR spectroscopy

This subsection summarises the accuracy achieved in detecting and predicting plant extracts added to fruit juices in various combinations and concentrations using hand-held and benchtop NIR spectroscopic devices. The modelling results based on spectra recorded with the different instruments are presented in comparison, as the same samples were analysed with both devices.

5.3.1. Detection results on sour cherry juices

Figure 77 presents the raw spectra obtained using the two instruments after the enrichment of sour cherry juices with various concentrations of plant extracts. The two instruments operate based on fundamentally different measurement setups. The hand-held device captures transflectance, while the benchtop instrument records transmission spectra. The spectra obtained with the benchtop instrument exhibited higher variability in the data. Besides, when applying second derivative pre-treatment, two peaks emerge between 1400-1500 nm, unlike the data recorded with the hand-held device (Figure 77c, d). PCA performed after smoothing and msc correction also confirms the differences between the instruments, and thus in the spectral data (Figure 50).

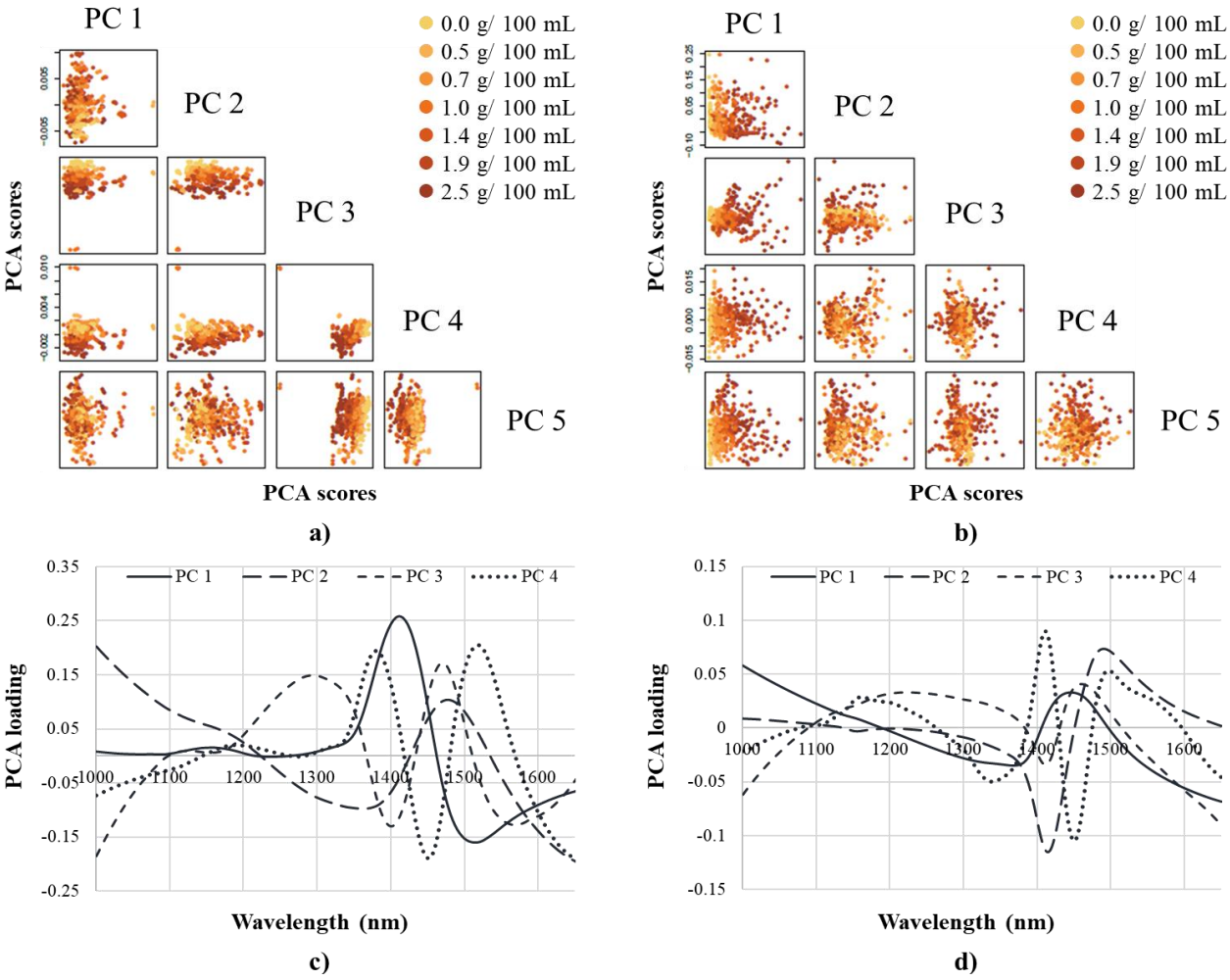

Figure 50. PCA on the NIR spectra of sour cherry juices when colouring was based on total extract content: PCA score plots on the data recorded with the hand-held NIR device (sgol-2-21-0, msc) (a); PCA score plots on the data recorded with the benchtop NIR device (sgol-2-43-0, msc) (b); PCA loading plot on the data recorded with the hand-held NIR device (c); PCA loading plot on the data recorded with the benchtop NIR device (d).

Based on the PCA score plots, separation trend according to the total extract content was more apparent along different PCs for the two instruments, respectively. For the hand-held device, this was observed mainly along the second and third PCs. In contrast, with the benchtop instrument, the separation based on extract content was already evident along the first and second PCs (Figure 50a, b). These are supported by that for the hand-held device, the first three, whereas for the benchtop device data, the first two PCs explained the 99% of the total variance in the data. Based on the two PCA loadings highlighted by NIR instrument, the relevant wavelengths that best describe separation according to total extract concentration are the following (Figure 50c, d):

- **Hand-held NIR instrument**
  PC 2 loading: 1155.9, 1409.8, 1515.1 nm;
  PC 3 loading: 1292.2, 1403.6, 1471.8, 1570.9 nm;

- **Benchtop NIR instrument**
  PC 1 loading: 1368.4, 1445.9 nm;
  PC 2 loading: 1155.3, 1414.8, 1490.8 nm.

Optimised PCA-LDA modelling was employed as a supervised classification method to determine the effectiveness of distinguishing between sour cherry juice samples containing simple, binary, or ternary combinations of plant extracts. The modelling involved all extract concertation levels; and the results obtained after the optimised spectral pre-processing are illustrated in Figure 51.

The PCA-LDA score plots displayed reveal a logical overlap among the juice blends. Particularly in the modelling based on data of the benchtop NIR instrument, it is evident that as the complexity of the blends increases, the data points representing these samples show a greater degree of superimposition of points corresponding to samples of partially similar compositions. In this highlighted example, the simple blends are arranged in a triangular shape within the space defined by LD 1 and LD 2. The vertices of the triangle represent the individual simple blends, while the binary blends are positioned between these vertices. At the centre, the ternary blends are located, potently illustrating how the complexity of the mixtures affects their positioning in the discriminant space (Figure 51c).

Table 17 summarises the classification results regarding sour cherry juices and their blends. The classification accuracies for the hand-held device data were 66.65 and 42.45%, while for the benchtop spectrometer data 71.67 and 56.33% during model building and validation, respectively. It was observed for the calibration sample sets that misclassification occurred primarily with samples containing extracts in binary or ternary blends. In addition, wavelengths that played a significant role in discrimination among juice blends were also identified based on their discriminating power plots (Figure 51b, d):

- **Hand-held NIR device**: 1106.3, 1131.1, 1279.8, 1329.3, 1354.1, 1385.1, 1409.8, 1434.6, 1453.2, 1478.0, 1509.0v1533.7, 1558.5, 1583.3 nm;
- **Benchtop NIR device:** 1257.5, 1352.1, 1382.0, 1405.3, 1427.8, 1447.6, 1471.5, 1497.9, 1542.3 nm.

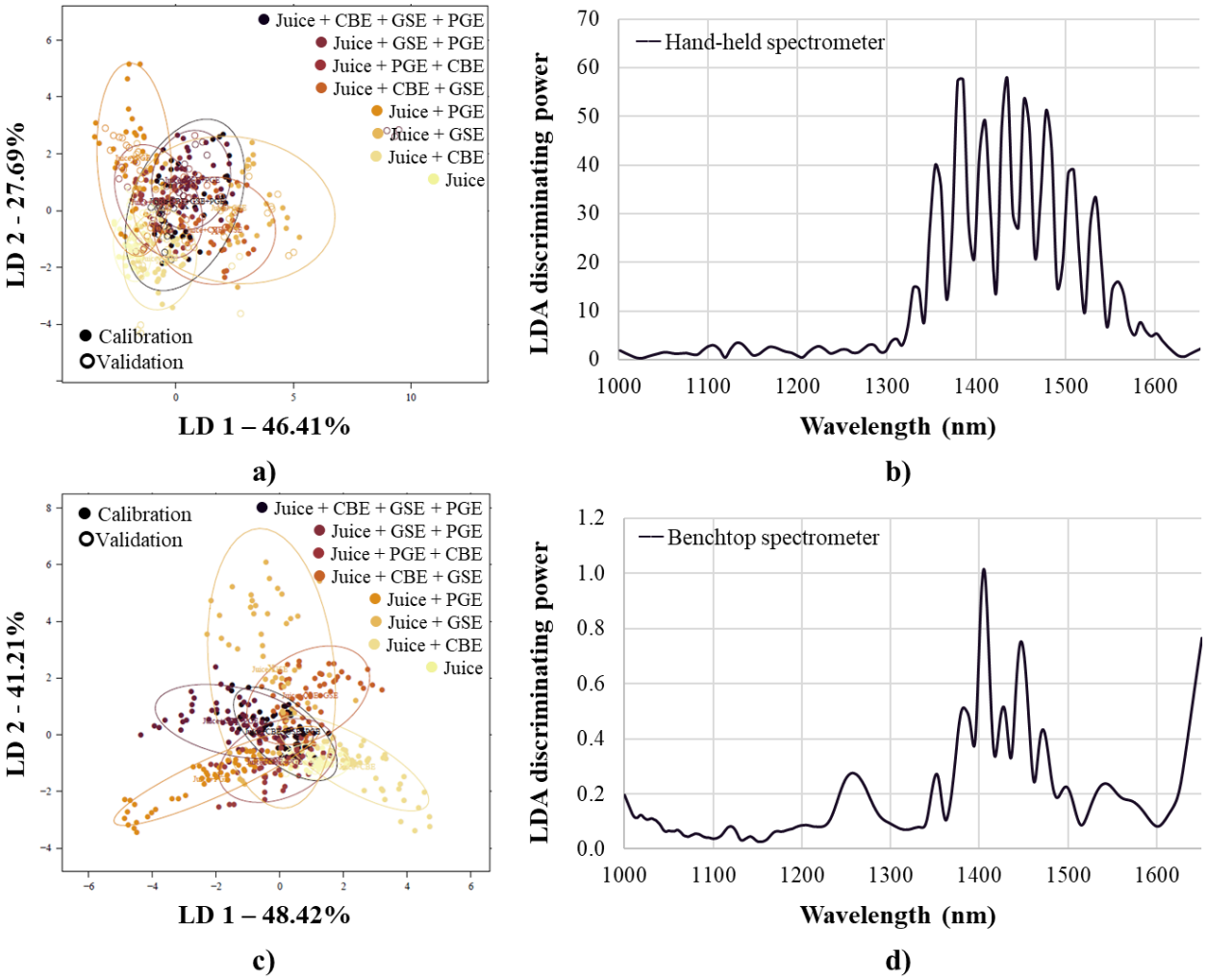

Figure 51. PCA-LDA on the NIR spectra of sour cherry juices when classification was based on the type of dosed plant extract: PCA-LDA score plot on the data recorded with the hand-held NIR device (a); LDA discriminating power plot on the data recorded with the hand-held NIR device (b); PCA-LDA score plot on the data recorded with the benchtop NIR device (c); LDA discriminating power plot on the data recorded with the benchtop NIR device (d).

It was considered important to investigate the accuracy with which the extract content of all the added extracts could be distinguished in sour cherry juices, quasi independently regardless of the composition of blends involved. For this purpose, optimised PCA-LDA modelling was also applied.

Table 47 summarises the classification results regarding sour cherry juices and their blends. The classification accuracies for the hand-held device data were 71.73 and 49.62%, while for the benchtop spectrometer data 76.02 and 58.29% during model building and validation, respectively. Misclassification was typically to adjacent lower or higher concentration levels.

Table 17. PCA-LDA on the spectra of sour cherry juices recorded different NIR instruments when classification was based on the type of plant extract added.

		Juice blends	Juice	+ CBE	+ GSE	+ PGE	+(CBE+GSE)	+(GSE+PGE)	+(PGE+CBE)	+(CBE+GSE+PGE)	Classification accuracy
MicroNIR hand-held device *	**Calibration**	**Juice**	93.89	5.56	0.93	6.02	5.56	1.39	7.41	0.93	**66.65%**
		Juice+CBE	2.78	79.63	1.39	0.00	3.70	0.00	2.78	12.96	
		Juice+GSE	0.00	0.00	58.33	0.00	13.43	6.02	0.93	3.70	
		Juice+PGE	0.00	0.00	2.78	69.91	0.00	4.63	16.67	1.39	
		Juice+(CBE+GSE)	0.00	0.00	13.43	0.00	62.04	6.48	0.00	6.94	
		Juice+(GSE+PGE)	0.00	0.00	5.09	1.39	5.56	62.50	6.48	8.80	
		Juice+(PGE+CBE)	3.33	9.72	16.20	22.69	0.93	5.09	52.31	10.65	
		Juice+(CBE+GSE+PGE)	0.00	5.09	1.85	0.00	8.80	13.89	13.43	54.63	
	Validation	**Juice**	71.11	11.11	3.70	16.67	11.11	5.56	18.52	0.00	**42.45%**
		Juice+CBE	11.11	55.56	5.56	0.00	7.41	1.85	12.96	24.07	
		Juice+GSE	0.00	1.85	42.59	0.00	20.37	16.67	0.00	5.56	
		Juice+PGE	0.00	0.00	11.11	62.96	0.00	7.41	27.78	5.56	
		Juice+(CBE+GSE)	0.00	7.41	14.81	0.00	31.48	9.26	0.00	7.41	
		Juice+(GSE+PGE)	0.00	5.56	7.41	5.56	12.96	27.78	11.11	14.81	
		Juice+(PGE+CBE)	11.11	9.26	5.56	11.11	0.00	14.81	18.52	12.96	
		Juice+(CBE+GSE+PGE)	6.67	9.26	9.26	3.70	16.67	16.67	11.11	29.63	
NIRflex benchtop device **	**Calibration**	**Juice**	96.11	17.13	3.30	1.39	4.63	3.24	11.79	4.63	**71.67%**
		Juice+CBE	0.00	75.46	0.00	0.00	0.00	0.00	0.47	1.85	
		Juice+GSE	0.00	0.00	60.85	0.00	12.50	0.00	0.00	0.00	
		Juice+PGE	0.00	0.00	1.89	70.37	0.00	5.09	11.79	0.00	
		Juice+(CBE+GSE)	0.00	0.00	16.51	0.00	72.22	0.93	0.00	9.72	
		Juice+(GSE+PGE)	0.00	0.00	0.94	4.63	0.00	78.24	3.30	18.06	
		Juice+(PGE+CBE)	3.89	1.85	12.74	22.69	0.46	2.31	60.85	6.48	
		Juice+(CBE+GSE+PGE)	0.00	5.56	3.77	0.93	10.19	10.19	11.79	59.26	
	Validation	**Juice**	93.33	24.07	9.43	7.41	11.11	5.56	24.53	14.81	**56.33%**
		Juice+CBE	2.22	66.67	0.00	0.00	3.70	0.00	5.66	9.26	
		Juice+GSE	0.00	0.00	62.26	0.00	12.96	0.00	0.00	1.85	
		Juice+PGE	0.00	0.00	3.77	66.67	0.00	12.96	9.43	0.00	
		Juice+(CBE+GSE)	0.00	0.00	7.55	0.00	50.00	0.00	0.00	11.11	
		Juice+(GSE+PGE)	0.00	0.00	3.77	11.11	14.81	57.41	18.87	24.07	
		Juice+(PGE+CBE)	4.44	5.56	3.77	14.81	0.00	9.26	32.08	16.67	
		Juice+(CBE+GSE+PGE)	0.00	3.70	9.43	0.00	7.41	14.81	9.43	22.22	

***** sgol-2-17-0, sgol-2-17-1; Nr = 423; NrPCs = 17

****** sgol-2-27-0, sgol-2-43-1; Nr = 421; NrPCs = 10

The findings are supported by the PCA-LDA score plots shown in Figure 78. In the illustrated discriminant space, increasing levels of extract concentration exhibited distinct clustering trends along LD 1. This indicates a clear separation based on extract concentration, suggesting that the model effectively captures variations in the spectral data associated with different concentrations. In addition, wavelengths that played a significant role in discrimination among juice blends were also identified based on their discriminating power plots (Figure 78b, d):

- **Hand-held NIR device**: 1323.1, 1347.9, 1378.9, 1409.8, 1440.8, 1471.8, 1502.8, 1533.7, 1558.5, 1589.5 nm;
- **Benchtop NIR device:** 1134.8, 1153.7, 1317.2, 1347.0, 1372.1, 1388.1, 1406.1, 1422.1, 1447.6, 1462.8, 1477.5, 1491.6, 1508.8, 1529.1, 1549.9 nm.

PLSR modelling was conducted to predict the concentrations of various extracts added to sour cherry juices. The models were developed using the whole dataset by instrument, then filtered for simple, binary, and ternary blends. In each instance, the models were optimised to suit the specific dataset. The prediction accuracies obtained during model calibration and validation of the different sample sets are summarised in Table 48 and Table 49. The best modelling results by each extract were achieved when constructing models for specific sample groups.

In the case of the hand-held NIR device, the prediction of CBE was made with Rcv^2 between 0.46 – 0.93; RMSEcv between 0.07 – 0.42 g/ 100 mL. The prediction of GSE was made with Rcv^2 between 0.65 – 0.93; RMSEcv between 0.07 – 0.34 g/ 100 g/mL. The prediction of PGE was made with Rcv^2 between 0.66 – 0.93; RMSEcv between 0.07 – 0.31 g/ 100 mL. The prediction of total extract content was made with Rcv^2 between 0.66 – 0.93; RMSEcv between 0.22 – 0.49 g/ 100 mL. Figure 52 illustrates the regression vectors obtained for simple fruit juice blends, respectively by extract, with the most prominent wavelengths listed below:

- **CBE**: 1063.0, 1100.1, 1149.7, 1193.0, 1248.8, 1329.3, 1354.1, 1391.3, 1422.2, 1453.2, 1490.4, 1515.1, 1570.9 nm;
- **GSE**: 1149.7, 1360.3, 1428.4, 1484.2, 1552.3 nm;
- **PGE**: 1112.5, 1137.3, 1347.9, 1422.2, 1471.8, 1546.1 nm.

In the case of the benchtop NIR instrument, the prediction of CBE was made with Rcv^2 between 0.86 – 0.98; RMSEcv between 0.04 – 0.21 g/ 100 mL. The prediction of GSE was made with Rcv^2 between 0.90 – 0.98; RMSEcv between 0.04 – 0.23 g/ 100 g/mL. The prediction of PGE was made with Rcv^2 between 0.86 – 0.98; RMSEcv between 0.04 – 0.16 g/ 100 mL. The prediction of total extract content was made with Rcv^2 between 0.86 – 0.98; RMSEcv between 0.12 – 0.32 g/ 100 mL. Figure 53 illustrates the regression vectors obtained for simple fruit juice blends, respectively by extract, with the most prominent wavelengths listed below:

- **CBE**: 1374.4, 1460.3 nm;
- **GSE**: 1123.1, 1129.2, 1340.5, 1362.4, 1398.2, 1431.8, 1495.2, 1570.4 nm;
- **PGE**: 1086.5, 1128.2, 1276.2, 1341.2, 1362.4, 1397.4, 1422.9, 1451.8, 1474.9, 1501.5, 1540.4, 1600.5 nm.

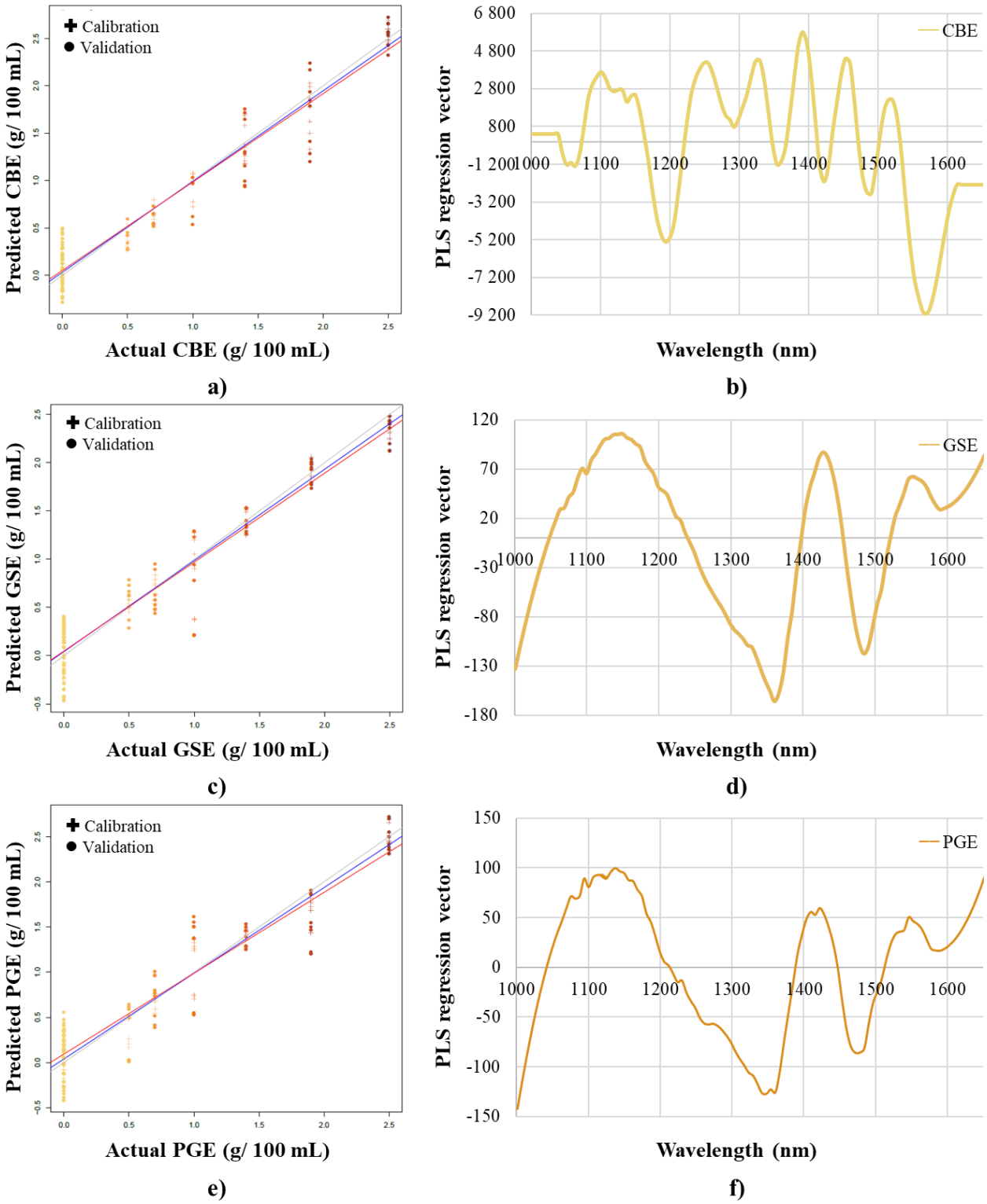

Figure 52. PLSR prediction of plant extract content of simple sour cherry juice blends scanned with the hand-held NIR instrument: Y-fit of CBE prediction (a); regression vectors of CBE prediction (b); Y-fit of GSE prediction (c); regression vectors of GSE prediction (d); Y-fit of PGE prediction (e); regression vectors of PGE prediction (f).

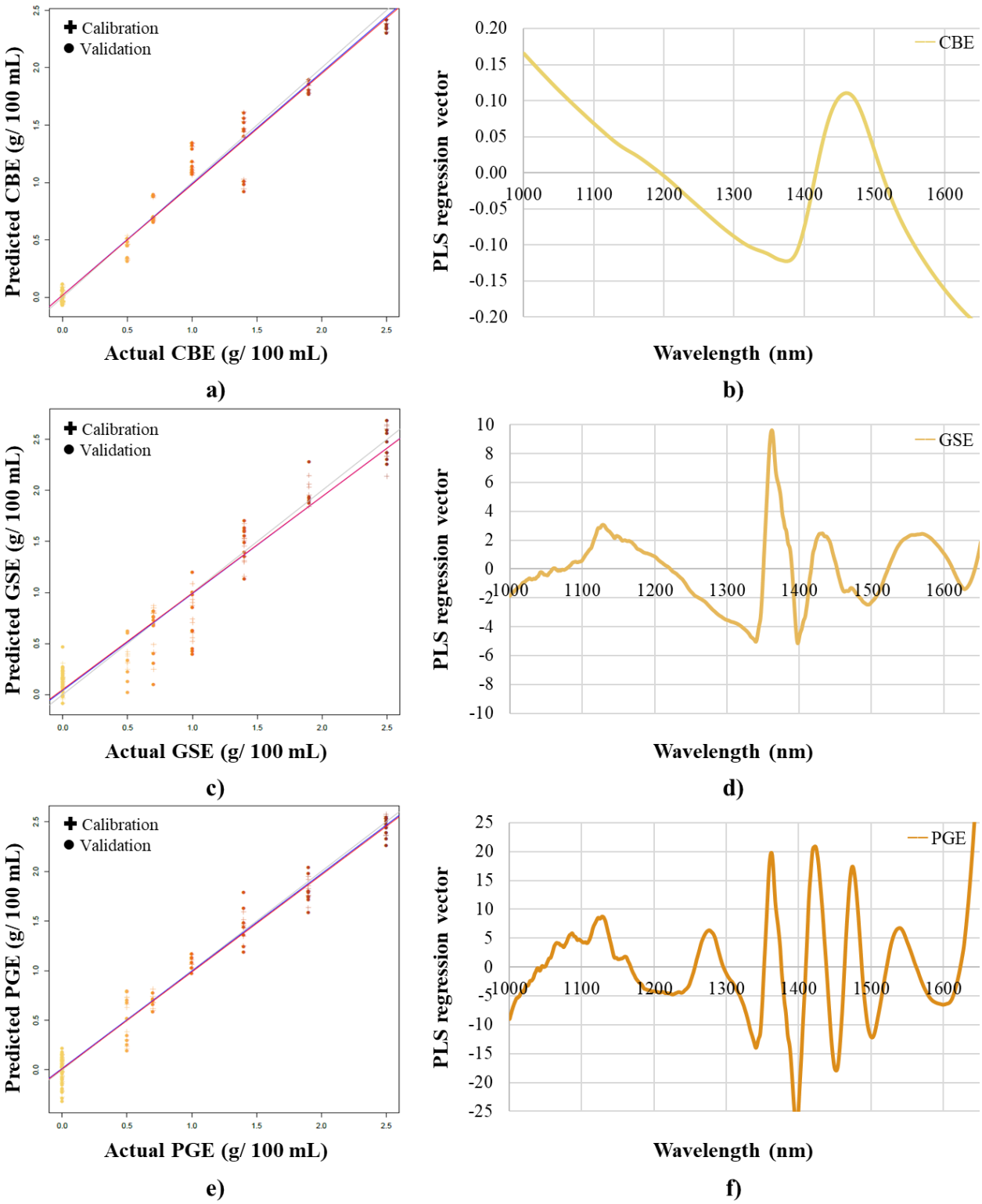

Figure 53. PLSR prediction of plant extract content of simple sour cherry juice blends scanned with the benchtop NIR instrument: Y-fit of CBE prediction (a); regression vectors of CBE prediction (b); Y-fit of GSE prediction (c); regression vectors of GSE prediction (d); Y-fit of PGE prediction (e); regression vectors of PGE prediction (f).

Based on the relevant wavelengths determined as partial results of the PCA, PCA-LDA and PLSR models, the absorption bands for sour cherry juice blends that contribute most to successful chemometric modelling were summarised. The obtained wavelength-frequency results are presented as absorption bands in Figure 54. The plots by instrument provide evidence of coincident absorption bands.

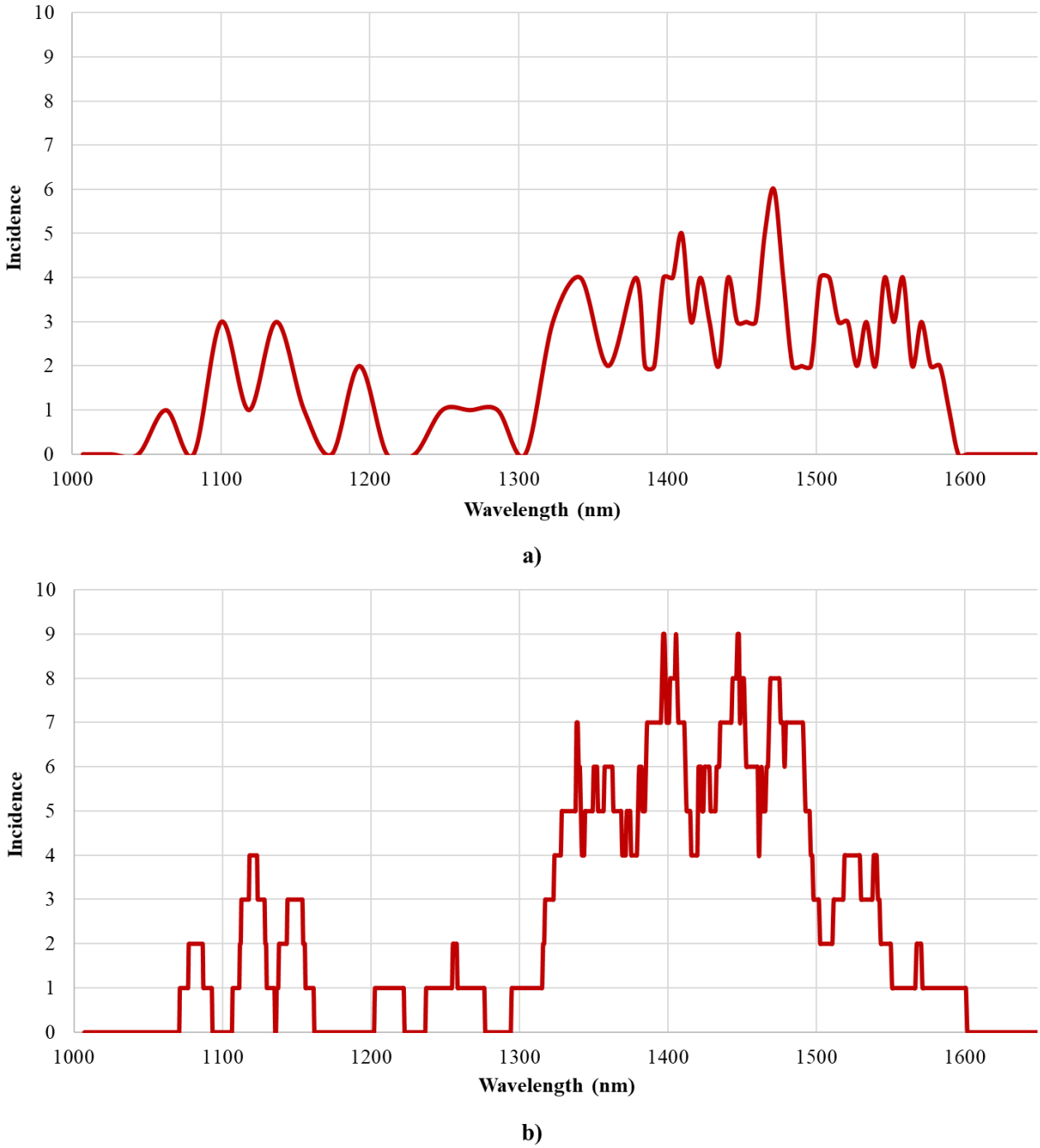

Figure 54. Absorbance bands frequently observed in chemometric modelling results of sour cherry juice enrichment with plant extracts: findings on the hand-held NIR spectrometer data (a); findings on the benchtop NIR spectrometer data (b)

5.3.2. Detection results on plum juices

Figure 79 presents the raw spectra obtained using the two instruments after the enrichment of plum juices with various concentrations of plant extracts. The spectra showed similar behaviour to what was observed for the sour cherry juices: as the concentration of the extracts increased, the absorbance of the blends also increased. The spectra obtained with the benchtop instrument exhibited higher variability. The application of second derivative pre-treatment also resulted in the occurrence of two negative peaks in the 1400-1500 nm wavelength range (Figure 79c, d).

PCA performed on the smoothed and msc-treated data also revealed differences inherent in the spectra, consistent with the findings for the sour cherry juice samples. The PCA score plots show that in the case of hand-held device data, a separation based on concentration is observed along the first and third PCs, while for the benchtop device data, this is more pronounced along the first and second PCs (Figure 55a, b). These are supported by that for the hand-held device, the first three, whereas for the benchtop device data, the first two PCs explained the 99% of the total variance in the data.

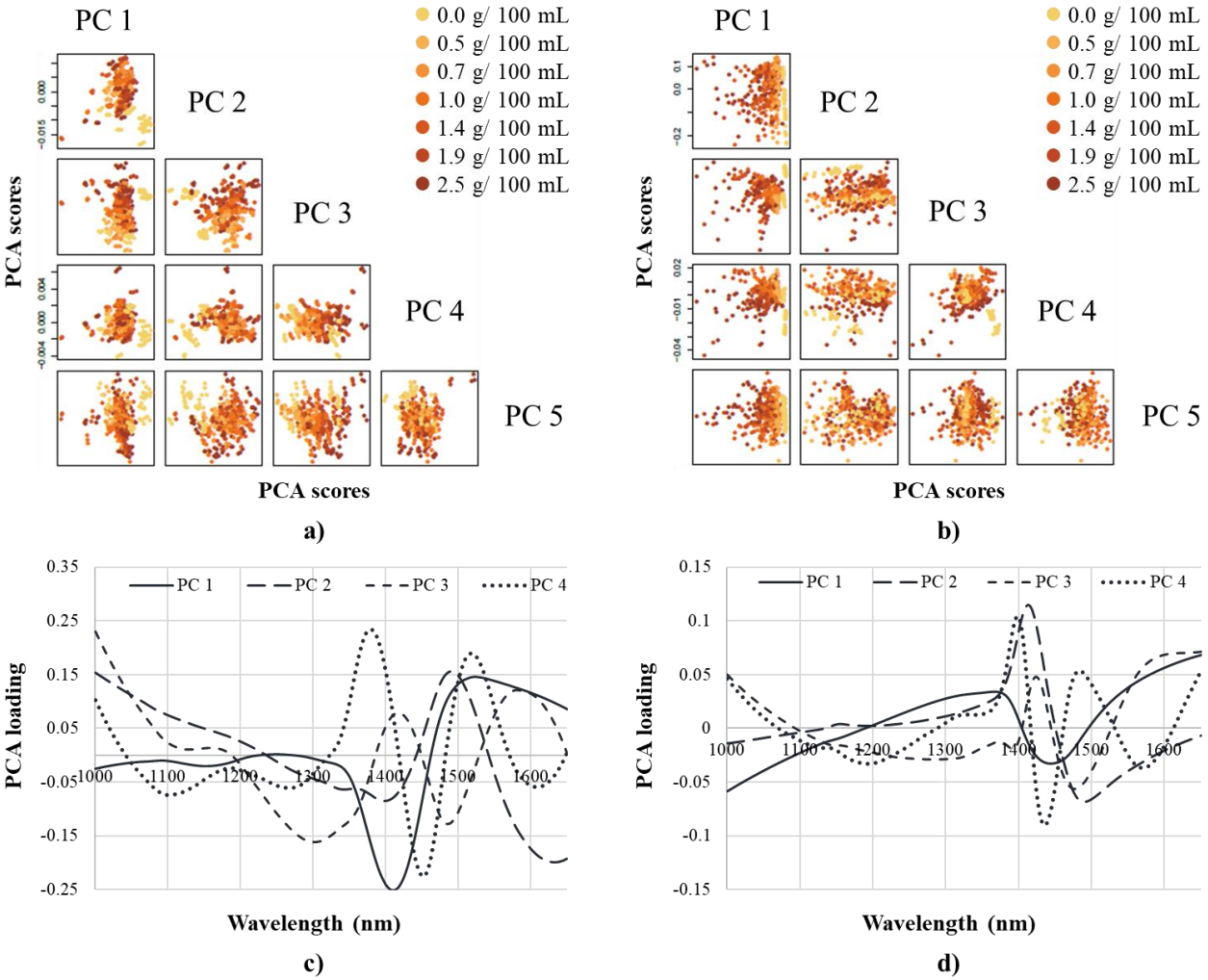

Figure 55. PCA on the NIR spectra of plum juices when colouring was based on total extract content: PCA score plots on the data recorded with a hand-held device (sgol-2-21-0, msc) (a); PCA score plots on the data recorded with a benchtop device (sgol-2-43-0, msc) (b); PCA loading plot on the data recorded with a hand-held device (c); PCA loading plot on the data recorded with a benchtop device (d).

Based on the two PCA loadings highlighted by NIR instrument, the relevant wavelengths that best describe separation according to total extract concentration are the following (Figure 55c, d):

- **Hand-held NIR instrument**
  PC 1 loading: 1149.7 1409.8 1521.3 nm;
  PC 3 loading: 1162.1 1304.5 1416.0 1484.2 1583.3 nm;

- **Benchtop NIR instrument**
  PC 1 loading: 1367.6 1444.3 nm;
  PC 2 loading: 1155.8 1413.2 1489.9 nm.

Optimised PCA-LDA modelling was employed as a supervised classification method to determine the effectiveness of distinguishing between plum juice samples containing simple, binary, or ternary combinations of plant extracts. The modelling involved all extract concertation levels; and the results obtained after the optimised spectral pre-processing are illustrated in Figure 80.

The PCA-LDA score plots display less logical overlap among the juice blends in comparison to sour cherry juices. In the modelling based on data of the benchtop NIR instrument, it is more pronounced that as the complexity of the blends increases, the data points representing these samples show a greater degree of superimposition of points corresponding to samples of partially similar compositions. It was also true for the plum juices that the simple blends arranged in a triangular shape within the space defined by LD 1 and LD 2. The vertices of the triangle represent the individual simple blends, while the binary and ternary blends positioned overlapping between these vertices. According to the PCA-score plots (Figure 80a, c), the pure plum juices were clearly distinguishable from the juice blends suggesting that the spectral characteristics are significantly different from those of the juices enriched with extracts.

Table 50 summarise the classification results regarding plum juices and their blends. The classification accuracies for the hand-held device data were 53.11 and 27.04%, while for the benchtop spectrometer data 55.08 and 34.04% during model building and validation, respectively. For the plum juice sample set, there was a higher degree of misclassification concerning sample groups that did not necessarily overlap in terms of added extracts. In addition, wavelengths that played a significant role in discrimination among juice blends were also identified based on their discriminating power plots (Figure 80b, d):

- **Hand-held NIR device**: 1075.3, 1093.9, 1217.8, 1329.3, 1409.8, 1440.8, 1471.8, 1490.4, 1509.0, 1539.9, 1570.9, 1595.7 nm;
- **Benchtop NIR device:** 1243.2, 1271.6, 1329.1, 1371.4, 1391.2, 1406.1, 1423.7, 1438.4, 1451.0, 1464.6, 1479.3, 1500.6, 1540.4, 1569.4, 1616.0 nm.

It was considered important to investigate the accuracy with which the extract content of all the added extracts could be distinguished in plum juices, quasi independently regardless of the composition of blends involved. For this purpose, optimised PCA-LDA modelling was also applied.

Table 18 summarises the classification results regarding plum juices and their blends. The classification accuracies for the hand-held device data were 58.07 and 41.45%, while for the benchtop spectrometer data 66.96 and 46.29% during model building and validation, respectively. Misclassification was typically to adjacent lower or higher concentration levels. Misclassification was more pronounced to adjacent lower or higher concentration levels.

The results are supported by the PCA-LDA score plots shown in Figure 56. It was also observed in these analyses that the data points representing pure fruit juice samples were distinctly separated from the blended samples. In both instruments, the individual extract concentration levels showed a clear clustering trend along LD 2 (Figure 56a, c). The most contributing wavelengths were determined based on the LDA discriminating power plots (Figure 56b, d) and listed below:

- **Hand-held NIR device**: 1131.1, 1205.4, 1286.0, 1385.1, 1465.6, 1539.9, 1583.3 nm;
- **Benchtop NIR device:** 1042.1, 1122.1, 1148.9, 1157.9, 1203.1, 1248.1, 1292.7, 1341.2, 1360.9, 1384.3, 1391.2, 1411.6, 1427.8, 1443.4, 1458.6, 1475.8, 1493.4, 1527.2, 1556.7 nm.

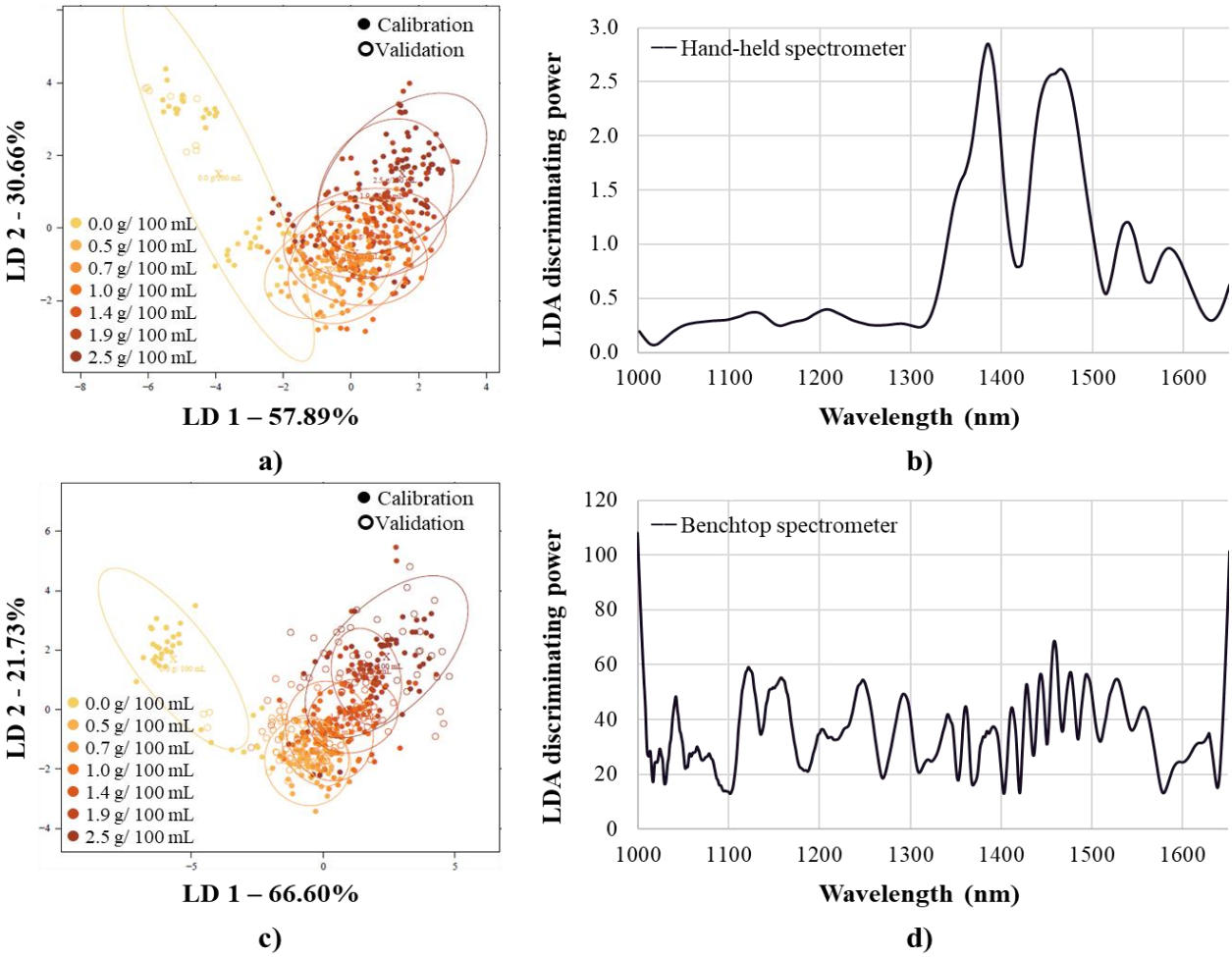

Figure 56. PCA-LDA on the NIR spectra of plum juices when classification was based on the dosed plant extract content: PCA-LDA score plot on the data recorded with a hand-held device (a); LDA discriminating power plot on the data recorded with a hand-held device (b); PCA-LDA score plot on the data recorded with a benchtop device (c); LDA discriminating power plot on the data recorded with a benchtop device (d).

Table 18. PCA-LDA on the spectra of plum juices recorded different NIR instruments when classification was based on total extract content.

		Total extract content	0.0 g/100 mL	0.5 g/100 mL	0.7 g/100 mL	1.0 g/100 mL	1.4 g/100 mL	1.9 g/100 mL	2.5 g/100 mL	Classification accuracy
MicroNIR hand-held device *	**Calibration**	**0.0 g/100 mL**	78.33	0.00	0.00	0.00	0.00	1.19	1.59	**58.07%**
		0.5 g/100 mL	17.78	65.87	30.16	13.49	10.71	2.78	3.17	
		0.7 g/100 mL	3.89	12.70	37.30	18.25	13.10	4.37	1.98	
		1.0 g/100 mL	0.00	15.87	14.68	52.38	11.51	10.71	7.54	
		1.4 g/100 mL	0.00	4.37	12.30	10.32	46.03	8.33	4.76	
		1.9 g/100 mL	0.00	1.19	1.98	5.56	8.33	58.73	13.10	
		2.5 g/100 mL	0.00	0.00	3.57	0.00	10.32	13.89	67.86	
	Validation	**0.0 g/100 mL**	60.00	0.00	0.00	0.00	0.00	0.00	1.59	**41.45%**
		0.5 g/100 mL	37.78	52.38	28.57	33.33	14.29	6.35	6.35	
		0.7 g/100 mL	2.22	19.05	34.92	14.29	19.05	12.70	0.00	
		1.0 g/100 mL	0.00	20.63	9.52	28.57	11.11	4.76	7.94	
		1.4 g/100 mL	0.00	3.17	14.29	9.52	31.75	14.29	12.70	
		1.9 g/100 mL	0.00	0.00	1.59	7.94	19.05	36.51	25.40	
		2.5 g/100 mL	0.00	4.76	11.11	6.35	4.76	25.40	46.03	
NIRflex benctop device **	**Calibration**	**0.0 g/100 mL**	74.44	0.83	0.00	0.00	1.19	0.00	0.76	**66.96%**
		0.5 g/100 mL	18.33	62.08	28.57	10.32	1.59	0.40	0.38	
		0.7 g/100 mL	7.22	22.92	52.38	13.49	0.79	0.00	6.82	
		1.0 g/100 mL	0.00	12.50	19.05	56.75	10.71	2.82	2.65	
		1.4 g/100 mL	0.00	1.25	0.00	15.87	74.21	8.87	1.52	
		1.9 g/100 mL	0.00	0.00	0.00	3.17	9.52	74.60	13.64	
		2.5 g/100 mL	0.00	0.42	0.00	0.40	1.98	13.31	74.24	
	Validation	**0.0 g/100 mL**	71.11	1.67	0.00	0.00	1.59	0.00	4.55	**46.29%**
		0.5 g/100 mL	22.22	60.00	57.14	26.98	4.76	4.84	7.58	
		0.7 g/100 mL	6.67	28.33	28.57	25.40	4.76	0.00	0.00	
		1.0 g/100 mL	0.00	8.33	12.70	22.22	14.29	0.00	1.52	
		1.4 g/100 mL	0.00	0.00	1.59	23.81	60.32	8.06	4.55	
		1.9 g/100 mL	0.00	1.67	0.00	1.59	11.11	50.00	50.00	
		2.5 g/100 mL	0.00	0.00	0.00	0.00	3.17	37.10	31.82	

***** sgol-2-17-0, sgol-2-13-1; Nr = 423; NrPCs = 12

****** sgol-2-43-0; Nr = 422; NrPCs = 20

PLSR modelling was conducted to predict the concentrations of various extracts added to plum juices. The models were developed using the whole dataset by instrument, then filtered for simple, binary, and ternary blends. In each instance, the models were optimised to suit the specific dataset. The prediction accuracies obtained during model calibration and validation of the different sample sets are summarised in Table 51 and Table 52. Comparing the prediction results of the two instruments, the indicators describing the accuracy of the model fits varied considerably.

In the case of the hand-held NIR device, the prediction of CBE was made with Rcv^2 between 0.53 – 0.84; RMSEcv between 0.13 – 0.59 g/ 100 mL. The prediction of GSE was made with Rcv^2 between 0.42 – 0.93; RMSEcv between 0.12 – 0.43 g/ 100 g/mL. The prediction of PGE was made with Rcv^2 between 0.47 – 0.93; RMSEcv between 0.12 – 0.62 g/ 100 mL. The prediction of total extract content was made with Rcv^2 between 0.77 – 0.93; RMSEcv between 0.23 – 0.40 g/ 100 mL. Figure 57 illustrates the regression vectors obtained for simple fruit juice blends, respectively by extract, with the most prominent wavelengths listed below:

- **CBE**: 1100.1, 1131.1, 1168.3, 1199.2, 1236.4, 1366.5, 1484.2, 1558.5 nm;
- **GSE**: 1131.1, 1199.2, 1286.0, 1378.9, 1478.0, 1533.7 nm;
- **PGE**: 1075.3, 1155.9, 1211.6, 1292.2, 1391.3, 1484.2, 1552.3 nm.

In the case of the benchtop NIR instrument, the prediction of CBE was made with Rcv^2 between 0.61 – 0.98; RMSEcv between 0.04 – 0.54 g/ 100 mL. The prediction of GSE was made with Rcv^2 between 0.59 – 0.98; RMSEcv between 0.04 – 0.37 g/ 100 g/mL. The prediction of PGE was made with Rcv^2 between 0.71 – 0.98; RMSEcv between 0.04 – 0.32 g/ 100 mL. The prediction of total extract content was made with Rcv^2 between 0.87 – 0.98; RMSEcv between 0.13 – 0.28 g/ 100 mL. Figure 58 illustrates the regression vectors obtained for simple fruit juice blends, respectively by extract, with the most prominent wavelengths listed below:

- **CBE**: 1136.4, 1167.7, 1188.2, 1315.1, 1362.4, 1399.8, 1426.1, 1450.1, 1481.9, 1563.5 nm;
- **GSE**: 1128.7, 1218.3, 1310.3, 1392.0, 1419.6, 1448.4, 1474.1, 1502.4, 1570.4 nm;
- **PGE**: 1115.6, 1132.2, 1150.0, 1292.0, 1314.4, 1381.2, 1401.3, 1418.8, 1435.1, 1468.0, 1486.3, 1509.7, 1564.5 nm.

Based on the relevant wavelengths determined as partial results of the PCA, PCA-LDA and PLSR models, the absorption bands for plum juice blends that contribute most to successful chemometric modelling were summarised. The obtained wavelength-frequency results are presented as absorption bands in Figure 59. The plots by instrument provide evidence of coincident absorption bands.

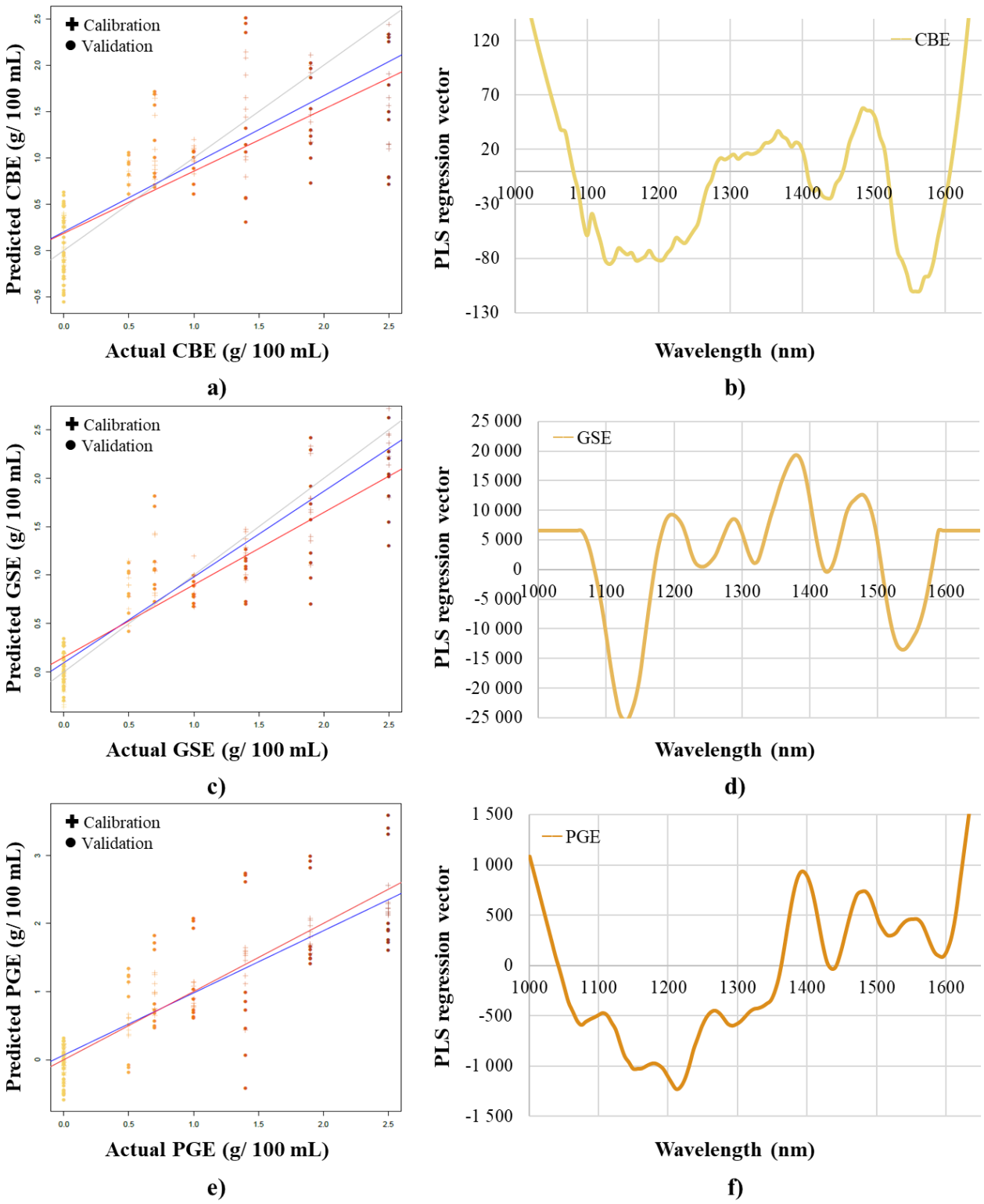

Figure 57. PLSR prediction of plant extract content of simple plum juice blends scanned with the hand-held NIR instrument: Y-fit of CBE prediction (a); regression vectors of CBE prediction (b); Y-fit of GSE prediction (c); regression vectors of GSE prediction (d); Y-fit of PGE prediction (e); regression vectors of PGE prediction (f).

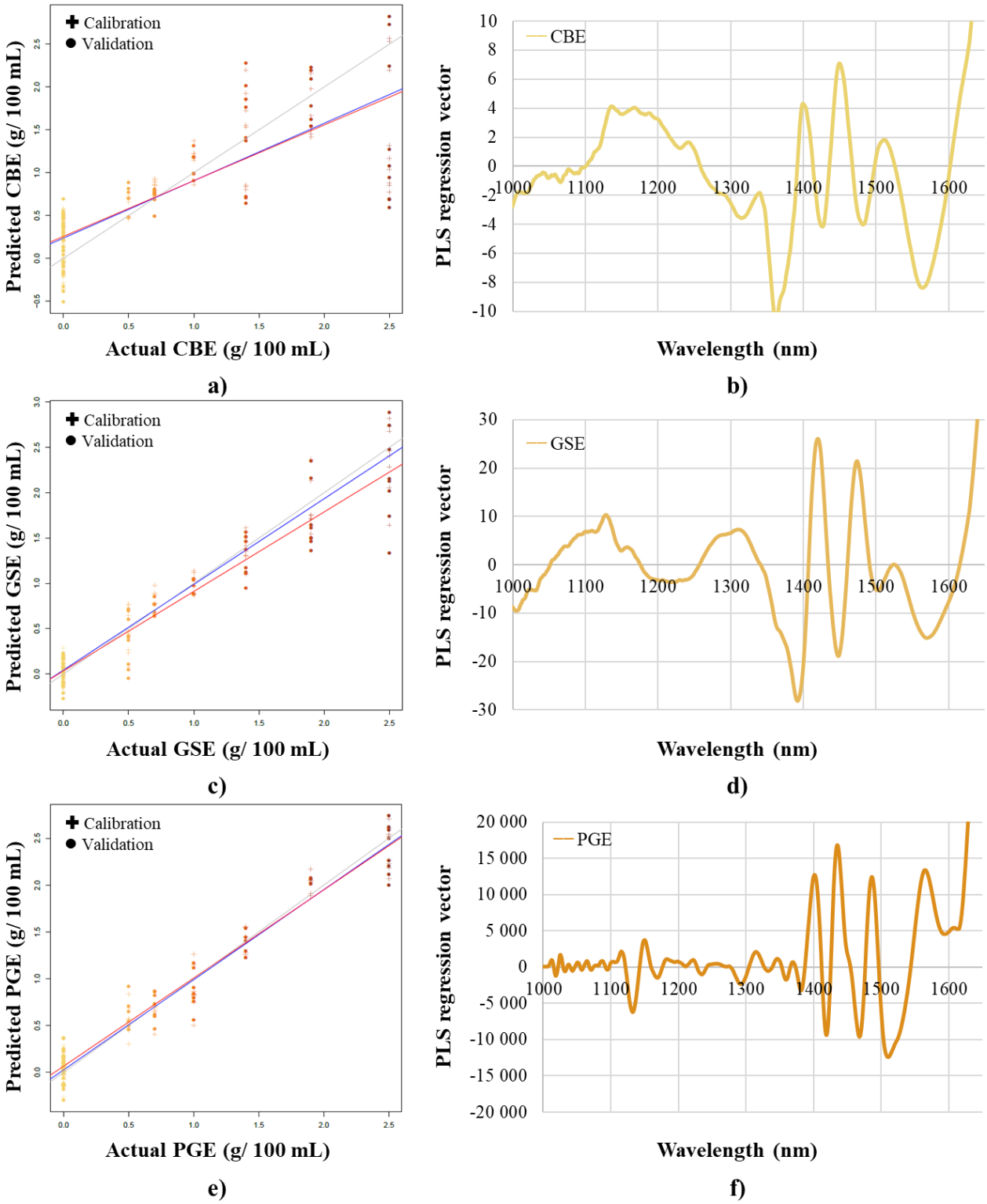

Figure 58. PLSR prediction of plant extract content of simple plum juice blends scanned with the benchtop NIR instrument: Y-fit of CBE prediction (a); regression vectors of CBE prediction (b); Y-fit of GSE prediction (c); regression vectors of GSE prediction (d); Y-fit of PGE prediction (e); regression vectors of PGE prediction (f).

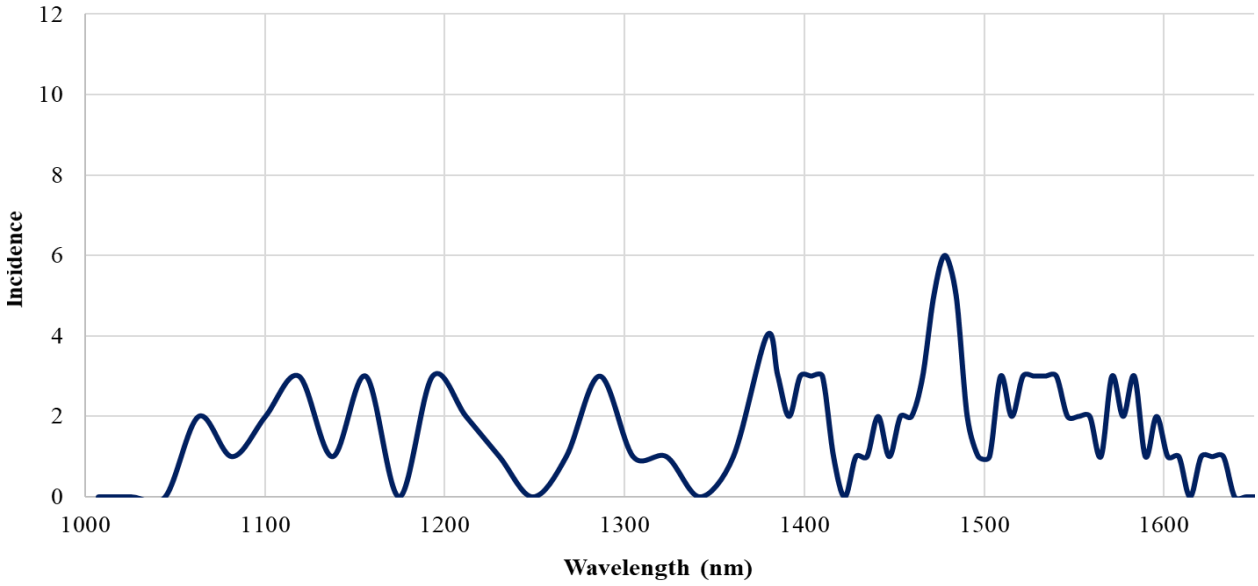

a)

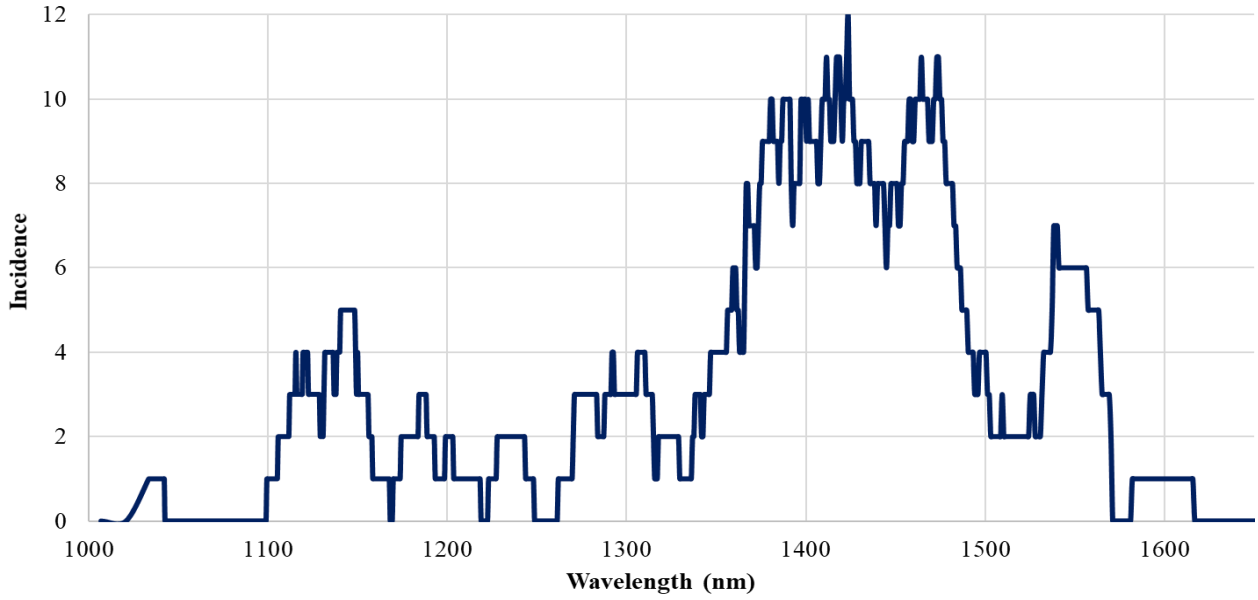

b)

Figure 59. Absorbance bands frequently observed in chemometric modelling results of plum juice enrichment with plant extracts: findings on the hand-held NIR spectrometer data (a); findings on the benchtop NIR spectrometer data (b).

There is relatively little available literature on the detectability of value enhancement and fortification of fruit juices. With the general profiling of fruit juices, more and more researchers are using NIR spectroscopy because of the advantages it offers. Aykac, Cavdaroglu, and Ozen (2023) worked on detecting the manipulation of pomegranate juice, a superfood. The authors reported 100% calibration and 97% validation accuracies for PLS-DA and OPLS-DA, respectively, when detecting 5-10% dilution in binary and ternary blends of sour cherry and black carrot juices. Vitalis et al. (2023) reported classification and prediction results on the probiotic enrichment of apple-sour cherry-plum fruit juice blend, demonstrating that simple and mixed bacterial cultures could be well differentiated, moreover fermentation time and acidity could be predicted accurately.

6. CONCLUSIONS AND RECOMMENDATIONS

As part of the doctoral research, multivariate statistical modelling was conducted based on NIR spectroscopy and hyperspectral imaging with the aim of mapping the key to effective application of the technique in the case of stone fruits and their products.

Sweet cherries, sour cherries and plums intended for the non-destructive assessment of fruits' physiological ripeness were harvested in a very inhomogeneous state according to ripeness. This allowed a wide spectrum of maturation to be studied, but also resulted in high variability in the outcomes. The former statement was mainly true for cherries. Sorting fruit by visually perceived ripeness (pre-classified samples) was often a challenge during the preparation of the measurements, as the available fruit stock did not have an equal quantitative distribution of fruit at different ripeness levels, therefore the number of fruits tested was also unequal in the larger ripeness clusters. To record the spectral characteristics of the fruits, a hand-held NIR device was employed, which is an easy-to-use tool for field studies in fruit production practice. The spectra were recorded on the more mature and immature sides of the fruits to test the effect of scanning location on the accuracy of prediction models.

For qualitative modelling, i.e., classification according to ripeness, spectral pre-treatment and NrPC-optimised LDA was used. To predict some of the fruits' value-measuring properties, spectral pre-treatment and NrLV-optimised PLS regression was employed. The results show that the accuracy of the prediction models was influenced by whether they are based on complete or partial datasets. However, for the latter case, if they were built on the data of more mature or the immature side can be dependent or sensitive to the variety of fruit and component under estimation.

Different varieties of sour cherries and plums were included in the experiments to detect *Monilinia* causing brown rot on fruits' surface. The spectra were obtained at three measurement points with the hand-held NIR device, and from nine surface areas with hyperspectral image processing. The latter's line scanning (push-broom) operation allowed fruit to be inspected without contact, as if they were moving on a conveyor belt. Separate sample sets were prepared for the two different instrumental analyses because the illuminating light of the HSI system used was very intense. Of the fruit infected with *M. fructigena* conidia in different ways and to different extents, only wound-infected samples stored above 20 °C showed signs of rotting and conidia formation. Within these sample sets, contrary to expectations, the "response" to infection of fruit that had been similarly inoculated and stored was different. Some fruits showed "meaningful" signs earlier, others later, if at all. In the recorded spectra, the increased amount of conidia on the surface of the fruit and the "dripping" of the wounds was disturbing. To reduce the effect of noise, various spectral pre-treatment techniques have been employed prior to qualitative modelling, otherwise the differentiation would have been based on light scattering only.

In general, there was a considerable, but not significant, divergence in the SIMCA models when the different modes of inoculation and storage were evaluated together on certain days of storage. The PCA-LDA models for classification according to initial conidia concentration based on spectra recorded on the first day of storage, showed varying classification accuracy, but it was

generally true that HSI gave more accurate models. Interestingly, for samples of EB, UF and TP varieties, the classification of the same sample sets by instrument was the most accurate. The highest average correct classification according to the appearance time of visible signs of *Monilinia* infection was based on hand-held NIR spectra for EB and TD samples, and HSI spectra for UF and TP samples.

The examination of fruit juices enriched with various extracts was conducted in transflexion and transmission arrangements using a hand-held NIR and a benchtop FT NIR spectrometer. The same samples were examined with both instruments. The characteristic of the prepared fruit juices was that the dosed extract did not always completely dissolve and the powdery particles tended to settle in the sample containers. After homogenization, when loading the sample solutions, we aimed to analyse a solution free of interfering components. During the qualitative and quantitative analysis of spectral data, spectral pre-processing, NrPC- or NrLV-optimised PCA-LDA and PLSR modelling were applied, respectively. Overall, it was found that chemometric modelling based on data recorded by the benchtop instrument resulted in more accurate classification and extract concentration prediction. This can be attributed, on the one hand, to the instrument's resolution, and on the other hand, to the measurement setup, highlighting that the transmission measurement approach is better suited for measuring transparent liquids like the juices we had. Comparing the modelling results of the examined fruit juices, it was found that sour cherry juices exhibited better model fitting. This is suspected to be due to some unidentified sample preparation anomaly in the case of plum juice samples.

Chemometric modelling results based on spectra recorded with HSI and NIR instruments show relatively high variability, especially during classifications. The primary reason for this is the naturally high variability of the fruits, despite the sample replicates. Our research, based partly on the development of measurement techniques and partly on statistical methods, is of great importance as it is based on the investigation of economically important fruits, for which there is very limited source material available, both in literature and in practice, for the non-destructive examination. Small-scale handheld NIR instruments can be used for on-site inspections, while line scan recording of HSI can support continuous production processes. In addition, prominent absorption bands obtained from chemometric modelling can contribute to the development of target instruments.

Based on the above summary, we have the following suggestions for the extension of studies:

- Preparation of fruit studies for larger sample sets,
- Involvement of untested factors in the modelling (e.g., different origin, season, etc.),
- Pre-sorting of fruits not only on the basis of their visual characteristics,
- Very precise setting of fruit storage and measurement conditions,
- Implementation of variable wavelength selection methods prior chemometrics,
- Involvement of other chemometric methods in data analysis (e.g., PLS-DA, SVM, k-NN),
- Calibration transfer between precision benchtop and hand-held instruments,
- Model testing with completely independent sample sets.

7. NEW SCIENTIFIC FINDINGS

In the new scientific results, the handheld near infrared (NIR) spectrometer used in fruit ripeness studies refers to NIR-S-G1 (InnoSpectra Co., Hsinchu, Taiwan). In the Monilinia detection studies, the hand-held NIR instrument refers to NIR-S-G1 (InnoSpectra Co., Hsinchu, Taiwan, and the hyperspectral imaging system refers to Headwall XEVA-1648 XC134. In the fruit juice studies, hand-held NIR device refers to MicroNIR (Viavi, Scottsdale, USA), and benchtop spectrometer refers to NIRFlex N-500 (Büchi Labortechnik AG, Flawil, Switzerland). Classification modelling refers to principal component analysis-based linear discriminant analysis (PCA-LDA), and predictive modelling refers to partial least squares regression (PLSR).

New scientific findings on the determination of stone fruit ripeness with hand-held NIR spectrometer (950-1650 nm)

1. The efficiency with which a hand-held NIR spectrometer could classify stone fruits according to ripeness has been determined.
   - For sweet cherries, the classification models performed with up to 91.7 and 78.0% accuracy during model building and validation, respectively.
   - For sour cherries, the classification models performed with up to 87.8 and 82.4% accuracy during model building and validation, respectively,
   - For plums, the classification models performed with up to 82.1 and 70.7% accuracy during model building and validation, respectively.

2. The efficiency with which a hand-held NIR spectrometer could predict dry matter content of stone fruits of different ripeness has been determined.
   - For sweet cherries, the modelling and validation was performed with a maximal Rc^2 of 0.88 and RMSEc of 2.07% m/m, Rcv^2 of 0.83 and RMSEcv of 2.50% m/m, respectively.
   - For sour cherries, the modelling and validation was performed with a maximal Rc^2 of 0.79 and RMSEc of 1.47% m/m, Rcv^2 of 0.72 and RMSEcv of 1.67% m/m, respectively.
   - For plums, the modelling and validation was performed with a maximal Rc^2 of 0.45 and RMSEc of 1.02% m/m, Rcv^2 of 0.35 and RMSEcv of 1.11% m/m, respectively.

3. The efficiency with which a hand-held NIR spectrometer could predict soluble solid content of stone fruits of different ripeness has been determined.
   - For sweet cherries, modelling and validation was performed with a maximal Rc^2 of 0.95 and RMSEc of 0.69% brix, Rcv^2 of 0.93 and RMSEcv of 0.79% brix, respectively.
   - For sour cherries, modelling and validation was performed with a maximal Rc^2 of 0.87 and RMSEc of 0.98% brix, Rcv^2 of 0.83 and RMSEcv of 1.10% brix, respectively.
   - For plums, modelling and validation was performed with a maximal Rc^2 of 0.97 and RMSEc of 0.32% brix, Rcv^2 of 0.95 and RMSEcv of 0.41% brix, respectively.

New scientific finding on the spectral detectability of Monilinia contamination in stone fruits with a hand-held NIR spectrometer or hyperspectral imaging (1000-1650 nm)

4. For the first time in the scientific literature, the performance of a hand-held NIR spectrometer for the detection of *Monilinia fructigena* on the surface stone fruits (with or without injury, stored at refrigerated or room temperature) has been determined based on spectral data recorded on the first day of storage after inoculation. Classification models were developed separately by storage condition to discriminate:

- sour cherries of four conidial contamination levels (in tenfold dilutions: ~ 100-10-1-0.1 conidium/μL), when classification accuracies for "Érdi bőtermő" sour cherries were between 63.1-77.6% and 23.5-34.1%, for "Újfehértói" cherries were between 58.2-85.1% and 24.6-42.0% during model building and validation, respectively.
- plums of three conidial contamination levels (in tenfold dilutions: ~ 100-10-1 conidium/μL), when classification accuracies for "Topend" plums were between 74.2-84.2% and 34.0-50.4%, for "Topend plus" plums were between 78.9-92.9% and 35.1-51.6% during model building and validation, respectively.

5. For the first time in the scientific literature, the performance of a hyperspectral imaging for the detection of *Monilinia fructigena* on the surface stone fruits (with or without injury, stored at refrigerated or room temperature) has been determined based on spectral data recorded on the first day of storage after inoculation. Classification models were developed separately by storage condition to discriminate:
- sour cherries of four conidial contamination levels (in tenfold dilutions: ~ 100-10-1-0.1 conidium/μL), when classification accuracies for "Érdi bőtermő" sour cherries were between 61.6-85.6% and 33.1-45.0%, for "Újfehértói" cherries were between 83.4-98.0% and 32.5-53.3% during model building and validation, respectively.
- plums of three conidial contamination levels (in tenfold dilutions: ~ 100-10-1 conidium/μL), when classification accuracies for "Topend" plums were between 81.6-97.1% and 42.8-75.2%, for "Topend plus" plums were between 78.9-87.1-100% and 50.0-79.3% during model building and validation, respectively.

New scientific findings on the predictability of fruit juice enrichment with NIR spectroscopy (1000-1650 nm)

6. The performance of a hand-held NIR spectrometer for the prediction of fruit juice enrichment with plant extracts has been determined.
- In simple sour cherry juice blends, cranberry extract was predicted with an Rcv^2 of 0.92 and RMSEcv of 0.25 g/100 mL, grape seed extract content with an Rcv^2 of 0.90 and RMSEcv of 0.27 g/100 mL, and pomegranate extract with an Rcv^2 of 0.87 and RMSEcv of 0.31 g/100 mL.
- In simple plum juice blends, cranberry extract was predicted with an Rcv^2 of 0.53 and RMSEcv of 0.59 g/100 mL, grape seed extract content with an Rcv^2 of 0.76 and RMSEcv of 0.42 g/100 mL, and pomegranate extract with an Rcv^2 of 0.47 and RMSEcv of 0.62 g/100 mL.

7. The performance of a benchtop NIR spectrometer for the prediction of fruit juice enrichment with plant extracts has been determined.
- In simple sour cherry juice blends, cranberry extract was predicted with an Rcv^2 of 0.97 and RMSEcv of 0.13 g/100 mL, grape seed extract content with an Rcv^2 of 0.92 and RMSEcv of 0.23 g/100 mL, and pomegranate extract with an Rcv^2 of 0.97 and RMSEcv of 0.15 g/100 mL.
- In simple plum juice blends, cranberry extract was predicted with an Rcv^2 of 0.61 and RMSEcv of 0.54g/100 mL, grape seed extract content with an Rcv^2 of 0.90 and RMSEcv of 0.27 g/100 mL, and pomegranate extract with an Rcv^2 of 0.98 and RMSEcv of 0.18 g/100 mL.

8. SUMMARY

Fruits, especially those species with highly valuable nutritional composition, have a major role to play in reforming human diets and shaping dietary trends. The very valuable nutritional properties of the sweet cherry, sour cherry and plum varieties involved in the present research justify the preservation of quality out of season, but this requires them to undergo very complex agricultural and food industrial processes. During fruit ripening, postharvest monitoring as well as in food processing and control, there is a trend towards the use of non-targeted analytical methods to obtain a comprehensive analytical image of the subject, preferably in a non-destructive and even non-contact manner. In collaboration with Agricolae Ltd., our research objectives included the novel application of digital fingerprinting approaches to assess their applicability for the prediction of certain qualitative and quantitative indicators of ripening fruit, monitoring of fruit decay during storage, and authentication of fruit juices enriched with various fruit-derived extracts.

To meet these objectives, we examined the near infrared light absorption patterns of our samples. The knowledge and application of spectral methods are well-known, but despite their successful application in e.g., cereal qualitative reception, it has been less widespread in fruit production and classification practice. When exploring the related literature, it was found that a significant portion of the published studies report very accurate classification and prediction modelling results in certain cases, but there is less discussion of the impact of, for example, spectral acquisition on modelling results. Interestingly, limited literature is available on the spectral detectability of *Monilinia* contamination and resulting decay, a major threat to sour cherry and plum production. The same is true for authenticity assessment of enriched of fruit juices.

During the fruit ripeness examinations, the non-destructive analyses of pre-classified stone fruits was conducted using a hand-held NIR device. The advantage of such instruments is that spectra can be recorded in a controlled manner due to internal illumination and contact measurement. Qualitative and quantitative chemometric modelling revealed that it varied by fruit variety, whether the models based on the more mature, immature, or the entire dataset performed better. To clearly determine the positive or negative impact of the location of spectrum scanning, it is necessary to extend the studies.

During the determination of *Monilinia* detectability on stone fruits, hand-held NIR and benchtop hyperspectral instruments were employed. Based on the results, the differences in storage conditions had a significant impact on the samples, while the mode of sample inoculation (with or without injury) had a less pronounced effect. The PCA-LDA results according to initial conidial contamination showed highly variable classification accuracies, but it was generally established that higher average correct classification was achieved using HSI. Based on the classification according to the appearance time of visible infection signs, this could not be stated so clearly. Interestingly, despite the fact that the available HSI system recorded the data in a reflectance measurement setup with external illumination, it allowed a more accurate classification of the samples tested. This verified for us that with average spectra obtained from several surface areas, a more complete analytical image of the samples emerges despite measurements more exposed to environmental influences (e.g., temperature, dust, etc.). To reduce the high variability observed during measurements and data evaluations, a larger initial sample size and instrumental sorting of the fruits would be necessary prior sample preparation.

Fruit juices enriched with different combinations and degrees of plant extracts were examined using two instruments with different measurement setups, a transflectance hand-held and a transmittance benchtop NIR device. The classification and predictition models reflect that the latter instrument, due to its high resolution and measurement arrangement, is more effectively applicable for analysing liquid samples similar to fruit juices. During the examination of fruit juice blends, a slight sedimentation of powder-like extract particles was observed. To mitigate this potential negative effect, it may be justified to remove the undissolved particles, for example, through filtration. To gain a deeper understanding of the impact of different instrument constructions (i.e., transmittance, transflectance) on prediction accuracy, it would be worthwhile to extend the investigations by comparing results obtained from identical measurement setups. In addition to these, it would be beneficial to implement a calibration transfer from precision instrumented data to hand-held data.

The method development presented in the dissertation is based partly on methodological and partly on statistical evaluation, demonstrates the easy applicability of the NIR technique for conducting laboratory and even on-site examinations. The applied chemometric approaches can be multi-used, as they can be relatively easily and quickly adapted for the analysis of new similar datasets or for refining existing models. Our long-term ambition is to create and continuously develop databases along with chemometric models that allow quantitative and qualitative mapping not “only” a portion of harvested fruits, but also orchards or even regions. In our opinion, this doctoral research will provide a good basis for determining the optimal harvest time of fruit, for effective intervention in case of emerging fruit diseases, for optimising processing procedures, and monitoring the composition of fruit products.

9. LIST OF PUBLICATIONS IN THE FIELD OF STUDY

9.1. Journal articles

9.1.1. Publications in journal quartiles

First author publications

Flora Vitalis, Jelena Muncan, Sukritta Anantywittayanon, Zoltan Kovacs, Roumiana Tsenkova (2023). Aquaphotomics Monitoring of Lettuce Freshness During Cold Storage. *Foods*, 12(2): 258. (DOI: 10.3390/foods12020258) – **Q1** (2023)

Flora Vitalis, David Tjandra Nugraha, Balkis Aouadi, Juan Pablo Aguinaga Bósquez, Zsanett Bodor, John-Lewis Zinia Zaukuu, Tamás Kocsis, Viktoria Zsom-Muha, Zoltan Gillay, Zoltan Kovacs (2021). Detection of Monilia Contamination in Plum and Plum Juice with NIR Spectroscopy and Electronic Tongue, *Chemosensors*, 9(12), 355. (DOI: 10.3390/chemosensors9120355) – **Q2** (2023)

Flora Vitalis, John-Lewis Zinia Zaukuu, Zsanett Bodor, Balkis Aouadi, Géza Hitka, Timea Kaszab, Viktoria Zsom-Muha, Zoltan Gillay, Zoltan Kovacs (2020). Detection and Quantification of Tomato Paste Adulteration Using Conventional and Rapid Analytical Methods, *Sensors*, 20(21), 6059. (DOI: 10.3390/s20216059) – **Q1** (2023)

Vitális Flóra, Bodor Zsanett, John-Lewis Zinia Zaukuu, Bázár György, Kovács Zoltán (2019)**.** Aquaphotomics: a közeli infravörös spektroszkópia innovatív, víz központú alkalmazása [Aquaphotomics: an innovative application of near-infrared spectroscopy focusing on water]. *Élelmiszervizsgálati Közlemények*, 65(4). pp. 2672-2687., 16 p. (ISSN: 2676-8704) – **Q4** (2023)

Co-authored publications

Gergo Szabo, **Flora Vitalis**, Zsuzsanna Horvath-Mezofi, Monika Gob, Aguinaga Juan Palblo Bosquez, Zoltan Gillay, Tamas Zsom, Lien Le Puong Nguyen, Geza Hitka, Zoltan Kovacs, Laszlo Friedrich (2023). Application of Near Infrared Spectroscopy to Monitor the Quality Change of Sour Cherry Stored Under Modified Atmosphere Conditions. *Sensors*. 23(1):479. (DOI: 10.3390/S23010479) – **Q1** (2023)

Lívia Darnay, **Flóra Vitális**, Anna Szepessy, Dávid Bencze, Tamás Csurka, József Surányi, Ferenc Firtha, Péter Laczay (2022). Comparison of different visual methods to follow the effect of milk heat treatment and microbial transglutaminase on appearance of semi-hard buffalo cheese. *Food Control*, 139, 109049. (DOI: 10.1016/j.foodcont.2022.109049) – **D1** (2023)

Balkis Aouadi, **Flora Vitalis**, Zsanett Bodor, John-Lewis Zinia Zaukuu, Istvan Kertesz, Zoltan Kovacs (2022). NIRS and Aquaphotomics Trace Robusta-to-Arabica Ratio in Liquid Coffee Blends, *Molecules*, 27(2), 388. (DOI: 10.3390/molecules27020388) – **Q1** (2023)

David Tjandra Nugraha, John-Lewis Zinia Zaukuu, Juan Pablo Aguinaga Bósquez, Zsanett Bodor, **Flora Vitalis**, Zoltan Kovacs (2021). Near-Infrared Spectroscopy and Aquaphotomics for Monitoring Mung Bean (Vigna radiata) Sprout Growth and Validation of Ascorbic Acid Content, *Sensors*, 21(2), 611. (DOI: 10.3390/s21020611) – **Q1** (2023)

Haruna Gado Yakubu, Zoltán Kovács, **Flóra Vitális**, György Bázár (2021). Near-infrared spectroscopy: rapid and effective tool for measuring fructose content [Közeli-infravörös spektroszkópia: gyors és hatékony eszköz a fruktóztartalom mérésére]. Élelmiszervizsgálati Közlemények, 67(1), pp. 3249-3268. (DOI: 10.52091/JFI-2021/1-1-ENG) – **Q4** (2023)

Balkis Aouadi, John-Lewis Zinia Zaukuu, **Flora Vitális**, Zsanett Bodor, Orsolya Fehér, Zoltán Gillay, George Bazar, Zoltan Kovacs (2020). Historical Evolution and Food Control Achievements of Near Infrared Spectroscopy, Electronic Nose, and Electronic Tongue—Critical Overview, *Sensors*, 20(19), 5479. (DOI: 10.3390/s20195479) – **Q1** (2023)

Zoltan Kovacs, Dániel Szöllősi, John-Lewis Zinia Zaukuu, Zsanett Bodor, **Flóra Vitális**, Balkis Aouadi, Zsom-Muha Viktória, Zoltan Gillay (2020). Factors influencing the long-term stability of electronic tongue and application of improved drift correction methods, *Biosensors*, 10(7), 74. (DOI: 10.3390/bios10070074) – **Q1** (2023)

Zaukuu, John Lewis Zinia, Aouadi, Balkis, Lukács, Mátyás, Bodor, Zsanett, Vitális, Flóra, Gillay, B., Gillay, Z., Friedrich, L., Kovacs, Z. (2020). Detecting Low Concentrations of Nitrogen-Based Adulterants in Whey Protein Powder Using Benchtop and Handheld NIR Spectrometers and the Feasibility of Scanning through Plastic Bag. *Molecules*, 25(11), 2522. (DOI: 10.3390/molecules25112522) – **Q1** (2023)

9.1.2. Publications in non-quartile journals

Flóra Vitális, Juan Pablo Aguinag Bósquez, Mátyás Lukács, Marietta Petróczy, Marietta Fodor, Zoltán Gillay, Zoltán Kovács (2024). Development of state-of-the-art correlative rapid methods for the non-destructive control of fruit products. Scientia et Securitas, 4(4), 258-264. (DOI: 10.1556/112.2023.00202)

Kata Józsa, **Flóra Vitális**, Zoltán Kovács, Gabriella Zsarnóczay (2022). Marhahús sertéshússal történő hamisításának kimutatása spektroszkópiás módszerekkel (1. rész). A Hús: A Magyar Húsipar Szakmai Folyóirata: Az Országos Húsipari Kutatóintézet Folyóirata 1: 1-2 pp. 16-21., 6 p. (DOI: 10.56616/meat.3411)

Vitális Flóra (2021). Növényi eredetű élelmiszerek eredetiségének meghatározása közeli infravörös spektroszkópiával. *Táplálkozástudományi Morzsák Hírlevél*, 4(3), pp. 11-13. (ISSN: 2630-8975)

9.2. Book chapters

John-Lewis Zinia Zaukuu, Zsanett Bodor, **Flóra Vitális**, and Zoltán Kovács (2023). 10. Detection Methods of Adulteration in Natural Foods. In Megh R. Goyal, Arijit Nath, Zoltan Kovacs (Ed.), Sustainable and Functional Foods from Plants (1st ed.). CRC Press. (ISBN: 9781774914540)

Jelena Muncan, Balkis Aouadi, **Flora Vitalis**, Zoltan Kovacs, Roumiana Tsenkova (2020). 10. Soil Aquaphotomics for Understanding Soil - Health Relation Through Water-Light Interaction. In Rattan Lal (Ed.), The Soil-Human Health-Nexus (1st ed.). CRC Press. (ISBN: 9780367822736)

10. APPENDICES

10.1. References

Agrios, George N. 2005. *Plant Pathology*. Elsevier.

Aiello, Dalia, Cristina Restuccia, Emilio Stefani, Alessandro Vitale, and Gabriella Cirvilleri. 2019. "Postharvest Biocontrol Ability of Pseudomonas Synxantha against Monilinia Fructicola and Monilinia Fructigena on Stone Fruit." *Postharvest Biology and Technology* 149:83–89.

Alsolmei, Faten A., Haiwen Li, Suzette L. Pereira, Padmavathy Krishnan, Paul W. Johns, and Rafat A. Siddiqui. 2019. "Polyphenol-Enriched Plum Extract Enhances Myotubule Formation and Anabolism While Attenuating Colon Cancer-Induced Cellular Damage in C2C12 Cells." *Nutrients* 11(5):1077.

Álvarez-Herrera, Javier G., Yuli Alexandra Deaquiz, and Ximena Rozo-Romero. 2021. "Effect of Storage Temperature and Maturity Stage on the Postharvest Period of'Horvin'Plums (Prunus Domestica L.)." *Ingeniería e Investigación* 41(2).

Aouadi, Balkis, John-Lewis Zinia Zaukuu, Flora Vitális, Zsanett Bodor, Orsolya Fehér, Zoltan Gillay, George Bazar, and Zoltan Kovacs. 2020. "Historical Evolution and Food Control Achievements of near Infrared Spectroscopy, Electronic Nose, and Electronic Tongue—Critical Overview." *Sensors* 20(19):5479.

Arjmandi, Bahram H., Sarah A. Johnson, Shirin Pourafshar, Negin Navaei, Kelli S. George, Shirin Hooshmand, Sheau C. Chai, and Neda S. Akhavan. 2017. "Bone-Protective Effects of Dried Plum in Postmenopausal Women: Efficacy and Possible Mechanisms." *Nutrients* 9(5):496.

Astacio, Juan Diego, Eduardo Antonio Espeso, Paloma Melgarejo, and Antonieta De Cal. 2023. "Monilinia Fructicola Response to White Light." *Journal of Fungi* 9(10):988.

Aykac, Basak, Cagri Cavdaroglu, and Banu Ozen. 2023. "Authentication of Pomegranate Juice in Binary and Ternary Mixtures with Spectroscopic Methods." *Journal of Food Composition and Analysis* 117:105100.

Aykas, Didem P., and Luis Rodriguez-Saona. 2024. "What's in Your Fruit Juice?—Rapid Quality Screening Based on Infrared (FT-IR) Spectroscopy." *Applied Sciences* 14(4):1654.

Bakuradze, Tamara, Angelina Tausend, Jens Galan, Isabel Anna Maria Groh, David Berry, Josep A. Tur, Doris Marko, and Elke Richling. 2019. "Antioxidative Activity and Health Benefits of Anthocyanin-Rich Fruit Juice in Healthy Volunteers." *Free Radical Research* 53(sup1):1045–55.

Barkai-Golan, Rivka. 2001. *Postharvest Diseases of Fruits and Vegetables: Development and Control*. Elsevier.

Barta, József, and Imre Körmendy. 2007. *Növényi Nyersanyagok Hőközléses Tartósító Technológiái*. Budapest: Mezőgazda Kiadó.

Barta, József, and Imre Körmendy. 2008. *Növényi Nyersanyagok Feldolgozástechnológiai Műveletei*. Budapest: Mezőgazda Kiadó.

Batra, Lekh R. 1991. *World Species of Monilinia (Fungi): Their Ecology, Biosystematics and Control.*

Beć, Krzysztof B., Justyna Grabska, and Christian W. Huck. 2022. "Miniaturized NIR Spectroscopy in Food Analysis and Quality Control: Promises, Challenges, and Perspectives." *Foods* 11:1–53. doi: 10.3390/foods11101465.

Bernat, M., J. Segarra, X. M. Xu, C. Casals, and J. Usall. 2017. "Influence of Temperature on Decay, Mycelium Development and Sporodochia Production Caused by Monilinia Fructicola and M. Laxa on Stone Fruits." *Food Microbiology* 64:112–18.

Bird, Kevin A., MacKenzie Jacobs, Audrey Sebolt, Kathleen E. Rhoades, Elizabeth I. Alger, Marivi Colle, Paulina K. Bies, Adare J. Cario, Ramya S. Chigurupati, Delaney R. Collazo, Brooke Garland, Kaitlyn M. Hein, Annie R. Hillenberg, Lawrence I. Kado, Vanessa R. Kilian, Philip F. Longueuil, Vibha Mahesha, Kat Munsell, Nicole M. L. Peters, Megan O. Steffes, Sathvik Suryadevara, Grace Urban, Aditya K. Walia, Taylor B. Wirsing, Michael R. McKain, Amy Iezzoni, and Patrick P. Edger. 2022. "Parental Origins of the Cultivated Tetraploid Sour Cherry (<scp><i>Prunus Cerasus</I></Scp> L.)." *Plants People Planet* 4(5):444–50. doi: 10.1002/ppp3.10267.

Bíró, György, and Károly Lindner. 1995. *Tápanyagtáblázat - Táplálkozástan És Tápanyag-Összetétel*. 12. edited by G. Bíró and K. Lindner. Budapest: Medicina Könyvkiadó.

Blando, Federica, and B. Dave Oomah. 2019. "Sweet and Sour Cherries: Origin, Distribution, Nutritional Composition and Health Benefits." *Trends in Food Science & Technology* 86:517–29. doi: https://doi.org/10.1016/j.tifs.2019.02.052.

Boca, Grațiela Dana. 2021. "Factors Influencing Consumer Behavior in Sustainable Fruit and Vegetable Consumption in Maramures County, Romania." *Sustainability* 13(4):1812. doi: 10.3390/su13041812.

BRC, FDF, and SSA. 2016. "Guidance on Authenticity of Herbs and Spices - Industry Best Practice on Assessing and Protecting Culinary Dried Herbs and Spices." Retrieved September 21, 2019 (Guidance on authenticity of herbs and spices-Industry Best).

Brettin, Thomas, R. Karle, E. L. Crowe, and Amy Iezzoni. 2000. "Brief Communication. Chloroplast Inheritance and DNA Variation in Sweet, Sour, and Ground Cherry." *Journal of Heredity* 91(1):75–79. doi: 10.1093/jhered/91.1.75.

Butac, Madalina. 2020. *Plum Breeding*. IntechOpen: London, UK.

Callahan, Ann M. 2008. "Plums." 93–120. doi: 10.1002/9781405181099.k0404.

Carrión-Antolí, Alberto, Domingo Martínez-Romero, Fabián Guillén, Pedro J. Zapata, María Serrano, and Daniel Valero. 2022. "Melatonin Pre-Harvest Treatments Leads to Maintenance of Sweet Cherry Quality during Storage by Increasing Antioxidant Systems." *Frontiers in Plant Science* 13:863467.

Cassani, Lucía, Mauricio Santos, Esteban Gerbino, María del Rosario Moreira, and Andrea Gómez-Zavaglia. 2018. "A Combined Approach of Infrared Spectroscopy and Multivariate Analysis for the Simultaneous Determination of Sugars and Fructans in Strawberry Juices during Storage." *Journal of Food Science* 83(3):631–38.

Castillo-Girones, S., R. Van Belleghem, N. Wouters, S. Munera, J. Blasco, and W. Saeys. 2024. "Detection of Subsurface Bruises in Plums Using Spectral Imaging and Deep Learning with Wavelength Selection." *Postharvest Biology and Technology* 207:112615.

Cattaneo, Tiziana M. P., and Annamaria Stellari. 2019. "NIR Spectroscopy as a Suitable Tool for the Investigation of the Horticultural Field." *Agronomy* 9(9):503.

Chełpiński, Piotr, Ireneusz Ochmian, and Paweł Forczmański. 2019. "Sweet Cherry Skin Colour Measurement as an Non-Destructive Indicator of Fruit Maturity." *Acta Universitatis Cibiniensis. Series E: Food Technology* 23(2):157–66.

Chen, Chaoqun, Hongxu Chen, Wenlong Yang, Jie Li, Wenjing Tang, and Ronggao Gong. 2022. "Transcriptomic and Metabolomic Analysis of Quality Changes during Sweet Cherry Fruit Development and Mining of Related Genes." *International Journal of Molecular Sciences* 23(13):7402.

Chockchaisawasdee, Suwimol, John B. Golding, Quan V Vuong, Konstantinos Papoutsis, and Costas E. Stathopoulos. 2016. "Sweet Cherry: Composition, Postharvest Preservation, Processing and Trends for Its Future Use." *Trends in Food Science & Technology* 55:72–83.

Cortés-Montaña, Daniel, María Josefa Bernalte-García, Manuel Joaquín Serradilla, and Belén Velardo-Micharet. 2023. "Optimal Preharvest Melatonin Applications to Enhance Endogenous Melatonin Content, Harvest and Postharvest Quality of Japanese Plum." *Agriculture* 13(7):1318.

Costa, Rosangela C., and Kássio M. G. de Lima. 2013. "Prediction of Parameters (Soluble Solid and PH) in Intact Plum Using NIR Spectroscopy and Wavelength Selection." *Journal of the Brazilian Chemical Society* 24:1351–56.

Creydt, Marina, and Markus Fischer. 2020. "Food Authentication in Real Life: How to Link Nontargeted Approaches with Routine Analytics?" *Electrophoresis* 41(20):1665–79.

Csapó, János, Csilla Albert, and Zsuzsanna Csapóné Kiss. 2016. *Élelmiszerhamisítás*. Debrecen: Debrecen University Press.

Cui, Jiefen, Yunhe Lian, Chengying Zhao, Hengjun Du, Yanhui Han, Wei Gao, Hang Xiao, and Jinkai Zheng. 2019. "Dietary Fibers from Fruits and Vegetables and Their Health Benefits via Modulation of Gut Microbiota." *Comprehensive Reviews in Food Science and Food Safety* 18(5):1514–32.

Das, Biswajit, N. Ahmed, and Pushkar Singh. 2011. “Prunus Diversity-Early and Present Development: A Review.” *Int J Biodivers Conserv* 3(14):721–34.

Dasenaki, Marilena E., and Nikolaos S. Thomaidis. 2019. “Quality and Authenticity Control of Fruit Juices - A Review.” *Molecules* 24(6):1–35.

Desiderio, Francesco, Samuel Szilagyi, Zsuzsanna Békefi, Gábor Boronkay, Valentina Usenik, Biserka Milić, Cristina Mihali, and Liviu Giurgiulescu. 2023. “Polyphenolic and Fruit Colorimetric Analysis of Hungarian Sour Cherry Genebank Accessions.” *Agriculture* 13(7):1287.

EC. 2001. “COUNCIL DIRECTIVE 2001/112/EC Relating to Fruit Juices and Certain Similar Products Intended for Human Consumption.” *Official Journal of the European Union* 1–9.

EC. 2002. “REGULATION (EC) No 178/2002 OF THE EUROPEAN PARLIAMENT AND OF THE COUNCIL Laying down the General Principles and Requirements of Food Law, Establishing the European Food Safety Authority and Laying down Procedures in Matters of Food Safety.” *Official Journal of the European Communities* 1–24.

EC. 2008a. “REGULATION (EC) No 1332/2008 OF THE EUROPEAN PARLIAMENT AND OF THE COUNCIL on Food Enzymes and Amending Council Directive 83/417/EEC, Council Regulation (EC) No 1493/1999, Directive 2000/13/EC, Council Directive 2001/112/EC and Regulation (EC) No 258/97.” *Official Journal of the European Union* 1–9.

EC. 2008b. “REGULATION (EC) No 1333/2008 OF THE EUROPEAN PARLIAMENT AND OF THE COUNCIL on Food Additives.” *Official Journal of the European Union* 1–18.

EC. 2008c. “REGULATION (EC) No 1334/2008 OF THE EUROPEAN PARLIAMENT AND OF THE COUNCIL on Flavourings and Certain Food Ingredients with Flavouring Properties for Use in and on Foods and Amending Council Regulation (EEC) No 1601/91, Regulations (EC) No 2232/96 and (EC) No 110/2008 and Directive 2000/13/EC.” *Official Journal of the European Union* 1–17.

EFSA. 2021. “Food Composition Data.” Retrieved November 17, 2024 (https://www.efsa.europa.eu/en/microstrategy/food-composition-data).

El-Beltagi, Hossam S., Abeer E. El-Ansary, Mai A. Mostafa, Teba A. Kamel, and Gehan Safwat. 2019. “Evaluation of the Phytochemical, Antioxidant, Antibacterial and Anticancer Activity of Prunus Domestica Fruit.” *Notulae Botanicae Horti Agrobotanici Cluj-Napoca* 47(2):395–404.

Elik, Aysel, Derya Kocak Yanik, Yildiray Istanbullu, Nurcan Aysar Guzelsoy, Arzu Yavuz, and Fahrettin Gogus. 2019. “Strategies to Reduce Post-Harvest Losses for Fruits and Vegetables.” *Strategies* 5(3):29–39.

Escribano, S., W. V Biasi, R. Lerud, D. C. Slaughter, and E. J. Mitcham. 2017. “Non-Destructive Prediction of Soluble Solids and Dry Matter Content Using NIR Spectroscopy and Its Relationship with Sensory Quality in Sweet Cherries.” *Postharvest Biology and Technology* 128:112–20.

Esslinger, S., J. Riedl, and C. Fauhl-Hassek. 2014. “Potential and Limitations of Non-Targeted Fingerprinting for Authentication of Food in Official Control.” *Food Research International* 60:189–204.

EU. 2011a. “COMMISSION IMPLEMENTING REGULATION (EU) No 543/2011 Laying down Detailed Rules for the Application of Council Regulation (EC) No 1234/2007 in Respect of the Fruit and Vegetables and Processed Fruit and Vegetables Sectors.” *Official Journal of the European Union* 1–163.

EU. 2011b. “COMMISSION REGULATION (EU) No 1129/2011 Amending Annex II to Regulation (EC) No 1333/2008 of the European Parliament and of the Council by Establishing a Union List of Food Additives.” *Official Journal of the European Union* 1–177.

EU. 2011c. “REGULATION (EU) No 1169/2011 OF THE EUROPEAN PARLIAMENT AND OF THE COUNCIL on the Provision of Food Information to Consumers.” *Official Journal of the European Union* 1–46.

EU. 2015. “REGULATION (EU) 2015/2283 OF THE EUROPEAN PARLIAMENT AND OF THE COUNCIL - on Novel Foods, Amending Regulation (EU) No 1169/2011 of the European Parliament and of the Council and Repealing Regulation (EC) No 258/97 of the European Parliament and of the Council and Commission Regulation (EC) No 1852/2001.” *Official Journal of the European Union* 1–22.

EU. 2018. “COMMISSION IMPLEMENTING REGULATION (EU) 2018/1023 Correcting Implementing Regulation (EU) 2017/2470 Establishing the Union List of Novel Foods.” *Official Journal of the European Union* 1–133.

Everstine, Karen, John Spink, and Shaun Kennedy. 2013. “Economically Motivated Adulteration (EMA) of Food: Common Characteristics of EMA Incidents.” *Journal of Food Protection* 76(4):723–35. doi: 10.4315/0362-028X.JFP-12-399.

Faienza, Maria Felicia, Filomena Corbo, Alessia Carocci, Alessia Catalano, Maria Lisa Clodoveo, Maria Grano, David Q. H. Wang, Gabriele D’amato, Marilena Muraglia, and Carlo Franchini. 2020. “Novel Insights in Health-Promoting Properties of Sweet Cherries.” *Journal of Functional Foods* 69:103945.

Fan, Jin-Yan, Li-Yun Guo, Jian-Ping Xu, Yong Luo, and Themis J. Michailides. 2010. “Genetic Diversity of Populations of Monilinia Fructicola (Fungi, Ascomycota, Helotiales) from China.” *Journal of Eukaryotic Microbiology* 57(2):206–12.

Fang, Zhi-Zhen, Dan-Rong Zhou, Xin-Fu Ye, Cui-Cui Jiang, and Shao-Lin Pan. 2016. “Identification of Candidate Anthocyanin-Related Genes by Transcriptomic Analysis of ‘Furongli’Plum (Prunus Salicina Lindl.) during Fruit Ripening Using RNA-Seq.” *Frontiers in Plant Science* 7:1338.

FAO. 2023a. “Production of Crops and Livestock Products by Year.” *FAOSTAT*. Retrieved September 24, 2024 (https://www.fao.org/faostat/en/#data/QCL).

FAO. 2023b. “Production Quantities of Crops and Livestock Products by Country.” *FAOSTAT*. Retrieved September 24, 2024 (https://www.fao.org/faostat/en/#data/QCL/visualize).

FAO, and WHO. 2005. “GENERAL STANDARD FOR FRUIT JUICES AND NECTARS (CXS-247-2005).” *Codex Alimentarius - International Standards* 1–20.

FAO, and WHO. n.d. “About Codex Alimentarius.” Retrieved October 20, 2024 (https://www.fao.org/fao-who-codexalimentarius/about-codex/en/#c453333).

Fazzari, Marco, Lana Fukumoto, Giuseppe Mazza, Maria A. Livrea, Luisa Tesoriere, and Luigi Di Marco. 2008. “In Vitro Bioavailability of Phenolic Compounds from Five Cultivars of Frozen Sweet Cherries (Prunus Avium L.).” *Journal of Agricultural and Food Chemistry* 56(10):3561–68.

FDA. 2009. “Economically Motivated Adulteration; Public Meeting.” *Federal Register* 74:15497–99.

Femenias, Antoni, Ferran Gatius, Antonio J. Ramos, Irene Teixido-Orries, and Sonia Marín. 2022. “Hyperspectral Imaging for the Classification of Individual Cereal Kernels According to Fungal and Mycotoxins Contamination: A Review.” *Food Research International* 155:111102. doi: https://doi.org/10.1016/j.foodres.2022.111102.

Firtha, F. 2011. “Argus Szoftver.”

Fodor, Marietta. 2022. “Development of FT-NIR Technique to Determine the Ripeness of Sweet Cherries and Sour Cherries.” *Processes* 10(11):2423.

Fodor, Marietta, Zsuzsa Jókai, Anna Matkovits, and Eszter Benes. 2023. “Assessment of Maturity of Plum Samples Using Fourier Transform Near-Infrared Technique Combined with Chemometric Methods.” *Foods* 12(16):3059.

Fotirić Akšić, Milica, Živoslav Tešić, Milica Kalaba, Ivanka Ćirić, Lato Pezo, Biljana Lončar, Uroš Gašić, Biljana Dojčinović, Tomislav Tosti, and Mekjell Meland. 2023. “Breakthrough Analysis of Chemical Composition and Applied Chemometrics of European Plum Cultivars Grown in Norway.” *Horticulturae* 9(4):477.

Frida Food Data. 2024a. “Cherry, Raw.” *Danish Food Composition Database*. Retrieved September 23, 2024 (https://frida.fooddata.dk/food/1854?lang=en).

Frida Food Data. 2024b. “Plum, Raw.” *Danish Food Composition Database*. Retrieved September 23, 2024 (https://frida.fooddata.dk/food/1852?lang=en).

Furulyás, Diána, Lilla Szalóki-Dorkó, M. Máté, and Éva Stefanovits-Bányai. 2024. “Enrichment of Apple Juice with Antioxidant-Rich Elderberry (Sambucus Nigra L) Pomace Extract.” *Acta Alimentaria* 53(2):327–35.

Garcia-Benitez, Carlos, Paloma Melgarejo, Antonieta De Cal, and Blanca Fontaniella. 2016. “Microscopic Analyses of Latent and Visible Monilinia Fructicola Infections in Nectarines.” *PloS One* 11(8):e0160675.

Geladi, Paul, Hans Grahn, and Marena Manley. 2010. “Data Analysis and Chemometrics for Hyperspectral Imaging.” *Raman, Infrared, and Near-infrared Chemical Imaging* 93–107.

Gell, Iray, Antonieta De Cal, Rosario Torres, Josep Usall, and Paloma Melgarejo. 2008. “Relationship between the Incidence of Latent Infections Caused by Monilinia Spp. and the Incidence of Brown Rot of Peach Fruit: Factors Affecting Latent Infection.” *European Journal of Plant Pathology* 121:487–98.

Gopal, Srinivasa. 2023. “Survey on Ordering and Eating Food Using Online Food Delivery Applications.” *International Journal for Multidisciplinary Research* 5(4). doi: 10.36948/ijfmr.2023.v05i04.5607.

Goryńska-Goldmann, Elżbieta. 2019. “Disadvantageous Behavior for Achieving Sustainable Food Consumption Accoridng to Consumer Opinions.” *Annals of the Polish Association of Agricultural and Agribusiness Economists* XXI(3):102–11. doi: 10.5604/01.3001.0013.4084.

Graef, Jennifer L., Ping Ouyang, Yan Wang, Elizabeth Rendina-Ruedy, Megan R. Lerner, Denver Marlow, Edralin A. Lucas, and Brenda J. Smith. 2018. “Dried Plum Polyphenolic Extract Combined with Vitamin K and Potassium Restores Trabecular and Cortical Bone in Osteopenic Model of Postmenopausal Bone Loss.” *Journal of Functional Foods* 42:262–70.

Guarino, Carmine, Simona Santoro, Luciana De Simone, and G. Cipriáni. 2009. “<i>Prunus Avium</I>: Nuclear DNA Study in Wild Populations and Sweet Cherry Cultivars.” *Genome* 52(4):320–37. doi: 10.1139/g09-007.

Guiné, Raquel, Sofia G. Florença, Daniela Teixeira Costa, Selda Çelik, Manuela Ferreira, Ana Paula Cardoso, Sümeyye Çetin, and Cristina Amaro da Costa. 2022. “Comparative Study About the Consumption of Organic Food Products on Samples of Portuguese and Turkish Consumers Under the COVID-19 Pandemic Context.” *Agronomy* 12(6):1385. doi: 10.3390/agronomy12061385.

Guo, Huixin, Fang Yan, Pingzhen Li, and Ming Li. 2022. “Determination of Storage Period of Harvested Plums by Near-infrared Spectroscopy and Quality Attributes.” *Journal of Food Processing and Preservation* 46(9):e16504.

Habib, Muzammil, Mudassir Bhat, B. N. Dar, and Ali Abas Wani. 2017. “Sweet Cherries from Farm to Table: A Review.” *Critical Reviews in Food Science and Nutrition* 57(8):1638–49.

Hasan, Md Mohidul, Hae-Keun Yun, Eun-Jung Kwak, and Kwang-Hyun Baek. 2014. “Preparation of Resveratrol-Enriched Grape Juice from Ultrasonication Treated Grape Fruits.” *Ultrasonics Sonochemistry* 21(2):729–34.

Hauck, Nathanael R., Kazuo Ikeda, Ryutaro Tao, and Amy Iezzoni. 2006. “The Mutated S1-Haplotype in Sour Cherry Has an Altered S-Haplotype–Specific F-Box Protein Gene.” *Journal of Heredity* 97(5):514–20. doi: 10.1093/jhered/esl029.

Hong, Mee Young, Mark Kern, Michelle Nakamichi-Lee, Nazanin Abbaspour, Arshya Ahouraei Far, and Shirin Hooshmand. 2021. “Dried Plum Consumption Improves Total Cholesterol and Antioxidant Capacity and Reduces Inflammation in Healthy Postmenopausal Women.” *Journal of Medicinal Food* 24(11):1161–68.

Horváth-Kerkai, Emőke, and Mónika Stéger-Máté. 2012. “Processed Fruit Products and Packaging.” Pp. 215–28 in *Handbook of Fruits and Fruit Processing*, edited by N. K. Sinha. Wiley-Blackwell.

Horváthné Petróczy, Marietta. 2009. “A Monilinia Fructicola És a Monilia Polystroma Megjelenése Magyasrországon És a Védekezés Újabb Lehetősége.” Corvinus University of Budapest, Budapest, Magyarország.

Hrustić, Jovana, Milica Mihajlović, and Brankica Tanović. 2020. “Morphological, Cultural and Ecological Characterization of Monilinia Spp., Pathogens of Stone Fruit in Serbia.” *Pesticides and Phytomedicine/Pesticidi i Fitomedicina* 35(1):39–48.

Huang, Zhenyu, Fei Shen, Yuling Chen, Ke Cao, and Lirong Wang. 2021. “Chromosome-scale Genome Assembly and Population Genomics Provide Insights Into the Adaptation, Domestication, and Flavonoid Metabolism of Chinese Plum.” *The Plant Journal* 108(4):1174–92. doi: 10.1111/tpj.15482.

Hussain, Syed Zameer, Bazila Naseer, Tahiya Qadri, Tabasum Fatima, and Tashooq Ahmad Bhat. 2021. “Plum (Prunus Domestica): Morphology, Taxonomy, Composition and Health Benefits.” Pp. 169–79 in *Fruits Grown in Highland Regions of the Himalayas: Nutritional and Health Benefits*. Springer.

Igwe, Ezinne O., and Karen E. Charlton. 2016. “A Systematic Review on the Health Effects of Plums (Prunus Domestica and Prunus Salicina).” *Phytotherapy Research* 30(5):701–31.

Igwe, Ezinne O., Karen E. Charlton, Steven Roodenrys, Katherine Kent, Kent Fanning, and Michael E. Netzel. 2017. “Anthocyanin-Rich Plum Juice Reduces Ambulatory Blood Pressure but Not Acute Cognitive Function in Younger and Older Adults: A Pilot Crossover Dose-Timing Study.” *Nutrition Research* 47:28–43.

Ivanišová, Eva, Helena Frančáková, Pavla Ritschlová, Štefan Dráb, Miriam Solgajová, and Marián Tokár. 2015. “Biological Activity of Apple Juice Enriched by Herbal Extracts.”

Ivić, Dario, Tina Fazinić, Jennifer Cole, and Adrijana Novak. 2014. “Monilinia Species Identified on Peach and Nectarine in Croatia, with the First Record of Monilinia Fructicola.” *EPPO Bulletin* 44(1):70–72.

Johnson, Renée. 2014. “Food Fraud and Economically Motivated Adulteration of Food and Food Ingredients.”

Jung, András, René Michels, and Graser Rainer. 2018. “Portable Snapshot Spectral Imaging for Agriculture.”

Jung, András, Michael Vohland, Marianna Magyar, László Kovács, Tímea Jung, Nóra Péterfalvi, Boglárka Keller, Fanni Sillinger, Renáta Rák, and Kornél Szalay. 2019. “Snapshot Hyperspectral Imaging for Field Data Acquisition in Agriculture (in Raspberry Plantation).” *DEUTSCHEN GESELLSCHAFT FUR PHOTOGRAMMETRIE UND FERNERKUNDUNG* 28:1–7.

Kállay, E., G. Bujdosó, G. Mester-Ficzek, Stéger-Máté, and M. Tóth. 2007. “Meggyfajták Érésmenetének Jellemzése a Gyümölcs Leválasztásához Szükséges Erő És a Beltartalmi Értékek Változásával (Characterization Ofripening Time Ofhungarian Bred Sour Cherry Cultivars with Changing of Fruit Removal Force and Components).” *Kertgazdaság* 38:21–26.

Kamiloglu, Senem. 2019. “Authenticity and Traceability in Beverages.” *Food Chemistry* 277:12–24. doi: 10.1016/j.foodchem.2018.10.091.

Kappel, Frank, Andrew Granger, Károly Hrotkó, and Mirko Schuster. 2012. “Cherry.” Pp. 459–504 in *Fruit Breeding*, edited by M. L. Badenes and D. H. Byrne. Boston, MA: Springer US.

Kelley, Darshan S., Yuriko Adkins, and Kevin D. Laugero. 2018. “A Review of the Health Benefits of Cherries.” *Nutrients* 10(3):368. doi: 10.3390/nu10030368.

Khan, Inayat Mustafa, Shakeel Ahmad Mir, M. H. Chesti, Amir H. Mir, S. P. Wani, S. A. Hakeem, Rakshanda Anayat, Muhammad Hayat Jaspal, Shereen Mehraj, and Asma Shakeel. 2022. “Studies on Mineral Nutrient Concentration of Different Cultivars of Sweet Cherry (Prunus Avium L.) in Kashmir.” *Journal of Experimental Agriculture International* 60–65. doi: 10.9734/jeai/2022/v44i130790.

Kodagoda, Gethmini, Hung T. Hong, Tim J. O’Hare, Yasmina Sultanbawa, Bruce Topp, and Michael E. Netzel. 2021. “Effect of Storage on the Nutritional Quality of Queen Garnet Plum.” *Foods* 10(2):352.

Kole, Chittaranjan, and Albert G. Abbott. 2012. *Genetics, Genomics and Breeding of Stone Fruits*. CRC Press.

Kondész, Csilla. 2005. “The Function of the Fruit-Growing and-Processing in the County of Szabolcs-Szatmár-Bereg.” *Scientific Bulletin Series C: Fascicle Mechanics, Tribology, Machine Manufacturing Technology* 19:1.

KSH. 2017. “Gyümölcstermesztés Magyarországon.” *STADAT*. Retrieved September 24, 2024 (https://www.ksh.hu/interaktiv/storytelling/gyumolcs/index.html).

KSH. 2024. “19.1.2.19. Gyümölcstermelés Vármegye És Régió Szerint.” *STADAT*. Retrieved September 24, 2024 (https://www.ksh.hu/stadat_files/mez/hu/mez0086.html).

Kuhn, Nathalie, Claudio Ponce, Macarena Arellano, Alson Time, Boris Sagredo, José Manuel Donoso, and Lee A. Meisel. 2020. “Gibberellic Acid Modifies the Transcript Abundance of ABA Pathway Orthologs and Modulates Sweet Cherry (Prunus Avium) Fruit Ripening in Early-and Mid-Season Varieties.” *Plants* 9(12):1796.

Laguna, Laura, Susana Fiszman, Patricia Puerta, Carolina Chaya, and Amparo Tárrega. 2020. “The Impact of COVID-19 Lockdown on Food Priorities. Results From a Preliminary Study Using Social Media

and an Online Survey With Spanish Consumers." *Food Quality and Preference* 86:104028. doi: 10.1016/j.foodqual.2020.104028.

Lao, Fei, and M. Monica Giusti. 2016. "Quantification of Purple Corn (Zea Mays L.) Anthocyanins Using Spectrophotometric and HPLC Approaches: Method Comparison and Correlation." *Food Analytical Methods* 9:1367–80.

Lara, María Valeria, Claudio Bonghi, Franco Famiani, Giannina Vizzotto, Robert P. Walker, and María Fabiana Drincovich. 2020. "Stone Fruit as Biofactories of Phytochemicals with Potential Roles in Human Nutrition and Health." *Frontiers in Plant Science* 11:1323.

Lee, Jungmin, Robert W. Durst, Ronald E. Wrolstad, and Collaborators: Eisele T. Giusti M. M. Hach J. Hofsommer H. Koswig S. Krueger D. A. Kupina; S. Martin S. K. Martinsen B. K. Miller T. C. Paquette F. Ryabkova A. Skrede G. Trenn U. Wightman J. D. 2005. "Determination of Total Monomeric Anthocyanin Pigment Content of Fruit Juices, Beverages, Natural Colorants, and Wines by the PH Differential Method: Collaborative Study." *Journal of AOAC International* 88(5):1269–78.

Lee, Sang Gil, Terrence M. Vance, Tae-Gyu Nam, Dae-Ok Kim, Sung I. Koo, and Ock K. Chun. 2016. "Evaluation of PH Differential and HPLC Methods Expressed as Cyanidin-3-Glucoside Equivalent for Measuring the Total Anthocyanin Contents of Berries." *Journal of Food Measurement and Characterization* 10:562–68.

Van Leeuwen, G. C. M., I. J. Holb, and M. J. Jeger. 2002. "Factors Affecting Mummification and Sporulation of Pome Fruit Infected by Monilinia Fructigena in Dutch Orchards." *Plant Pathology* 51(6):787–93.

Li, Kuo-Tan. 2012. "Physiology and Classification of Fruits." Pp. 3–12 in *Handbook of Fruits and Fruit Processing*, edited by N. K. Sinha. Wiley-Blackwell.

Li, Ming, Wenbo Lv, Rui Zhao, Huixin Guo, Jing Liu, and Donghai Han. 2017. "Non-Destructive Assessment of Quality Parameters in 'Friar' Plums during Low Temperature Storage Using Visible/near Infrared Spectroscopy." *Food Control* 73:1334–41.

Li, Qian, Pei Chen, Shengjie Dai, Yufei Sun, Bing Yuan, Wenbin Kai, Yuelin Pei, Suihuan He, Bin Liang, and Yushu Zhang. 2015. "PacCYP707A2 Negatively Regulates Cherry Fruit Ripening While PacCYP707A1 Mediates Drought Tolerance." *Journal of Experimental Botany* 66(13):3765–74.

Li, Quan, Xiao-Xiao Chang, Hong Wang, Charles Stephen Brennan, and Xin-Bo Guo. 2019. "Phytochemicals Accumulation in Sanhua Plum (Prunus Salicina L.) during Fruit Development and Their Potential Use as Antioxidants." *Journal of Agricultural and Food Chemistry* 67(9):2459–66.

Li, Shanshan, Zein Kallas, Djamel Rahmani, and José M. Gil. 2021. "Trends in Food Preferences and Sustainable Behavior During the COVID-19 Lockdown: Evidence From Spanish Consumers." *Foods* 10(8):1898. doi: 10.3390/foods10081898.

Li, Xiaoli, Yuzhen Wei, Jie Xu, Xuping Feng, Feiyue Wu, Ruiqing Zhou, Juanjuan Jin, Kaiwen Xu, Xinjie Yu, and Yong He. 2018. "SSC and PH for Sweet Assessment and Maturity Classification of Harvested Cherry Fruit Based on NIR Hyperspectral Imaging Technology." *Postharvest Biology and Technology* 143:112–18.

Li, Xiong, Yande Liu, Xiaogang Jiang, and Guantian Wang. 2021. "Supervised Classification of Slightly Bruised Peaches with Respect to the Time after Bruising by Using Hyperspectral Imaging Technology." *Infrared Physics & Technology* 113:103557.

Louw, Esmé D., and Karen I. Theron. 2010. "Robust Prediction Models for Quality Parameters in Japanese Plums (Prunus Salicina L.) Using NIR Spectroscopy." *Postharvest Biology and Technology* 58(3):176–84.

Lovas Kiss, Antal. 2014. "A helyi értékek és hungarikumok használatának és értelmezésének néhány lokális és etnikus sajátossága: A panyolai példa."

Magyar Élelmiszerkönyv Bizottság. 2009. "A Magyar Élelmiszerkönyv 1-3-2001/112 Számú Előírása a Gyümölcslevekről És Egyes Hasonló, Emberi Fogyasztásra Szánt Termékekről." 1–11.

Magyar Élelmiszerkönyv Bizottság. 2010. "Magyar Élelmiszerkönyv 2-101 Számú Irányelv - Megkülönböztető Minőségi Jelöléssel Ellátott Egyes Feldolgozott Gyümölcstermékek." 1–8.

Magyar Élelmiszerkönyv Bizottság. 2013. "Magyar Élelmiszerkönyv 2-601 Számú Irányelv - Hőkezeléssel Tartósított Élelmiszerek." 1–22.

Mahfoudhi, Nesrine, and Salem Hamdi. 2015. “Use of Almond Gum and Gum Arabic as Novel Edible Coating to Delay Postharvest Ripening and to Maintain Sweet Cherry (P Runus Avium) Quality during Storage.” *Journal of Food Processing and Preservation* 39(6):1499–1508.

Mahmood, Tahir, Farooq Anwar, Mateen Abbas, Mary C. Boyce, and Nazamid Saari. 2012. “Compositional Variation in Sugars and Organic Acids at Different Maturity Stages in Selected Small Fruits from Pakistan.” *International Journal of Molecular Sciences* 13(2):1380–92.

Manley, Marena. 2014. “Near-Infrared Spectroscopy and Hyperspectral Imaging: Non-Destructive Analysis of Biological Materials.” *Chemical Society Reviews* 43(24):8200–8214.

Manley, Marena, Gerard Downey, and Vincent Baeten. 2008. “Spectroscopic Technique: Near-Infrared (NIR) Spectroscopy.” P. 689 in *Modern Techniques for Food Authentication*, edited by D.-W. Sun. Elsevier/Academic Press.

María-Jesús Rodrigo, Berta Alquéezar, Fernando Alférez, and Lorenzo Zacarías. 2012. “Biochemistry of Fruits and Fruit Products.” Pp. 13–34 in *Handbook of Fruits and Fruit Processing*, edited by N. K. Sinha.

Martínez-Esplá, Alejandra, María Serrano, Daniel Valero, Domingo Martínez-Romero, Salvador Castillo, and Pedro J. Zapata. 2017. “Enhancement of Antioxidant Systems and Storability of Two Plum Cultivars by Preharvest Treatments with Salicylates.” *International Journal of Molecular Sciences* 18(9):1911.

Martínez-García, Pedro J., Jorge Mas-Gómez, Ángela S. Prudencio, Juan José Barriuso, and Celia M. Cantín. 2023. “Genome-Wide Association Analysis of Monilinia Fructicola Lesion in a Collection of Spanish Peach Landraces.” *Frontiers in Plant Science* 14:1165847.

Di Matteo, Antonio, Rosa Russo, Giulia Graziani, Alberto Ritieni, and Claudio Di Vaio. 2017. “Characterization of Autochthonous Sweet Cherry Cultivars (Prunus Avium L.) of Southern Italy for Fruit Quality, Bioactive Compounds and Antioxidant Activity.” *Journal of the Science of Food and Agriculture* 97(9):2782–94.

De Miccolis Angelini, Rita Milvia, Lucia Landi, Celeste Raguseo, Stefania Pollastro, Francesco Faretra, and Gianfranco Romanazzi. 2022. “Tracking of Diversity and Evolution in the Brown Rot Fungi Monilinia Fructicola, Monilinia Fructigena, and Monilinia Laxa.” *Frontiers in Microbiology* 13:854852.

Michailidis, Michail, Georgia Tanou, Eirini Sarrou, Evangelos Karagiannis, Ioannis Ganopoulos, Stefan Martens, and Athanassios Molassiotis. 2021. “Pre-and Post-Harvest Melatonin Application Boosted Phenolic Compounds Accumulation and Altered Respiratory Characters in Sweet Cherry Fruit.” *Frontiers in Nutrition* 8:695061.

Milić, Anita, Tatjana Daničić, Aleksandra Tepić Horecki, Zdravko Šumić, Danijela Bursać Kovačević, Predrag Putnik, and Branimir Pavlić. 2021. “Maximizing Contents of Phytochemicals Obtained from Dried Sour Cherries by Ultrasound-Assisted Extraction.” *Separations* 8(9):155.

Miranda-Castro, Susana Patricia. 2016. “Chapter 3 - Application of Chitosan in Fresh and Minimally Processed Fruits and Vegetables.” Pp. 67–113 in *Chitosan in the Preservation of AgricultApplication of Chitosan in Fresh and Minimally Processed Fruits and Vegetablesural Commodities*. Academic Press.

Moore, Jeffrey C., John Spink, and Markus Lipp. 2012. “Development and Application of a Database of Food Ingredient Fraud and Economically Motivated Adulteration from 1980 to 2010.” *Journal of Food Science* 77(4):R118–26. doi: 10.1111/j.1750-3841.2012.02657.x.

Mulabagal, Vanisree, Gregory A. Lang, David L. DeWitt, Sanjeev S. Dalavoy, and Muraleedharan G. Nair. 2009. “Anthocyanin Content, Lipid Peroxidation and Cyclooxygenase Enzyme Inhibitory Activities of Sweet and Sour Cherries.” *Journal of Agricultural and Food Chemistry* 57(4):1239–46.

Naseem, Zahida, Sajad Ahmad Mir, Sajad Mohd Wani, Molvi Abdul Rouf, Iqra Bashir, and Aiman Zehra. 2023. “Probiotic-Fortified Fruit Juices: Health Benefits, Challenges, and Future Perspective.” *Nutrition* 115:112154.

Neveu, Vanessa, Jara Perez-Jiménez, Femke Vos, Vanessa Crespy, Lerman du Chaffaut, Louise Mennen, Craig Knox, Roman Eisner, J. Cruz, and D. Wishart. 2010. “Phenol-Explorer: An Online Comprehensive Database on Polyphenol Contents in Foods.” *Database* 2010.

Norris, Karl H. 1964. “Design and Development of a New Moisture Meter.” *Agric. Eng* 45(7):370–72.

Norris, Karl H. 1992. “Early History of near Infrared for Agricultural Applications.” *NIR News* 3(1):12–13. doi: 10.1255/nirn.105.

Oliveira Lino, Leandro, Igor Pacheco, Vincent Mercier, Franco Faoro, Daniele Bassi, Isabelle Bornard, and Bénédicte Quilot-Turion. 2016. “Brown Rot Strikes Prunus Fruit: An Ancient Fight Almost Always Lost.” *Journal of Agricultural and Food Chemistry* 64(20):4029–47. doi: 10.1021/acs.jafc.6b00104.

Padayachee, A., L. Day, K. Howell, and M. J. Gidley. 2017. “Complexity and Health Functionality of Plant Cell Wall Fibers from Fruits and Vegetables.” *Critical Reviews in Food Science and Nutrition* 57(1):59–81.

Panda, Sauris, Juan José Molina Martín, Itziar Aguinagalde, and Aparajita Mohanty. 2003. “Chloroplast DNA Variation in Cultivated and Wild <i>Prunus Avium</I> L: A Comparative Study.” *Plant Breeding* 122(1):92–94. doi: 10.1046/j.1439-0523.2003.00768.x.

Papp, J., J. Nyéki, and M. Soltész. 2004. “Fruit Production and Research in Hungary-An Overview.” *International Journal of Horticultural Science* 10(4):7–11.

Park, Bosoon, and Renfu Lu. 2015. *Hyperspectral Imaging Technology in Food and Agriculture*. Vol. 1. Springer.

Pátkai, Györgyi. 2012. “Fruit and Fruit Products as Ingredients.” Pp. 263–75 in *Handbook of Fruits and Fruit Processing*, edited by N. K. Sinha. Wiley-Blackwell.

Pereira, Wagner V, Amanda C. N. Padilha, Jéssica A. O. Kaiser, Cristiano N. Nesi, Juliana M. M. Fischer, and Louise L. May-De-Mio. 2019. “Monilinia Spp. from Imported Stone Fruits May Represent a Risk to Brazilian Fruit Production.” *Tropical Plant Pathology* 44(2):120–31.

Petróczy, M., and L. Palkovics. 2005. “First Occurrence of the Quarantine Pathogen Monilinia Fructicola on Imported Peach in Hungary.”

Petróczy, Marietta, and László Palkovics. 2006. “First Report of Brown Rot Caused by Monilinia Fructicola on Imported Peach in Hungary.” *Plant Disease* 90(3):375.

Pollner, Bernhard, and Zoltan Kovacs. 2016. “Multivariate Data Analysis Tools for R Including Aquaphotomics Methods, Aquap2.”

Posom, Jetsada, Junjira Klaprachan, Kamonpan Rattanasopa, Panmanas Sirisomboon, Khwantri Saengprachatanarug, and Seree Wongpichet. 2020. “Predicting Marian Plum Fruit Quality without Environmental Condition Impact by Handheld Visible–near-Infrared Spectroscopy.” *ACS Omega* 5(43):27909–21.

Prinsi, Bhakti, Alfredo S. Negri, Luca Espen, and M. Claudia Piagnani. 2016. “Proteomic Comparison of Fruit Ripening between ‘Hedelfinger’Sweet Cherry (Prunus Avium L.) and Its Somaclonal Variant ‘HS.’” *Journal of Agricultural and Food Chemistry* 64(20):4171–81.

Pullanagari, Reddy R., and Mo Li. 2021. “Uncertainty Assessment for Firmness and Total Soluble Solids of Sweet Cherries Using Hyperspectral Imaging and Multivariate Statistics.” *Journal of Food Engineering* 289:110177.

Qu, Jia Huan, Dan Liu, Jun Hu Cheng, Da Wen Sun, Ji Ma, Hongbin Pu, and Xin An Zeng. 2015. “Applications of Near-Infrared Spectroscopy in Food Safety Evaluation and Control: A Review of Recent Research Advances.” *Critical Reviews in Food Science and Nutrition* 55(13):1939–54. doi: 10.1080/10408398.2013.871693.

Salgó, András. 2014. “Obituary: Károly Kaffka: The Hungarian Pioneer of near Infrared Spectroscopy.” *NIR News* 25(7):13–14.

Savitzky, Abraham, and Marcel J. E. Golay. 1951. “Smoothing and Differentiation of Data by Simplified Least Squares Procedures.” *Analytical Chemistry* 36(2):1627–39.

Schuck, P., A. Dolivet, and R. Jeantet. 2012. “Determination of Dry Matter and Total Dry Matter.” *Analytical Methods for Food and Dairy Powders; Schuck, P., Dolivet, A., Jeantet, R., Eds* 45–57.

Serradilla, Manuel Joaquín, M. Fotirić Akšić, George A. Manganaris, Sezai Ercisli, David González-Gómez, and Daniel Valero. 2017. “Fruit Chemistry, Nutritional Benefits and Social Aspects of Cherries.” Pp. 420–41 in *Cherries: Botany, production and uses*. CABI Wallingford UK.

Serradilla, Manuel Joaquín, Alejandro Hernández, Margarita López-Corrales, Santiago Ruiz-Moyano, María de Guía Córdoba, and Alberto Martín. 2016. "Composition of the Cherry (Prunus Avium L. and Prunus Cerasus L.; Rosaceae)." Pp. 127–47 in *Nutritional composition of fruit cultivars*. Elsevier.

Serradilla, Manuel Joaquín, Alberto Martin, Alejandro Hernandez, Margarita Lopez-Corrales, Mercedes Lozano, and María de Guía Córdoba. 2010. "Effect of the Commercial Ripening Stage and Postharvest Storage on Microbial and Aroma Changes of 'Ambrunés' Sweet Cherries." *Journal of Agricultural and Food Chemistry* 58(16):9157–63.

Serrano, María, Huertas M. Díaz-Mula, Pedro Javier Zapata, Salvador Castillo, Fabián Guillén, Domingo Martínez-Romero, Juan M. Valverde, and Daniel Valero. 2009. "Maturity Stage at Harvest Determines the Fruit Quality and Antioxidant Potential after Storage of Sweet Cherry Cultivars." *Journal of Agricultural and Food Chemistry* 57(8):3240–46.

Serrano, María, Fabián Guillén, Domingo Martínez-Romero, Salvador Castillo, and Daniel Valero. 2005. "Chemical Constituents and Antioxidant Activity of Sweet Cherry at Different Ripening Stages." *Journal of Agricultural and Food Chemistry* 53(7):2741–45.

Shah, Syed Sohaib Ali, Ayesha Zeb, Waqar S. Qureshi, Muhammad Arslan, Aman Ullah Malik, Waleed Alasmary, and Eisa Alanazi. 2020. "Towards Fruit Maturity Estimation Using NIR Spectroscopy." *Infrared Physics & Technology* 111:103479.

Shamloufard, Pouneh, Mark Kern, and Shirin Hooshmand. 2017. "Bowel Function of Postmenopausal Women: Effects of Daily Consumption of Dried Plum." *International Journal of Food Properties* 20(12):3006–13.

Shao, Yuanyuan, Guantao Xuan, Zhichao Hu, Zongmei Gao, and Lei Liu. 2019. "Determination of the Bruise Degree for Cherry Using Vis-NIR Reflection Spectroscopy Coupled with Multivariate Analysis." *PLos One* 14(9):e0222633.

Sharpe, Richard M., Benjamin Killian, Tyson Koepke, Rishikesh Ghogare, Nnadozie Oraguzie, Matthew Whiting, Lee Meisel, Herman Silva, and Amit Dhingra. 2022a. "Draft Genome Data of Prunus Avium Cv 'Stella.'" *Data in Brief* 45:108611. doi: 10.1016/j.dib.2022.108611.

Sharpe, Richard M., Benjamin Killian, Tyson Koepke, Rishikesh Ghogare, Nnadozie Oraguzie, Matthew Whiting, Lee Meisel, Herman Silva, and Amit Dhingra. 2022b. "Draft Genome Data of Prunus Avium Cv 'Stella.'" *Data in Brief* 45:108611. doi: 10.1016/j.dib.2022.108611.

Siedliska, Anna, Monika Zubik, Piotr Baranowski, and Wojciech Mazurek. 2017. "Algorithms for Detecting Cherry Pits on the Basis of Transmittance Mode Hyperspectral Data." *International Agrophysics* 31(4):539–49.

Singh, Dinesh, and R. R. Sharma. 2018. *Postharvest Diseases of Fruits and Vegetables and Their Management*. Elsevier Inc.

Sinha, Nirmal K. 2012. *Handbook of Fruits and Fruit Processing*. 2nd ed. Wiley-Blackwell.

Śmiglak-Krajewska, Magdalena, and Julia Wojciechowska-Solis. 2021. "Consumer Versus Organic Products in the COVID-19 Pandemic: Opportunities and Barriers to Market Development." *Energies* 14(17):5566. doi: 10.3390/en14175566.

Sottile, Francesco, Chiara Caltagirone, Giovanna Giacalone, Cristiana Peano, and Ettore Barone. 2022. "Unlocking Plum Genetic Potential: Where Are We At?" *Horticulturae* 8(2):128. doi: 10.3390/horticulturae8020128.

Spink, J. 2014. "Safety of Food and Beverages: Risks of Food Adulteration." Pp. 413–16 in *Encyclopedia of Food Safety*, edited by Y. Motarjemi. Waltham: Academic Press.

Spink, John, and Douglas C. Moyer. 2011. "Defining the Public Health Threat of Food Fraud." *Journal of Food Science* 76(9):R157–63. doi: 10.1111/j.1750-3841.2011.02417.x.

Stacewicz-Sapuntzakis, M. 2013. "Dried Plums and Their Products: Composition and Health Effects–an Updated Review." *Critical Reviews in Food Science and Nutrition* 53(12):1277–1302.

Stéger-Máté, Mónika. 2012. "Sweet and Tart Cherries." Pp. 433–46 in *Handbook of Fruits and Fruit Processing*, edited by N. K. Sinha. Wiley-Blackwell.

Sun, Ye, Kangli Wei, Qiang Liu, Leiqing Pan, and Kang Tu. 2018. “Classification and Discrimination of Different Fungal Diseases of Three Infection Levels on Peaches Using Hyperspectral Reflectance Imaging Analysis.” *Sensors* 18(4):1295.

Sun, Ye, Hui Xiao, Sicong Tu, Ke Sun, Leiqing Pan, and Kang Tu. 2018. “Detecting Decayed Peach Using a Rotating Hyperspectral Imaging Testbed.” *LWT* 87:326–32.

Szabo, Gergo, Flora Vitalis, Zsuzsanna Horvath-Mezofi, Monika Gob, Juan Pablo Aguinaga Bosquez, Zoltan Gillay, Tamás Zsom, Lien Le Phuong Nguyen, Geza Hitka, and Zoltan Kovacs. 2023. “Application of Near Infrared Spectroscopy to Monitor the Quality Change of Sour Cherry Stored under Modified Atmosphere Conditions.” *Sensors* 23(1):479.

Tijero, Verónica, Natalia Teribia, Paula Muñoz, and Sergi Munné-Bosch. 2016. “Implication of Abscisic Acid on Ripening and Quality in Sweet Cherries: Differential Effects during Pre-and Post-Harvest.” *Frontiers in Plant Science* 7:602.

Time, Alson, Claudio Ponce, Nathalie Kuhn, Macarena Arellano, Boris Sagredo, José Manuel Donoso, and Lee A. Meisel. 2021. “Canopy Spraying of Abscisic Acid to Improve Fruit Quality of Different Sweet Cherry Cultivars.” *Agronomy* 11(10):1947.

Toivonen, P. M. A., Adrian Batista, and Brenda Lannard. 2017. “Development of a Predictive Model for ‘Lapins’ Sweet Cherry Dry Matter Content Using a Visible/near-Infrared Spectrometer and Its Potential Application to Other Cultivars.” *Canadian Journal of Plant Science* 97(6):1030–35.

Topp, Bruce L., Dougal M. Russell, Michael Neumüller, Marco A. Dalbó, and Weisheng Liu. 2012. “Plum.” *Fruit Breeding* 571–621.

Toydemir, Gamze, Esra Capanoglu, Maria Victoria Gomez Roldan, Ric C. H. de Vos, Dilek Boyacioglu, Robert D. Hall, and Jules Beekwilder. 2013. “Industrial Processing Effects on Phenolic Compounds in Sour Cherry (Prunus Cerasus L.) Fruit.” *Food Research International* 53(1):218–25. doi: 10.1016/j.foodres.2013.04.009.

Tyl, Catrin, and George D. Sadler. 2017. “PH and Titratable Acidity.” *Food Analysis* 389–406.

USDA. 2019a. “Cherries, Sour, Red, Raw.” *USDA Agricultural Research Service*. Retrieved September 23, 2024 (https://fdc.nal.usda.gov/fdc-app.html#/food-details/173954/nutrients).

USDA. 2019b. “Cherries, Sweet, Raw.” *USDA Agricultural Research Service*. Retrieved September 23, 2024 (https://fdc.nal.usda.gov/fdc-app.html#/food-details/171719/nutrients).

USDA. 2019c. “Plums, Raw.” *USDA Agricultural Research Service*. Retrieved September 23, 2024 (https://fdc.nal.usda.gov/fdc-app.html#/food-details/169949/nutrients).

Usenik, Valentina, Damijana Kastelec, Robert Veberič, and Franci Štampar. 2008. “Quality Changes during Ripening of Plums (Prunus Domestica L.).” *Food Chemistry* 111(4):830–36.

Usenik, Valentina, Franci Štampar, and Robert Veberič. 2009. “Anthocyanins and Fruit Colour in Plums (Prunus Domestica L.) during Ripening.” *Food Chemistry* 114(2):529–34.

Valderrama-Soto, Diego, J. Salazar, Ailynne Sepúlveda-González, Claudia Silva-Andrade, Claudio Gardana, Héctor Morales, Benjamín Battistoni, Pablo Jiménez-Muñoz, Maurício González, Álvaro Peña-Neira, Rodrigo Infante, and Igor Pacheco. 2021. “Detection of Quantitative Trait Loci Controlling the Content of Phenolic Compounds in an Asian Plum (Prunus Salicina L.) F1 Population.” *Frontiers in Plant Science* 12. doi: 10.3389/fpls.2021.679059.

Valero, Daniel, Huertas M. Diaz-Mula, Pedro Javier Zapata, Salvador Castillo, Fabian Guillen, Domingo Martinez-Romero, and Maria Serrano. 2011. “Postharvest Treatments with Salicylic Acid, Acetylsalicylic Acid or Oxalic Acid Delayed Ripening and Enhanced Bioactive Compounds and Antioxidant Capacity in Sweet Cherry.” *Journal of Agricultural and Food Chemistry* 59(10):5483–89.

Valero, Daniel, and María Serrano. 2010. *Postharvest Biology and Technology for Preserving Fruit Quality*. CRC press.

Vargas, Adabella Suárez, Porfirio Juarez-Lopez, Victor Lopez-Martinez, Laura Josefina Pérez Flores, Dagoberto Guillén Sánchez, and Iran Alia-Tejacal. 2017. “Botany and Physiology Antioxidant Activity and Physicochemical Parameters in ‘Cuernavaqueña’ Mexican Plum (Spondias Purpurea L.) at Different Ripening Stages.” *Revista Brasileira de Fruticultura* 39:e-787.

Viljevac, Marija, Krunoslav Dugalić, Vlatka Jurković, Ines Mihaljević, Vesna Tomaš, Boris Puškar, Hrvoje Lepeduš, Rezica Sudar, and Zorica Jurković. 2012. "Relation between Polyphenols Content and Skin Colour in Sour Cherry Fruits." *Journal of Agricultural Sciences, Belgrade* 57(2):57–67.

Villarino, M., Paloma Melgarejo, J. Usall, J. Segarra, N. Lamarca, and A. De Cal. 2012. "Secondary Inoculum Dynamics of Monilinia Spp. and Relationship to the Incidence of Postharvest Brown Rot in Peaches and the Weather Conditions during the Growing Season." *European Journal of Plant Pathology* 133:585–98.

Villavicencio, Juan D., Juan P. Zoffoli, Anne Plotto, and Carolina Contreras. 2021. "Aroma Compounds Are Responsible for an Herbaceous Off-Flavor in the Sweet Cherry (Prunus Avium L.) Cv. Regina during Fruit Development." *Agronomy* 11(10):2020.

Vitalis, Flora, Juan Pablo Aguinaga Bósquez, Balkis Aouadi, Zsanett Bodor, John-Lewis Zinia Zaukuu, and Zoltan Kovacs. 2021. "Monitoring of Brown Rot Caused by Monilia Fructigena on Plums with the Aquaphotomics Approach." Pp. 122–23 in *Proceeding of The 4th Aquaphotomics International Conference,* edited by R. Tsenkova, M. Yasui, Z. Kovacs, and J. Muncan. Kobe, Japan.

Vitalis, Flora, Lueji Regatieri Santos, Erika Bujna, Quang Nguyen D., and Zoltan Kovacs. 2023. "Tracing Fermentation Processes Hidden in the near Infrared Spectra of Probiotic Fruit Juices by Aquaphotomics." P. 16 in, edited by R. Tsenkova, Z. Kovacs, C. Huck, C. Malegori, F. Marini, J. Muncan, T. Cattaneo, and S. Atanasova. Rome: Società Italiana di Spettroscopia NIR, International Aquaphotomics Society.

Vitalis, Flora, David Tjandra Nugraha, Balkis Aouadi, Juan Pablo Aguinaga Bósquez, Zsanett Bodor, John-Lewis Zinia Zaukuu, Tamás Kocsis, Viktória Zsom-Muha, Zoltan Gillay, and Zoltan Kovacs. 2021. "Detection of Monilia Contamination in Plum and Plum Juice with NIR Spectroscopy and Electronic Tongue." *Chemosensors* 9(12):355.

Walkowiak-Tomczak, Dorota, Julita Regula, and Angelika Smidowicz. 2018. "Effect of Prune Prunus Domestica Consumption on Blood Lipid Profile in Patients with Moderate Hypercholesterolemia." *Acta Scientiarum Polonorum. Hortorum Cultus* 17(6).

Walsh, K. B., V. A. McGlone, and D. H. Han. 2020. "The Uses of near Infra-Red Spectroscopy in Postharvest Decision Support: A Review." *Postharvest Biology and Technology* 163:111139.

Wang, Jianming, Thuy Linh Pham, and Van Thac Dang. 2020. "Environmental Consciousness and Organic Food Purchase Intention: A Moderated Mediation Model of Perceived Food Quality and Price Sensitivity." *International Journal of Environmental Research and Public Health* 17(3):850. doi: 10.3390/ijerph17030850.

Wang, Qinghao, Luyang Jing, Yue Xu, Weiwei Zheng, and Wangshu Zhang. 2023. "Transcriptomic Analysis of Anthocyanin and Carotenoid Biosynthesis in Red and Yellow Fruits of Sweet Cherry (Prunus Avium L.) during Ripening." *Horticulturae* 9(4):516.

Wang, Tao, Jian Chen, Yangyang Fan, Zhengjun Qiu, and Yong He. 2018. "SeeFruits: Design and Evaluation of a Cloud-Based Ultra-Portable NIRS System for Sweet Cherry Quality Detection." *Computers and Electronics in Agriculture* 152:302–13.

Wei, Hairong, Xin Chen, Xiaojuan Zong, Huairui Shu, Dongsheng Gao, and Qingzhong Liu. 2015. "Comparative Transcriptome Analysis of Genes Involved in Anthocyanin Biosynthesis in the Red and Yellow Fruits of Sweet Cherry (Prunus Avium L.)." *PLoS One* 10(3):e0121164.

Whitham, Hilary K., Preethi Sundararaman, Daniel Dewey-Mattia, Karunya Manikonda, Katherine E. Marshall, Patricia M. Griffin, Brigette Gleason, Sanjana Subramhanya, and Samuel J. Crowe. 2021. "Novel Outbreak-Associated Food Vehicles, United States." *Emerging Infectious Diseases* 27(10):2554–59. doi: 10.3201/eid2710.204080.

Williams, Phil, and Karl Norris. 1987. *Near-Infrared Technology in the Agricultural and Food Industries.* American Association of Cereal Chemists, Inc.

Wojdyło, Aneta, Paulina Nowicka, Piotr Laskowski, and Jan Oszmiański. 2014. "Evaluation of Sour Cherry (Prunus Cerasus L.) Fruits for Their Polyphenol Content, Antioxidant Properties, and Nutritional Components." *Journal of Agricultural and Food Chemistry* 62(51):12332–45.

Wold, Svante, and Michael Sjostrom. 1977. "SIMCA: A Method for Analyzing Chemical Data in Terms of Similarity and Analogy." Pp. 243–82 in.

Wu, Di, and Da-Wen Sun. 2013. “Advanced Applications of Hyperspectral Imaging Technology for Food Quality and Safety Analysis and Assessment: A Review—Part I: Fundamentals.” *Innovative Food Science & Emerging Technologies* 19:1–14.

Wu, Fuwang, Dandan Zhang, Haiyan Zhang, Guoqiang Jiang, Xinguo Su, Hongxia Qu, Yueming Jiang, and Xuewu Duan. 2011. “Physiological and Biochemical Response of Harvested Plum Fruit to Oxalic Acid during Ripening or Shelf-Life.” *Food Research International* 44(5):1299–1305.

Wu, Yue, Zhongyuan Xu, Wenjian Yang, Zhiqiang Ning, and Hao Dong. 2022. “Review on the Application of Hyperspectral Imaging Technology of the Exposed Cortex in Cerebral Surgery.” *Frontiers in Bioengineering and Biotechnology* 10:906728.

Xiao, Wei, Fei Shen, Qiuping Zhang, Liu Ning, Yuping Zhang, Ming Xu, Shuo Liu, Yujun Zhang, Xiaoxue Ma, and Weisheng Liu. 2021. “Genetic Diversity Analysis of Chinese Plum (Prunus Salicina L.) Based on Whole-Genome Resequencing.” *Tree Genetics & Genomes* 17(3). doi: 10.1007/s11295-021-01506-x.

Yahaya, SM, and AY Mardiyya. 2019. “Review of Post-Harvest Losses of Fruits and Vegetables.” *Biomedical Journal of Scientific & Technical Research* 13(4):10192–200. doi: 10.26717/bjstr.2019.13.002448.

Zaukuu, John-Lewis Zinia, Eszter Benes, György Bázár, Zoltán Kovács, and Marietta Fodor. 2022. “Agricultural Potentials of Molecular Spectroscopy and Advances for Food Authentication: An Overview.” *Processes* 10(2):214.

Zhao, Z. L., Y. W. Wang, D. J. Gong, X. Y. Niu, Wei Cheng, and Y. H. Gu. 2016. “Discrimination of Plum Browning with near Infrared Spectroscopy.” *Guang Pu Xue Yu Guang Pu Fen Xi= Guang Pu* 36(7):2089–93.

10.2. Supplementary materials

10.2.1. Annexes for the materials and methods used

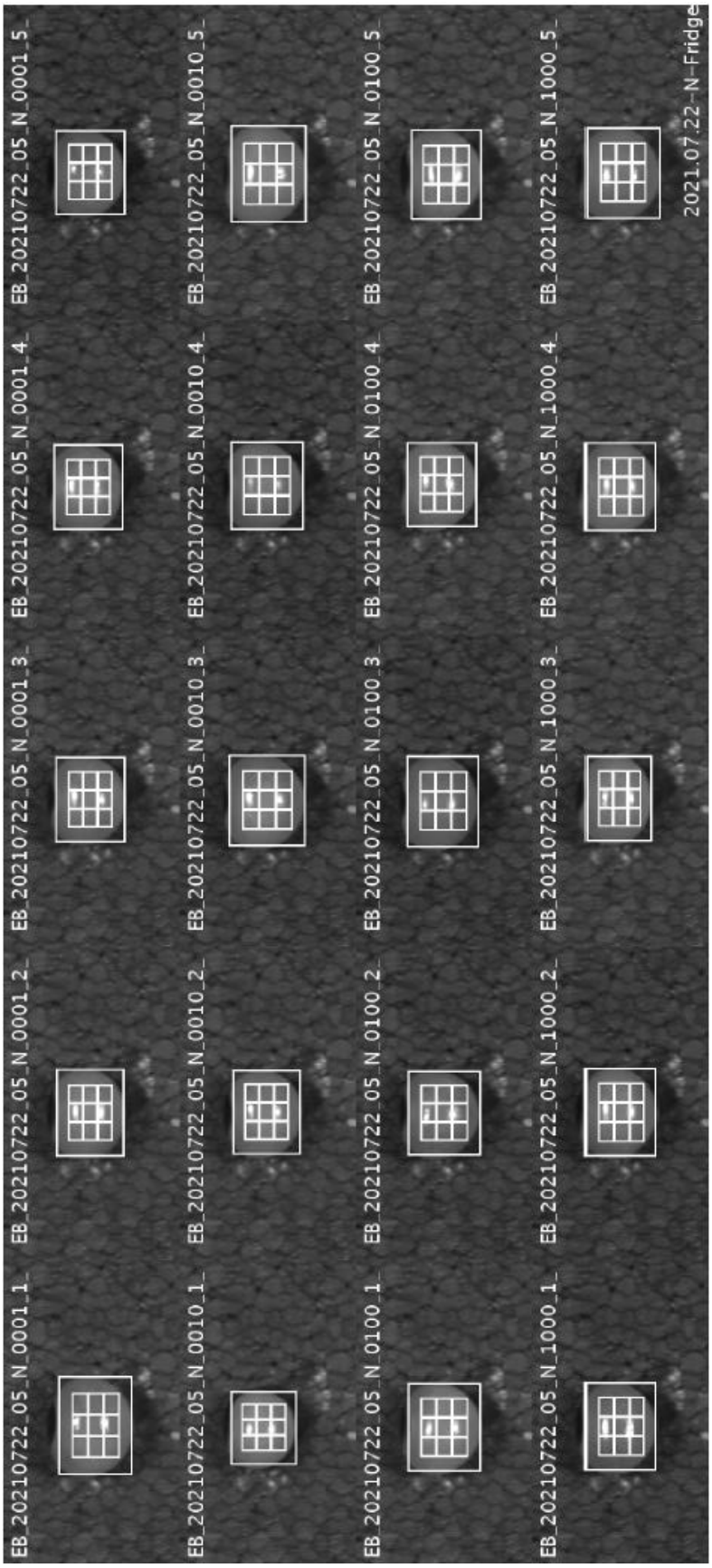

Figure 60. Hyperspectral images of intact "Érdi bőtermő" sour cherry samples stored under refrigerated conditions on the first day of storage (example).

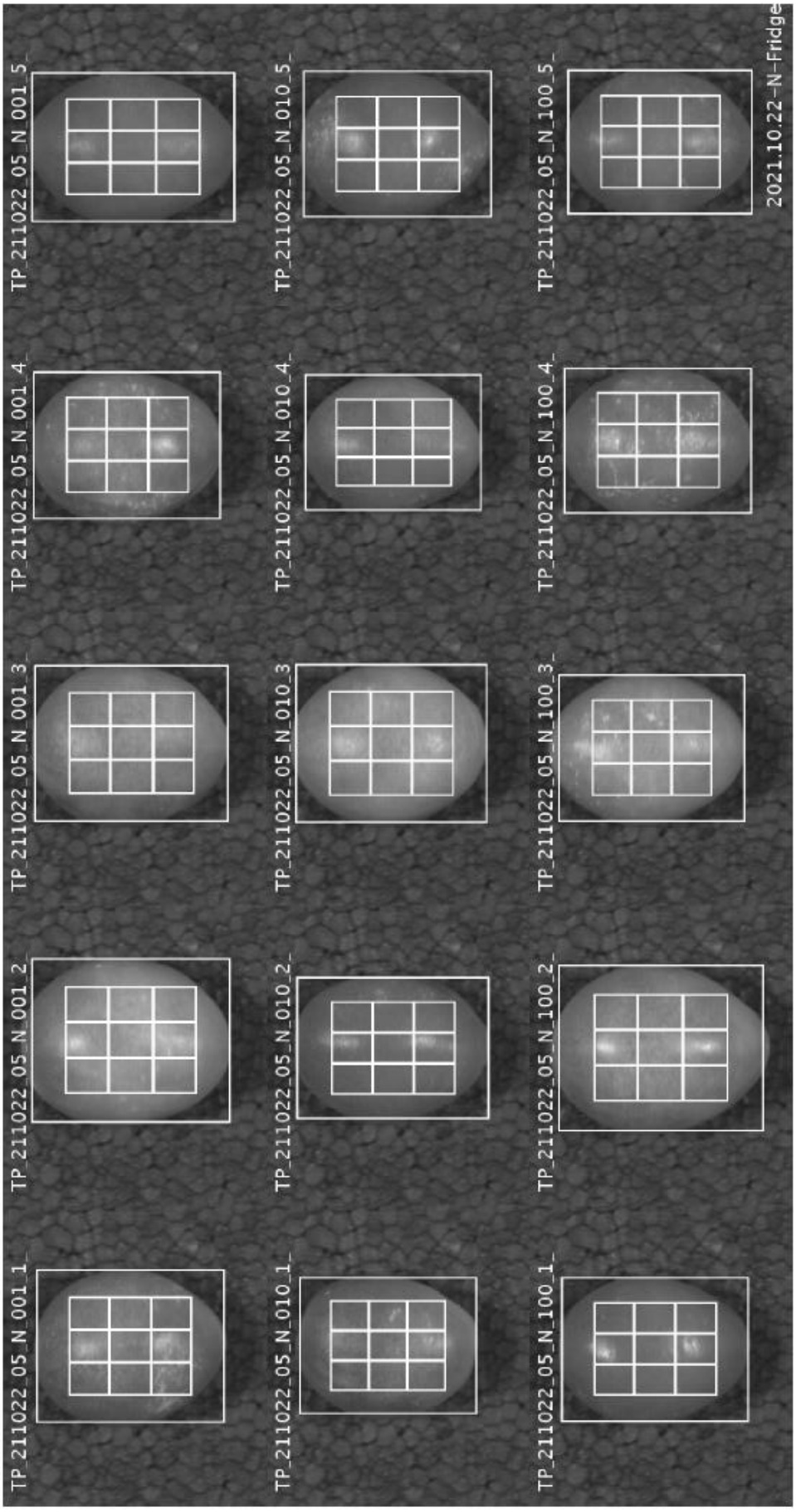

Figure 61. Hyperspectral images of intact "Topend" plum samples stored under refrigerated conditions on the first day of storage (example)

Table 19. Pre-classified stone fruit varieties, their presumed ripeness clusters and the indicating colours.

Sweet cherry varieties

Bigarreau Burlat

1	2	3	4	5	6	7	8	9	10	11	12	13	14	15	16	17	18	19	20	21	22	23	24	25	26
L1				L2			L3				L4			L5								L6			

Valerij Cskalov

1	2	3	4	5	6	7	8	9	10	11	12	13	14	15	16	17	18	19	20	21
L1	L2			L3				L4		L5						L6				

Sour cherry varieties

Kántorjánosi

1	2	3	4	5	6	7	8	9	10	11	12	13	14	15	16	17	18	19	20
L2				L3					L4				L5						

Újfehértói

1	2	3	4	5	6	7	8	9	10	11	12	13	14	15	16	17	18	19	20	21
L2				L3						L4				L5						

Plum varieties

Elena

1	2	3	4	5	6	7	8	9	10	11	12	13	14	15	16	17	18	19	20
L1									L2	L3				L4			L5		

Stanley

1	2	3	4	5	6	7	8	9	10	11	12	13	14	15	16	17	18	19	20
L1						L2				L3	L4								

Table 20. Plant extracts and their concentrations added to fruit juices in varying concentration.

	CBE concentration (g/ 100 mL)	GSE concentration (g/ 100 mL)	PGE concentration (g/ 100 mL)	Total extract concentration (g/ 100 mL)
Pure juices	0.00	0.00	0.00	0.00
Simple blends	0.50	0.00	0.00	0.50
	0.70	0.00	0.00	0.70
	1.00	0.00	0.00	1.00
	1.40	0.00	0.00	1.40
	1.90	0.00	0.00	1.90
	2.50	0.00	0.00	2.50
	0.00	0.50	0.00	0.50
	0.00	0.70	0.00	0.70
	0.00	1.00	0.00	1.00
	0.00	1.40	0.00	1.40
	0.00	1.90	0.00	1.90
	0.00	2.50	0.00	2.50
	0.00	0.00	0.50	0.50
	0.00	0.00	0.70	0.70
	0.00	0.00	1.00	1.00
	0.00	0.00	1.40	1.40
	0.00	0.00	1.90	1.90
	0.00	0.00	2.50	2.50
Binary blends	0.25	0.25	0.00	0.50
	0.35	0.35	0.00	0.70
	0.50	0.50	0.00	1.00
	0.70	0.70	0.00	1.40
	0.95	0.95	0.00	1.90
	1.25	1.25	0.00	2.50
	0.00	0.25	0.25	0.50
	0.00	0.35	0.35	0.70
	0.00	0.50	0.50	1.00
	0.00	0.70	0.70	1.40
	0.00	0.95	0.95	1.90
	0.00	1.25	1.25	2.50
	0.25	0.00	0.25	0.50
	0.35	0.00	0.35	0.70
	0.50	0.00	0.50	1.00
	0.70	0.00	0.70	1.40
	0.95	0.00	0.95	1.90
	1.25	0.00	1.25	2.50
Ternary blends	0.17	0.17	0.17	0.50
	0.23	0.23	0.23	0.70
	0.33	0.33	0.33	1.00
	0.47	0.47	0.47	1.40
	0.63	0.63	0.63	1.90
	0.83	0.83	0.83	2.50

Table 21. Applied spectral pre-treatments during the evaluation of data obtained with hyperspectral imaging, hand-held and benchtop spectrometers (I).

Use		Pre-treatment	Polynomial	Data frame	Derivation	Abbreviation	Basic purposes of application
✓	1	Savitzky-Golay smoothing	2nd order	13 points	–	sgol-2-13-0	Reduction of spectral noise
		Savitzky-Golay smoothing	2nd order	17 points	–	sgol-2-17-0	Reduction of spectral noise
		Savitzky-Golay smoothing	2nd order	21 points	–	sgol-2-21-0	Reduction of spectral noise
		detrending	2nd order	–	–	deTr	Elimination of polynomial trends
		multiplicative scatter correction	2nd order	–	–	msc	Reduction of baseline shift
		derivatives	2nd order	13 points	1st der	sgol-2-13-1	Elimination of constant offset
		derivatives	2nd order	17 points	1st der	sgol-2-17-1	Elimination of constant offset
		derivatives	2nd order	21 points	1st der	sgol-2-21-1	Elimination of constant offset
		derivatives	2nd order	13 points	2nd der	sgol-2-13-2	Elimination of constant and linear offsets
		derivatives	2nd order	17 points	2nd der	sgol-2-17-2	Elimination of constant and linear offsets
		derivatives	2nd order	21 points	2nd der	sgol-2-21-2	Elimination of constant and linear offsets
✓	2	smoothing and detrending	2nd order	21 points	–	sgol-2-21-0, deTr	Reduction of spectral noise; Elimination of polynomial trends
✓	3	smoothing and multiplicative scatter correction	2nd order	21 points	–	sgol-2-21-0, msc	Reduction of spectral noise; Reduction of baseline shift
✓	4	smoothing and derivation	2nd order	13 points; 13 points	1st der	sgol-2-13-0, sgol-2-13-1	Reduction of spectral noise; Elimination of constant offset
✓	5	smoothing and derivation	2nd order	17 points; 13 points	1st der	sgol-2-17-0, sgol-2-13-1	Reduction of spectral noise; Elimination of constant offset
✓	6	smoothing and derivation	2nd order	21 points; 13 points	1st der	sgol-2-21-0, sgol-2-13-1	Reduction of spectral noise; Elimination of constant offset
✓	7	smoothing and derivation	2nd order	13 points; 13 points	2nd der	sgol-2-13-0, sgol-2-13-2	Reduction of spectral noise; Elimination of constant and linear offset
✓	8	smoothing and derivation	2nd order	17 points; 13 points	2nd der	sgol-2-17-0, sgol-2-13-2	Reduction of spectral noise; Elimination of constant and linear offset
✓	9	smoothing and derivation	2nd order	21 points; 13 points	2nd der	sgol-2-21-0, sgol-2-13-2	Reduction of spectral noise; Elimination of constant and linear offset

Table 22. Applied spectral pre-treatments during the evaluation of data obtained with hyperspectral imaging, hand-held and benchtop spectrometers (II).

Use		Pre-treatment	Polynomial	Data frame	Derivation	Abbreviation	Basic purposes of application
✓	10	smoothing and derivation	2nd order	13 points; 17 points	1st der	sgol-2-13-0, sgol-2-17-1	Reduction of spectral noise; Elimination of constant offset
✓	11	smoothing and derivation	2nd order	17 points; 17 points	1st der	sgol-2-17-0, sgol-2-17-1	Reduction of spectral noise; Elimination of constant offset
✓	12	smoothing and derivation	2nd order	21 points; 17 points	1st der	sgol-2-21-0, sgol-2-17-1	Reduction of spectral noise; Elimination of constant offset
✓	13	smoothing and derivation	2nd order	13 points; 17 points	2nd der	sgol-2-13-0, sgol-2-17-2	Reduction of spectral noise; Elimination of constant and linear offset
✓	14	smoothing and derivation	2nd order	17 points; 17 points	2nd der	sgol-2-17-0, sgol-2-17-2	Reduction of spectral noise; Elimination of constant and linear offset
✓	15	smoothing and derivation	2nd order	21 points; 17 points	2nd der	sgol-2-21-0, sgol-2-17-2	Reduction of spectral noise; Elimination of constant and linear offset
✓	16	smoothing and derivation	2nd order	13 points; 21 points	1st der	sgol-2-13-0, sgol-2-21-1	Reduction of spectral noise; Elimination of constant offset
✓	17	smoothing and derivation	2nd order	17 points; 21 points	1st der	sgol-2-17-0, sgol-2-21-1	Reduction of spectral noise; Elimination of constant offset
✓	18	smoothing and derivation	2nd order	21 points; 21 points	1st der	sgol-2-21-0, sgol-2-21-1	Reduction of spectral noise; Elimination of constant offset
✓	19	smoothing and derivation	2nd order	13 points; 21 points	2nd der	sgol-2-13-0, sgol-2-21-2	Reduction of spectral noise; Elimination of constant and linear offset
✓	20	smoothing and derivation	2nd order	17 points; 21 points	2nd der	sgol-2-17-0, sgol-2-21-2	Reduction of spectral noise; Elimination of constant and linear offset
✓	21	smoothing and derivation	2nd order	21 points; 21 points	2nd der	sgol-2-21-0, sgol-2-21-2	Reduction of spectral noise; Elimination of constant and linear offset

✦ data frame for the smoothing of spectra recorded with the benchtop NIR spectrometer: 43 points

✦ data frame for the 1st or 2nd derivation of spectra recorded with the benchtop NIR spectrometer: 27 points

✶ data frame for the 1st or 2nd derivation of spectra recorded with the benchtop NIR spectrometer: 35 points

✷ data frame for the 1st or 2nd derivation of spectra recorded with the benchtop NIR spectrometer: 43 points

10.2.2. Annexes to the fruit ripeness assessment results

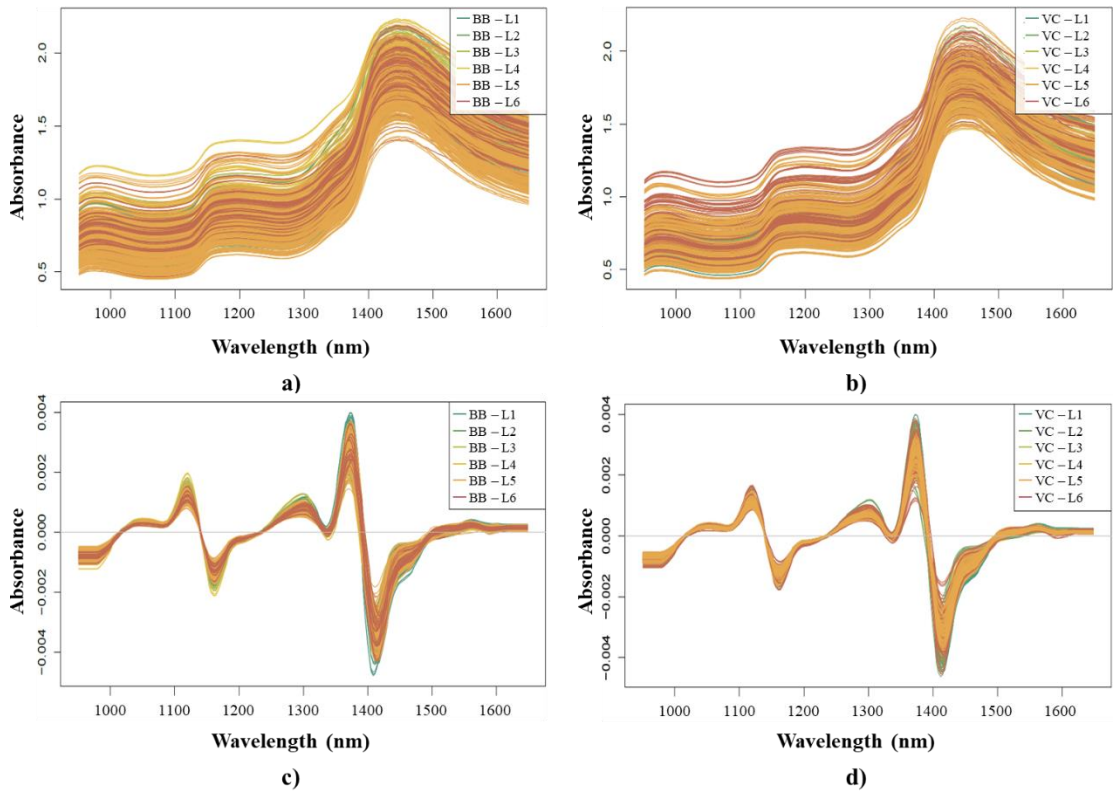

Figure 62. NIR spectra of sweet cherries of different ripeness: raw spectra of BB cherries (a); raw spectra of VC cherries (b); 2nd derivative spectra of BB cherries (c); 2nd derivative spectra of VC cherries (d).

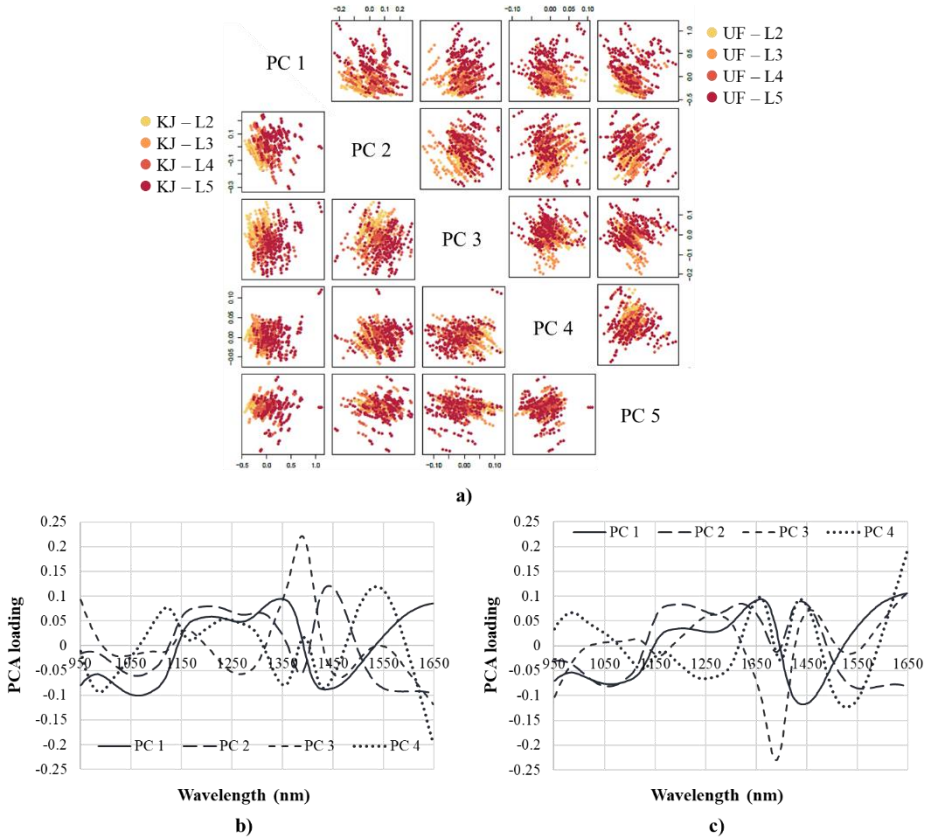

Figure 63. Preliminary PCA on the NIR spectra of sour cherries when colouring was based on fruit ripeness (sgol-2-21-0, msc): PCA score plots of cherries of different ripeness (a); PCA loading plot of KJ cherries (b); PCA loading plot of UF cherries (c).

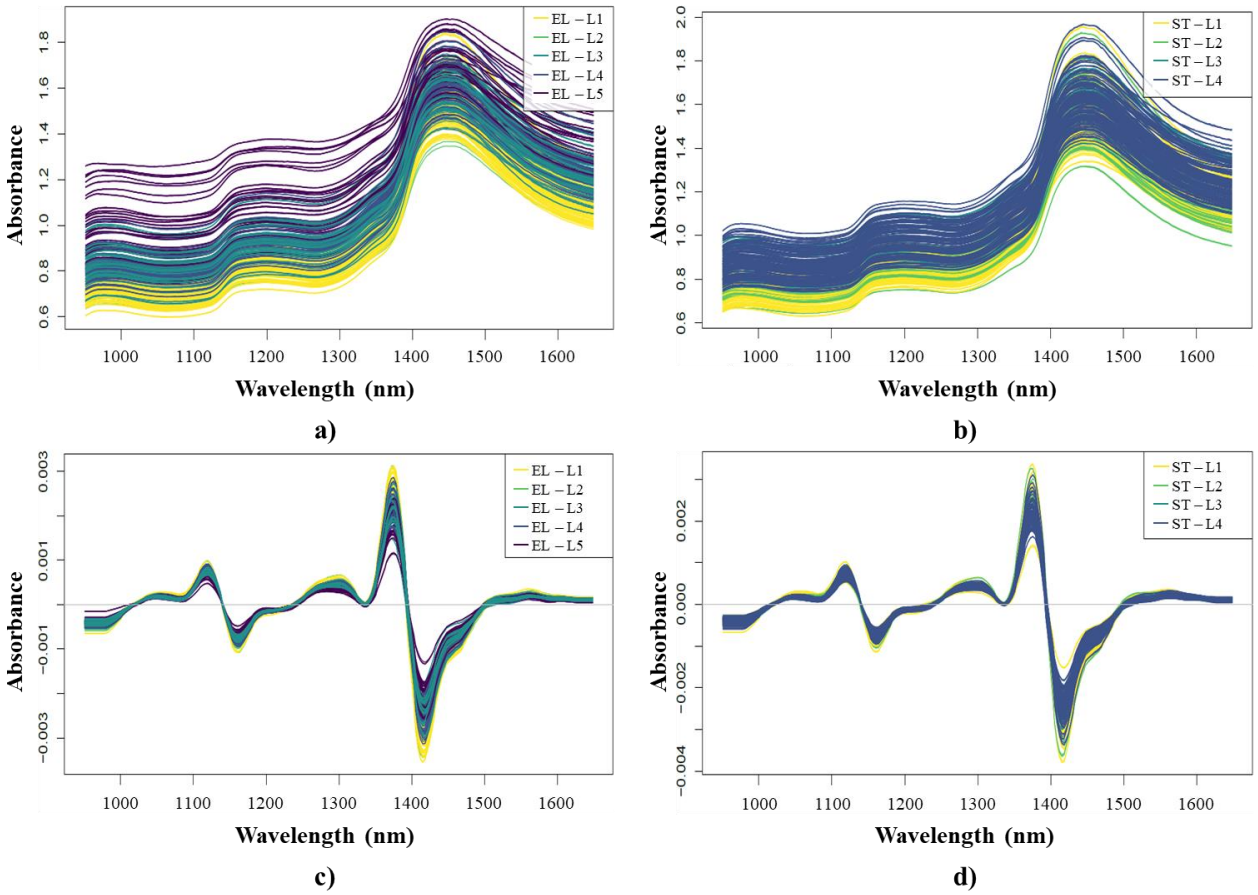

Figure 64. NIR spectra of plums of different ripeness: raw spectra of EL plums (a); raw spectra of ST plums (b); 2nd derivative spectra of EL plums (c); 2nd derivative spectra of ST plums (d).

Table 23. PCA-LDA classification accuracies on the NIR spectra of BB cherries when classification was based on fruit ripeness.

BB			BB_L1	BB_L2	BB_L3	BB_L4	BB_L5	BB_L6	Classification accuracy
Both sides *	**Calibration**	**BB_L1**	62.8	20.6	4.0	2.5	0.0	0.0	**66.6%**
		BB_L2	27.2	64.4	9.4	5.0	0.3	0.0	
		BB_L3	9.2	12.8	71.5	29.4	2.0	0.0	
		BB_L4	0.0	0.8	12.1	50.6	7.1	2.9	
		BB_L5	0.8	1.4	3.1	8.6	81.9	28.8	
		BB_L6	0.0	0.0	0.0	3.9	8.6	68.3	
	Validation	**BB_L1**	44.4	25.6	5.0	3.3	0.0	0.0	**55.5%**
		BB_L2	43.3	52.2	11.7	3.3	0.4	0.0	
		BB_L3	12.2	20.0	59.2	36.7	3.0	0.0	
		BB_L4	0.0	0.0	19.2	42.2	7.8	2.5	
		BB_L5	0.0	2.2	5.0	14.4	78.2	40.8	
		BB_L6	0.0	0.0	0.0	0.0	10.7	56.7	
Green side **	**Calibration**	**BB_L1**	91.1	0.0	0.0	0.0	0.0	0.0	**94.1%**
		BB_L2	6.7	91.1	3.3	2.2	0.0	0.0	
		BB_L3	2.2	8.9	93.3	4.4	1.5	0.0	
		BB_L4	0.0	0.0	3.3	93.3	0.7	0.0	
		BB_L5	0.0	0.0	0.0	0.0	95.6	0.0	
		BB_L6	0.0	0.0	0.0	0.0	2.2	100.0	
	Validation	**BB_L1**	32.2	14.4	10.4	8.9	0.6	1.7	**42.5%**
		BB_L2	46.7	47.2	37.1	18.9	5.6	1.7	
		BB_L3	16.7	30.0	31.3	40.0	4.8	2.9	
		BB_L4	4.4	2.8	13.8	22.2	6.1	5.0	
		BB_L5	0.0	3.9	6.3	7.2	68.5	35.0	
		BB_L6	0.0	1.7	1.3	2.8	14.4	53.8	
Ripe side ***	**Calibration**	**BB_L1**	73.9	9.4	6.3	0.0	0.0	0.0	**74.3%**
		BB_L2	14.4	77.8	5.4	2.2	2.4	0.0	
		BB_L3	11.1	8.3	78.3	27.2	2.8	0.0	
		BB_L4	0.0	3.3	5.4	58.3	6.9	0.0	
		BB_L5	0.6	1.1	4.6	12.2	80.0	22.5	
		BB_L6	0.0	0.0	0.0	0.0	8.0	77.5	
	Validation	**BB_L1**	57.8	20.0	10.0	2.2	0.0	0.0	**54.4%**
		BB_L2	24.4	57.8	15.0	6.7	4.4	0.0	
		BB_L3	13.3	13.3	50.0	48.9	3.0	1.7	
		BB_L4	4.4	6.7	20.0	24.4	10.4	0.0	
		BB_L5	0.0	2.2	5.0	17.8	71.1	33.3	
		BB_L6	0.0	0.0	0.0	0.0	11.1	65.0	

* sgol-2-21-0; Nr = 780; NrPC = 16

** sgol-2-17-0, sgol-2-13-1; Nr = 390, NrPC = 16

*** sgol-2-21-0; Nr = 390; NrPC = 17

Table 24. PCA-LDA classification accuracies on the NIR spectra of VC sweet cherries when classification was based on fruit ripeness.

VC			VC_L1	VC_L2	VC_L3	VC_L4	VC_L5	VC_L6	Classification accuracy
Both sides *	**Calibration**	**VC_L1**	93.3	1.1	0.0	0.0	0.0	0.0	**83.3%**
		VC_L2	6.7	81.4	6.0	0.0	0.0	0.0	
		VC_L3	0.0	16.7	88.3	34.6	1.5	0.0	
		VC_L4	0.0	0.6	5.6	60.0	3.2	0.0	
		VC_L5	0.0	0.3	0.0	5.4	90.8	14.0	
		VC_L6	0.0	0.0	0.0	0.0	4.4	86.1	
	Validation	**VC_L1**	90.0	2.2	0.0	0.0	0.0	0.0	**74.5%**
		VC_L2	10.0	74.4	7.5	0.0	0.0	0.0	
		VC_L3	0.0	21.1	82.5	50.0	1.7	0.0	
		VC_L4	0.0	1.1	10.0	36.7	6.1	0.0	
		VC_L5	0.0	1.1	0.0	13.3	81.1	17.7	
		VC_L6	0.0	0.0	0.0	0.0	11.1	82.3	
Green side **	**Calibration**	**VC_L1**	100.0	0.0	0.0	0.0	0.0	0.0	**98.3%**
		VC_L2	0.0	100.0	3.3	0.0	0.0	0.0	
		VC_L3	0.0	0.0	96.7	6.7	0.0	0.0	
		VC_L4	0.0	0.0	0.0	93.3	0.0	0.0	
		VC_L5	0.0	0.0	0.0	0.0	100.0	0.0	
		VC_L6	0.0	0.0	0.0	0.0	0.0	100.0	
	Validation	**VC_L1**	63.3	9.4	1.3	0.8	0.0	1.0	**48.8%**
		VC_L2	35.0	51.1	23.8	9.2	0.6	0.0	
		VC_L3	1.7	27.8	46.3	51.7	9.2	3.8	
		VC_L4	0.0	11.7	16.3	16.7	10.3	11.8	
		VC_L5	0.0	0.0	12.1	20.8	64.2	32.3	
		VC_L6	0.0	0.0	0.4	0.8	15.8	51.0	
Ripe side ***	**Calibration**	**VC_L1**	100.0	0.0	0.0	0.0	0.0	0.0	**91.7%**
		VC_L2	0.0	87.2	2.1	0.0	0.0	0.0	
		VC_L3	0.0	12.8	97.9	14.2	1.1	0.0	
		VC_L4	0.0	0.0	0.0	83.3	0.8	0.0	
		VC_L5	0.0	0.0	0.0	2.5	93.3	11.3	
		VC_L6	0.0	0.0	0.0	0.0	4.7	88.7	
	Validation	**VC_L1**	100.0	0.0	0.0	0.0	0.0	0.0	**78.0%**
		VC_L2	0.0	73.3	5.0	0.0	0.0	0.0	
		VC_L3	0.0	26.7	90.0	43.3	4.4	0.0	
		VC_L4	0.0	0.0	5.0	53.3	2.2	0.0	
		VC_L5	0.0	0.0	0.0	3.3	76.7	25.3	
		VC_L6	0.0	0.0	0.0	0.0	16.7	74.7	

* sgol-2-21-0, sgol-2-17-2; Nr = 312; NrPC = 16

** sgol-2-21-0, sgol-2-21-1; Nr = 315; NrPC = 19

*** sgol-2-21-0; Nr = 621; NrPC = 19

Table 25. PLSR prediction results of certain quality traits of BB sweet cherries of different ripeness.

BB	Quality trait	Pre-treatment	Nr	NrLV	R_C^2	$RMSE_C$	R_{CV}^2	$RMSE_{CV}$
Both sides	**L***	sgol-2-21-0	537	15	0.76	5.42	0.72	5.87
	a*	sgol-2-21-0; msc	538	5	0.23	8.74	0.16	9.15
	b*	sgol-2-21-0	552	12	0.69	2.90	0.64	3.12
	DMC (% *m/m*)	sgol-2-13-0; sgol-2-17-1	650	19	0.85	2.35	0.82	2.55
	SSC (% *brix*)	sgol-2-13-0; sgol-2-21-1	647	12	0.86	1.20	0.84	1.31
	TA (mg/ g)	sgol-2-21-0	651	20	0.72	0.48	0.65	0.54
	TAC (mg/ L)	sgol-2-21-0; sgol-2-17-1	651	6	0.79	14.81	0.78	15.28
	average L*	sgol-2-21-0	712	15	0.75	5.41	0.71	5.83
	average a*	sgol-2-21-0; sgol-2-21-1	673	29	0.44	6.29	0.22	7.47
	average b*	sgol-2-13-0; sgol-2-13-1	713	10	0.72	2.52	0.68	2.71
Green side	**L***	sgol-2-17-0; sgol-2-17-1	260	26	0.84	4.80	0.73	6.23
	a*	sgol-2-21-0; sgol-2-13-1	264	25	0.49	5.54	0.21	6.92
	b*	sgol-2-21-0	268	12	0.69	2.98	0.57	3.51
	DMC (% *m/m*)	sgol-2-13-0; sgol-2-17-1	319	18	0.88	2.07	0.83	2.50
	SSC (% *brix*)	sgol-2-13-0; sgol-2-21-1	336	13	0.88	1.13	0.83	1.31
	TA (mg/ g)	sgol-2-13-0; sgol-2-13-1	307	20	0.76	0.44	0.65	0.53
	TAC (mg/ L)	sgol-2-21-0; sgol-2-21-1	323	5	0.75	16.10	0.73	16.81
	average L*	sgol-2-13-0; sgol-2-17-1	260	30	0.85	4.23	0.71	5.79
	average a*	sgol-2-21-0; sgol-2-13-1	260	25	0.54	5.65	0.21	7.39
	average b*	sgol-2-21-0; sgol-2-13-2	266	7	0.76	2.33	0.70	2.60
Ripe side	**L***	sgol-2-21-0	266	12	0.75	5.00	0.69	5.60
	a*	sgol-2-21-0	266	10	0.34	9.62	0.19	10.60
	b*	sgol-2-21-0	270	15	0.74	2.38	0.64	2.80
	DMC (% *m/m*)	sgol-2-13-0; sgol-2-17-1	303	7	0.83	2.55	0.80	2.74
	SSC (% *brix*)	sgol-2-21-0; msc	316	10	0.89	1.09	0.86	1.23
	TA (mg/ g)	sgol-2-21-0	322	10	0.68	0.50	0.62	0.54
	TAC (mg/ L)	sgol-2-21-0; msc	306	12	0.86	12.14	0.83	13.51
	average L*	sgol-2-21-0	262	14	0.79	4.91	0.71	5.78
	average a*	sgol-2-17-0; sgol-2-17-1	260	15	0.46	6.11	0.27	7.13
	average b*	sgol-2-13-0; sgol-2-13-1	267	9	0.74	2.42	0.67	2.75

Table 26. PLSR prediction results of certain quality traits of VC sweet cherries of different ripeness.

VC	Quality trait	Pre-treatment	Nr	NrLV	R_C^2	$RMSE_C$	R_{CV}^2	$RMSE_{CV}$
Both	**L***	sgol-2-21-0, sgol-2-21-1	425	30	0.86	4.50	0.79	5.41
sides	**a***	sgol-2-13-0, sgol-2-21-1	428	22	0.60	6.05	0.50	6.80
	b*	sgol-2-21-0	442	14	0.73	2.39	0.68	2.59
	DMC (% *m/m*)	sgol-2-13-0, sgol-2-13-1	527	18	0.72	2.63	0.63	2.99
	SSC (% *brix*)	sgol-2-21-0	497	21	0.95	0.70	0.92	0.82
	TA (mg/ g)	sgol-2-13-0, sgol-2-13-1	486	18	0.47	0.67	0.37	0.72
	TAC (mg/ L)	sgol-2-21-0, msc	507	14	0.85	20.93	0.83	22.64
	average L*	sgol-2-21-0, sgol-2-21-1	552	30	0.86	4.32	0.81	5.09
	average a*	sgol-2-17-0, sgol-2-13-1	548	30	0.70	4.81	0.61	5.45
	average b*	sgol-2-21-0	563	15	0.84	1.72	0.80	1.90
Green	**L***	sgol-2-17-0, sgol-2-17-2	208	14	0.89	4.27	0.83	5.32
side	**a***	sgol-2-21-0	210	13	0.58	5.65	0.45	6.50
	b*	sgol-2-21-0, sgol-2-21-2	216	5	0.76	2.21	0.73	2.37
	DMC (% *m/m*)	sgol-2-13-0, sgol-2-13-2	244	5	0.68	2.71	0.60	3.05
	SSC (% *brix*)	sgol-2-21-0, sgol-2-17-1	239	10	0.95	0.69	0.93	0.79
	TA (mg/ g)	sgol-2-21-0	252	11	0.42	0.65	0.12	0.80
	TAC (mg/ L)	sgol-2-21-0	253	15	0.91	16.20	0.87	19.86
	average L*	sgol-2-13-0, sgol-2-17-2	211	17	0.89	3.79	0.83	4.77
	average a*	sgol-2-21-0	208	13	0.69	4.83	0.58	5.61
	average b*	sgol-2-13-0, sgol-2-13-1	214	9	0.85	1.69	0.79	1.98
Ripe	**L***	sgol-2-21-0, sgol-2-13-2	210	10	0.83	4.40	0.74	5.36
side	**a***	sgol-2-21-0, sgol-2-21-1	215	21	0.79	4.72	0.68	5.80
	b*	sgol-2-13-0, sgol-2-17-1	217	10	0.69	2.55	0.59	2.95
	DMC (% *m/m*)	sgol-2-21-0, sgol-2-21-1	254	10	0.78	2.34	0.72	2.62
	SSC (% *brix*)	sgol-2-17-0, sgol-2-13-2	228	19	0.96	0.60	0.92	0.89
	TA (mg/ g)	sgol-2-21-0	249	17	0.55	0.63	0.34	0.76
	TAC (mg/ L)	sgol-2-13-0, sgol-2-13-2	244	16	0.88	18.88	0.78	26.22
	average L*	sgol-2-17-0, sgol-2-17-2	214	8	0.83	4.76	0.78	5.44
	average a*	sgol-2-17-0, sgol-2-21-1	210	16	0.71	4.63	0.58	5.62
	average b*	sgol-2-21-0, sgol-2-21-1	214	15	0.86	1.63	0.76	2.10

Table 27. PCA-LDA classification accuracies on the NIR spectra of KJ sour cherries when classification was based on fruit ripeness.

KJ			KJ_L2	KJ_L3	KJ_L4	KJ_L5	Classification accuracy
Both sides *	**Calibration**	**KJ_L2**	96.9	2.2	0.0	0.0	**87.8%**
		KJ_L3	3.1	93.8	16.9	0.1	
		KJ_L4	0.0	4.0	62.7	2.3	
		KJ_L5	0.0	0.0	20.4	97.6	
	Validation	**KJ_L2**	95.0	5.3	0.0	0.0	**82.4%**
		KJ_L3	5.0	86.0	21.7	1.9	
		KJ_L4	0.0	8.7	55.8	5.3	
		KJ_L5	0.0	0.0	22.5	92.8	
Green side **	**Calibration**	**KJ_L2**	99.2	3.0	0.0	0.0	**89.6%**
		KJ_L3	0.8	92.7	15.0	0.0	
		KJ_L4	0.0	4.3	67.1	0.7	
		KJ_L5	0.0	0.0	17.9	99.3	
	Validation	**KJ_L2**	93.3	6.7	0.0	0.0	**76.8%**
		KJ_L3	6.7	80.0	28.3	1.0	
		KJ_L4	0.0	13.3	41.7	6.7	
		KJ_L5	0.0	0.0	30.0	92.4	
Ripe side ***	**Calibration**	**KJ_L2**	98.3	1.3	0.0	0.0	**93.1%**
		KJ_L3	1.7	93.3	6.7	0.0	
		KJ_L4	0.0	5.3	80.8	0.0	
		KJ_L5	0.0	0.0	12.5	100.0	
	Validation	**KJ_L2**	95.0	2.7	0.0	0.0	**80.7%**
		KJ_L3	5.0	84.0	21.7	0.0	
		KJ_L4	0.0	13.3	51.7	7.8	
		KJ_L5	0.0	0.0	26.7	92.2	

* sgol-2-21-0; Nr = 597; NrPC = 20

** sgol-2-21-0; Nr = 300; NrPC = 20

*** sgol-2-21-0; Nr = 297; NrPC = 19

Table 28. PCA-LDA classification accuracies on the NIR spectra of UF sour cherries when classification was based on fruit ripeness.

UF			UF_L2	UF_L3	UF_L4	UF_L5	Classification accuracy
Both sides *	**Calibration**	**UF_L2**	90.8	1.9	0.0	0.0	**87.0%**
		UF_L3	9.2	88.6	11.0	0.0	
		UF_L4	0.0	8.5	76.3	7.7	
		UF_L5	0.0	1.0	12.7	92.3	
	Validation	**UF_L2**	85.0	5.0	0.0	0.0	**78.3%**
		UF_L3	15.0	82.8	19.2	1.5	
		UF_L4	0.0	11.1	59.2	12.4	
		UF_L5	0.0	1.1	21.7	86.1	
Green side **	**Calibration**	**UF_L2**	93.8	0.0	0.0	0.0	**91.6%**
		UF_L3	6.3	93.6	7.9	0.0	
		UF_L4	0.0	6.4	82.1	3.2	
		UF_L5	0.0	0.0	10.0	96.8	
	Validation	**UF_L2**	81.7	3.3	0.0	0.0	**80.9%**
		UF_L3	18.3	83.3	16.7	0.0	
		UF_L4	0.0	13.3	68.3	9.8	
		UF_L5	0.0	0.0	15.0	90.2	
Ripe side ***	**Calibration**	**UF_L2**	91.7	2.2	0.0	0.0	**86.6%**
		UF_L3	5.0	87.2	16.7	1.8	
		UF_L4	3.3	9.2	81.3	11.9	
		UF_L5	0.0	1.4	2.1	86.4	
	Validation	**UF_L2**	90.0	4.4	0.0	0.0	**78.4%**
		UF_L3	6.7	81.1	28.3	4.0	
		UF_L4	3.3	10.0	61.7	15.2	
		UF_L5	0.0	4.4	10.0	80.8	

* sgol-2-21-0; Nr = 621; NrPC = 19

** sgol-2-21-0; Nr = 312; NrPC = 20

*** sgol-2-21-0, sgol-2-17-2; Nr = 309; NrPC = 11

Table 29. PLSR prediction results for certain quality traits of KJ sour cherries of different ripeness.

KJ	Quality trait	Pre-treatment	Nr	NrLV	R_C^2	$RMSE_C$	R_{CV}^2	$RMSE_{CV}$
Both sides	**L***	sgol-2-21-0	410	18	0.81	2.59	0.74	3.03
	a*	sgol-2-21-0	416	6	0.73	4.42	0.72	4.52
	b*	sgol-2-21-0	437	8	0.90	1.62	0.88	1.73
	DMC (% *m/m*)	sgol-2-21-0; sgol-2-17-1	493	7	0.69	1.77	0.64	1.89
	SSC (% *brix*)	sgol-2-21-0; msc	499	12	0.50	1.34	0.44	1.42
	TA (mg/ g)	sgol-2-21-0; sgol-2-21-1	510	12	0.57	2.08	0.52	2.22
	TAC (mg/ L)	sgol-2-21-0	483	18	0.89	16.57	0.86	18.77
	average L*	sgol-2-21-0	555	16	0.83	2.30	0.78	2.60
	average a*	sgol-2-21-0	587	7	0.80	3.41	0.78	3.59
	average b*	sgol-2-21-0	557	12	0.91	1.50	0.88	1.68
Green side	**L***	sgol-2-21-0	206	11	0.83	2.60	0.75	3.18
	a*	sgol-2-21-0	202	5	0.58	4.85	0.56	4.98
	b*	sgol-2-21-0	204	12	0.93	1.42	0.90	1.69
	DMC (% *m/m*)	sgol-2-21-0	247	9	0.68	1.78	0.56	2.10
	SSC (% *brix*)	sgol-2-21-0; msc	229	10	0.51	1.36	0.42	1.47
	TA (mg/ g)	sgol-2-21-0	242	12	0.67	1.79	0.54	2.09
	TAC (mg/ L)	sgol-2-21-0	244	14	0.91	15.14	0.87	18.03
	average L*	sgol-2-21-0	200	17	0.89	1.88	0.81	2.44
	average a*	sgol-2-21-0	200	7	0.82	3.24	0.80	3.42
	average b*	sgol-2-21-0	204	12	0.93	1.26	0.91	1.51
Ripe side	**L***	sgol-2-21-0	200	14	0.86	1.92	0.80	2.31
	a*	sgol-2-21-0	208	5	0.92	2.59	0.91	2.77
	b*	sgol-2-21-0	202	5	0.90	1.50	0.89	1.57
	DMC (% *m/m*)	sgol-2-21-0	232	9	0.79	1.47	0.72	1.67
	SSC (% *brix*)	sgol-2-21-0; deTr	256	5	0.59	1.23	0.55	1.28
	TA (mg/ g)	sgol-2-21-0	237	9	0.62	1.91	0.55	2.09
	TAC (mg/ L)	sgol-2-21-0	233	14	0.88	17.22	0.79	22.57
	average L*	sgol-2-21-0	198	13	0.87	2.01	0.82	2.42
	average a*	sgol-2-21-0	198	7	0.82	3.24	0.78	3.58
	average b*	sgol-2-21-0	204	13	0.93	1.28	0.89	1.62

Table 30. PLSR prediction results of certain quality traits of UF sour cherries of different ripeness.

UF	Quality trait	Pre-treatment	Nr	NrLV	R_C^2	$RMSE_C$	R_{CV}^2	$RMSE_{CV}$
Both	**L***	sgol-2-21-0	444	14	0.81	2.70	0.77	2.93
sides	**a***	sgol-2-21-0	429	6	0.57	5.14	0.55	5.26
	b*	sgol-2-21-0	439	20	0.89	1.78	0.84	2.18
	DMC (% *m/m*)	sgol-2-21-0	502	15	0.58	1.51	0.50	1.65
	SSC (% *brix*)	sgol-2-21-0	531	15	0.85	1.02	0.82	1.13
	TA (mg/ g)	sgol-2-13-0, sgol-2-13-2	523	9	0.48	1.45	0.39	1.57
	TAC (mg/ L)	sgol-2-21-0	540	16	0.86	21.59	0.83	23.75
	average L*	sgol-2-21-0	564	24	0.85	2.31	0.79	2.74
	average a*	sgol-2-21-0	547	27	0.80	3.12	0.69	3.90
	average b*	sgol-2-21-0	573	17	0.90	1.69	0.87	1.94
Green	**L***	sgol-2-21-0	215	16	0.88	2.52	0.76	3.53
side	**a***	sgol-2-21-0	212	6	0.48	5.12	0.40	5.50
	b*	sgol-2-21-0	214	13	0.90	1.93	0.86	2.29
	DMC (% *m/m*)	sgol-2-21-0	260	9	0.47	1.72	0.29	1.99
	SSC (% *brix*)	sgol-2-21-0	271	18	0.88	0.91	0.81	1.15
	TA (mg/ g)	sgol-2-21-0, sgol-2-13-2	264	9	0.49	1.43	0.35	1.60
	TAC (mg/ L)	sgol-2-21-0	242	10	0.89	18.67	0.87	20.98
	average L*	sgol-2-21-0	209	16	0.88	2.03	0.78	2.76
	average a*	sgol-2-21-0	211	6	0.71	3.79	0.67	4.09
	average b*	sgol-2-21-0	210	11	0.91	1.54	0.89	1.78
Ripe	**L***	sgol-2-21-0	216	10	0.79	2.25	0.73	2.52
side	**a***	sgol-2-21-0	210	15	0.88	2.95	0.81	3.71
	b*	sgol-2-21-0	218	15	0.91	1.42	0.86	1.77
	Dry matter	sgol-2-21-0	254	16	0.70	1.37	0.56	1.65
	Soluble solids	sgol-2-21-0, sgol-2-13-2	249	9	0.87	0.98	0.83	1.10
	Total acidity	sgol-2-21-0, deTr	245	7	0.53	1.41	0.43	1.56
	Anthocyanin content	sgol-2-21-0	248	9	0.82	24.22	0.79	26.57
	average L*	sgol-2-21-0	208	12	0.83	2.44	0.74	3.01
	average a*	sgol-2-21-0	208	10	0.71	3.77	0.61	4.41
	average b*	sgol-2-21-0	208	20	0.91	1.59	0.82	2.25

Table 31. PCA-LDA classification accuracies on the NIR spectra of EL plums when classification was based on fruit ripeness.

EL			EL_L1	EL_L2	EL_L3	EL_L4	EL_L5	Classification accuracy
Both sides *	**Calibration**	**EL_L1**	98.3	20.0	0.0	0.0	0.0	**76.8%**
		EL_L2	1.7	80.0	0.0	0.0	0.0	
		EL_L3	0.0	0.0	74.2	29.4	16.4	
		EL_L4	0.0	0.0	18.1	63.9	15.8	
		EL_L5	0.0	0.0	7.7	6.7	67.8	
	Validation	**EL_L1**	97.0	33.3	0.0	0.0	0.0	**66.5%**
		EL_L2	3.0	66.7	0.0	0.0	0.0	
		EL_L3	0.0	0.0	53.3	37.8	23.3	
		EL_L4	0.0	0.0	32.5	55.6	16.7	
		EL_L5	0.0	0.0	14.2	6.7	60.0	
Green side **	**Calibration**	**EL_L1**	99.1	21.7	0.0	0.0	0.0	**82.1%**
		EL_L2	0.2	78.3	0.0	0.0	0.0	
		EL_L3	0.7	0.0	79.6	28.9	8.3	
		EL_L4	0.0	0.0	15.0	71.1	9.4	
		EL_L5	0.0	0.0	5.4	0.0	82.2	
	Validation	**EL_L1**	99.3	46.7	0.0	0.0	0.0	**70.7%**
		EL_L2	0.7	53.3	0.0	0.0	0.0	
		EL_L3	0.0	0.0	63.3	31.1	20.0	
		EL_L4	0.0	0.0	23.3	68.9	11.1	
		EL_L5	0.0	0.0	13.3	0.0	68.9	
Ripe side ***	**Calibration**	**EL_L1**	97.78	16.67	0	0	0	**79.75%**
		EL_L2	2.2	83.3	0.0	0.0	0.0	
		EL_L3	0.0	0.0	75.4	11.7	17.8	
		EL_L4	0.0	0.0	13.8	78.9	18.9	
		EL_L5	0.0	0.0	10.8	9.4	63.3	
	Validation	**EL_L1**	96.3	53.3	0.0	0.0	0.0	**60.1%**
		EL_L2	3.7	46.7	0.0	0.0	0.0	
		EL_L3	0.0	0.0	46.7	26.7	33.3	
		EL_L4	0.0	0.0	31.7	60.0	15.6	
		EL_L5	0.0	0.0	21.7	13.3	51.1	

* sgol-2-21-0; Nr = 297; NrPC = 19

** sgol-2-13-0, sgol-2-17-1; Nr = 600; NrPC = 15

*** sgol-2-21-0, sgol-2-21-1; Nr = 300; NrPC = 12

Table 32. PCA-LDA classification accuracies on the NIR spectra of ST plums when classification was based on fruit ripeness.

ST			ST_L1	ST_L2	ST_L3	ST_L4	Classification accuracy
Both sides *	**Calibration**	**ST_L1**	81.0	46.5	0.0	0.0	**71.1%**
		ST_L2	19.0	53.5	0.0	0.0	
		ST_L3	0.0	0.0	52.5	2.4	
		ST_L4	0.0	0.0	47.5	97.6	
	Validation	**ST_L1**	80.0	61.7	0.0	0.0	**59.5%**
		ST_L2	19.4	38.3	0.0	0.0	
		ST_L3	0.0	0.0	23.3	3.8	
		ST_L4	0.6	0.0	76.7	96.3	
Green side **	**Calibration**	**ST_L1**	85.6	25.0	0.0	0.0	**88.2%**
		ST_L2	14.4	75.0	0.0	0.0	
		ST_L3	0.0	0.0	95.0	2.8	
		ST_L4	0.0	0.0	5.0	97.2	
	Validation	**ST_L1**	73.3	48.3	0.0	0.0	**58.7%**
		ST_L2	26.7	51.7	0.0	0.0	
		ST_L3	0.0	0.0	20.0	10.4	
		ST_L4	0.0	0.0	80.0	89.6	
Ripe side ***	**Calibration**	**ST_L1**	86.1	15.4	0.0	0.0	**85.4%**
		ST_L2	13.9	84.6	0.0	0.0	
		ST_L3	0.0	0.0	71.7	0.6	
		ST_L4	0.0	0.0	28.3	99.4	
	Validation	**ST_L1**	76.7	30.0	0.0	0.0	**68.0%**
		ST_L2	23.3	70.0	0.0	0.0	
		ST_L3	0.0	0.0	26.7	1.5	
		ST_L4	0.0	0.0	73.3	98.5	

* sgol-2-21-0, deTr; Nr = 597; NrPC = 13

** sgol-2-21-0, msc; Nr = 300; NrPC = 20

*** sgol-2-21-0, deTr; Nr = 297; NrPC = 13

Table 33. PLSR prediction results of certain quality traits of EL plums of different ripeness.

EL	Quality trait	Pre-treatment	Nr	NrLV	R_C^2	$RMSE_C$	R_{CV}^2	$RMSE_{CV}$
Both	**L***	sgol-2-21-0	412	18	0.83	4.10	0.76	4.82
sides	**a***	sgol-2-21-0, sgol-2-17-2	432	13	0.79	2.90	0.74	3.27
	b*	sgol-2-17-0, sgol-2-13-1	410	16	0.82	3.94	0.75	4.60
	DMC (% *m/m*)	sgol-2-21-0, sgol-2-21-2	510	6	0.24	1.11	0.16	1.17
	SSC (% *brix*)	sgol-2-13-0, sgol-2-13-2	492	12	0.96	0.35	0.95	0.40
	TA (mg/ g)	sgol-2-21-0	508	15	0.96	0.66	0.96	0.74
	TAC (mg/ L)	sgol-2-21-0	496	3	0.77	1.04	0.76	1.06
	average L*	sgol-2-21-0	545	18	0.91	2.67	0.87	3.17
	average a*	sgol-2-13-0, sgol-2-13-2	525	9	0.89	1.94	0.86	2.17
	average b*	sgol-2-21-0	527	12	0.89	2.76	0.85	3.14
Green	**L***	sgol-2-21-0	200	9	0.80	3.79	0.74	4.29
side	**a***	sgol-2-21-0, sgol-2-17-1	210	20	0.89	2.10	0.83	2.62
	b*	sgol-2-21-0	202	8	0.80	3.53	0.76	3.88
	DMC (% *m/m*)	sgol-2-21-0, deTr	264	7	0.45	1.02	0.35	1.11
	SSC (% *brix*)	sgol-2-17-0, sgol-2-17-2	238	12	0.97	0.32	0.95	0.41
	TA (mg/ g)	sgol-2-17-0, sgol-2-13-1	243	13	0.97	0.58	0.95	0.74
	TAC (mg/ L)	sgol-2-21-0, sgol-2-21-1	236	6	0.82	0.90	0.75	1.04
	average L*	sgol-2-21-0	206	12	0.91	2.62	0.88	3.10
	average a*	sgol-2-17-0, sgol-2-13-2	208	7	0.88	1.98	0.85	2.28
	average b*	sgol-2-17-0, sgol-2-13-1	200	29	0.93	2.22	0.86	3.07
Ripe	**L***	sgol-2-13-0, sgol-2-13-2	204	8	0.92	2.92	0.86	3.87
side	**a***	sgol-2-13-0, sgol-2-21-2	211	6	0.76	2.99	0.70	3.36
	b*	sgol-2-13-0, sgol-2-21-1	205	13	0.91	2.81	0.87	3.44
	Dry matter	sgol-2-21-0, sgol-2-21-2	239	6	0.30	1.08	0.12	1.22
	Soluble solids	sgol-2-13-0, sgol-2-13-2	251	12	0.97	0.34	0.93	0.49
	Total acidity	sgol-2-21-0	234	15	0.98	0.50	0.97	0.62
	Anthocyanin content	sgol-2-21-0, msc	256	6	0.76	1.01	0.71	1.12
	average L*	sgol-2-21-0	206	11	0.91	2.65	0.85	3.38
	average a*	sgol-2-17-0, sgol-2-17-2	208	12	0.91	1.72	0.85	2.27
	average b*	sgol-2-21-0, sgol-2-21-1	200	13	0.92	2.40	0.88	2.84

Table 34. PLSR prediction results of certain quality traits of ST plums of different ripeness.

ST	Quality trait	Pre-treatment	Nr	NrLV	R_C^2	$RMSE_C$	R_{CV}^2	$RMSE_{CV}$
Both	**L***	sgol-2-17-0, sgol-2-17-2	403	30	0.82	3.70	0.71	4.65
sides	**a***	sgol-2-13-0, sgol-2-21-2	424	21	0.62	3.78	0.50	4.37
	b*	sgol-2-17-0, sgol-2-13-1	420	11	0.73	4.54	0.67	5.07
	DMC (% *m/m*)	sgol-2-21-0	515	4	0.23	0.99	0.18	1.02
	SSC (% *brix*)	sgol-2-17-0, sgol-2-21-2	476	18	0.91	0.44	0.88	0.51
	TA (mg/ g)	sgol-2-21-0, sgol-2-13-2	492	19	0.93	0.59	0.90	0.69
	average L*	sgol-2-21-0	556	15	0.86	2.75	0.82	3.12
	average a*	sgol-2-13-0, sgol-2-21-1	528	30	0.80	2.09	0.73	2.40
	average b*	sgol-2-13-0, sgol-2-13-2	542	7	0.80	3.16	0.76	3.45
Green	**L***	sgol-2-21-0, sgol-2-21-2	201	27	0.92	2.24	0.81	3.42
side	**a***	sgol-2-17-0, sgol-2-13-2	209	7	0.95	1.52	0.92	1.94
	b*	sgol-2-21-0, sgol-2-17-2	201	9	0.84	3.06	0.76	3.82
	DMC (% *m/m*)	sgol-2-21-0	247	3	0.20	1.01	0.13	1.06
	SSC (% *brix*)	sgol-2-21-0	240	16	0.93	0.40	0.86	0.55
	TA (mg/ g)	sgol-2-21-0	245	17	0.92	0.61	0.85	0.84
	TAC (mg/ L)	sgol-2-17-0, sgol-2-17-2	253	4	0.29	4.42	0.18	4.75
	average L*	sgol-2-13-0, sgol-2-13-2	201	7	0.87	2.67	0.78	3.46
	average a*	sgol-2-21-0, deTr	204	19	0.82	1.94	0.67	2.61
	average b*	sgol-2-13-0, sgol-2-13-2	200	6	0.81	3.09	0.72	3.71
Ripe	**L***	sgol-2-17-0, sgol-2-17-2	201	6	0.72	4.04	0.65	4.58
side	**a***	sgol-2-13-0, sgol-2-13-2	207	4	0.28	3.69	0.17	3.98
	b*	sgol-2-13-0, sgol-2-13-1	203	8	0.72	3.99	0.65	4.51
	DMC (% *m/m*)	sgol-2-21-0	222	3	0.36	0.86	0.28	0.91
	SSC (% *brix*)	sgol-2-17-0, sgol-2-21-2	233	7	0.90	0.46	0.88	0.52
	TA (mg/ g)	sgol-2-21-0, sgol-2-13-1	231	18	0.94	0.52	0.90	0.66
	TAC (mg/ L)	sgol-2-21-0	228	2	0.26	4.95	0.22	5.06
	average L*	sgol-2-21-0, sgol-2-13-2	199	7	0.86	2.71	0.81	3.20
	average a*	sgol-2-13-0, sgol-2-21-2	205	10	0.80	2.02	0.73	2.35
	average b*	sgol-2-17-0, sgol-2-13-2	198	7	0.83	2.87	0.79	3.22

10.2.3. Annexes to the *Monilinia* detection results

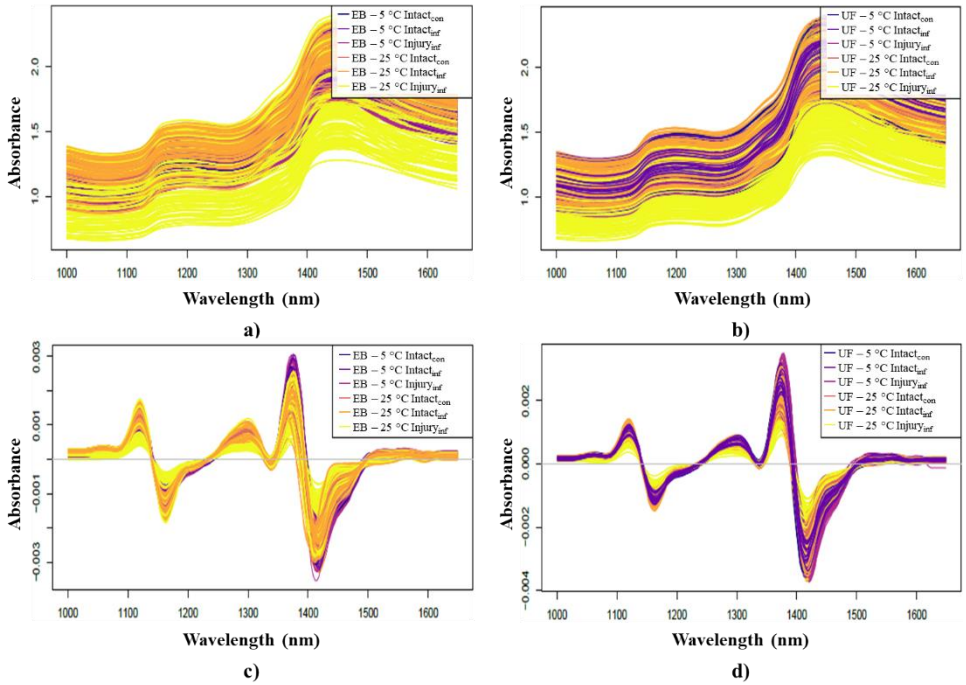

Figure 65. NIR spectra of sour cherries treated in different ways: raw spectra of EB cherries (a); raw spectra of UF cherries (b); 2nd derivative spectra of EB cherries (c); 2nd derivative spectra of UF cherries (d).

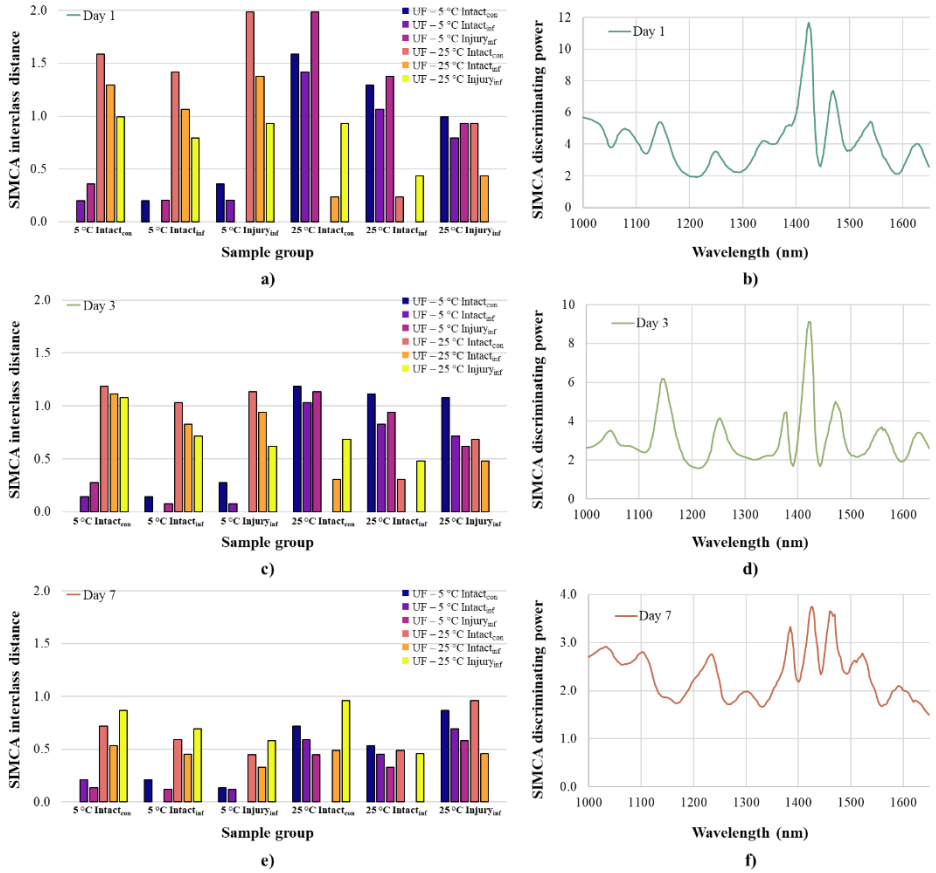

Figure 66. SIMCA on the NIR spectra of UF cherries when discrimination was based on fruit treatment on certain storage days (sgol-2-21-0, msc): SIMCA interclass distances on the 1st day of storage (a); SIMCA discrimination power plot on the 1st day of storage (b); SIMCA interclass distances on the 3rd day of storage (c); SIMCA discrimination power plot on the 3rd day of storage (d); SIMCA interclass distances on the 7th day of storage (e); SIMCA discrimination power plot on the 7th day of storage (f).

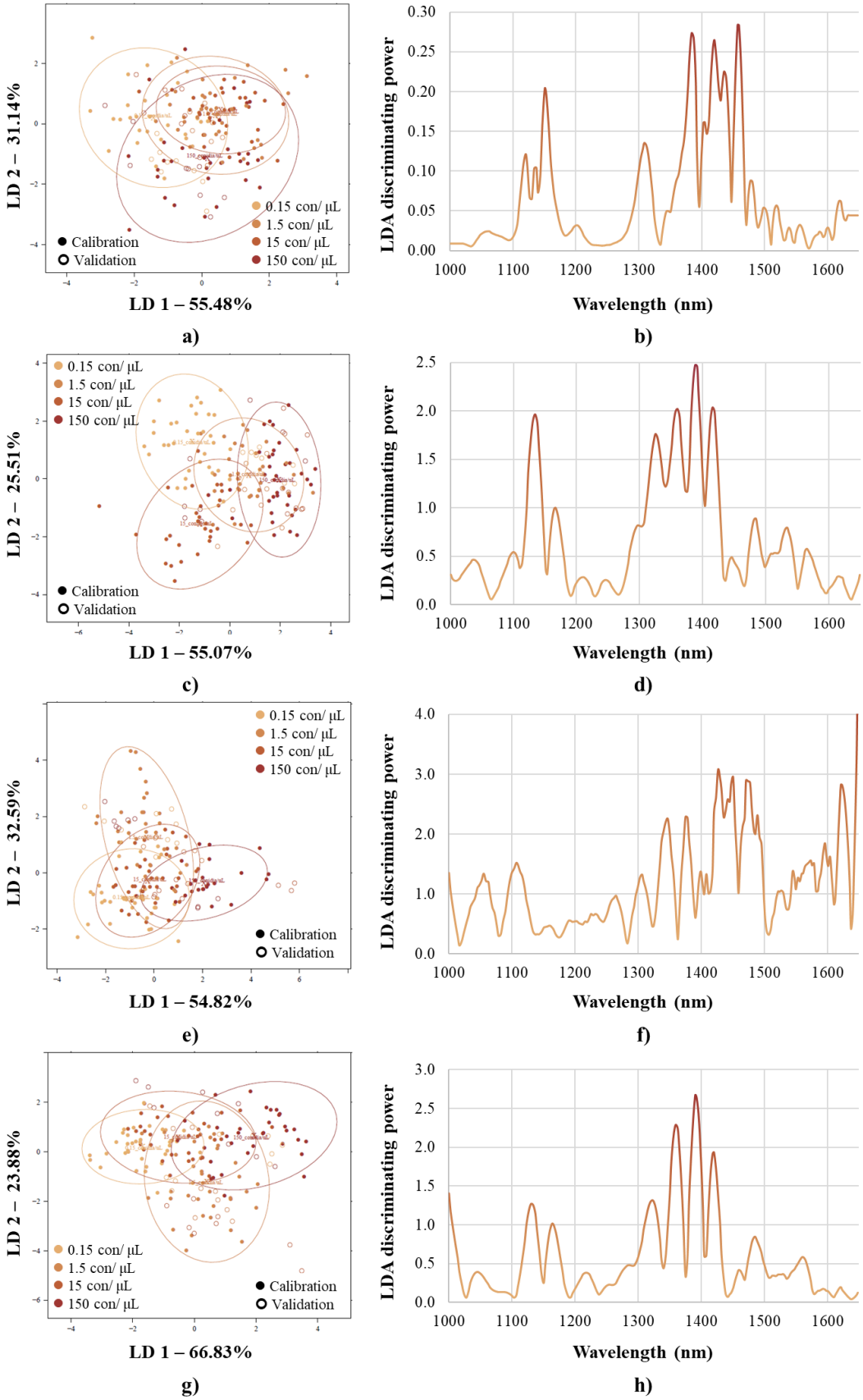

Figure 67. PCA-LDA on the NIR spectra of EB cherries when classification was based on initial conidial contamination: PCA-LDA score plot of "5 °C Injury" samples (a); LDA discriminating power plot of "5 °C Injury" samples (b); PCA-LDA score plot of "5 °C Intact" samples (c); LDA discriminating power plot of "5 °C Intact" samples (d); PCA-LDA score plot of "25 °C Injury" samples (e); LDA discriminating power plot of "25 °C Injury" samples (f); PCA-LDA score plot of "25 °C Intact" samples (g); LDA discriminating power plot of "25 °C Intact" samples (h).

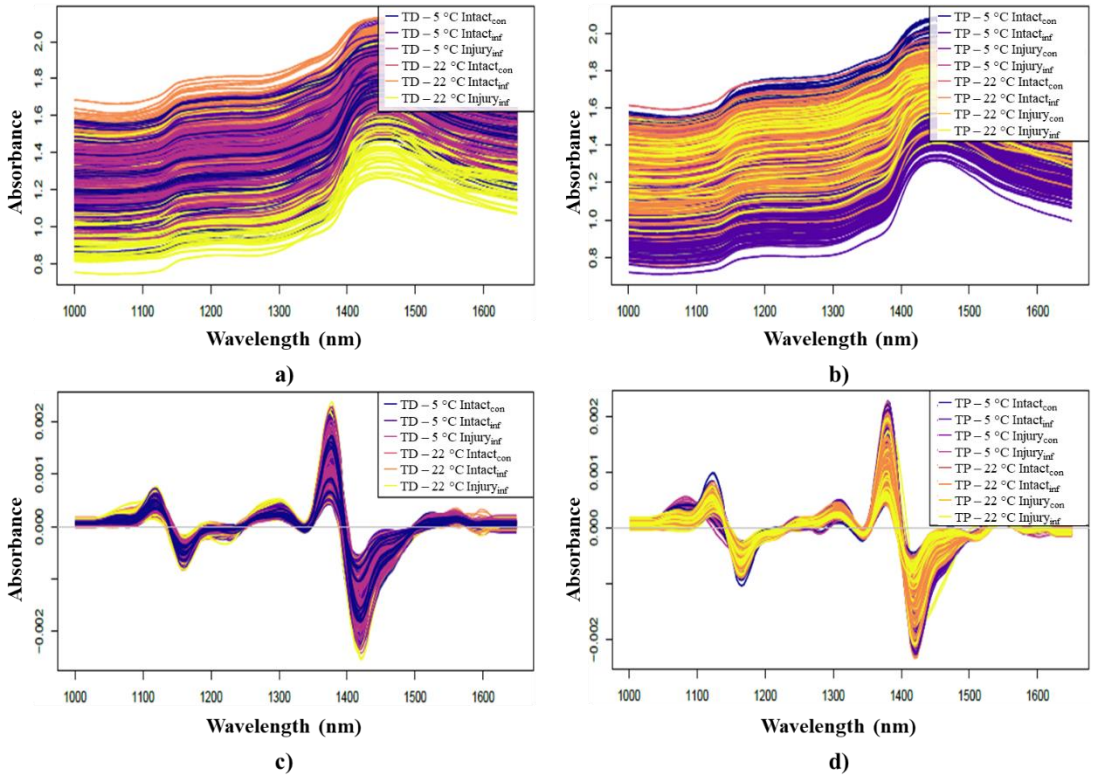

Figure 68. NIR spectra of plums treated in different ways: raw spectra of TD plums (a); raw spectra of TP plums (b); 2nd derivative spectra of TD plums (c); 2nd derivative spectra of TP plums (d).

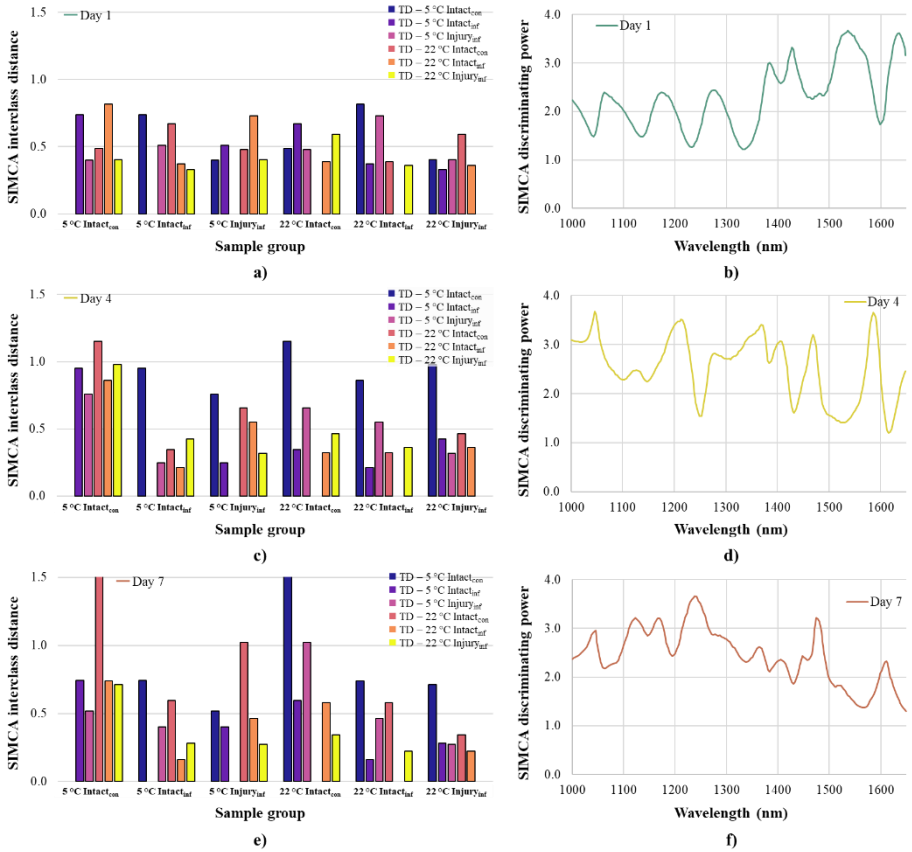

Figure 69. SIMCA on NIR spectra of TD plums when discrimination was based on fruit treatment on certain storage days (sgol-2-21-0, msc): SIMCA interclass distances on the 1st day of storage (a); SIMCA discrimination power plot on the 1st day of storage (b); SIMCA interclass distances on the 4th day of storage (c); SIMCA discrimination power plot on the 4th day of storage (d); SIMCA interclass distances on the 7th day of storage (e); SIMCA discrimination power plot on the 7th day of storage (f).

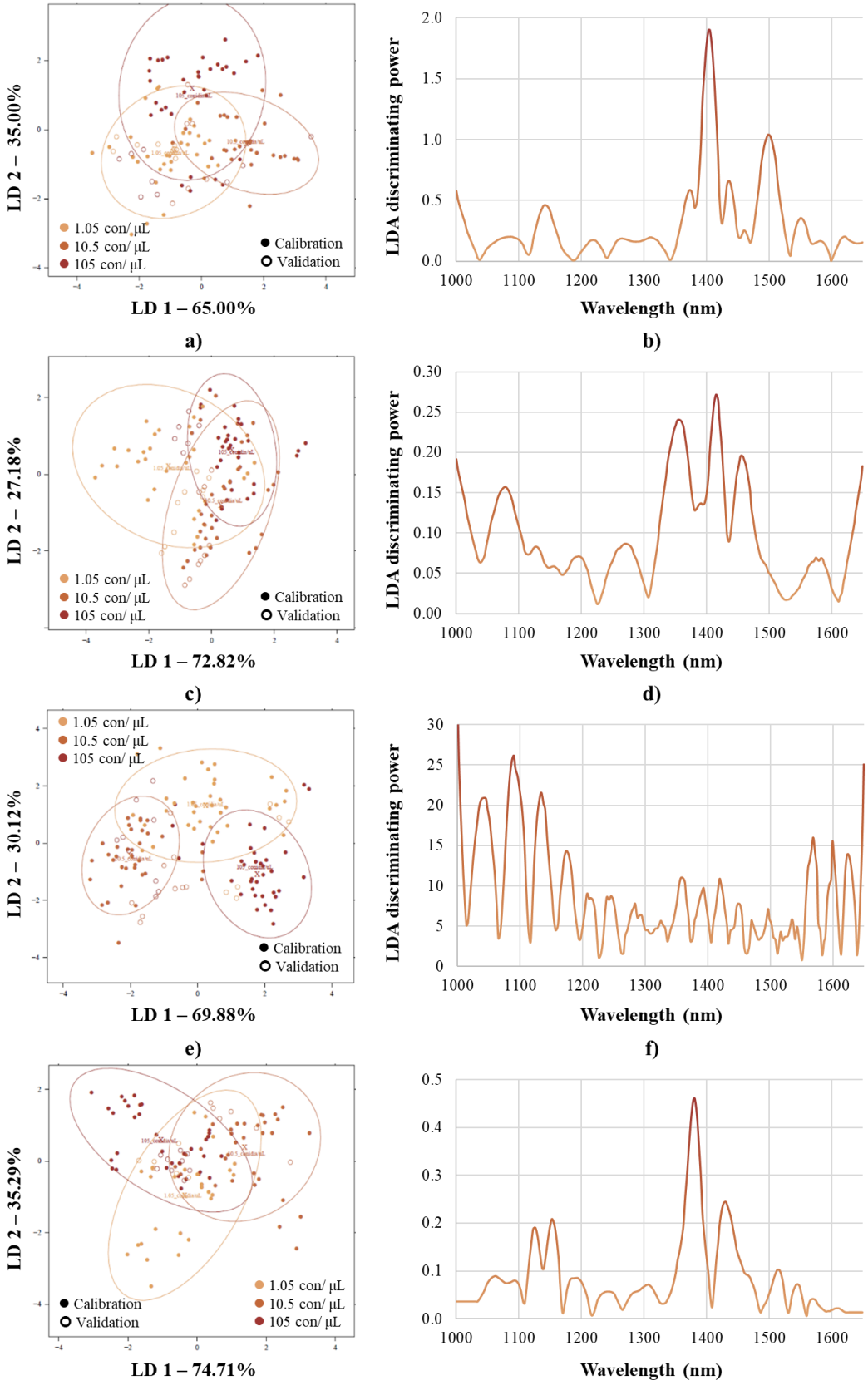

Figure 70. PCA-LDA on the NIR spectra of TD plums when classification was based on initial conidial contamination: PCA-LDA score plot of "5 °C Injury" samples (a); LDA discriminating power plot of "5 °C Injury" samples (b); PCA-LDA score plot of "5 °C Intact" samples (c); LDA discriminating power plot of "5 °C Intact" samples (d); PCA-LDA score plot of "22 °C Injury" samples (e); LDA discriminating power plot of "22 °C Injury" samples (f); PCA-LDA score plot of "22 °C Intact" samples (g); LDA discriminating power plot of "22 °C Intact" samples (h).

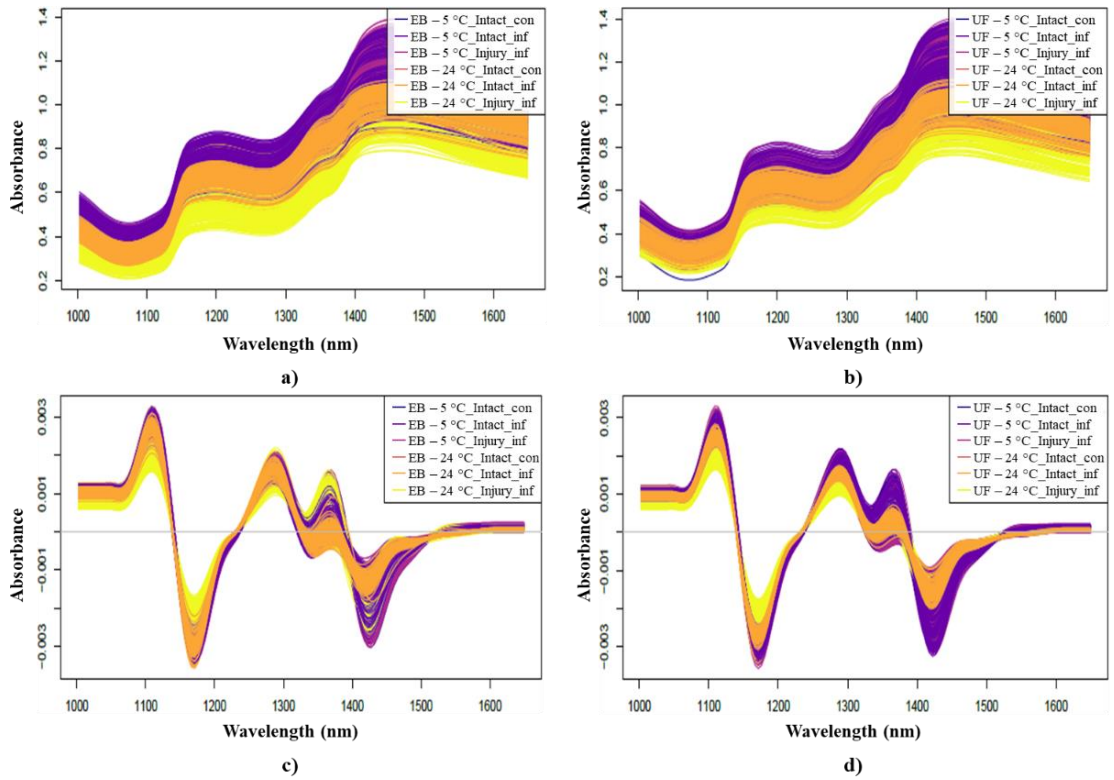

Figure 71. HSI spectra of sour cherries treated in different ways: raw spectra of EB cherries (a); raw spectra of UF cherries (b); 2nd derivative spectra of EB cherries (c); 2nd derivative spectra of UF cherries (d).

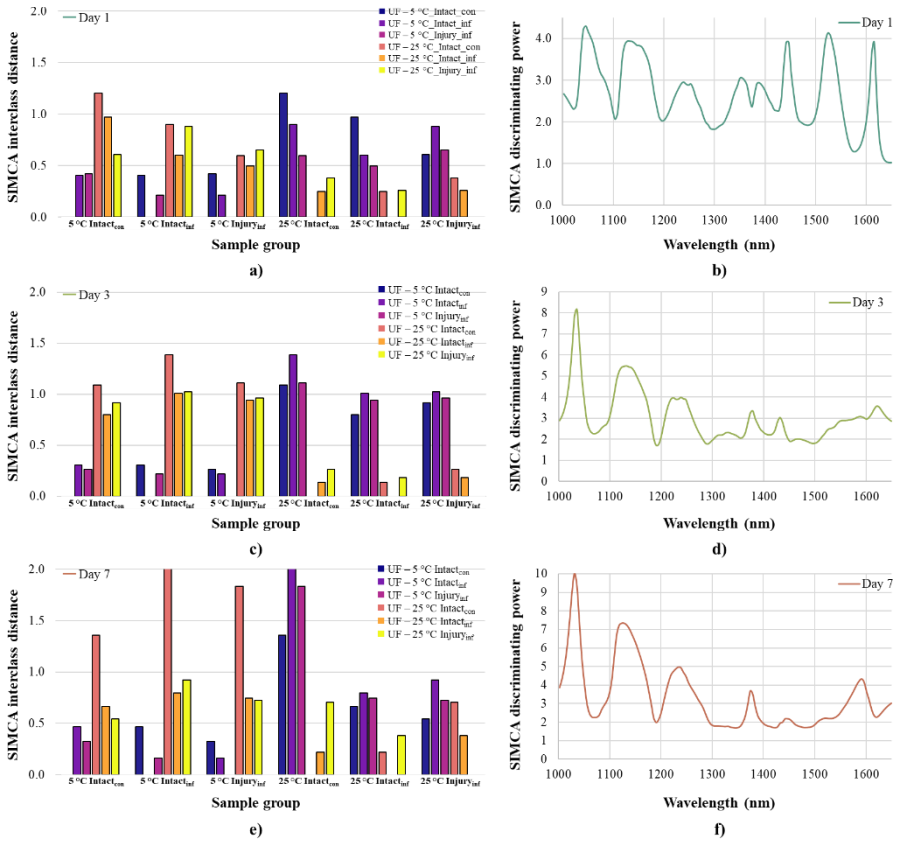

Figure 72. SIMCA on the HSI spectra of UF cherries when discrimination was based on fruit treatment on certain storage days (sgol-2-21-0, msc): SIMCA interclass distances on the 1st day of storage (a); SIMCA discrimination power plot on the 1st day of storage (b); SIMCA interclass distances on the 3rd day of storage (c); SIMCA discrimination power plot on the 3rd day of storage (d); SIMCA interclass distances on the 7th day of storage (e); SIMCA discrimination power plot on the 7th day of storage (f).

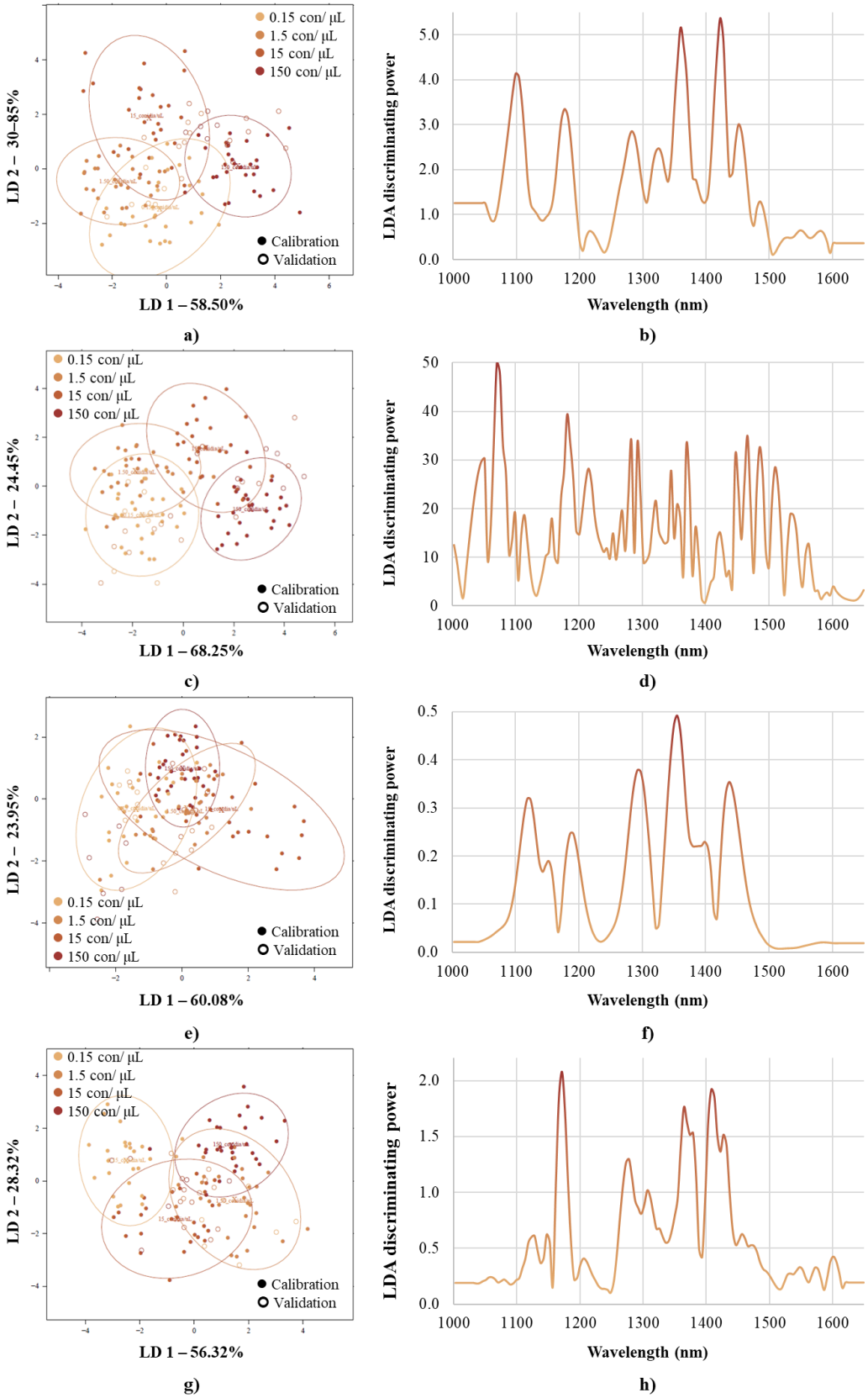

Figure 73. PCA-LDA on the HSI spectra of EB cherries when classification was based on initial conidial contamination: PCA-LDA score plot of "5 °C Injury" samples (a); LDA discriminating power plot of "5 °C Injury" samples (b); PCA-LDA score plot of "5 °C Intact" samples (c); LDA discriminating power plot of "5 °C Intact" samples (d); PCA-LDA score plot of "25 °C Injury" samples (e); LDA discriminating power plot of "25 °C Injury" samples (f); PCA-LDA score plot of "25 °C Intact" samples (g); LDA discriminating power plot of "25 °C Intact" samples (h).

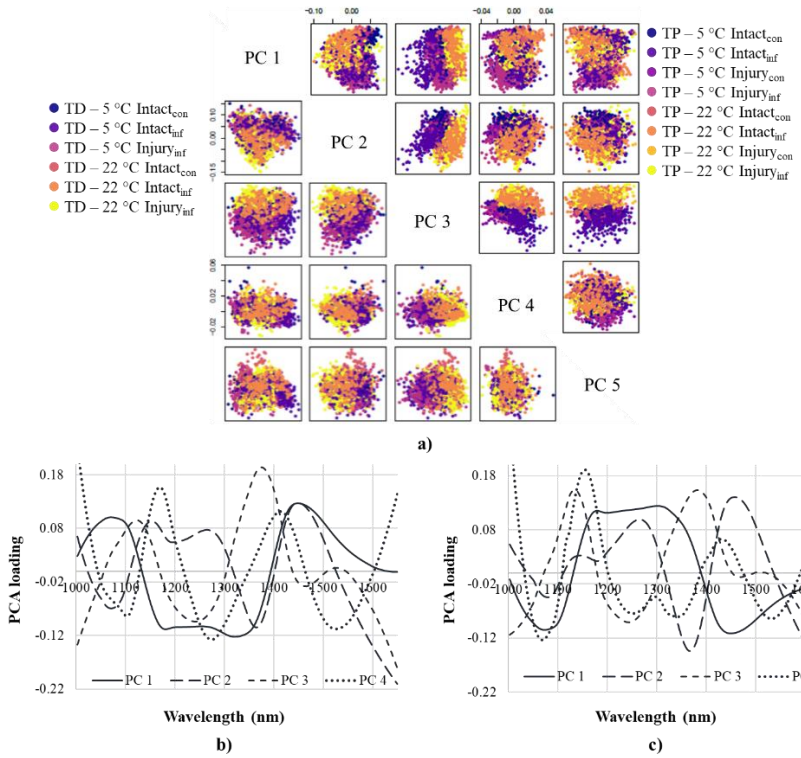

Figure 74. PCA on the HSI spectra of plums when colouring was based on fruit treatment (sgol-2-21-0, msc): PCA score plots of plums treated in different ways (a); PCA loading plot of TD plums (b); PCA loading plot of TP plums (c).

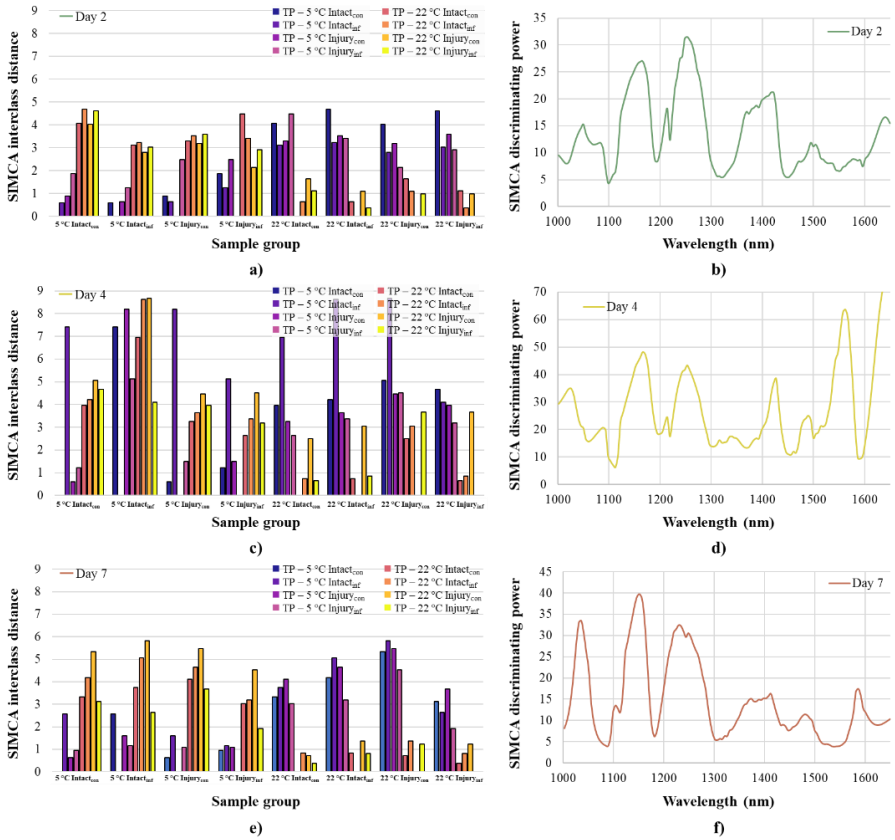

Figure 75. SIMCA on the HSI spectra of TP plums when discrimination was based on fruit treatment on certain storage days (sgol-2-21-0, msc): SIMCA interclass distances on the 2nd day of storage (a); SIMCA discrimination power plot on the 2nd day of storage (b); SIMCA interclass distances on the 4th day of storage (c); SIMCA discrimination power plot on the 4th day of storage (d); SIMCA interclass distances on the 7th day of storage (e); SIMCA discrimination power plot on the 7th day of storage (f).

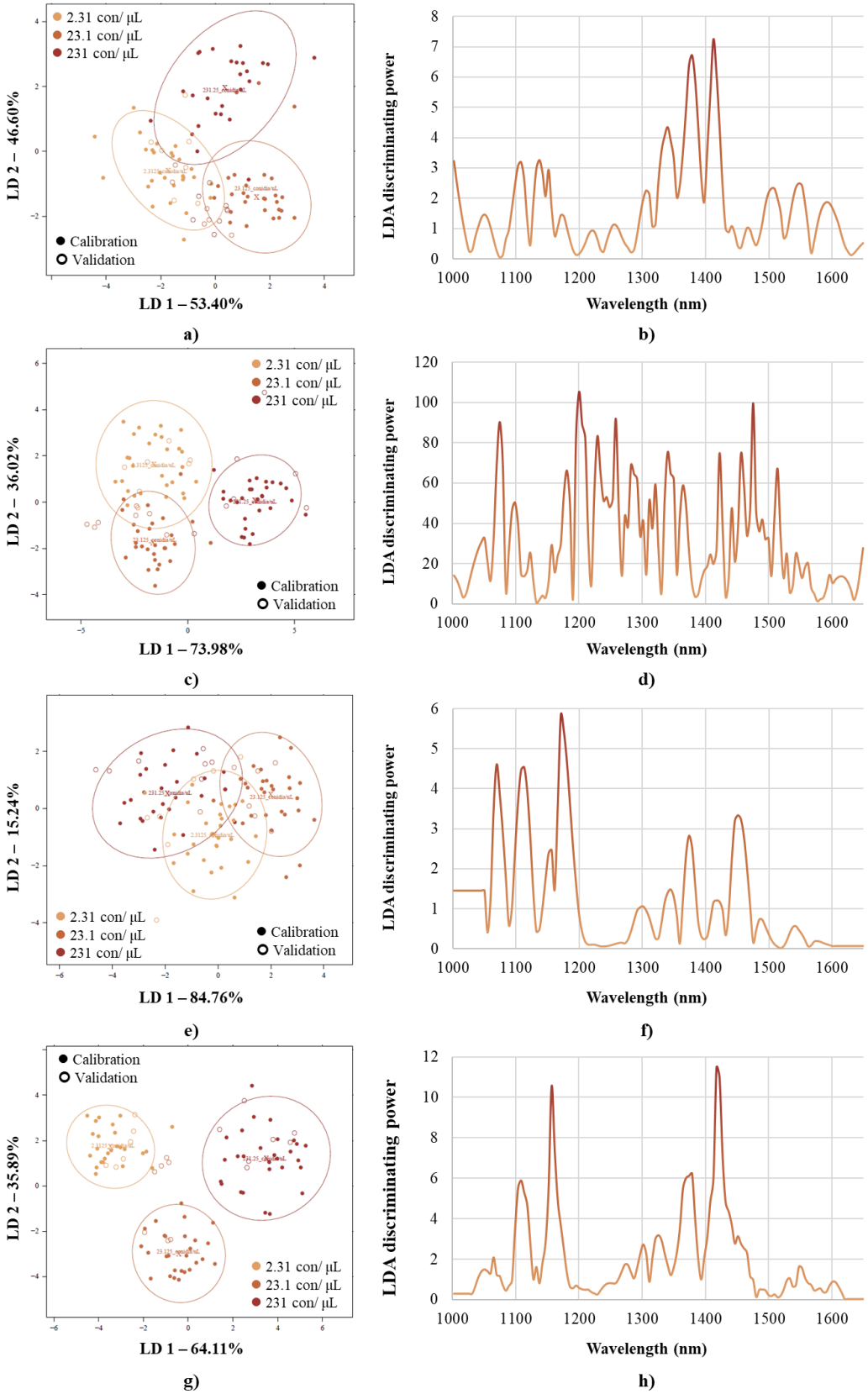

Figure 76. PCA-LDA on the HSI spectra of TP plums when classification was based on initial conidial contamination: PCA-LDA score plot of "5 °C Injury" samples (a); LDA discriminating power plot of "5 °C Injury" samples (b); PCA-LDA score plot of "5 °C Intact" samples (c); LDA discriminating power plot of "5 °C Intact" samples (d); PCA-LDA score plot of "22 °C Injury" samples (e); LDA discriminating power plot of "22 °C Injury" samples (f); PCA-LDA score plot of "22 °C Intact" samples (g); LDA discriminating power plot of "22 °C Intact" samples (h).

Table 35. PCA-LDA classification accuracies on the NIR spectra of EB sour cherries when classification was based on initial conidial contamination.

EB		Initial conidium conc.	0.15 con./µL	1.5 con./µL	15 con./µL	150 con./µL	Classification accuracies
5 °C Injury *	**Calibration**	**0.15 con./µL**	65.8	9.4	7.7	13.4	**63.1%**
		1.5 con./µL	3.3	65.6	28.2	13.4	
		15 con./µL	13.2	17.8	54.5	6.7	
		150 con./µL	17.8	7.2	9.6	66.5	
	Validation	**0.15 con./µL**	36.8	11.1	10.3	19.5	**34.1%**
		1.5 con./µL	13.2	37.8	48.7	24.4	
		15 con./µL	15.8	26.7	20.5	14.6	
		150 con./µL	34.2	24.4	20.5	41.5	
5 °C Intact **	**Calibration**	**0.15 con./µL**	84.3	12.2	6.3	0.6	**77.6%**
		1.5 con./µL	5.8	65.9	11.9	4.6	
		15 con./µL	6.4	9.2	77.5	11.9	
		150 con./µL	3.5	12.8	4.4	83.0	
	Validation	**0.15 con./µL**	37.2	39.0	12.5	9.1	**30.5%**
		1.5 con./µL	18.6	7.3	25.0	20.5	
		15 con./µL	27.9	14.6	27.5	20.5	
		150 con./µL	16.3	39.0	35.0	50.0	
25 °C Injury ***	**Calibration**	**0.15 con./µL**	77.8	11.9	15.6	6.8	**72.6%**
		1.5 con./µL	8.9	67.9	11.1	5.3	
		15 con./µL	10.0	11.9	66.7	9.9	
		150 con./µL	3.3	8.3	6.7	78.0	
	Validation	**0.15 con./µL**	31.1	31.0	40.0	12.1	**23.5%**
		1.5 con./µL	26.7	21.4	22.2	27.3	
		15 con./µL	24.4	28.6	11.1	30.3	
		150 con./µL	17.8	19.1	26.7	30.3	
25 °C Intact ****	**Calibration**	**0.15 con./µL**	76.7	8.9	17.1	3.6	**75.4%**
		1.5 con./µL	6.1	72.8	6.7	8.9	
		15 con./µL	15.0	11.7	67.7	3.0	
		150 con./µL	2.2	6.7	8.5	84.5	
	Validation	**0.15 con./µL**	37.8	35.6	31.7	23.8	**31.0%**
		1.5 con./µL	24.4	31.1	36.6	19.1	
		15 con./µL	15.6	17.8	12.2	14.3	
		150 con./µL	22.2	15.6	19.5	42.9	

* sgol-2-13-0, sgol-2-13-2; Nr = 163; NrPCs = 12

** sgol-2-17-0, sgol-2-21-1; Nr = 168; NrPCs = 20

*** sgol-2-21-0, msc; Nr = 165; NrPCs = 19

**** sgol-2-13-0, sgol-2-21-1; Nr = 173; NrPCs = 19

Table 36. PCA-LDA classification accuracies on the NIR spectra of UF sour cherries when classification was based on initial conidial contamination.

UF		Initial conidium conc.	0.17 con./µL	1.7 con./µL	17 con./µL	170 con./µL	Classification accuracies
5 °C Injury *	**Calibration**	**0.17 con./µL**	93.0	0.0	0.6	0.0	**85.1%**
		1.7 con./µL	2.0	72.2	3.0	13.7	
		17 con./µL	4.0	10.0	91.1	2.4	
		170 con./µL	1.0	17.8	5.4	83.9	
	Validation	**0.17 con./µL**	56.0	6.7	4.8	4.8	**40.9%**
		1.7 con./µL	20.0	24.4	19.1	40.5	
		17 con./µL	20.0	31.1	50.0	21.4	
		170 con./µL	4.0	37.8	26.2	33.3	
5 °C Intact **	**Calibration**	**0.17 con./µL**	72.0	5.1	7.1	17.3	**70.6%**
		1.7 con./µL	13.1	71.2	8.9	5.8	
		17 con./µL	4.2	11.5	72.0	9.6	
		170 con./µL	10.7	12.2	11.9	67.3	
	Validation	**0.17 con./µL**	45.2	10.3	16.7	30.8	**42.0%**
		1.7 con./µL	26.2	51.3	21.4	7.7	
		17 con./µL	7.1	28.2	38.1	28.2	
		170 con./µL	21.4	10.3	23.8	33.3	
25 °C Injury ***	**Calibration**	**0.17 con./µL**	61.9	10.0	10.7	19.4	**58.2%**
		1.7 con./µL	8.3	63.3	16.1	15.0	
		17 con./µL	11.9	15.0	60.7	18.9	
		170 con./µL	17.9	11.7	12.5	46.7	
	Validation	**0.17 con./µL**	35.7	28.9	14.3	35.6	**24.6%**
		1.7 con./µL	11.9	17.8	21.4	26.7	
		17 con./µL	23.8	35.6	40.5	33.3	
		170 con./µL	28.6	17.8	23.8	4.4	
25 °C Intact ****	**Calibration**	**0.17 con./µL**	68.5	17.2	10.3	9.7	**69.7%**
		1.7 con./µL	19.1	66.1	7.1	8.3	
		17 con./µL	4.2	12.2	76.3	13.9	
		170 con./µL	8.3	4.4	6.4	68.1	
	Validation	**0.17 con./µL**	42.9	44.4	18.0	33.3	**31.5%**
		1.7 con./µL	14.3	8.9	23.1	13.9	
		17 con./µL	21.4	44.4	41.0	19.4	
		170 con./µL	21.4	2.2	18.0	33.3	

* sgol-2-21-0; Nr = 154; NrPCs = 20

** sgol-2-17-0, sgol-2-21-1; Nr = 162; NrPCs = 11

*** sgol-2-13-0, sgol-2-17-2; Nr = 174; NrPCs = 13

**** sgol-2-21-0, sgol-2-21-1; Nr = 162; NrPCs = 14

Table 37. PCA-LDA classification accuracies on the NIR spectra of sour cherries showing monilial activity when classification was based on the day of appearance of visible infection signs ± 2 days.

			-2 days	-1 day	0 day	+1 day	+2 days	Classification accuracies
EB *	**Calibration**	**-2 days**	85.2	12.4	6.1	2.2	0.0	**77.2%**
		-1 days	11.1	64.8	20.7	0.0	0.0	
		0 days	3.7	22.2	65.7	2.2	0.0	
		+1 days	0.0	0.6	3.0	75.6	5.1	
		+2 days	0.0	0.0	4.6	20.0	94.9	
	Validation	**-2 days**	52.4	37.0	18.2	13.3	0.0	**48.2%**
		-1 days	30.2	25.9	16.7	0.0	0.0	
		0 days	14.3	31.5	51.5	26.7	3.9	
		+1 days	1.6	1.9	4.6	26.7	11.5	
		+2 days	1.6	3.7	9.1	33.3	84.6	
UF **	**Calibration**	**-2 days**	35.3	9.34	7.6	2.8	0.4	**49.1%**
		-1 days	39.2	57.07	26.6	8.7	13.9	
		0 days	15.7	24.75	45.1	23.6	25.4	
		+1 days	7.4	5.05	9.5	50.7	3.2	
		+2 days	2.5	3.79	11.1	14.2	57.1	
	Validation	**-2 days**	17.7	30.3	14.1	6.9	1.6	**31.7%**
		-1 days	54.9	34.34	15.2	11.1	25.4	
		0 days	15.7	13.13	33.7	37.5	19.1	
		+1 days	7.8	13.13	13.0	25.0	6.4	
		+2 days	3.9	9.09	23.9	19.4	47.6	

* sgol-2-13-0, sgol-2-21-1; Nr = 224; NrPCs = 19

** sgol-2-21-0; Nr = 377; NrPCs = 13

Table 38. PCA-LDA classification accuracies on the NIR spectra of TD plums when classification was based on initial conidial contamination.

TD		Initial conidium conc.	1.05 con./µL	10.5 con./µL	105 con./µL	Classification accuracies
5 °C Injury *	**Calibration**	**1.05 con./µL**	80.4	9.3	21.4	**76.5%**
		10.5 con./µL	3.6	80.0	9.5	
		105 con./µL	16.1	10.7	69.1	
	Validation	**1.05 con./µL**	47.6	45.7	38.1	**34.0%**
		10.5 con./µL	21.4	25.7	33.3	
		105 con./µL	31.0	28.6	28.6	
5 °C Intact **	**Calibration**	**1.05 con./µL**	75.6	5.4	10.5	**74.2%**
		10.5 con./µL	12.8	72.0	14.5	
		105 con./µL	11.5	22.6	75.0	
	Validation	**1.05 con./µL**	53.9	26.2	34.2	**50.4%**
		10.5 con./µL	25.6	50.0	18.4	
		105 con./µL	20.5	23.8	47.4	
22 °C Injury ***	**Calibration**	**1.05 con./µL**	80.4	1.7	13.6	**84.2%**
		10.5 con./µL	7.1	90.6	4.6	
		105 con./µL	12.5	7.8	81.8	
	Validation	**1.05 con./µL**	50.0	26.7	29.6	**47.3%**
		10.5 con./µL	21.4	53.3	31.8	
		105 con./µL	28.6	20.0	38.6	
22 °C Intact ****	**Calibration**	**1.05 con./µL**	68.2	5.8	16.7	**77.8%**
		10.5 con./µL	11.4	89.1	7.1	
		105 con./µL	20.5	5.1	76.2	
	Validation	**1.05 con./µL**	18.2	5.1	33.3	**39.2%**
		10.5 con./µL	24.2	59.0	26.2	
		105 con./µL	57.6	35.9	40.5	

***** sgol-2-17-0, sgol-2-21-1; Nr = 119; NrPCs = 15

****** sgol-2-21-0, msc; Nr = 119; NrPCs = 8

******* sgol-2-21-0; Nr = 131; NrPCs = 18

******** sgol-2-17-0, sgol-2-21-2; Nr = 114; NrPCs = 10

Table 39. PCA-LDA classification accuracies on the NIR spectra of TP plums when classification was based on initial conidial contamination.

TP		Initial conidium conc.	2.31 con./µL	23.1 con./µL	231 con./µL	Classification accuracies
5 °C Injury *	**Calibration**	**2.31 con./µL**	82.0	1.9	0.0	**92.9%**
		23.1 con./µL	15.0	98.1	1.4	
		231 con./µL	3.0	0.0	98.6	
	Validation	**2.31 con./µL**	20.0	51.3	8.3	**47.2%**
		23.1 con./µL	64.0	41.0	11.1	
		231 con./µL	16.0	7.7	80.6	
5 °C Intact **	**Calibration**	**2.31 con./µL**	82.8	15.2	9.4	**78.9%**
		23.1 con./µL	15.6	76.2	12.8	
		231 con./µL	1.7	8.5	77.8	
	Validation	**2.31 con./µL**	48.9	56.1	26.7	**35.1%**
		23.1 con./µL	44.4	9.8	26.7	
		231 con./µL	6.7	34.2	46.7	
22 °C Injury ***	**Calibration**	**2.31 con./µL**	88.6	3.5	8.3	**89.4%**
		23.1 con./µL	3.0	91.0	3.2	
		231 con./µL	8.3	5.6	88.5	
	Validation	**2.31 con./µL**	36.4	11.1	35.9	**47.2%**
		23.1 con./µL	27.3	69.4	28.2	
		231 con./µL	36.4	19.4	35.9	
22 °C Intact ****	**Calibration**	**2.31 con./µL**	83.9	6.6	5.4	**87.9%**
		23.1 con./µL	7.8	89.9	4.8	
		231 con./µL	8.3	3.6	89.9	
	Validation	**2.31 con./µL**	33.3	45.2	23.8	**51.6%**
		23.1 con./µL	33.3	54.8	9.5	
		231 con./µL	33.3	0.0	66.7	

* sgol-2-21-0; Nr = 100; NrPCs = 18

** sgol-2-21-0, sgol-2-17-2; Nr = 131; NrPCs = 12

*** sgol-2-21-0, sgol-2-17-2; Nr = 108; NrPCs = 19

**** sgol-2-13-0, sgol-2-13-1; Nr = 129; NrPCs = 19

Table 40. PCA-LDA classification accuracies on the NIR spectra of plums showing monilial activity when classification was based on the day of appearance of visible infection signs ± 2 days.

			-2 days	-1 day	0 day	+1 day	+2 days	Classification accuracies
TD *	**Calibration**	**-2 days**	69.5	18.6	11.0	13.0	5.7	**61.0%**
		-1 days	16.4	55.5	18.8	12.0	6.1	
		0 days	8.9	17.3	60.4	12.7	10.2	
		+1 days	3.1	8.7	6.9	48.6	6.8	
		+2 days	2.2	0.0	3.0	13.8	71.2	
	Validation	**-2 days**	56.7	21.8	10.7	14.5	3.0	**49.6%**
		-1 days	22.1	49.5	22.6	20.3	7.6	
		0 days	9.6	18.8	39.3	7.3	15.2	
		+1 days	7.7	9.9	13.1	44.9	16.7	
		+2 days	3.9	0.0	14.3	13.0	57.6	
TP **	**Calibration**	**-2 days**	61.6	15.32	22.0	18.8	31.8	**38.9%**
		-1 days	18.5	49.73	28.0	27.9	37.9	
		0 days	13.4	27.42	41.6	15.4	9.1	
		+1 days	6.0	6.45	5.4	34.6	14.4	
		+2 days	0.6	1.08	3.0	3.3	6.8	
	Validation	**-2 days**	50.0	32.26	31.3	25.0	42.4	**25.3%**
		-1 days	21.4	29.03	36.1	25.0	21.2	
		0 days	20.2	31.18	24.1	23.3	27.3	
		+1 days	4.8	2.15	7.2	23.3	9.1	
		+2 days	3.6	5.38	1.2	3.3	0.0	

* sgol-2-13-0, sgol-2-13-1; Nr = 424; NrPCs = 20

** sgol-2-21-0, sgol-2-17-2; Nr = 353; NrPCs = 11

Table 41. PCA-LDA classification accuracies on the HSI spectra of EB sour cherries when classification was based on initial conidial contamination.

EB		Initial conidium conc.	0.15 con./µL	1.5 con./µL	15 con./µL	150 con./µL	Classification accuracies
5 °C Injury *	**Calibration**	**0.15 con./µL**	85.3	8.6	5.3	2.1	**85.5%**
		1.5 con./µL	9.6	85.0	7.6	0.0	
		15 con./µL	1.5	4.3	78.0	4.3	
		150 con./µL	3.7	2.1	9.1	93.6	
	Validation	**0.15 con./µL**	70.6	22.9	18.2	14.3	**45.0%**
		1.5 con./µL	11.8	45.7	48.5	11.4	
		15 con./µL	5.9	28.6	12.1	22.9	
		150 con./µL	11.8	2.9	21.2	51.4	
5 °C Intact **	**Calibration**	**0.15 con./µL**	85.0	12.1	2.9	0.0	**85.6%**
		1.5 con./µL	12.1	83.6	1.5	0.0	
		15 con./µL	2.9	3.6	82.4	8.3	
		150 con./µL	0.0	0.7	13.2	91.7	
	Validation	**0.15 con./µL**	37.1	54.3	5.9	3.0	**33.1%**
		1.5 con./µL	42.9	14.3	29.4	0.0	
		15 con./µL	17.1	28.6	29.4	45.5	
		150 con./µL	2.9	2.9	35.3	51.5	
25 °C Injury ***	**Calibration**	**0.15 con./µL**	73.5	7.9	7.1	16.4	**61.6%**
		1.5 con./µL	8.1	57.9	16.4	14.3	
		15 con./µL	0.7	17.1	55.7	10.0	
		150 con./µL	17.7	17.1	20.7	59.3	
	Validation	**0.15 con./µL**	47.1	11.4	14.3	20.0	**39.6%**
		1.5 con./µL	38.2	42.9	31.4	22.9	
		15 con./µL	5.9	22.9	40.0	28.6	
		150 con./µL	8.8	22.9	14.3	28.6	
25 °C Intact ****	**Calibration**	**0.15 con./µL**	80.5	7.1	6.8	5.9	**83.0%**
		1.5 con./µL	4.7	85.0	7.6	5.2	
		15 con./µL	6.3	2.1	81.1	3.7	
		150 con./µL	8.6	5.7	4.6	85.3	
	Validation	**0.15 con./µL**	31.3	22.9	21.2	20.6	**36.6%**
		1.5 con./µL	28.1	28.6	27.3	17.7	
		15 con./µL	25.0	22.9	39.4	14.7	
		150 con./µL	15.6	25.7	12.1	47.1	

* sgol-2-13-0, sgol-2-21-2; Nr = 137; NrPCs = 18

** sgol-2-21-0, msc; Nr = 137; NrPCs = 20

*** sgol-2-21-0, sgol-2-17-2; Nr = 139; NrPCs = 6

**** sgol-2-13-0, sgol-2-13-2; Nr = 134; NrPCs = 20

Table 42. PCA-LDA classification accuracies on the HSI spectra of UF sour cherries when classification was based on initial conidial contamination.

UF		Initial conidium conc.	0.17 con./µL	1.7 con./µL	17 con./µL	170 con./µL	Classification accuracies
5 °C Injury *	**Calibration**	**0.17 con./µL**	100.0	0.0	0.0	0.0	**92.6%**
		1.7 con./µL	0.0	92.9	8.9	4.7	
		17 con./µL	0.0	3.6	82.1	0.0	
		170 con./µL	0.0	3.6	8.9	95.3	
	Validation	**0.17 con./µL**	80.0	7.1	7.1	0.0	**45.2%**
		1.7 con./µL	0.0	28.6	14.3	25.0	
		17 con./µL	0.0	50.0	28.6	31.3	
		170 con./µL	20.0	14.3	50.0	43.8	
5 °C Intact **	**Calibration**	**0.17 con./µL**	100.0	0.0	0.0	0.0	**98.0%**
		1.7 con./µL	0.0	100.0	0.0	0.0	
		17 con./µL	0.0	0.0	96.4	4.4	
		170 con./µL	0.0	0.0	3.6	95.6	
	Validation	**0.17 con./µL**	41.7	10.5	7.1	0.0	**53.3%**
		1.7 con./µL	50.0	84.2	21.4	11.8	
		17 con./µL	8.3	5.3	28.6	29.4	
		170 con./µL	0.0	0.0	42.9	58.8	
25 °C Injury ***	**Calibration**	**0.17 con./µL**	90.6	3.6	6.5	4.6	**83.4%**
		1.7 con./µL	3.1	73.8	4.8	3.4	
		17 con./µL	0.8	14.3	83.9	6.8	
		170 con./µL	5.5	8.3	4.8	85.2	
	Validation	**0.17 con./µL**	59.4	33.3	25.8	22.7	**32.5%**
		1.7 con./µL	12.5	0.0	25.8	18.2	
		17 con./µL	9.4	47.6	38.7	27.3	
		170 con./µL	18.8	19.1	9.7	31.8	
25 °C Intact ****	**Calibration**	**0.17 con./µL**	87.5	4.5	3.4	4.4	**89.1%**
		1.7 con./µL	7.1	91.1	6.8	5.4	
		17 con./µL	2.7	0.9	88.6	1.1	
		170 con./µL	2.7	3.6	1.1	89.1	
	Validation	**0.17 con./µL**	50.0	21.4	13.6	39.1	**46.3%**
		1.7 con./µL	21.4	50.0	27.3	21.7	
		17 con./µL	7.1	7.1	59.1	13.0	
		170 con./µL	21.4	21.4	0.0	26.1	

* sgol-2-21-0, sgol-2-13-1; Nr = 54; NrPCs = 18

** sgol-2-21-0, sgol-2-21-1; Nr = 62; NrPCs = 20

*** sgol-2-17-0, sgol-2-21-2; Nr = 106; NrPCs = 18

**** sgol-2-13-0, sgol-2-13-2; Nr = 101; NrPCs = 20

Table 43. PCA-LDA classification accuracies on the HSI spectra of sour cherries showing monilial activity when classification was based on the day of appearance of visible infection signs ± 2 days.

			-2 days	-1 day	0 day	+1 day	+2 days	Classification accuracies
EB *	**Calibration**	**-2 days**	73.8	16.4	9.9	0.0	0.0	**72.6%**
		-1 days	7.1	77.9	7.8	0.0	0.0	
		0 days	12.5	5.7	58.3	21.0	14.4	
		+1 days	6.6	0.0	13.5	73.0	5.8	
		+2 days	0.0	0.0	10.4	6.0	79.8	
	Validation	**-2 days**	59.5	51.4	25.0	12.0	19.2	**25.9%**
		-1 days	14.3	17.1	16.7	4.0	0.0	
		0 days	11.9	22.9	29.2	40.0	26.9	
		+1 days	9.5	2.9	14.6	12.0	42.3	
		+2 days	4.8	5.7	14.6	32.0	11.5	
UF **	**Calibration**	**-2 days**	91.7	0	4.0	8.3	0.0	**86.5%**
		-1 days	5.9	89.58	1.6	0.5	0.0	
		0 days	1.5	10.42	90.5	5.2	21.7	
		+1 days	1.0	0	2.4	84.9	2.2	
		+2 days	0.0	0	1.6	1.0	76.1	
	Validation	**-2 days**	78.4	41.67	15.9	14.6	0.0	**57.4%**
		-1 days	7.8	25	15.9	0.0	0.0	
		0 days	11.8	33.33	54.0	2.1	26.1	
		+1 days	2.0	0	6.4	72.9	17.4	
		+2 days	0.0	0	7.9	10.4	56.5	

* sgol-2-17-0, sgol-2-17-2; Nr = 176; NrPCs = 17

** sgol-2-13-0, sgol-2-13-2; Nr = 197; NrPCs = 20

Table 44. PCA-LDA classification accuracies on the HSI spectra of TD plums when classification was based on initial conidial contamination.

TD		Initial conidium conc.	1.05 con./µL	10.5 con./µL	105 con./µL	Classification accuracies
5 °C Injury *	**Calibration**	**1.05 con./µL**	86.4	14.3	6.4	**83.8%**
		10.5 con./µL	8.6	77.1	5.7	
		105 con./µL	5.0	8.6	87.9	
	Validation	**1.05 con./µL**	54.3	37.1	17.1	**55.2%**
		10.5 con./µL	37.1	54.3	25.7	
		105 con./µL	8.6	8.6	57.1	
5 °C Intact **	**Calibration**	**1.05 con./µL**	94.1	1.4	0.0	**92.9%**
		10.5 con./µL	2.9	94.3	9.9	
		105 con./µL	2.9	4.3	90.2	
	Validation	**1.05 con./µL**	67.7	25.7	21.2	**54.1%**
		10.5 con./µL	17.7	40.0	24.2	
		105 con./µL	14.7	34.3	54.6	
22 °C Injury ***	**Calibration**	**1.05 con./µL**	95.7	4.3	0.0	**97.1%**
		10.5 con./µL	4.3	95.7	0.0	
		105 con./µL	0.0	0.0	100.0	
	Validation	**1.05 con./µL**	65.7	28.6	2.9	**75.2%**
		10.5 con./µL	25.7	68.6	5.9	
		105 con./µL	8.6	2.9	91.2	
22 °C Intact ****	**Calibration**	**1.05 con./µL**	78.7	11.4	11.4	**81.6%**
		10.5 con./µL	11.8	82.6	5.0	
		105 con./µL	9.6	6.1	83.6	
	Validation	**1.05 con./µL**	52.9	36.4	28.6	**42.8%**
		10.5 con./µL	14.7	21.2	17.1	
		105 con./µL	32.4	42.4	54.3	

* sgol-2-17-0, sgol-2-17-2; Nr = 105; NrPCs = 15
** sgol-2-13-0, sgol-2-17-2; Nr = 102; NrPCs = 20
*** sgol-2-17-0, sgol-2-21-1; Nr = 104; NrPCs = 19
**** sgol-2-13-0, sgol-2-13-2; Nr = 102; NrPCs = 12

Table 45. PCA-LDA classification accuracies on the HSI spectra of TP plums when classification was based on initial conidial contamination.

TP		Initial conidium conc.	2.31 con./µL	23.1 con./µL	231 con./µL	Classification accuracies
5 °C Injury *	**Calibration**	**2.31 con./µL**	92.9	0.7	7.6	**92.0%**
		23.1 con./µL	2.9	92.9	2.3	
		231 con./µL	4.3	6.4	90.2	
	Validation	**2.31 con./µL**	74.3	17.1	36.4	**50.0%**
		23.1 con./µL	14.3	48.6	36.4	
		231 con./µL	11.4	34.3	27.3	
5 °C Intact **	**Calibration**	**2.31 con./µL**	96.4	5.7	0.0	**96.9%**
		23.1 con./µL	2.1	94.3	0.0	
		231 con./µL	1.4	0.0	100.0	
	Validation	**2.31 con./µL**	65.7	25.7	17.1	**69.5%**
		23.1 con./µL	31.4	71.4	11.4	
		231 con./µL	2.9	2.9	71.4	
22 °C Injury ***	**Calibration**	**2.31 con./µL**	83.6	6.4	10.0	**87.1%**
		23.1 con./µL	6.4	90.0	2.1	
		231 con./µL	10.0	3.6	87.9	
	Validation	**2.31 con./µL**	48.6	8.6	31.4	**61.9%**
		23.1 con./µL	8.6	82.9	14.3	
		231 con./µL	42.9	8.6	54.3	
22 °C Intact ****	**Calibration**	**2.31 con./µL**	100.0	0.0	0.0	**100%**
		23.1 con./µL	0.0	100.0	0.0	
		231 con./µL	0.0	0.0	100.0	
	Validation	**2.31 con./µL**	87.1	14.7	2.9	**79.3%**
		23.1 con./µL	12.9	79.4	25.7	
		231 con./µL	0.0	5.9	71.4	

* sgol-2-21-0, sgol-2-13-1; Nr = 103; NrPCs = 18

** sgol-2-21-0, deTr; Nr = 105; NrPCs = 20

*** sgol-2-21-0, sgol-2-21-2; Nr = 105; NrPCs = 12

**** sgol-2-13-0, sgol-2-13-2; Nr = 100; NrPCs = 19

Table 46. PCA-LDA classification accuracies on the HSI spectra of plums showing monilial activity when classification was based on brown rot signs by day of appearance.

			-2 days	-1 day	0 day	+1 day	+2 days	Classification accuracies
TD *	**Calibration**	**-2 days**	68.9	11.1	10.0	0.4	0.4	**65.3%**
		-1 days	16.1	53.9	17.1	5.3	0.4	
		0 days	15.0	29.3	59.6	18.0	3.6	
		+1 days	0.0	5.7	11.1	60.2	12.1	
		+2 days	0.0	0.0	2.1	16.2	83.6	
	Validation	**-2 days**	48.6	37.1	18.6	2.8	4.3	**46.5%**
		-1 days	30.0	25.7	14.3	9.9	2.9	
		0 days	17.1	21.4	48.6	26.8	1.4	
		+1 days	0.0	15.7	11.4	38.0	20.0	
		+2 days	4.3	0.0	7.1	22.5	71.4	
TP **	**Calibration**	**-2 days**	64.2	12.14	13.6	3.8	0.0	**57.3%**
		-1 days	17.8	60.71	19.2	11.4	3.3	
		0 days	8.4	9.29	38.0	16.6	5.9	
		+1 days	8.7	13.81	12.8	59.2	26.3	
		+2 days	0.9	4.05	16.5	9.0	64.5	
	Validation	**-2 days**	43.4	20.95	16.0	9.8	0.0	**33.5%**
		-1 days	28.9	34.29	24.5	21.7	5.3	
		0 days	9.6	16.19	9.6	19.6	7.9	
		+1 days	14.5	15.24	26.6	31.5	38.2	
		+2 days	3.6	13.33	23.4	17.4	48.7	

* sgol-2-17-0, sgol-2-21-1; Nr = 351; NrPCs = 18

** sgol-2-13-0, sgol-2-13-2; Nr = 450; NrPCs = 15

10.2.4. Annexes to the fruit juice fortification results

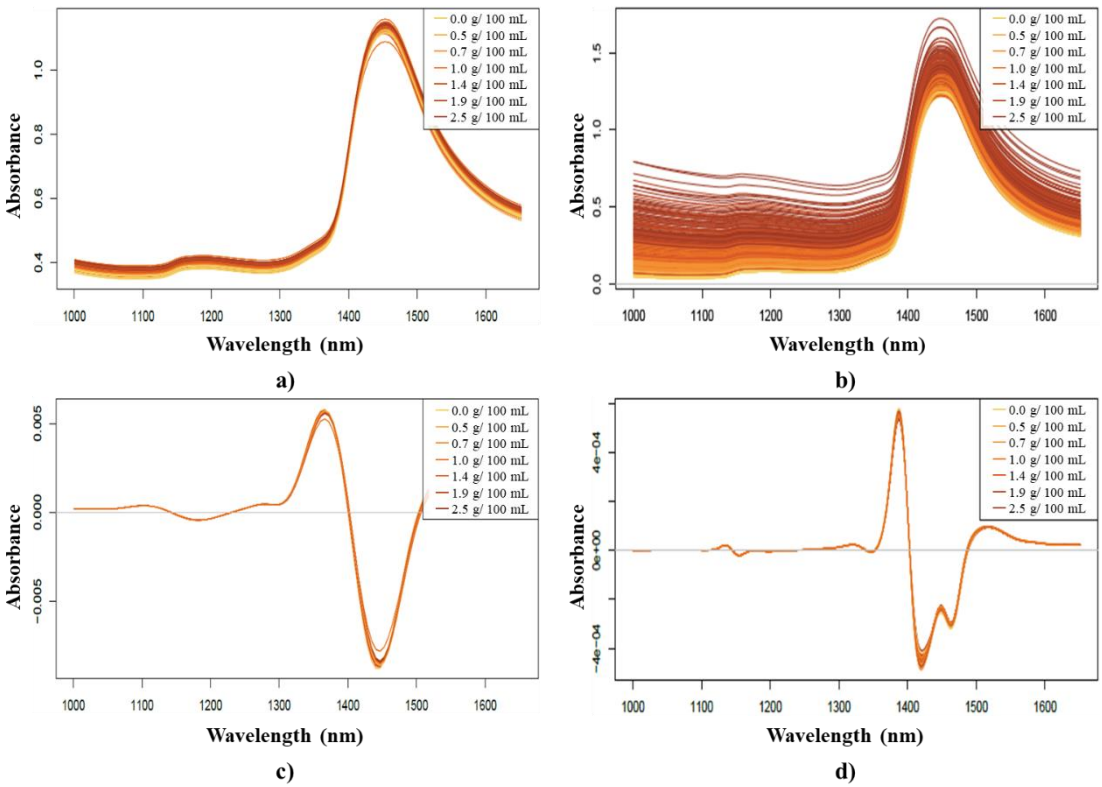

Figure 77. NIR spectra of sour cherry juices when colouring was based on total extract content: raw spectra recorded with the hand-held NIR device (a); raw spectra recorded with the benchtop NIR device (b); 2nd derivative spectra recorded with the hand-held NIR device (c); 2nd derivative spectra recorded with the benchtop NIR device (d).

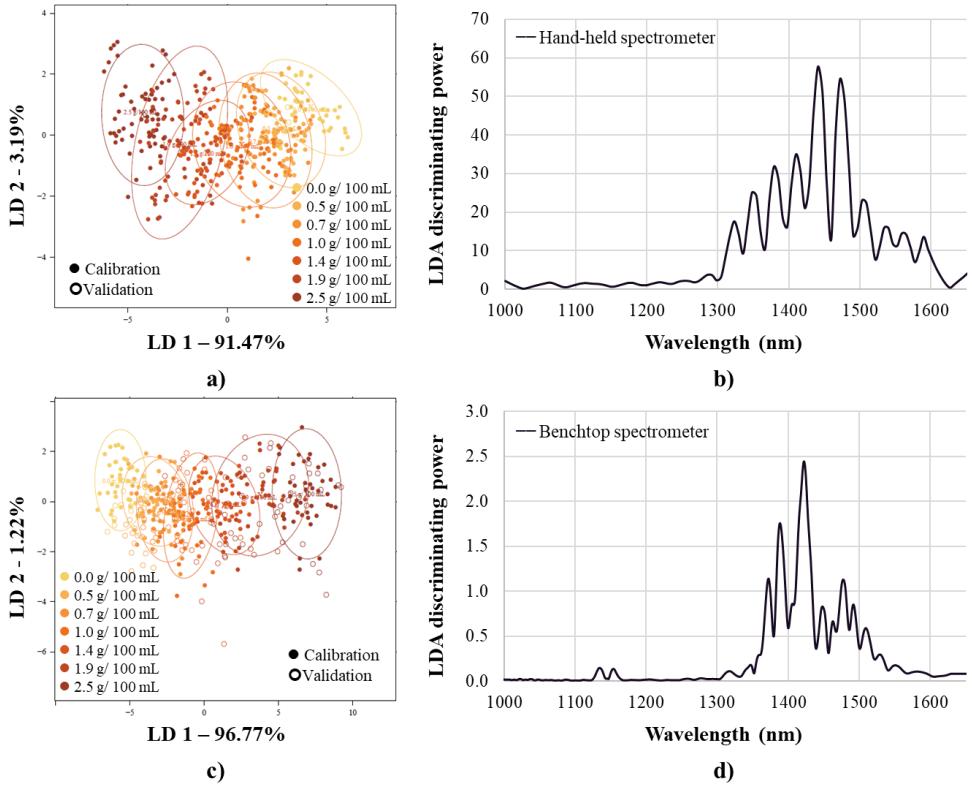

Figure 78. PCA-LDA on the NIR spectra of sour cherry juices when classification was based on the dosed plant extract content: PCA-LDA score plot on the data recorded with the hand-held NIR device (a); LDA discriminating power plot on the data recorded with the hand-held NIR device (b); PCA-LDA score plot on the data recorded with the benchtop NIR device (c); LDA discriminating power plot on the data recorded with the benchtop NIR device (d).

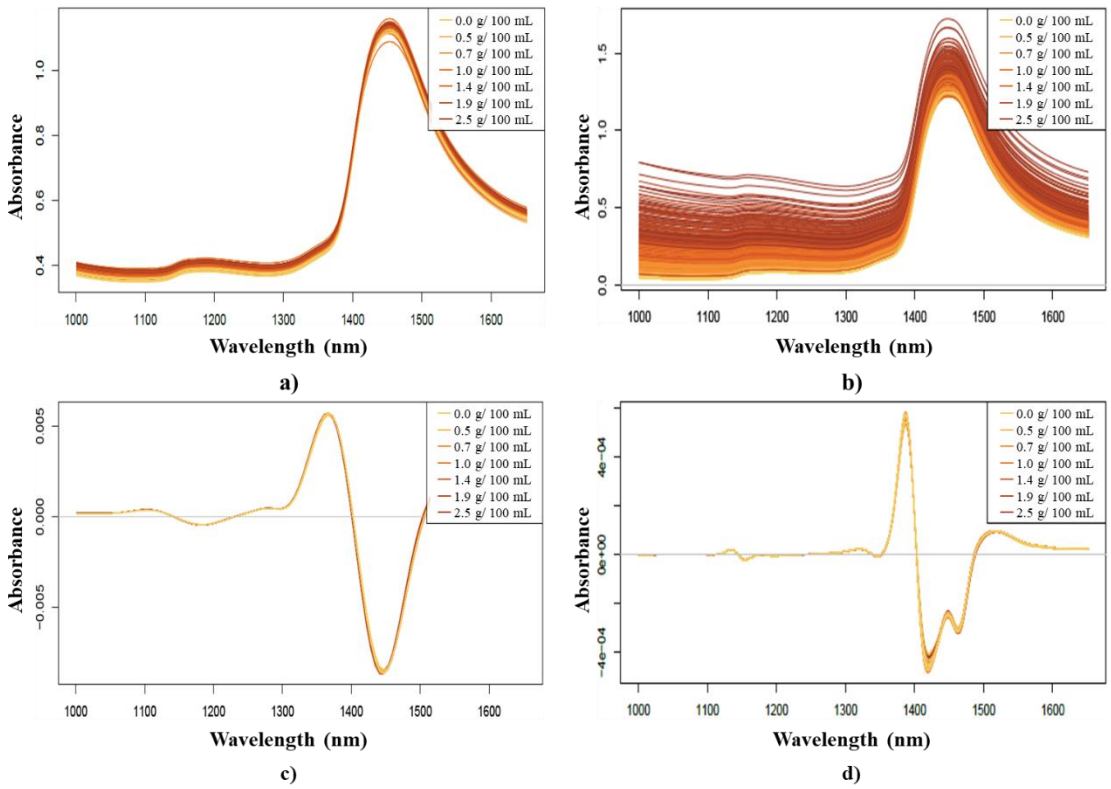

Figure 79. NIR spectra of plum juices when colouring was based on total extract content: raw spectra recorded with the hand-held NIR device (a); raw spectra recorded with the benchtop NIR device (b); 2nd derivative spectra recorded with the hand-held NIR device (c); 2nd derivative spectra recorded with the benchtop NIR device (d).

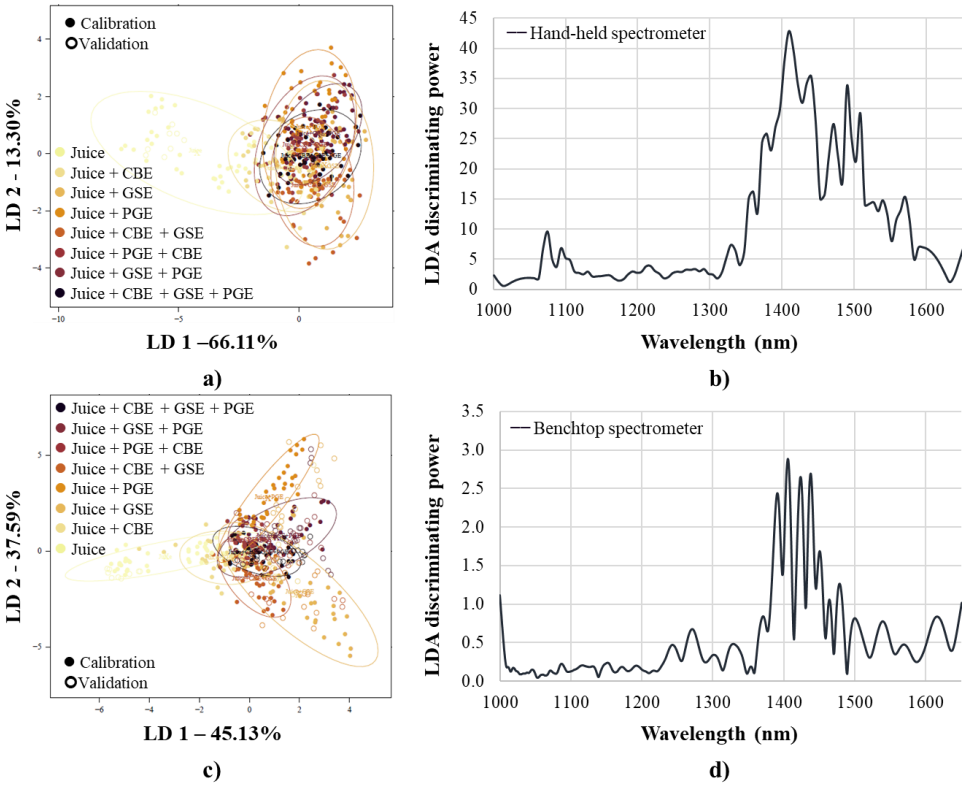

Figure 80. PCA-LDA on the NIR spectra of plum juices when classification was based on the type of dosed plant extract: PCA-LDA score plot on the data recorded with the hand-held NIR device (a); LDA discriminating power plot on the data recorded with the hand-held NIR device (b); PCA-LDA score plot on the data recorded with the benchtop NIR device (c); LDA discriminating power plot on the data recorded with the benchtop NIR device (d).

Table 47. PCA-LDA classification accuracies on the spectra of sour cherry juices recorded different NIR instruments when classification was based on total extract content.

		Total extract content	0.0 g/100 mL	0.5 g/100 mL	0.7 g/100 mL	1.0 g/100 mL	1.4 g/100 mL	1.9 g/100 mL	2.5 g/100 mL	Classification accuracy
MicroNIR hand-held device *	**Calibration**	**0.0 g/100 mL**	83.89	6.35	4.76	0.00	0.00	0.00	0.00	**71.73%**
		0.5 g/100 mL	9.44	68.25	21.83	7.14	0.00	0.00	0.00	
		0.7 g/100 mL	6.67	18.25	61.11	23.02	1.59	0.00	0.00	
		1.0 g/100 mL	0.00	4.37	12.30	55.16	10.32	1.19	0.00	
		1.4 g/100 mL	0.00	2.78	0.00	12.70	73.02	18.25	0.00	
		1.9 g/100 mL	0.00	0.00	0.00	1.98	15.08	69.84	9.13	
		2.5 g/100 mL	0.00	0.00	0.00	0.00	0.00	10.71	90.87	
	Validation	**0.0 g/100 mL**	60.00	28.57	12.70	0.00	0.00	0.00	0.00	**49.62%**
		0.5 g/100 mL	22.22	38.10	19.05	14.29	0.00	0.00	0.00	
		0.7 g/100 mL	13.33	11.11	36.51	22.22	6.35	1.59	0.00	
		1.0 g/100 mL	4.44	12.70	20.63	25.40	20.63	6.35	0.00	
		1.4 g/100 mL	0.00	9.52	11.11	26.98	52.38	14.29	0.00	
		1.9 g/100 mL	0.00	0.00	0.00	6.35	20.63	57.14	22.22	
		2.5 g/100 mL	0.00	0.00	0.00	4.76	0.00	20.63	77.78	
NIRflex benchtop device **	**Calibration**	**0.0 g/100 mL**	85.00	4.76	1.59	0.00	0.00	0.00	0.00	**76.02%**
		0.5 g/100 mL	14.44	72.22	23.81	2.38	0.40	0.00	0.00	
		0.7 g/100 mL	0.56	19.44	59.13	12.30	1.98	0.00	0.00	
		1.0 g/100 mL	0.00	3.57	15.48	75.79	13.10	0.00	0.00	
		1.4 g/100 mL	0.00	0.00	0.00	9.52	71.03	16.53	0.00	
		1.9 g/100 mL	0.00	0.00	0.00	0.00	13.49	75.00	6.05	
		2.5 g/100 mL	0.00	0.00	0.00	0.00	0.00	8.47	93.95	
	Validation	**0.0 g/100 mL**	86.67	7.94	1.59	0.00	0.00	0.00	0.00	**58.29%**
		0.5 g/100 mL	13.33	47.62	38.10	6.35	4.76	0.00	0.00	
		0.7 g/100 mL	0.00	28.57	33.33	20.63	0.00	0.00	0.00	
		1.0 g/100 mL	0.00	12.70	17.46	41.27	17.46	0.00	0.00	
		1.4 g/100 mL	0.00	0.00	9.52	31.75	55.56	27.42	0.00	
		1.9 g/100 mL	0.00	3.17	0.00	0.00	22.22	59.68	16.13	
		2.5 g/100 mL	0.00	0.00	0.00	0.00	0.00	12.90	83.87	

* sgol-2-21-0, sgol-2-21-1; Nr = 423; NrPCs = 14

** sgol-2-43-0, sgol-2-43-2; Nr = 421; NrPCs = 20

Table 48. PLSR prediction of plant extract concentration (g/ 100 mL) based on the spectra of sour cherry juices recorded with the hand-held NIR device.

Sour cherry	juice	Extract	Pretreatment	Nr	NrLV	R_C^2	$RMSE_C$	R_{CV}^2	$RMSE_{CV}$
All		**CBE conc.**	sgol-2-13-0, sgol-2-21-2	369	4	0.50	0.40	0.46	0.42
blends		**GSE conc.**	sgol-2-21-0, sgol-2-13-1	345	15	0.71	0.31	0.65	0.34
		PGE conc.	sgol-2-21-0	346	17	0.90	0.17	0.85	0.21
		Total extacts	sgol-2-17-0, sgol-2-21-1	343	7	0.90	0.25	0.87	0.29
Simple	+ CBE	**CBE conc.**	sgol-2-13-0, sgol-2-13-2	86	6	0.96	0.18	0.92	0.25
blends		**GSE conc.**	–	–	–	–	–	–	–
		PGE conc.	–	–	–	–	–	–	–
		Total extacts	–	–	–	–	–	–	–
	+ GSE	**CBE conc.**	–	–	–	–	–	–	–
		GSE conc.	sgol-2-21-0, deTr	91	5	0.94	0.20	0.90	0.27
		PGE conc.	–	–	–	–	–	–	–
		Total extacts	–	–	–	–	–	–	–
	+ PGE	**CBE conc.**	–	–	–	–	–	–	–
		GSE conc.	–	–	–	–	–	–	–
		PGE conc.	sgol-2-21-0, deTr	95	5	0.95	0.19	0.87	0.31
		Total extacts	–	–	–	–	–	–	–
Binary	+ CBE	**CBE conc.**	sgol-2-21-0	88	5	0.96	0.09	0.91	0.13
blends	+ GSE	**GSE conc.**	sgol-2-21-0	88	5	0.96	0.09	0.91	0.13
		PGE conc.	–	–	–	–	–	–	–
		Total extacts	sgol-2-21-0	88	5	0.96	0.17	0.91	0.26
		CBE conc.	–	–	–	–	–	–	–
	+ GSE	**GSE conc.**	sgol-2-21-0, msc	94	2	0.72	0.22	0.66	0.25
	+ PGE	**PGE conc.**	sgol-2-21-0, msc	94	2	0.72	0.22	0.66	0.25
		Total extacts	sgol-2-21-0, msc	94	2	0.72	0.45	0.66	0.49
	+ CBE	**CBE conc.**	sgol-2-13-0, sgol-2-13-1	87	7	0.93	0.11	0.85	0.16
		GSE conc.	–	–	–	–	–	–	–
	+ PGE	**PGE conc.**	sgol-2-13-0, sgol-2-13-1	87	7	0.93	0.11	0.85	0.16
		Total extacts	sgol-2-13-0, sgol-2-13-1	87	7	0.93	0.22	0.85	0.33
Ternary	+ CBE	**CBE conc.**	sgol-2-13-0, sgol-2-13-1	87	7	0.97	0.05	0.93	0.07
blends	+ GSE	**GSE conc.**	sgol-2-13-0, sgol-2-13-1	87	7	0.97	0.05	0.93	0.07
	+ PGE	**PGE conc.**	sgol-2-13-0, sgol-2-13-1	87	7	0.97	0.05	0.93	0.07
		Total extacts	sgol-2-13-0, sgol-2-13-1	87	7	0.97	0.15	0.93	0.22

Table 49. PLSR prediction of plant extract concentration (g/ 100 mL) based on the spectra of sour cherry juices recorded with the benchtop NIR device.

Sour cherry	juice	Extract	Pre-treatment	Nr	NrLV	R_C^2	$RMSE_C$	R_{CV}^2	$RMSE_{CV}$
All		**CBE conc.**	sgol-2-35-0, sgol-2-27-1	346	17	0.93	0.16	0.87	0.21
blends		**GSE conc.**	sgol-2-43-0, msc	360	12	0.91	0.17	0.90	0.17
		PGE conc.	sgol-2-43-0	343	16	0.98	0.09	0.97	0.10
		Total extacts	sgol-2-27-0, sgol-2-27-1	345	7	0.96	0.16	0.95	0.18
Simple	+ CBE	**CBE conc.**	sgol-2-43-0, msc	85	2	0.97	0.13	0.97	0.13
blends		**GSE conc.**	–	–	–	–	–	–	–
		PGE conc.	–	–	–	–	–	–	–
		Total extacts	–	–	–	–	–	–	–
	+ GSE	**CBE conc.**	_	_	–	–	–	–	–
		GSE conc.	sgol-2-43-0, deTr	73	6	0.95	0.18	0.92	0.23
		PGE conc.	–	–	–	–	–	–	–
		Total extacts	–	–	–	–	–	–	–
	+ PGE	**CBE conc.**	–	–	–	–	–	–	–
		GSE conc.	–	–	–	–	–	–	–
		PGE conc.	sgol-2-35-0, sgol-2-27-2	80	7	0.98	0.12	0.97	0.15
		Total extacts	–	–	–	–	–	–	–
Binary	+ CBE	**CBE conc.**	sgol-2-43-0, deTr	90	3	0.9686	0.08	0.95	0.09
blends	+ GSE	**GSE conc.**	sgol-2-43-0, deTr	90	3	0.9686	0.08	0.95	0.09
		PGE conc.	–	–	–	–	–	–	–
		Total extacts	sgol-2-43-0, deTr	90	3	0.97	0.15	0.95	0.19
	+ GSE	**CBE conc.**	–	–	–	–	–	–	–
		GSE conc.	sgol-2-43-0, sgol-2-43-2	74	7	0.98	0.07	0.97	0.08
	+ PGE	**PGE conc.**	sgol-2-43-0, sgol-2-43-2	74	7	0.98	0.07	0.97	0.08
		Total extacts	sgol-2-43-0, sgol-2-43-2	74	7	0.98	0.13	0.97	0.16
	+ CBE	**CBE conc.**	sgol-2-43-0, sgol-2-35-2	80	7	0.94	0.11	0.86	0.16
		GSE conc.	_	_	–	–	–	–	–
	+ PGE	**PGE conc.**	sgol-2-43-0, sgol-2-35-2	80	7	0.94	0.11	0.86	0.16
		Total extacts	sgol-2-43-0, sgol-2-35-2	80	7	0.94	0.21	0.86	0.32
Ternary	+ CBE	**CBE conc.**	sgol-2-43-0, msc	82	7	0.99	0.03	0.98	0.04
blends	+ GSE	**GSE conc.**	sgol-2-43-0, msc	82	7	0.99	0.03	0.98	0.04
	+ PGE	**PGE conc.**	sgol-2-43-0, msc	82	7	0.99	0.03	0.98	0.04
		Total extacts	sgol-2-43-0, msc	82	7	0.99	0.09	0.98	0.12

Table 50. PCA-LDA classification accuracies on the spectra of plum juices recorded different NIR instruments when classification was based on the type of plant extract added.

		Juice blends	Juice	+ CBE	+ GSE	+ PGE	+(CBE+GSE)	+(GSE+PGE)	+(PGE+CBE)	+(CBE+GSE+PGE)	Classification accuracy
MicroNIR hand-held device *	**Calibration**	**Juice**	74.44	1.39	0.00	0.00	0.00	0.00	0.00	0.00	**53.11%**
		Juice+CBE	18.33	79.63	1.85	10.65	10.65	1.85	18.98	6.02	
		Juice+GSE	0.00	0.00	43.52	7.41	11.57	6.94	0.93	5.09	
		Juice+PGE	0.00	0.00	6.48	48.15	5.56	8.80	9.72	4.17	
		Juice+(CBE+GSE)	0.00	7.87	12.50	2.31	51.39	2.78	10.65	10.65	
		Juice+(GSE+PGE)	0.00	0.00	18.52	11.11	3.70	43.98	18.98	16.67	
		Juice+(PGE+CBE)	7.22	5.56	14.35	12.50	4.63	16.67	36.11	9.72	
		Juice+(CBE+GSE+PGE)	0.00	5.56	2.78	7.87	12.50	18.98	4.63	47.69	
	Validation	**Juice**	64.44	0.00	0.00	0.00	0.00	0.00	0.00	0.00	**27.04%**
		Juice+CBE	22.22	51.85	7.41	16.67	12.96	5.56	18.52	14.81	
		Juice+GSE	0.00	11.11	11.11	20.37	29.63	16.67	5.56	14.81	
		Juice+PGE	2.22	9.26	20.37	11.11	5.56	16.67	14.81	7.41	
		Juice+(CBE+GSE)	0.00	18.52	33.33	9.26	16.67	5.56	11.11	12.96	
		Juice+(GSE+PGE)	0.00	0.00	9.26	18.52	12.96	22.22	22.22	12.96	
		Juice+(PGE+CBE)	11.11	7.41	7.41	7.41	9.26	14.81	16.67	14.81	
		Juice+(CBE+GSE+PGE)	0.00	1.85	11.11	16.67	12.96	18.52	11.11	22.22	
NIRflex benchtop device **	**Calibration**	**Juice**	72.22	0.00	0.00	0.00	0.00	0.00	0.00	0.00	**55.08%**
		Juice+CBE	15.56	66.20	0.93	0.47	10.65	0.00	5.09	2.78	
		Juice+GSE	0.00	0.46	46.30	13.21	8.80	7.87	0.93	7.41	
		Juice+PGE	0.00	0.00	13.89	45.28	0.00	16.67	3.70	11.57	
		Juice+(CBE+GSE)	2.22	10.65	8.33	4.72	53.70	1.85	6.02	7.41	
		Juice+(GSE+PGE)	0.56	2.78	14.35	13.21	1.85	45.37	5.09	5.56	
		Juice+(PGE+CBE)	2.78	11.57	9.26	14.62	10.65	12.96	61.57	15.28	
		Juice+(CBE+GSE+PGE)	6.67	8.33	6.94	8.49	14.35	15.28	17.59	50.00	
	Validation	**Juice**	66.67	0.00	0.00	0.00	0.00	0.00	0.00	0.00	**34.04%**
		Juice+CBE	17.78	35.19	0.00	0.00	1.85	0.00	5.56	9.26	
		Juice+GSE	0.00	0.00	25.93	37.74	7.41	14.81	0.00	11.11	
		Juice+PGE	0.00	1.85	22.22	3.77	0.00	12.96	9.26	3.70	
		Juice+(CBE+GSE)	8.89	29.63	14.81	5.66	35.19	9.26	3.70	12.96	
		Juice+(GSE+PGE)	2.22	5.56	16.67	28.30	3.70	29.63	14.81	12.96	
		Juice+(PGE+CBE)	2.22	12.96	9.26	16.98	12.96	18.52	44.44	18.52	
		Juice+(CBE+GSE+PGE)	2.22	14.81	11.11	7.55	38.89	14.81	22.22	31.48	

* sgol-2-21-0, deTr; Nr = 423; NrPCs = 20

** sgol-2-35-0, sgol-2-27-1; Nr = 422; NrPCs = 16

Table 51. PLSR prediction of plant extract concentration (g/ 100 mL) based on the spectra of plum juices recorded with the hand-held NIR device.

Plum	juice	Extract	Pretreatment	Nr	NrLV	R_C^2	$RMSE_C$	R_{CV}^2	$RMSE_{CV}$
All		**CBE conc.**	sgol-2-21-0	348	8	0.15	0.54	0.00	0.58
blends		**GSE conc.**	sgol-2-21-0, msc	374	4	0.46	0.42	0.42	0.43
		PGE conc.	sgol-2-13-0, sgol-2-21-2	348	16	0.69	0.32	0.55	0.39
		Total extacts	sgol-2-21-0, msc	323	7	0.82	0.32	0.80	0.34
Simple	+ CBE	**CBE conc.**	sgol-2-21-0	91	7	0.73	0.44	0.53	0.59
blends		**GSE conc.**	–	–	–	–	–	–	–
		PGE conc.	–	–	–	–	–	–	–
		Total extacts	–	–	–	–	–	–	–
	+ GSE	**CBE conc.**	–	–	–	–	–	–	–
		GSE conc.	sgol-2-17-0, sgol-2-21-2	79	6	0.89	0.29	0.76	0.42
		PGE conc.	–	–	–	–	–	–	–
		Total extacts	–	–	–	–	–	–	–
	+ PGE	**CBE conc.**	–	–	–	–	–	–	–
		GSE conc.	–	–	–	–	–	–	–
		PGE conc.	sgol-2-13-0, sgol-2-13-1	91	7	0.91	0.25	0.47	0.62
		Total extacts	–	–	–	–	–	–	–
Binary	+ CBE	**CBE conc.**	sgol-2-21-0, deTr	91	3	0.84	0.17	0.77	0.20
blends	+ GSE	**GSE conc.**	sgol-2-21-0, deTr	91	3	0.84	0.17	0.77	0.20
		PGE conc.	–	–	–	–	–	–	–
		Total extacts	sgol-2-21-0, deTr	91	3	0.84	0.34	0.77	0.40
		CBE conc.	–	–	–	–	–	–	–
	+ GSE	**GSE conc.**	sgol-2-21-0, msc	87	6	0.96	0.09	0.93	0.12
	+ PGE	**PGE conc.**	sgol-2-21-0, msc	87	6	0.96	0.09	0.93	0.12
		Total extacts	sgol-2-21-0, msc	87	6	0.96	0.17	0.93	0.23
	+ CBE	**CBE conc.**	sgol-2-21-0, msc	81	7	0.92	0.12	0.84	0.17
		GSE conc.	–	–	–	–	–	–	–
	+ PGE	**PGE conc.**	sgol-2-21-0, msc	81	7	0.92	0.12	0.84	0.17
		Total extacts	sgol-2-21-0, msc	81	7	0.92	0.25	0.84	0.34
Ternary	+ CBE	**CBE conc.**	sgol-2-13-0, sgol-2-21-1	88	7	0.91	0.08	0.77	0.13
blends	+ GSE	**GSE conc.**	sgol-2-13-0, sgol-2-21-1	88	7	0.91	0.08	0.77	0.13
	+ PGE	**PGE conc.**	sgol-2-13-0, sgol-2-21-1	88	7	0.91	0.08	0.77	0.13
		Total extacts	sgol-2-13-0, sgol-2-21-1	88	7	0.91	0.25	0.77	0.39

Table 52. PLSR prediction of plant extract concentration (g/ 100 mL) based on the spectra of plum juices recorded with the benchtop NIR device.

Plum	juice	Extract	Pre-treatment	Nr	NrLV	R_C^2	$RMSE_C$	R_{CV}^2	$RMSE_{CV}$
All		**CBE conc.**	sgol-2-43-0, deTr	342	17	0.76	0.28	0.66	0.33
blends		**GSE conc.**	sgol-2-35-0, sgol-2-43-1	340	7	0.70	0.32	0.59	0.37
		PGE conc.	sgol-2-43-0, msc	333	12	0.78	0.28	0.71	0.32
		Total extacts	sgol-2-27-0, sgol-2-27-1	339	7	0.90	0.24	0.87	0.28
Simple	+ CBE	**CBE conc.**	sgol-2-43-0, msc	88	6	0.67	0.50	0.61	0.54
blends		**GSE conc.**	–	–	–	–	–	–	–
		PGE conc.	–	–	–	–	–	–	–
		Total extacts	–	–	–	–	–	–	–
		CBE conc.	–	–	–	–	–	–	–
	+ GSE	**GSE conc.**	sgol-2-43-0, deTr	80	8	0.95	0.20	0.90	0.27
		PGE conc.	–	–	–	–	–	–	–
		Total extacts	–	–	–	–	–	–	–
		CBE conc.	–	–	–	–	–	–	–
		GSE conc.	–	–	–	–	–	–	–
	+ PGE	**PGE conc.**	sgol-2-35-0, sgol-2-35-2	75	6	0.96	0.16	0.95	0.18
		Total extacts	–	–	–	–	–	–	–
Binary	+ CBE	**CBE conc.**	sgol-2-43-0, sgol-2-35-2	75	7	0.95	0.10	0.94	0.10
blends	+ GSE	**GSE conc.**	sgol-2-43-0, sgol-2-35-2	75	7	0.95	0.10	0.94	0.10
		PGE conc.	–	–	–	–	–	–	–
		Total extacts	sgol-2-43-0, sgol-2-27-2	73	7	0.96	0.17	0.93	0.24
		CBE conc.	–	–	–	–	–	–	–
	+ GSE	**GSE conc.**	sgol-2-27-0, sgol-2-27-2	81	7	0.96	0.08	0.94	0.09
	+ PGE	**PGE conc.**	sgol-2-27-0, sgol-2-27-2	81	7	0.96	0.08	0.94	0.09
		Total extacts	sgol-2-27-0, sgol-2-27-2	81	7	0.96	0.15	0.94	0.19
	+ CBE	**CBE conc.**	sgol-2-35-0, sgol-2-43-1	83	5	0.97	0.07	0.96	0.08
		GSE conc.	–	–	–	–	–	–	–
	+ PGE	**PGE conc.**	sgol-2-35-0, sgol-2-43-1	83	5	0.97	0.07	0.96	0.08
		Total extacts	sgol-2-35-0, sgol-2-43-1	83	5	0.97	0.15	0.96	0.17
Ternary	+ CBE	**CBE conc.**	sgol-2-43-0	79	6	0.98	0.03	0.98	0.04
blends	+ GSE	**GSE conc.**	sgol-2-43-0	79	6	0.98	0.03	0.98	0.04
	+ PGE	**PGE conc.**	sgol-2-43-0	79	6	0.98	0.03	0.98	0.04
		Total extacts	sgol-2-43-0	79	6	0.98	0.10	0.98	0.13

ACKNOWLEDGEMENT

I wish to thank my supervisor, Dr. Zoltán Kovács, for trusting me and inviting me to be a member of his research group since 2019. Your words of encouragement and remarks have motivated me to exceed my own limitations and aim for eminence. I also would like to thank for the opportunity to measure myself as a science strategic analyst in the academic community.

I owe appreciation to Csaba Bíró, managing director, as well as to Csaba Saliga and Szabolcs Molnár, former and present colleagues at Agricolae Ltd., for the collaborative goals we developed that supported to complete my PhD dissertation.

I would like to thank my colleagues at the Department of Food Measurement and Process Control for the warm welcome, the shared ideas, inspiration and the always delightful conversations. Thanks to Dr. Zoltán Gillay, Dr. Viktória Zsomné Muha, Dr. Tímea Kaszab and Dr. Ferenc Firtha, with whom I have had the opportunity to work more in-depth on projects. Special thanks to the fellows of the PhD room, especially Juan Pablo Aguinaga Bósquez, Dr. Balkis Aouadi, Mátyás Lukács and Lueji Regatieri Santos, with whom I have had the chance to cooperate on various projects over the past years.

I would like to thank Dr. Gergő Szabó and Dr. Marietta Fodor for their technical and analytical support during the fruit ripeness assessments. Many thanks to Dr. Marietta Horváthné Petróczy, Ivett Kocsis (Institute of Plant Protection, MATE), Dr. Tamás Kocsis and William Ofori Appaw (Department of Food Science and Technology, KNUST) for their irreplaceable help in the preparation and contribution of fruit decay trials. Many thanks to Redeemer Kofi Agbolegbe (Department of Food Science and Technology, KNUST) invaluable assistance in the preparation and analyses of fruit juices.

I would like to acknowledge the support of the Erasmus+ and CEEPUS mobility programmes, which enabled me to visit the Aquaphotomics Research Department at Kobe University (Japan) and the Institute of Analytical and Radiochemistry at the University of Innsbruck (Austria), among others. These study visits have enabled me to work with great minds and researchers such as Prof. Dr. Christian W. Huck, Prof. Dr. Roumiana Tsenkova, Dr Jelena Muncan and Dr. Krzysztof B. Beć.

I would especially like to thank my former PhD colleagues, my long-time collaborators, Dr. Zsanett Bodor (Semmelweis University) and Dr. John Lewis Zinia Zaukuu (KNUST, Ghana) for their valuable advice, scientific and emotional encouragement, whose humility, dedication and enthusiasm for science and collaboration will always be an example to me to admire.

Finally, I would like to express my deep appreciation to my close and distant family, as well as to all my wonderful friends who have unconditionally encouraged and supported me along the challenging road to my research and doctorate.

The research was supported by the Doctoral School of Food Science (MATE), the Cooperative Doctoral Programme (KDP-2021, C1769369), TéT mobility grant (2023-1.2.4-TÉT).